



City Research Online

City, University of London Institutional Repository

Citation: O'Connor, M.A. (1991). The prediction of moment-rotation curves of extended endplate connections for use in semi-rigid analysis of steel frameworks. (Unpublished Doctoral thesis, City, University of London)

This is the accepted version of the paper.

This version of the publication may differ from the final published version.

Permanent repository link: <https://openaccess.city.ac.uk/id/eprint/28542/>

Link to published version:

Copyright: City Research Online aims to make research outputs of City, University of London available to a wider audience. Copyright and Moral Rights remain with the author(s) and/or copyright holders. URLs from City Research Online may be freely distributed and linked to.

Reuse: Copies of full items can be used for personal research or study, educational, or not-for-profit purposes without prior permission or charge. Provided that the authors, title and full bibliographic details are credited, a hyperlink and/or URL is given for the original metadata page and the content is not changed in any way.

City Research Online:

<http://openaccess.city.ac.uk/>

publications@city.ac.uk

THE PREDICTION OF MOMENT-ROTATION CURVES
OF EXTENDED ENDPLATE CONNECTIONS
FOR USE IN SEMI-RIGID ANALYSIS
OF STEEL FRAMEWORKS.

by

Mark Anthony O'Connor , B.Sc

A thesis in partial fulfilment for the degree of
Doctor of Philosophy
submitted to The City University

Department of Civil Engineering,
The City University,
London,
England.
November 1991

ACKNOWLEDGEMENTS

I would first like to thank my supervisor, Dr. L.F. Boswell for his advice and guidance throughout the course of my research.

The work presented in this thesis has been supported by a Research grant provided by SERC which I gratefully acknowledge.

I would like to thank the many individuals in the Department of Civil Engineering for their help with the experimental work. In particular, I am very grateful to Mr. A. Bonomini, Mr. A. Jones, Mr. L. Ansdell, Mr. C. Logan, Mr. V. Bullemor and Mr. G. Gatehouse of the Structures department. I am also grateful to Professor M.A.R. Cooper, Mr.D.Stirling and Mr.J.Hooker for their help and advice on the photogrammetric aspects of the experimental work.

I am indebted to my parents and parents-in-law for their patience and support throughout the course of my academic study. Most of all, though, I would like to thank my wife, Naomi, for her help in typing this thesis and her constant encouragement without which I would not have been able to complete this research.

SUMMARY

THE PREDICTION OF MOMENT-ROTATION CURVES OF EXTENDED ENDPLATE CONNECTIONS FOR USE IN THE SEMI-RIGID ANALYSIS OF STEEL FRAMEWORKS.

Methods of analysis which incorporate the semi-rigidity of connections already exist. At present, the only way of providing the reliable connection moment-rotation data required for these analyses is by conducting expensive full-scale testing of connection subassemblies. There is a need for methods of prediction for all types of steel framework connections.

In this study a method of predicting the behaviour of extended endplate connections has been presented. Connections are classified according to their position in the steel framework and the geometry of the individual connection. A review of existing full-scale tests on extended endplate connections is given along with a review of the existing mathematical models used to represent connection behaviour. An existing physically based moment-rotation model has been taken and some of the parameters are recalculated. In particular a more rigorous representation of the column flange in the tension region of the connection has been derived. An outline of the calculation of the parameters for the potentially different behaviour of connections due to their position in the framework is given.

A series of 13 full-scale tests on internal/internal extended endplate connection specimens has been carried out. Four different methods of connection rotation measurement have been used throughout the study. The best method of measurement is a transducer based method which allows the contribution of the various connection components to overall connection rotation to be assessed.

The moment-rotation curves obtained are compared and evaluated. The proposed method of prediction compares favourably with most experimental results.

A plane semi-rigid framework analysis program has been written by the author so that the effect of using predicted and experimentally obtained moment-rotation curves on framework behaviour can be established. This program has also been used to predict the behaviour of a full-scale plane frame test carried out at BRE by Hatfield Polytechnic. The connection curves used in this analysis have been derived using the prediction method. The results of the frame analysis are compared with the experimental values and agreement is found to be satisfactory.

It is concluded that moment-rotation curves of internal/internal extended endplate connections can be predicted with sufficient accuracy for use in the semi-rigid analysis of steel frameworks. Recommendations for further research include more experimental work on different classes of extended endplate connections and applying the physically based mathematical model which has been used to different connection types.

CONTENTS

	Page
ACKNOWLEDGEMENTS	i
SUMMARY	ii
CONTENTS	iii
LIST OF TABLES	viii
LIST OF FIGURES	xii
NOTATION	xxii
1. INTRODUCTION	1
1.1 Introduction	1
1.2 The aim of the study	3
1.3 Outline of this thesis	4
1.4 Factors affecting the moment-rotation behaviour of extended endplate connections	5
Figures 1.1 - 1.5	8
2. LITERATURE REVIEW	13
2.1 Introduction	13
2.2 Review of previous experimental work	14
2.2.1 Introduction	14
2.2.2 Experimental work	15
2.3 Numerical models used to represent connection behaviour	28
2.3.1 Introduction	28
2.3.2 Linear based models	29
2.3.3 Polynomial based models	31

CONTENTS (Cont.)	Page
2.3.4 Power models	33
2.3.5 Exponential models	34
2.3.6 Finite element models	36
2.3.7 Summary	37
Table 2.1	38
Figure 2.1 - 2.5	39
3. THEORETICAL DEVELOPMENT	44
3.1 Introduction	44
3.2 Calculation of initial stiffness	46
3.2.1 Introduction	46
3.2.2 Deflection of endplate/column flange in the tension region	50
3.2.2.1 Introduction	50
3.2.2.2 Endplate deflection	52
3.2.2.3 Column flange deflection	56
3.2.2.4 Compatibility equations	70
3.2.3 Deflection of the column web at the beam tension flange	75
3.2.4 Deflection of the column web in the compression region	80
3.2.5 Summary	82
3.3 Calculation of plastic moment (M_p)	84
3.3.1 Introduction	84
3.3.2 Endplate failure	84
3.3.3 Column flange failure in the tension region	85

CONTENTS (Cont.)	Page
3.3.4 Column web shear failure	87
3.3.5 Column web buckling failure	87
3.3.6 Column web crippling failure	88
3.3.7 Bolt failure	88
3.3.8 Section failure	89
3.4 Summary of theoretical development	89
Figures 3.1 - 3.16	90
4. EXPERIMENTAL STUDY	106
4.1 Introduction	106
4.2 Test specimens	106
4.3 Test rig	110
4.4 Instrumentation	111
4.4.1 Rotation and deflection measurement	111
4.4.2 Load measurement	115
4.4.3 Strain gauge measurements	115
4.5 Test procedure	116
4.6 Summary of tests	118
4.6.1 Test series A	118
4.6.2 Test series B	122
4.6.3 Test series C	123
4.6.4 Test D1	124
4.7 Summary of test programme	125
Tables 4.1 - 4.4	126
Figures 4.1 - 4.22	130

CONTENTS (Cont.)	Page
5. COMPARISON AND DISCUSSION OF RESULTS	144
5.1 Introduction	144
5.2 Comparison of the methods of rotation measurement	144
5.3 Comparison of moment-rotation curves obtained	149
5.4 Component contributions to rotation	153
5.5 Comparison of the method of prediction with the experimental results	162
5.5.1 Introduction	162
5.5.2 Curve fitting of experimental results	163
5.5.3 Comparison of the theoretical model with the 'best' fit curves	165
5.5.4 Comparison of the predicted curves with the experimentally obtained curves	177
5.5.5 Summary	177
5.6 Comparison of the method of prediction with other experimental results	178
Tables 5.1 - 5.22	181
Figures 5.1 - 5.67	205
6. ASSESSMENT OF APPLICABILITY OF MOMENT-ROTATION CURVES	272
6.1 Introduction	272

CONTENTS (Cont.)	Page
6.2 A semi-rigid plane framework analysis program	273
6.3 Selection of moment-rotation curves for analysis	277
6.4 The effect of actual and predicted moment-rotation curves on frame behaviour	278
6.5 The Hatfield test frame	283
6.5.1 Introduction	283
6.5.2 Moment-rotation data generation	284
6.5.3 Comparison of analysis and experimental results	285
6.6 Applicability of moment-rotation curves	288
6.7 Summary	291
Tables 6.1 - 6.3	292
Figures 6.1 - 6.18	295
 7. CONCLUSIONS AND RECOMMENDATIONS	 313
7.1 Conclusions	313
7.2 Recommendations for future research	320
 REFERENCES	 322
APPENDICES	

LIST OF TABLES

	Page
2.1	38
Summary of Existing Extended Endplate Connection Experimental Data	
4.1	126
Sizes of Previous Endplate Specimens	
4.2	127
Definition of Test Specimens	
4.3	128
Dimensions of Endplates	
4.4	129
Summary of Tensile Specimen Testing	
5.1(a)	181
Values of Offset Stiffness for each Test Series	
5.1(b)	181
Comparison of the Initial Connection Stiffness Measured from Offset and Transducer Readings	
5.2	182
Contribution of the Various Connection Components to Initial Stiffness	
5.3	183
Deflections of the Various Connection Components at Yield	
5.4	184
Effect of Theoretically Changing Contact Position on the Tension Region Contribution to Initial Stiffness (Test A2)	
5.5	185
Effect of Theoretically Changing Contact Position on the Tension Region Contribution to Initial Stiffness (Test A3)	

LIST OF TABLES (Cont.)		Page
5.6	Effect of Theoretically Changing Contact Position on the Tension Region Contribution to Initial Stiffness (Test A4)	186
5.7	Effect of Theoretically Changing Contact Position on the Tension Region Contribution to Initial Stiffness (Test A5)	187
5.8	Effect of Theoretically Changing Contact Position on the Tension Region Contribution to Initial Stiffness (Test A6)	188
5.9	Effect of Theoretically Changing Contact Position on the Tension Region Contribution to Initial Stiffness (Test A7)	189
5.10	Effect of Theoretically Changing Contact Position on the Tension Region Contribution to Initial Stiffness (Test A8)	190
5.11	Effect of Theoretically Changing Contact Position on the Tension Region Contribution to Initial Stiffness (Test B1)	191

LIST OF TABLES (Cont.)		Page
5.12	Effect of Theoretically Changing Contact Position on the Tension Region Contribution to Initial Stiffness (Test B2)	192
5.13	Effect of Theoretically Changing Contact Position on the Tension Region Contribution to Initial Stiffness (Test C1 - 4 bolts)	193
5.14	Effect of Theoretically Changing Contact Position on the Tension Region Contribution to Initial Stiffness (Test C2 - 4 bolts)	194
5.15	Effect of Theoretically Changing Contact Position on the Tension Region Contribution to Initial Stiffness (Test C1 - 6 bolts)	195
5.16	Effect of Theoretically Changing Contact Position on the Tension Region Contribution to Initial Stiffness (Test C2 - 6 bolts)	196
5.17	Effect of Theoretically Changing Contact Position on the Tension Region Contribution to Initial Stiffness (Test D1)	197
5.18	Tension Region Contribution to Initial Stiffness	198

LIST OF TABLES (Cont.)		Page
5.19	Compression Contribution to Initial Stiffness	199
5.20	Comparison of the Predicted and Experimental Initial Stiffness	200
5.21	Comparison of Theoretical and Experimental Plastic Moment	201
5.22	Comparison of Theoretical Plastic Moment with Existing Test Data Plastic Moment	202
5.23	Comparison of Theoretical Initial Stiffness with Existing Test Data Initial Stiffness	204
6.1	Difference in Central Deflection and End Moment for a Straight Line Model and Actual Connection Curve at the Beam Elastic Design Moment	292
6.2	Parameters used for Connections in the Hatfield Test Frame Analysis	293
6.3	Comparison of Results of the Hatfield Frame Test and the Predicted Analysis	294

LIST OF FIGURES

	Page	
1.1	Definition of a Moment-Rotation Curve	8
1.2	Typical Moment-Rotation Curves	9
1.3	The Extended Endplate Connection	10
1.4	Types of Connection in a Typical Framework	11
1.5	Various Stiffener Arrangements for Endplate Connections	12
2.1	Types of Specimen for Connection Testing	39
2.2	Surtees and Mann's Method of Connection Rotation Measurement	40
2.3	Methods of Rotation Measurement	41
2.4	Models used to Represent Connection Data (1)	42
2.5	Models used to Represent Connection Data (2)	43
3.1	Moment-Rotation Model	90
3.2	Connection Rotation expressed in terms of the Deflection at the Beam Flange Levels	91
3.3	Force Interaction between the Column Flange and Endplate	92
3.4	Column Flange and Endplate Modelled using the T-stub Analogy	93
3.5	Free Body Diagram of the Tension region of the Endplate	94

LIST OF FIGURES (Cont.)		Page
3.6	Derivation of the Deflection of a Semi-infinite Cantilever Plate Simply Supported at the Edge under Concentrated Load	95
3.7	Derivation of the Deflection of a Cantilever Plate Simply Supported at each Side under Concentrated Load	96
3.8	Exaggerated Deflection of One-dimensional Endplate and Two-dimensional Column Flange Models	97
3.9	Variation in Location of Prying Force with changing Relative Rigidity of Column Flange and T-stub	98
3.10	Derivation of the Compatibility Equation	99
3.11	Shear Deformation of the Column Web	100
3.12	Unbalanced Internal Connection	101
3.13	Derivation of Compression Stiffener Deflection	102
3.14	Endplate Yield Line Mechanism (Reference 13)	103
3.15	Unstiffened Column Flange Yield Line Mechanism (Reference 8)	104
3.16	Stiffened Column Flange Yield Line Mechanism (Reference 8)	105
4.1	Test Rig Layout	130

LIST OF FIGURES (Cont.)		Page
4.2	Transducer Measuring Frame	131
4.3	Transducer and Mounting	132
4.4	Data Logging System	132
4.5	Column Web Transducer Placement	133
4.6	Transducer Positions	134
4.7	Load Cell and Roller Arrangement	133
4.8	Placement of Endplate Transducers	135
4.9	Test set-up	136
4.10	Deformation of Endplate at Failure (Test A1)	135
4.11	Endplate Deflection Profile (Test A2)	137
4.12	Column Flange Deflection Profile (Test A2)	138
4.13	Lateral Deflection at Failure (Test A3)	139
4.14	Endplate Deflection at Failure (Test A5)	139
4.15	Separation of Endplate and Column Flange (Test A6)	140
4.16	Separation at Failure	140
4.17	Deflection of Test A8 at Failure	141
4.18	Beam Tension Flange Weld Failure (Test B1)	141
4.19	Weld Cross-section showing Slag Inclusion (Test B1)	142
4.20	Deflection of Endplate and Column Flange at Failure (Test B2)	142
4.21	Proximity of Endplate to Specimen End (Test C1)	143

LIST OF FIGURES (Cont.)		Page
4.22	Endplate Deflection at Failure (Test D1)	143
5.1	Comparison of Methods of Rotation Measurement (Test A2)	205
5.2	Comparison of Methods of Rotation Measurement (Test A3)	206
5.3	Comparison of Methods of Rotation Measurement (Test A4)	207
5.4	Comparison of Methods of Rotation Measurement (Test A5)	208
5.5	Comparison of Methods of Rotation Measurement (Test A6)	209
5.6	Comparison of Methods of Rotation Measurement (Test A7)	210
5.7	Comparison of Methods of Rotation Measurement (Test A8)	211
5.8	Comparison of Methods of Rotation Measurement (Test B1)	212
5.9	Comparison of Methods of Rotation Measurement (Test B2)	213
5.10	Comparison of Methods of Rotation Measurement (Test C1)	214
5.11	Comparison of Methods of Rotation Measurement (Test C2)	215
5.12	Comparison of Methods of Rotation Measurement (Test D1)	216
5.13	Endplate Deflection (Test D1)	217
5.14	Column Flange Deflection (Test D1)	218

LIST OF FIGURES (Cont.)		Page
5.15	Column Flange Deflection in the Compression Region	219
5.16	Comparison of Moment-Rotation Data - Series A	220
5.17	Comparison of Moment-Rotation Data - Series A	221
5.18	Comparison of Moment-Rotation Data - Series A	222
5.19	Comparison of Moment-Rotation Data - Series A & D	223
5.20	Comparison of Moment-Rotation Data - Series A	224
5.21	Comparison of Moment-Rotation Data - Series A	225
5.22	Comparison of Moment-Rotation Data - Series A	226
5.23	Comparison of Moment-Rotation Data - Series B	227
5.24	Comparison of Moment-Rotation Data - Series C	228
5.25	Comparison of Moment-Rotation Data - Design Connections	229
5.26	Comparison of Moment-Rotation Data - Stiffened Connections	230
5.27	Component Contributions v. Moment (Test A2)	231

LIST OF FIGURES (Cont.)			Page
5.28	Component Contributions v. Moment (Test A3)		232
5.29	Component Contributions v. Moment (Test A4)		233
5.30	Component Contributions v. Moment (Test A5)		234
5.31	Component Contributions v. Moment (Test A6)		235
5.32	Component Contributions v. Moment (Test A7)		236
5.33	Component Contributions v. Moment (Test A8)		237
5.34	Component Contributions v. Moment (Test B1)		238
5.35	Component Contributions v. Moment (Test B2)		239
5.36	Component Contributions v. Moment (Test C1)		240
5.37	Component Contributions v. Moment (Test C2)		241
5.38	Component Contributions v. Moment (Test D1)		242
5.39	Effect of Varying Model Parameters on Moment-Rotation Behaviour		243
5.40	Modelling of Connection Data using Yee Model (Test A2)		244

LIST OF FIGURES (Cont.)		Page
5.41	Modelling of Connection Data using Yee Model (Test A3)	245
5.42	Modelling of Connection Data using Yee Model (Test A4)	246
5.43	Modelling of Connection Data using Yee Model (Test A5)	247
5.44	Modelling of Connection Data using Yee Model (Test A6)	248
5.45	Modelling of Connection Data using Yee Model (Test A7)	249
5.46	Modelling of Connection Data using Yee Model (Test A8)	250
5.47	Modelling of Connection Data using Yee Model (Test B1)	251
5.48	Modelling of Connection Data using Yee Model (Test B2)	252
5.49	Modelling of Connection Data using Yee Model (Test C1)	253
5.50	Modelling of Connection Data using Yee Model (Test C2)	254
5.51	Modelling of Connection Data using Yee Model (Test D1)	255
5.52	Factors used to Define Contact Positions	256
5.53	Contact Positions for Endplate and Column Flanges of Varying Thickness as Derived by Ioanniddes (Reference 10)	257

LIST OF FIGURES (Cont.)		Page
5.54	Comparison of Prediction with Connection Data (Test A2)	258
5.55	Comparison of Prediction with Connection Data (Test A3)	259
5.56	Comparison of Prediction with Connection Data (Test A4)	260
5.57	Comparison of Prediction with Connection Data (Test A5)	261
5.58	Comparison of Prediction with Connection Data (Test A6)	262
5.59	Comparison of Prediction with Connection Data (Test A7)	263
5.60	Comparison of Prediction with Connection Data (Test A8)	264
5.61	Comparison of Prediction with Connection Data (Test B1)	265
5.62	Comparison of Prediction with Connection Data (Test B2)	266
5.63	Comparison of Prediction with Connection Data (Test C1)	267
5.64	Comparison of Prediction with Connection Data (Test C2)	268
5.65	Comparison of Prediction with Connection Data (Test D1)	269
5.66	Comparison of Prediction with Other Test Data - Davison (14)	270

LIST OF FIGURES (Cont.)		Page
5.66	Comparison of Prediction with Other Test Data - Moore & Simms (18)	271
6.1	Definition of Beam Stiffness Equation Parameters	295
6.2	Convergence of Solution at the End of the Beam	296
6.3	Subassemblage used to Examine the Effect of Semi-rigidity	297
6.4	Comparison of the Effect of Actual, Predicted, Offset and Rigid Connections on Framework Behaviour - Test A2	298
6.5	Comparison of the Effect of Actual, Predicted, Offset and Rigid Connections on Framework Behaviour - Test A3	299
6.6	Comparison of the Effect of Actual, Predicted, Offset and Rigid Connections on Framework Behaviour - Test A4	300
6.7	Comparison of the Effect of Actual, Predicted, Offset and Rigid Connections on Framework Behaviour - Test A5	301
6.8	Comparison of the Effect of Actual, Predicted, Offset and Rigid Connections on Framework Behaviour - Test A6	302

LIST OF FIGURES (Cont.)		Page
6.9	Comparison of the Effect of Actual, Predicted, Offset and Rigid Connections on Framework Behaviour - Test A7	303
6.10	Comparison of the Effect of Actual, Predicted, Offset and Rigid Connections on Framework Behaviour - Test A8	304
6.11	Comparison of the Effect of Actual, Predicted, Offset and Rigid Connections on Framework Behaviour - Test B1	305
6.12	Comparison of the Effect of Actual, Predicted, Offset and Rigid Connections on Framework Behaviour - Test B2	306
6.13	Comparison of the Effect of Actual, Predicted, Offset and Rigid Connections on Framework Behaviour - Test D1	307
6.14	Hatfield Test Frame - Dimensions and Detailing	308
6.15	Hatfield Test Frame - Numbering System	309
6.16	Unloading and Reloading Behaviour of Connection	310
6.17	Criteria for Connections in Plastically Designed Frames (after Witteveen et al. (49))	311
6.18	Beam-Line Method (after Batho(19))	312

NOTATION

A	Arbitrary constant (Chapter 3)
A	Axial area of section (Chapter 6)
A_{bo}	Net tensile area of bolt
A_c	Area of column section
A_{cw}	Area of column web
A_h	Horizontal bolt gauge
A_s	Area of compression stiffener
B	Arbitrary constant
B_n	Net bolt force at boltline n
B_u	Ultimate bolt failure force
C	Arbitrary constant
C_{ep}	Endplate vertical bolt gauge
C_n	Curve fitting constants (Chapter 2)
C_v	Column flange vertical bolt gauge
D	Arbitrary constant
D_b	Depth of beam section
D_{bf}	Distance between beam flange centrelines
D_c	Column flange flexural rigidity
D_c	Distance between column flanges
E	Young's modulus
F	Beam flange force
F'	Half beam flange force
F_A, F_B	Beam flange force either side of column
F_p	Beam flange force at plastic moment of connection
F_u	Unbalanced force across a connection
G	Shear modulus

NOTATION (Cont.)

I	Section moment of inertia (Chapter 6)
I_c	Column section moment of inertia
I_e	Endplate moment of inertia
K'	Effective initial stiffness
K_c	Connection secant stiffness
K_i	Connection initial stiffness
K_m	Beam offset stiffness
K_n	Connection stiffness in linear connection modelling
K_p	Connection strain hardening stiffness
M	Moment at connection
$M_{1,2}$	Beam-column end moment (Chapter 6)
M_n	Transition moment
$N_{1,2}$	Beam-column axial force (Chapter 6)
P	General concentrated load on column flange
S	Standardisation parameter
$S_{1,2}$	Beam-column shear force (Chapter 6)
Z_p	Section plastic modulus
a_c	Column flange width (Figure 3.6)
a_e	Endplate model dimension (Figure 3.5)
a_{ep}	Endplate dimension (Table 4.3)
b_c	Distance from boltline to tension stiffener (Figure 3.6)
b_e	Endplate model dimension (Figure 3.5)
b_s	Compression stiffener width (Figure 3.13)
c	Curve fitting constant
c_c	Distance from fixed edge to force (Figure 3.6)

NOTATION (Cont.)

c_e	Endplate model dimension (Figure 3.5)
d_{bh}	Diameter of bolthole
d_{bo}	Nominal diameter of bolt
d_c	Depth of column flange between stiffeners (Figure 3.7)
d_e	Depth of endplate acting in tension (Figure 3.5)
e_c	Distance from column force to stiffener (Figure 3.7)
f_{ep}	Endplate dimension (Table 4.3)
f_k	Ratio of depth of endplate in tension to beam depth
g_{ep}	Endplate dimension (Table 4.3)
h_{ep}	Endplate dimension (Table 4.3)
j	Scaling factor (Chapter 2)
k	Connection form constant - shear deflection
k_t	Connection type constant - shear deflection
k_{uv}	Column flange deflection factor at u due to load at v
l	Beam-column length (Chapter 6)
ll	Weld leg length
l_s	Length of stiffener
m	Column flange yield line dimension (Figure 3.15)
n	Curve-fitting parameter (Chapter 2)
n	Column flange yield line dimension (Figure 3.15)
p_y	Beam-column uniformly distributed load in y-direction
r	Relative rigidity parameter (Figure 5.52)
r_k	Root fillet radius
t_{bf}	Beam flange thickness

NOTATION (Cont.)

t_{bp}	Column flange backing plate thickness
t_{bw}	Beam web thickness
t_{cf}	Column flange thickness
t_{cw}	Column web thickness
t_{ep}	Endplate thickness
t_s	Compression stiffener thickness
$u_{1,2}$	Axial deflection of beam-column (Chapter 6)
v	Stiffened column flange yield line dimension (Fig. 3.16)
$v_{1,2}$	Transverse deflection of beam-column (Chapter 6)
w	General deflection of column flange
w_1, w_2	Components of general column flange deflection
w_b	Bolt deflection
w_{cb}	Column flange deflection at boltline
w_{cq}	Column flange deflection at prying force position
w_e	Endplate model deflection
w_{eb}	Endplate deflection at boltline
w_{ep}	Endplate width (Table 4.3)
w_{uv}	Deflection of column flange at u due to load at v
z_n	Distance from force to point of interest (Endplate model)
Δ_{cw}	Column web deflection at compression flange (unstiffened)
Δ_{ec}	Endplate/column flange deflection at the beam tension flange
Δ_i	Connection deflection at the beam compression flange

NOTATION (Cont.)

Δ_{sc}	Column web deflection at compression flange (stiffened)
Δ_u	Connection deflection at the beam tension flange
Δ_{wt}	Column web deflection at the beam tension flange
α	Unbalanced connection factor
α_n	Complex roots of infinite column flange solution
$\alpha_{1,2}$	Rotation at end of beam-column (Chapter 6)
β_n	Complex roots of infinite column flange solution
δ	Dimensionless variable for stiffened column flange (Figure 3.7)
ϵ	Strain of column stiffener
ϕ_i	Stability function (Chapter 6)
η	Dimensionless variable used to define position on infinite cantilever plate
κ	Ratio of depth of endplate in tension to depth of beam for yield line analysis of endplate
λ_n	Ratio of boltforce n to flange force F
ν	Poissons ratio for steel
θ	Connection rotation
σ	Stress
σ_{bo}	Bolt nominal yield stress
σ_y	Section nominal yield stress
σ_{ybp}	Backing plate nominal yield stress
σ_{yc}	Column nominal yield stress
σ_{yep}	Endplate nominal yield stress

NOTATION (Cont.)

- ξ Dimensionless variable used to define position on infinite cantilever plate
- ψ Dimensionless variable used to define position from stiffener on column flange(Figure 3.6/3.7)
- ζ Dimensionless variable used to define position of force on infinite cantilever plate

CHAPTER 1

INTRODUCTION

1.1 Introduction

Steel frameworks are designed assuming that the joints are either rigid or pinned. Real connections, however, do not behave in this manner, their true behaviour falling somewhere between the two extremes. It would be more correct, therefore, to classify all steel frames as semi-rigid.

The advantages of taking real behaviour into account when designing or analysing steel frameworks lie in a better understanding of framework behaviour resulting in more consistent and less conservative design methods. Generally, taking the actual behaviour of the connections into account results in a reduction in the design moment of beams for both nominally rigid and pinned frameworks. This reduction in design moment is accompanied by an increase or decrease in deflections for rigid and pinned design methods respectively.

Although semi-rigid design of frameworks is allowed by current design rules (1), it is subject to stringent conditions. BS 5950 (1) states that all analysis of steel frameworks must be based upon connection data obtained in experimental studies. Alternatively, an allowance can be made for the end restraint

moment provided by a nominally pinned connection provided it does not exceed 10% of the free moment applied to the beam. The rest of the framework must be designed assuming simple design methods. These conditions make the design of true semi-rigid structures impractical at present.

Analytical procedures which take semi-rigidity into account are well-documented (2,3,4,5). These procedures are usually computer based and present little difficulty to designers with access to computers. The analyses, however, depend on the availability of reliable data describing the structural characteristics of the various types of connection. The most important structural characteristic required for such analyses to proceed is the moment-rotation relationship of the connection.

The moment-rotation characteristic of a connection is defined as the relationship between the moment transmitted by that connection and the relative angular change of the beam and column centrelines (Figure 1.1). Typical moment-rotation curves for various connections are shown in Figure 1.2. These curves range from 'pinned' web cleat connections to 'rigid' extended endplate connections. Perfectly pinned and perfectly rigid connections are defined by the x-axis and y-axis respectively. Moment-rotation curves are highly nonlinear due to the deformation and changing interaction of the various components which make up the connection.

The complexity of the connection behaviour means that, at present, moment-rotation characteristics can only be obtained from the results of tests on actual beam-to-column connections. If the number of different types and sizes of connection is considered, coupled with the expense of full-scale testing, then the considerable research effort needed to provide reliable data for semi-rigid design purposes can be appreciated. There is a need, therefore, for the prediction of moment-rotation behaviour for all sizes and type of connection.

The connection studied in this project is the extended endplate connection, Figure 1.3. This connection is a popular and widely used connection due to its economy and ease of site erection. It consists of a plate, welded to the end of the beam and extending past the beam tension flange, which is then bolted to the column flange or web. The extended endplate connection is considered a 'rigid' connection and, if suitably designed, is capable of transmitting the full plastic moment of the beam to the column. It provides an upper bound to the range of connections classed as semi-rigid.

1.2 The aim of the study.

The aim of this study is to develop a reliable method of predicting the moment-rotation behaviour of extended endplate connections for use in the semi-rigid analysis of steel frameworks.

The method should be able to predict the connection behaviour throughout the loading range and for all connection sizes and types. It should express the moment-rotation curve as accurately and as simply as possible.

Experimental observations are required to formulate and assess the performance of the proposed method. It would be beneficial if any method developed could be compared with previous full-scale tests carried out on this type of connection.

1.3 Outline of this thesis.

This thesis describes a program of research which has been undertaken to obtain the moment-rotation relationship of endplate connections. A series of large scale experiments have been completed. The current chapter provides an introduction to the programme of research.

Chapter two reviews the previous experimental work concerning the extended endplate connection and presents and discusses previous methods used to model connection data. The third chapter presents the modifications made to the calculation of the parameters of a previously developed model representing moment-rotation behaviour of extended endplate connections.

The experimental procedure and the observations of the full-scale testing programme are given in chapter four. Discussion of these results and the comparison of the predicted and observed moment-

rotation behaviour is carried out in the next chapter.

The applications of the predicted curves are presented in the sixth chapter with particular reference to tests on two full-scale frames carried out at the Building Research Establishment by researchers from Hatfield Polytechnic. Finally the main conclusions and recommendations are summarised in chapter seven.

1.4 Factors affecting the moment-rotation behaviour of extended endplate connections.

In this section some of the factors that affect the moment-rotation behaviour of extended endplate connections will be outlined to demonstrate the flexibility required of any method of prediction.

Factors which affect the moment-rotation behaviour can be split into two broad categories. Firstly, factors which are present due to the position of the connection in the frame and secondly, geometric factors which are due to the various components which make up each individual connection.

A typical framework is shown in Figure 1.4. It can be seen that there are four types of connection classified by their position in the frame. Each of these connections has factors which are unique. For example, external connections are potentially weaker than internal connections due to unbalanced loading across the connection. This leads to shear deformation in the column web

of the connection. Additionally, eave connections are potentially weaker than internal connections due to the absence of the restraint provided by the column above the connection. Finally, connections lower down the frame are affected by the increasing axial forces present in column sections.

Amongst the more obvious geometric factors that affect moment-rotation behaviour are endplate and column flange thickness, bolt centres and endplate width and depth. A less obvious factor is the bolt type, size and amount of pretension. Also, the behaviour of a particular connection may be affected by minor axis connections joining the column at the same level as the major axis connection. Further geometric factors are introduced if stiffening arrangements are included in the connection.

Stiffeners are required as some unstiffened extended endplate connections are unable to transfer the full plastic moment of the beam to the column due to premature local failure of some part of the column. In these connections, the stiffeners can drastically alter the behaviour of the connection. Various types of stiffener employed with this connection type are shown in Figure 1.5. Each type or combination of stiffener will affect the moment-rotation behaviour in a different manner. Some stiffeners hinder the placement of minor axis connections and are, therefore, often precluded.

Summarising, the moment-rotation behaviour is dependent on many factors, not only on geometrical considerations but also on the

loading conditions at the connection. Therefore the flexibility required of any proposed method of prediction has been demonstrated. The proposed method of prediction will also have to be verified by appropriate experimentation.

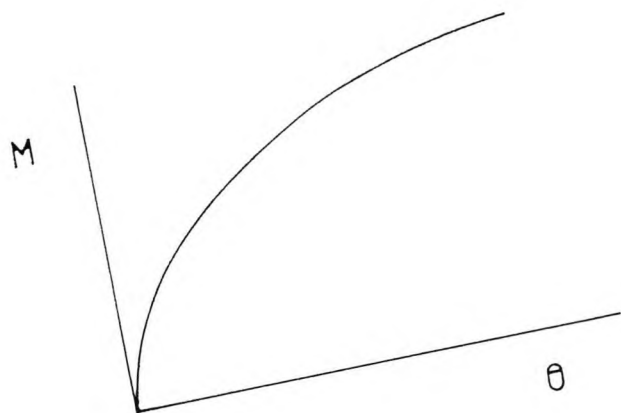
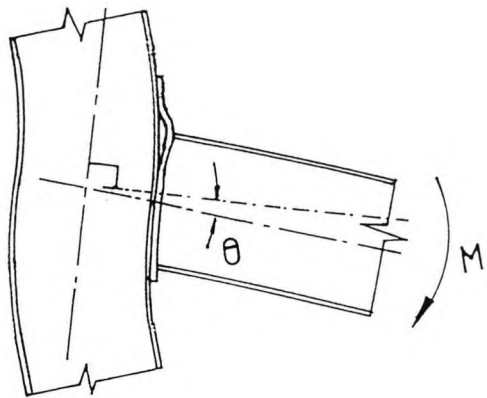
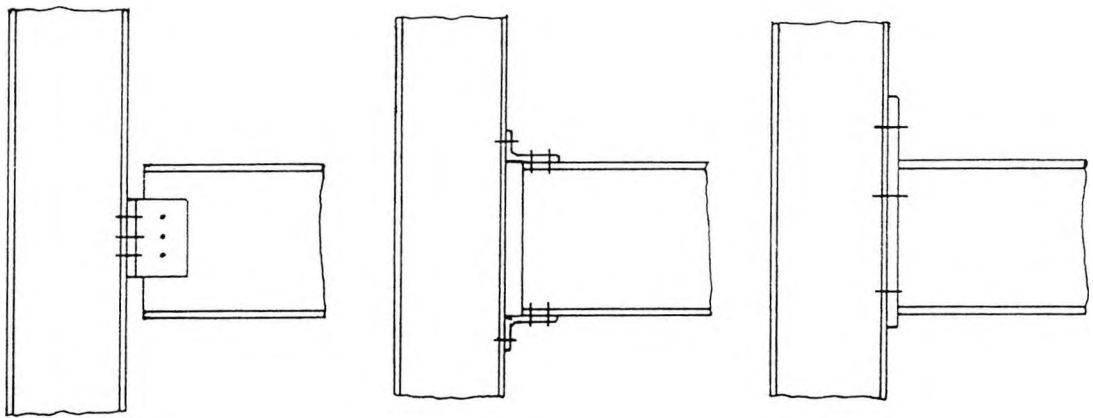
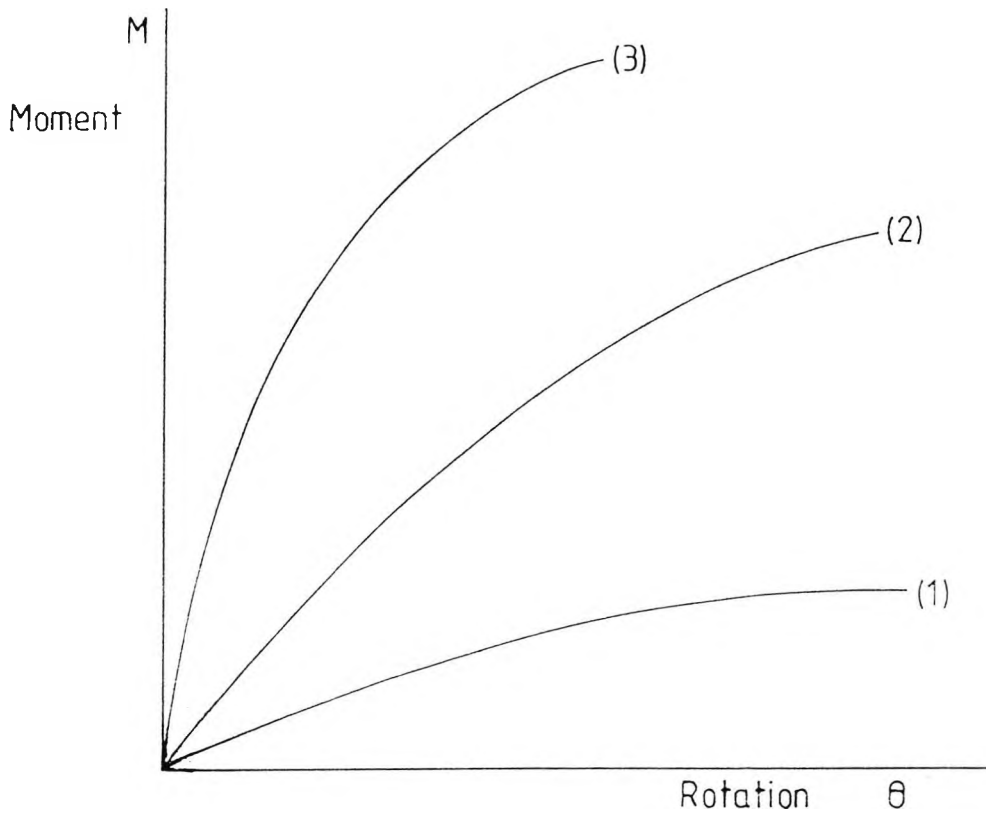


Figure 1.1 Definition of a Moment-Rotation Curve.



(1) Web cleat connection. (2) Top and seat angle connection. (3) Endplate connection.

Figure 1.2 Typical Moment-Rotation Curves.

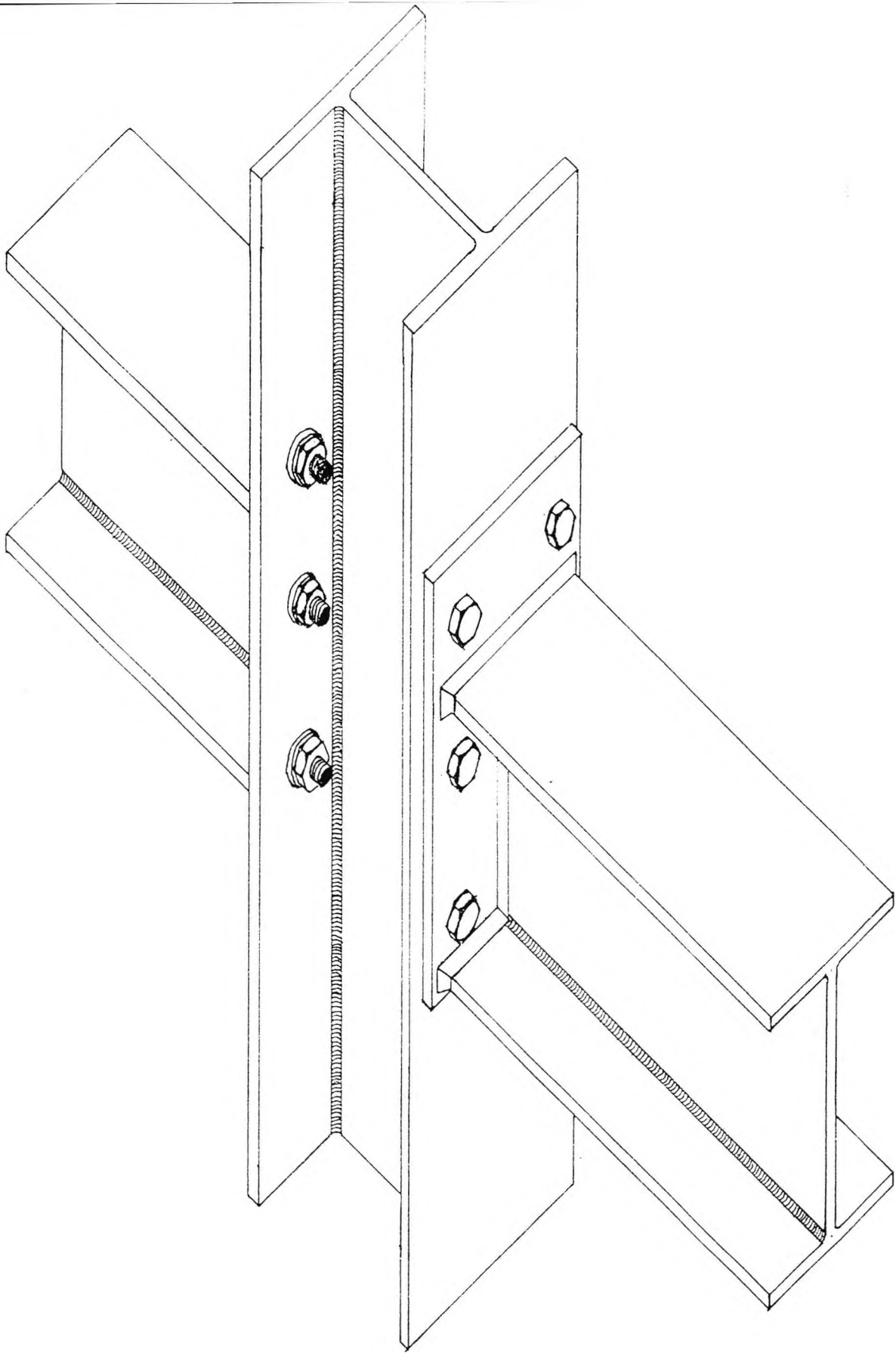
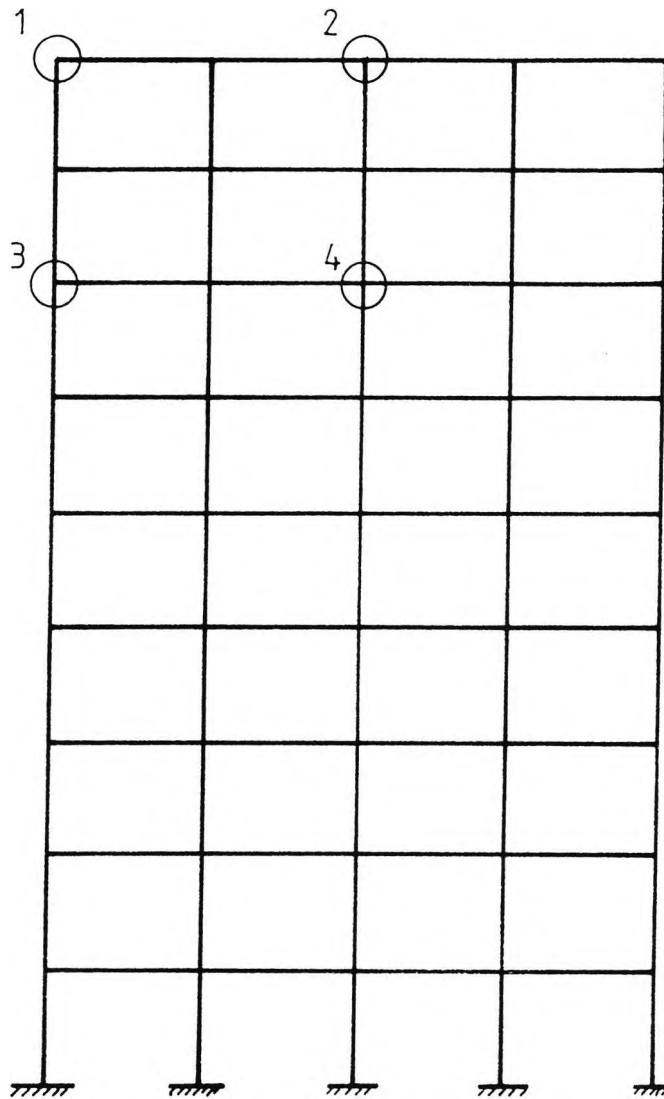
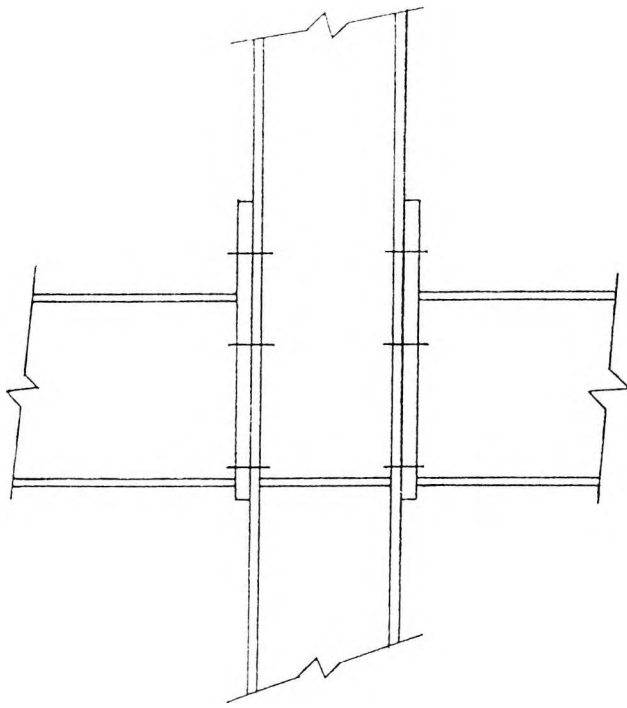


Figure 1.3 The Extended Endplate Connection.

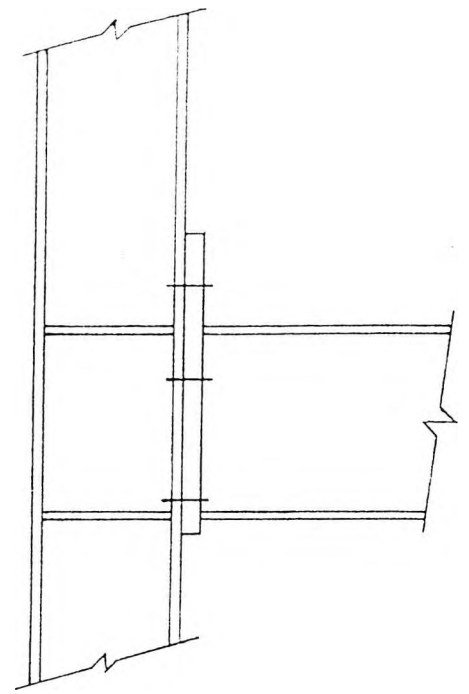


1. External / eave connection
2. Internal / eave connection
3. External / internal connection
4. Internal / internal connection

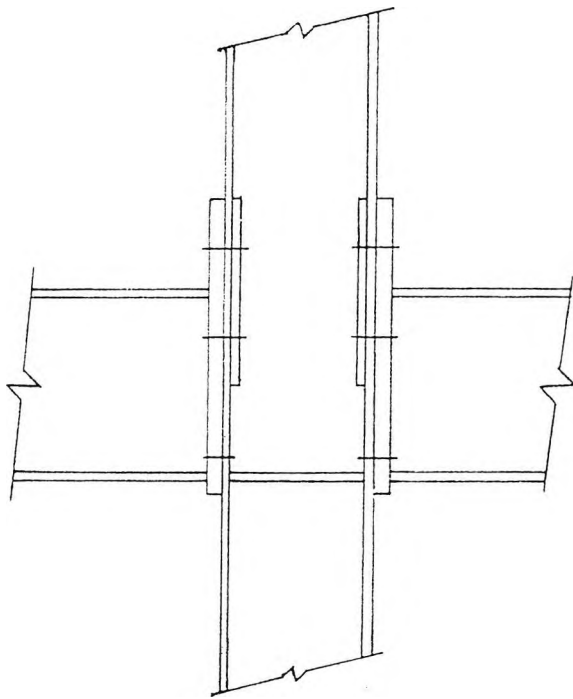
Figure 1.4 Types of Connection in a Typical Framework.



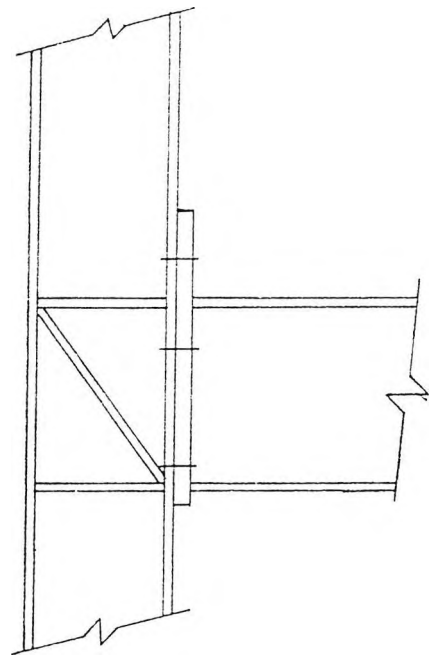
Compression Stiffener Only.



Compression and Tension Stiffeners.



Compression Stiffener with Backing Plate.



Shear Stiffener.

Figure 1.5 Various Stiffener Arrangements for Endplate Connections.

CHAPTER 2

LITERATURE REVIEW

2.1 Introduction

The aim of this research project is to develop a method of predicting the moment-rotation behaviour of extended endplate connections for use in the semi-rigid design of steel frameworks. Any proposed method will need to be compared with actual connection data, preferably obtained from full-scale testing. This chapter presents a review of previous full-scale tests on extended endplate connections. In particular, the review will concentrate on the suitability and accuracy of the data presented.

Any proposed method of prediction needs to be based upon a mathematical model. It was decided to review existing mathematical models to evaluate if any were suitable for adaptation to the particular connection examined in this study. The variety and usefulness of existing models has been the subject of many well-documented reviews (2,3). Some of these models are presented and their relevant merits discussed in a section following the review of connection tests. As a result of this review a suitable model for use in the author's work was identified and further refined to cover the full range of extended endplate connections.

2.2 Review of previous experimental work.

2.2.1 Introduction

The majority of the existing tests on endplate connections have been carried out to establish satisfactory strength criteria. In recent years some experimental work has been carried out to specifically obtain moment-rotation data and some tests have been conducted to obtain the behaviour of the connection under axial load. All the tests reviewed here deal with major axis connections i.e. beams adjoining column flanges. A summary of these tests is given in Table 2.1.

Each series of tests concentrates on one type of connection specimen. These specimens fall into one of four categories. These categories are shown in Figure 2.1 and roughly correspond to the position of the connection in the steel framework as outlined in section 1.4. The description of the specimen type tested in each series of tests refers back to Figure 2.1.

Before each series of tests are discussed it should be noted that as the extended endplate is a 'rigid' connection, rotations under working load are usually small. This means that some method of magnification needs to be employed if rotations are to be determined accurately. The method of rotation measurement adopted needs to be consistent and should not affect the normal behaviour of the connection. Very little information regarding

rotation measurement is given in reports of previous connection tests, and hence the accuracy of the various moment-rotation curves presented is difficult to assess.

2.2.2 Experimental Work

With the advent of plastic methods of design, researchers became more interested in 'rigid' connections, especially bolted connections due to their ease of site erection. This led Sherborne (4) to examine the behaviour of extended endplate connections with a series of tests on internal/internal type specimens (type(a)). Sherborne thought that it was contradictory to have connections which were designed elastically in frames which were designed plastically. Therefore, it was proposed that all the components of the connection should be designed to fail simultaneously at the plastic moment of the beam. This ensured that the plastic hinge that formed at the end of the beam formed in the connection itself and gave adequate rotational capacity to allow for the formation of a further hinge at the centre of the beam. Formulae were advanced for the determination of the endplate thickness, bolt size and the assessment of column stiffening requirements.

Endplate thickness was determined by assuming that the endplate between the two tension bolts acted as a clamped beam. The beam

tension flange force was then equated to the plastic moment capacity of the endplate at the beam flange. A quartic expression for the endplate thickness, t_{ep} , is obtained from which this thickness can be found.

Bolts were designed to carry the plastic moment of the beam at proof load as sudden bolt fracture is undesirable as a failure mode. It was noted that to obtain the bolt size design conditions, each bolt had to carry equal load at failure. This was the case for thin endplates where redistribution of force could take place due to the plastic yielding of the endplate. For thick endplates however force redistribution could not take place and failure of the bolts below the tension flange of the beam was possible before the plastic capacity of the beam was reached.

It was observed that the thickness of the column compression stiffeners had little effect on the moment capacity of the connection. This was because the failure mode of unstiffened columns in the compression region was usually column web buckling or crippling and stiffeners were only required for stability against out of plane movement of the column web.

Since Sherborne was only interested in the strength of the connections, specimen moment-rotation relationships were not deduced or measured. However, the load deflection relationship of the specimen was measured since any significant deviation from rigid elastic behaviour represented failure of the connection.

Bailey (5) continued the above work in 1970 with a series of tests on internal/internal type specimens with the column fixed, but without axial load (type (c)). The main aim of this research was to verify Sherborne's proposals. These were found to be adequate for design purposes and a formula for the design of welds was put forward. Again, only load-deflection curves were presented, although the deflections were modified to account for column flexure and the movement of the supporting baseplate.

Surtees and Mann (6) published the results of their research on the behaviour of external/internal type connections (type (b) - without axial load) with particular reference to the requirements of connection performance in a plastically designed multi-storey frame.

Their main design recommendations suggested that the prying force between the endplate and column flange should be taken into account when sizing bolts. It was proposed that an allowance of 33% of the total force carried by the bolts be added to the bolt design force to account for the prying effect. In addition, it was proposed that the calculation of the endplate ultimate load should be based on a more rigorous yield line mechanism. For the first time, it was recommended that the flange force used in the design process should be directly related to the plastic moment of the beam section, (M_p). This design flange force was equal to the plastic moment (M_p) divided by the depth of the beam section (D_{bf}). This calculation is based upon the assumption that the

moment at the end of the beam can be split into a couple acting at the beam flanges. This assumption was verified experimentally.

Moment-rotation relationships for each test were presented for the first time by Surtees and Mann and some comments regarding the method of measurement follow.

Rotation was measured using a combination of mirrors and dial gauges. Since the specimens tested were external/internal type connections, column and beam flexure needed to be taken into account when assessing rotation data. The mirrors were attached to the beam and column at sufficient distances away from the connection for local distortion effects to be minimised. The relative angular movement between the two mirrors was then found by sighting a distant target scale via the two mirrors (Figure 2.2).

Rotation was additionally measured by clamping dial gauges with magnetic stands to the beam flanges. The gauges were set on the column flanges at a distance away from the connection. Rotation was deduced from the difference in the movement of the two gauges knowing their distance apart (Figure 2.2). It was recognised that interface, shear and flexural deformations contributed to the connection rotation. It was suggested that by measuring rotation in two different ways the contributions of each of the deformations to connection rotation could be found.

In this case, the exact method of reduction of measurements to connection rotation has not been published. Therefore, it is difficult to make an assessment of the validity of the moment-rotation relationships given.

After a substantial experimental programme, a method of designing the tension region of bolted end-plate and t-stub connections was published by Zoetmeijer (7). The endplate was designed in the tension region as if it was a t-stub. The theoretical ultimate strength of an unstiffened column flange was found by assessing various straight line yield mechanisms. It was recognised that in t-stub to column flange subassemblages the position of the prying force was dependent upon the relative rigidities of the t-stub and column flange. It was concluded that this varying position had little effect on the ultimate failure condition as at failure the relative rigidities were roughly equal and the prying force could therefore be assumed to be acting at the corner of the t-stub.

The theoretical determinations of strength obtained using the straight line yield mechanisms were compared with the results of tests on t-stub to column flange and beam to column flange subassemblages and were found to be satisfactory. Additionally the behaviour of connections in a test framework was observed. The connections tested in this way included extended endplate connections.

Some moment-rotation curves for the connections tested were given, mainly to assess their ability to transmit the plastic moment of the beam with adequate rotational capacity. The method of rotation measurement is not discussed and hence an assessment of the data presented cannot be carried out. From photographs of the experimental set-up, it can be seen that some kind of rotation arm offset from the connection was used.

The yield line method of determining column flange capacity in the tension region was taken a stage further by Packer and Morris (8) with the use of curved yield lines and the derivation of a mechanism for stiffened flanges. Various yield line mechanisms were compared with the results of a series of internal/internal type connections (type (a)). Both stiffened and unstiffened column sections were tested. The formulae advanced were found to be satisfactory although it was recognised that they represented an upper bound to the column flange failure load.

The results of three unstiffened beam-to-column tests were presented as moment-rotation curves. These curves are deduced from the deflection at the centre of the specimen relative to the specimen supports. Rotation values must be obtained by simply dividing the deflections by the lever arm of the specimen. This is supported by noting that on the moment-rotation curves given, a line denoting the elastic deflection of a perfectly rigid connection is drawn. These curves are not moment-connection rotation curves as they include beam flexure. It demonstrates

that the method of connection rotation measurement needs to be carefully scrutinised before using moment-rotation curves from previous experiments.

The behaviour of the extended end-plate connections under axial load was investigated at Vanderbilt University, Tennessee. Firstly, Dews (9) studied the effect of axial load upon external/internal type connections (type (b)). The connection components were designed to carry the plastic moment of the beam. The axial load appears to have little effect on the plastic moment capacity of the connection as all tests deviated from linear elastic behaviour at or around the design moment of the connection.

Moment-rotation curves were presented for each test. These relationships were derived from dial gauge readings only and neglect beam and column flexure.

Ioanniddes (10) studied the effect of axial load on internal/internal type specimens (type (c)). The results of these tests were to be compared with a method of predicting the initial stiffness of the endplate and column flange using finite element analysis.

The moment-rotation relationship for each test is given. Rotation measurements were derived from dial gauge readings at the beam tension and compression flanges. These readings were taken relative to an external fixed datum. Tension readings only

have been used while, as will be seen later, the compression deflection also contributes to connection rotation. In addition, the results are erratic due to the nature of the loading system. When the column is fixed the beams have to be loaded on either side of the connection. It is difficult to load the beams at exactly the same rate. Therefore, the connection specimen moves to one side or the other until the load stabilises. As the dial gauge readings are taken relative to an external datum, the deflection of the connection at the beam tension and compression flange levels relative to the column centreline cannot easily be deduced. This has led to errors in the deduction of moment-rotation curves from these readings.

Grundy, Thomas and Bennetts (11) investigated the strength of two internal/internal type specimens (type (a)). Load-deflection measurements only were taken and the connections used had eight bolts in two rows about the tension flange. The comparison of these results with other specimens is, therefore, not valid.

The effect of varying the moment/shear ratio on the behaviour of unstiffened internal/internal type connections (type (a)) was studied by Graham (12). Bolt behaviour was also closely monitored. In particular, the value of the prying force was determined and compared with a method of prediction in the elastic range and at ultimate load.

It was concluded that the moment/shear ratio had little significant effect on the behaviour of endplate connections. The

magnitude of prying forces depended on the area of contact between the endplate and column flange. These areas of contact change throughout the loading range. This makes the prediction of prying force magnitude at any load difficult.

Rotation of the connection specimens was measured by placing two dial gauges on each beam and dividing the difference in their readings by their distance apart. These rotation values take a large amount of beam flexure into account. Unfortunately, data which would enable an approximate measure of connection rotation to be deduced was not presented.

A method of predicting the moment-rotation behaviour of external/eave connections (type (d)) was presented by Yee (13). A series of tests were performed to validate the method. Correlation between the predicted and observed behaviour of the specimen was found to be satisfactory. It was suggested that the method of prediction could be expanded to incorporate other types of endplate connection.

Yee measured rotation using two transducers placed on the column and beam at a sufficient distance away from the connection to minimize any local distortion effects. The rotation transducer consisted of a metal strip which was attached to the beam or column at one end and to a damped heavy weight at the other (Figure 2.3(a)). The strain in the metal strip on bending was measured using an electrical resistance strain gauge. Upon bending a linear relationship between the gauge readings and the

rotation of the strip was obtained. When calibrated the transducer could measure rotation to a precision of $\pm 0.5 \times 10^{-3}$ rads.

Specimen rotation was the difference in the two transducer readings. The rotation due to the offsets of the beam and column were taken into account when comparing the predicted experimental curves.

A test on an internal/internal type specimen was carried out as part of a series on a range of connection types by Davison (14). The purpose of the test was to provide basic moment-rotation data for use in methods of predicting the behaviour of beam-column subassemblages and frameworks.

T-bars welded to the beam and column were used to amplify connection rotation at a point. Rotation of each bar was then determined by measuring the change in length of a system of taut wires using linear displacement transducers (Figure 2.3(b)). The T-bars were placed at the beam column centreline intersection and at offsets from the connection on the beam centreline. The value of the offset rotation was assumed to be negligible. This is valid for nominally pinned connections but not for endplate connections as the stiffness of the connection is of the same order of magnitude as the offset stiffness. As all the test data is presented, an allowance for offset rotation can be made for comparison with the method of prediction.

Aggarwal and Coates (15) tested a series of external/eave connections under both static and cyclic load conditions. The load appears to have been applied in the opposite direction to that which would normally occur in a framework i.e. opposite to the direction of the load as shown in Figure 2.1(d). The results of these tests, therefore, are not easily compared with others in the literature.

Rotation was measured by an optical technique in which the rotations of the beam and column were determined by monitoring the movement of mirrors attached to the beam and column centrelines. The angular rotation of the mirrors could be deduced by measuring the movement of a distant scale, via the mirrors, with a theodolite.

A method of predicting the moment-rotation behaviour of extended and flush endplate connections using the finite element method was proposed by Jenkins, Tong and Prescott (16). The method was compared with a series of stiffened internal/internal type specimens and agreement was found to be reasonable. It was also proposed that endplate details be standardised and a suggested table of dimensions for flush and extended endplates was presented based upon an industry survey on present connection design practice. It was suggested that standardization would lead to economies in design time and fabrication costs as well as lending itself to computer aided design. A design method for flush endplates was presented based on the generated moment-rotation relationship.

The experimental work presented by Jenkins et al. was considered in more detail in Prescott's Ph.D thesis (17). Rotation was measured using dial gauges bearing on light extension arms to amplify rotation. The extension arms were placed as close as possible to the connection. The exact distance from the connection to the rotation arm position is not given. This means that an assessment of the validity of these results is not possible.

Certain unstiffened connections cannot transmit the full plastic moment of the beam to the column due to premature failure of the column flange in the tension region. This problem can be overcome by introducing transverse stiffeners between the column flanges to increase the strength of the connection. The presence of these stiffeners ,however, can hinder the placement of minor axis connections. An alternative method of stiffening the column flange in the tension region is to provide backing plates to the flange. This method requires minimal fabrication and hence is more economic than traditional stiffening systems.

Moore and Sims (18) carried out a preliminary investigation into the effect of these backing plates on the behaviour of extended endplate connections. The investigation was limited to the determination of the ultimate strength of these connections. Various yield line patterns were examined and the yield values obtained theoretically were compared with the experimental results on internal/internal type connection specimens. Correlation between the yield line failure loads and the

experimental failure loads was deemed to be satisfactory. It should be noted that the backing plates increased the strength of the connection but appeared to have little effect on the initial stiffness of the connection.

Moment-rotation curves were presented. Rotation was derived from accelerometer readings offset from the connection on the beam centreline and at the beam-column centreline intersection. Offset stiffness has not been taken into account.

Summarising this survey of previous experimental data on the extended endplate connection, the measurement of connection rotation has not been considered carefully enough. This is due to the fact that the majority of the previous tests have been carried out to establish strength criteria. However, tests carried out to provide moment-rotation data specifically still fail to take offset stiffness into account. Offset stiffness should be taken into account for extended endplate connections as it is of the same order of magnitude as the initial connection stiffness.

2.3 Numerical models used to represent connection behaviour

2.3.1 Introduction

Almost all curves used in the analysis of semi-rigid frameworks are obtained from experimental studies. This experimental data needs to be expressed mathematically so that it can be included in computer analyses. Various models have been proposed to represent moment-rotation data, ranging from simple linear expressions to complex piecewise polynomials. Whilst some models are used solely to curve-fit experimental data, others attempt to predict the behaviour of certain connection types. Prediction models fall into two categories. Firstly models based on regression analysis of existing moment-rotation data and secondly models based upon the physical behaviour of the connection.

The advantage of models based on the regression analysis is that they are usually easy to formulate. Different sizes of connection are accounted for by the introduction of standardisation parameters. However, large amounts of data are required to give a good prediction equation. This data will often come from varying sources and, as outlined in the last section, its reliability will not always be known. Other disadvantages of regression analysis include the facts that these models are usually only valid over a limited range and that although standardisation parameters are loosely based on connection geometry, they have little physical meaning.

The advantage of a physically based approach is that once the model is set up it should be able to accommodate all sizes of connection. However, due to the intricate interaction between the various components of the connection, this model is bound to be complex. This will often preclude its use from normal design procedures.

A fundamental requirement of all models, whether curve-fitted or physically based, is that the model should fit the data as accurately as possible throughout the loading range with as few parameters as possible to minimise the storage requirements of computer-based methods of analysis. It is also desirable that the model should be easily differentiable to enable the tangent stiffness at any point to be found. The models previously used to model and predict moment-rotation behaviour are briefly discussed below.

2.3.2 Linear based models.

Linear based models representing moment-rotation behaviour are shown in Figure 2.4(a). The simplest of these is the linear model which is expressed as

$$M_1 = K_1\theta$$

(2.1)

This model was used by various researchers (19,20,21) to represent connection stiffness in slope deflection and moment

distribution methods of semi-rigid analysis. While representing the moment-rotation behaviour accurately in the early stages of loading, it deviates from the true connection behaviour in the later stages.

A closer approximation to connection behaviour was proposed by Lionberger and Weaver (22) and Romstad and Subramian (23) who used a bilinear model (K_1, M_2, K_3 - Figure 2.4(a)) in a computer-based matrix method of analysis. Three parameters, two stiffnesses and a transition moment, are required for this model. Numerical difficulties ensue when using the model with tangent stiffness methods of analysis due to the sudden change in stiffness at the transition moment.

Trilinear (K_1, M_1, K_2, M_3, K_3) and quadlinear ($K_1, M_1, K_2, M_3, K_3, M_4, K_4$) models represent connection curves even more closely. These were proposed by Moncarz and Gertsle (24) and Melchers and Kaur (25). The main disadvantage with these models is the number of parameters needed to model each connection, five and seven respectively.

Several researchers developed physically based models which calculated the initial stiffness of connections. For example, Lothers (26) developed a method of predicting the initial stiffness of double web angle connections by considering the deformation of the angles. The deflection of the column flanges to which the angles were bolted was assumed to be negligible.

Huang et al (27) derived a theoretical quadlinear model for the column web panel of a connection based on the representation of the web as a beam under various support conditions and at various stages of plastic collapse.

2.3.3 Polynomial based models

Sommer (28) first used polynomial curve-fitting techniques (Figure 2.4) in his analysis of welded header plate connections. Frye and Morris (29) extended this method of curve-fitting to other types of connection including extended endplate connections. The model relating rotation, θ to moment M is of the form

$$\theta = C_1(SM) + C_2(SM)^3 + C_3(SM)^5$$

(2.2)

where S is the standardisation parameter
and C_1, C_2, C_3 are curve fitting constants.

The main disadvantage of this model is that maxima and minima are produced, these often lie within the working range of the connection. This can cause numerical difficulty when using tangent stiffness based analyses as the slope of the moment-rotation curve can become negative at some stage.

The above problem can be overcome by splitting the moment-rotation curve into sections, fitting a different cubic

polynomial within each small range and ensuring first and second derivative continuity at the changes in section. This method of representation, called a cubic B-spline curve, is extremely accurate and was first used for connection curve modelling by Jones, Kirby and Nethercot (2). The major drawback of this modelling technique is that a large number of parameters are usually needed to model the moment-rotation behaviour. This can lead to excessive data storage requirements in computer based analyses of large structures.

Another polynomial type model was presented by Ang and Morris (30) . It is in the form

$$\frac{\theta}{\theta_0} = \frac{SM}{(SM)_0} \left(1 + \left(\frac{SM}{(SM)_0} \right)^{n-1} \right)$$

(2.3)

where θ_0 , (SM) and n are parameters defined in Figure 2.5(c) and S is a standardisation parameter.

Rearranging this equation gives

$$\theta = \frac{\theta_0}{(SM)_0} (SM) + \frac{\theta_0}{(SM)_0^n} (SM)^n$$

(2.4)

which is in a similar form to equation (2.2).

This model is only a four parameter model and represents the

behaviour of connections reasonably well.

2.3.4 Power models.

Batho and Lash (31) were the first to suggest a nonlinear fit of experimental data. They suggested that for web cleat connections moment-rotation behaviour could be expressed by the equation

$$M = c\theta^{0.412}$$

(2.5)

where c and 0.412 are curve fitting constants.

Unfortunately this model gives an infinite stiffness at $\theta = 0$.

Later Krishnamurthy (32) suggested a similar model of the form

$$\theta = cM^{1.58}$$

(2.6)

where c and 1.58 were found from a parametric study of 2-dimensional and 3-dimensional finite element models of extended endplate connections.

Colson (33) suggested a model of the form

$$\theta = \frac{M}{K_i} \frac{1}{\left(1 - \left(\frac{M}{M_p}\right)^n\right)}$$

(2.7)

where K_i = the initial stiffness of the connection
 M_p = the ultimate moment capacity of the
connection
and n = a parameter to control the curvature of
the model.

This model is shown in Figure 2.5(d). The advantage of this model is that two out of three of the parameters are physically based and only three parameters are needed to give a reasonable fit to the data. The disadvantage of the model is that if a connection contains significant strain hardening then this cannot be easily incorporated into the model.

2.3.5 Exponential models.

Yee (13) developed an exponential model to predict the behaviour of extended endplate eave connections. This model is perfectly general as it is based upon the physical characteristics of any

connection viz. the initial elastic stiffness (K_i), the ultimate moment capacity (M_p) and the strain hardening stiffness (K_p). The model takes the form

$$M = M_p \left(1 - e^{-\frac{(K_i - K_p + c\theta)\theta}{M_p}} \right) + K_p \theta$$

(2.8)

where c is a parameter introduced to control the rate of decay of the curve.

This model gives a reasonable fit to the moment-rotation data with only four parameters.

A more complex exponential model for curve fitting was proposed by Lui and Chen (3). This model takes the form

$$M = \sum_{j=1}^m c_j \left(1 - e^{-\frac{\theta}{2j\alpha}} \right) + M_0 + K_p \theta$$

(2.9)

where c_j = curve fitting constants
 M_0 = starting value of connection moment to the curve
 K_p = strain hardening stiffness
 j = scaling factor for numerical stability.

This model fits moment-rotation behaviour extremely well with four to six curve fitting constants. However, these constants have little physical meaning and seven to nine parameters overall are needed to model each connection curve.

2.3.6 Finite element models.

These models are used exclusively for the prediction of moment-rotation behaviour. The cost and time involved make this technique unacceptable for everyday practical use. The main difficulty is that the connection problem is 3-dimensional and different elements lying in different planes are needed for different parts of the connection. The elements that are needed are not always compatible. This means that any analysis of the components of the connection have to be carried out separately and iteratively. The analysis becomes extremely lengthy and impractical.

Krishnamurthy (32), Lipson and Hague (35), Ioanniddes (10), Chen and Patel (36) and Jenkins, Tong and Prescott (16) have all used finite element models to try to assess moment-rotation behaviour. All have met with limited success while some have simplified the problem by using only an elastic analysis of the connection. The straight line model that is produced is subject to the same limitations as the linear model discussed previously.

However, the advent of more powerful and cheaper computers has made the 3-dimensional modelling of connections more feasible for

research purposes. Therefore finite element modelling of connection behaviour is becoming more cost-effective especially coupled with selective large scale testing of connection specimens but is still at the research stage.

2.3.7 Summary

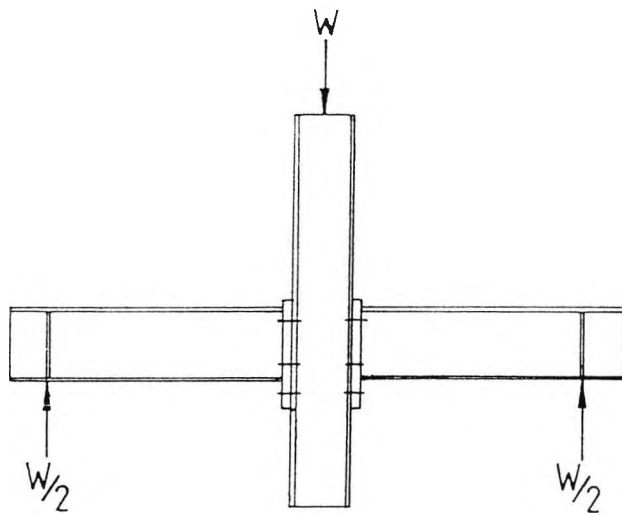
Various models used to previously model moment-rotation data for all connection types have been presented. The model which satisfied most of the criteria for modelling extended endplate connection behaviour was the Yee exponential model (section 2.3.5) as it had been derived specifically for extended endplate connections.

It had been demonstrated (13) that the Yee model can represent the moment-rotation behaviour of external/eave extended endplate connections with reasonable accuracy using only four parameters. Moreover three of these four parameters are physically based which means that the method of prediction can easily be extended and refined to include the whole range of extended endplate connections classified by position in the steel framework. The model is easily differentiable and can incorporate the strain hardening behaviour of the connection if so desired.

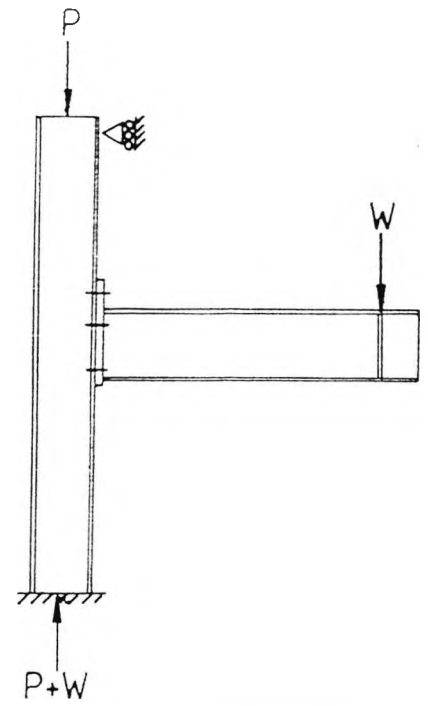
The author decided to investigate and refine the Yee model further in this study.

Name	Year	Ref.	No. of Tests	Specimen Type
Sherborne	1961	4	5	Int/Int (a)
Bailey	1970	5	13	Int/Int (c)
Surtees & Mann	1970	6	6	Ext/Int (b)
Zoetmeijer	1974	7	8	Ext+Int/Int (b/c)
Packer & Morris	1977	8	5	Int/Int (a)
Dews	1979	9	3	Ext/Int (b)
Ioanniddes	1980	10	6	Int/Int (c)
Grundy et al.	1980	11	2	Int/Int (a)
Graham	1981	12	21	Int/Int (a)
Yee	1984	13	16	Ext/Eave (d)
Davison	1985	14	1	Int/Int (a)
Aggarwal & Coates	1986	15	10	Ext/Eave (d)
Jenkins et al.	1986	16	16	Int/Int (a)
Moore & Sims	1986	18	4	Int/Int (a)
Total			116	

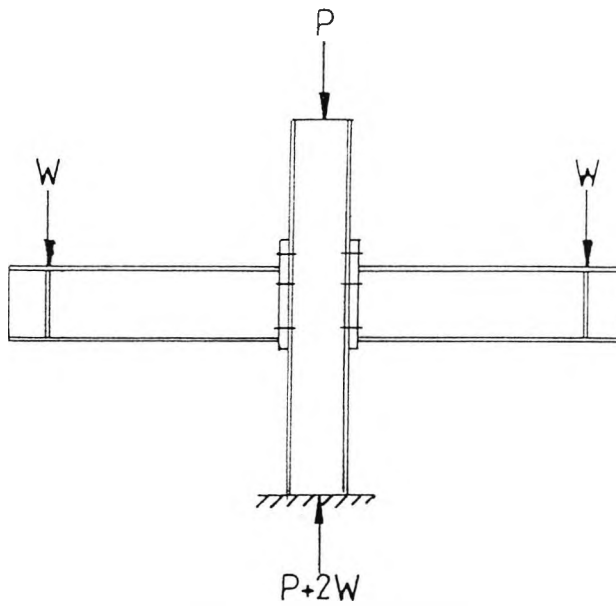
Table 2.1 Summary of Existing Extended Endplate Connection Experimental Data.



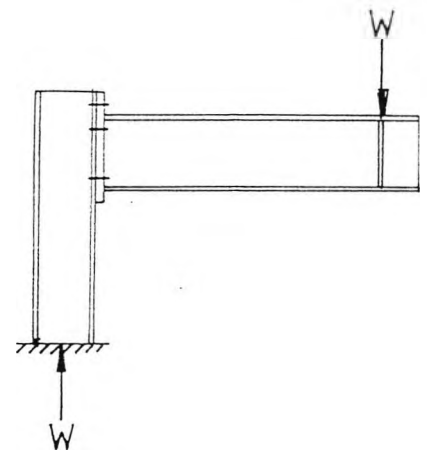
a) Internal/internal cruciform type
- column free



b) External/internal type

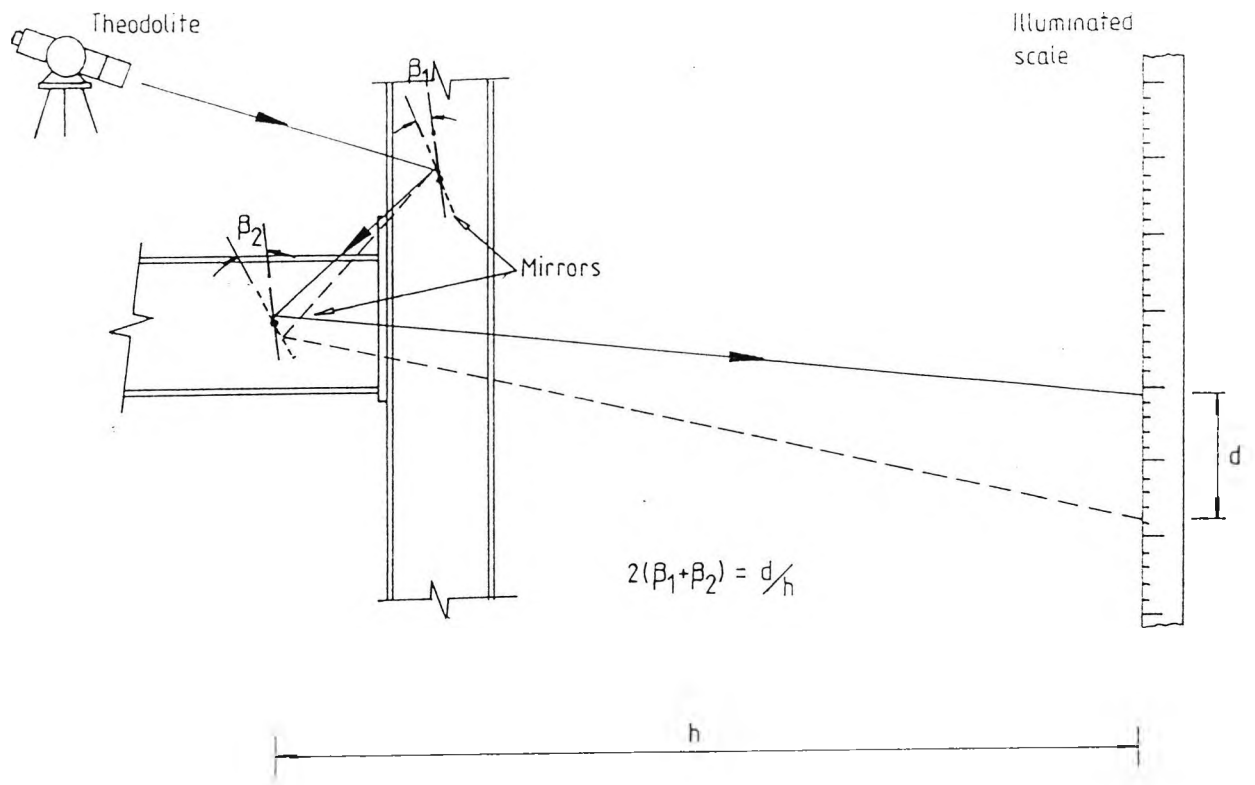


c) Internal/internal cruciform type
- column fixed

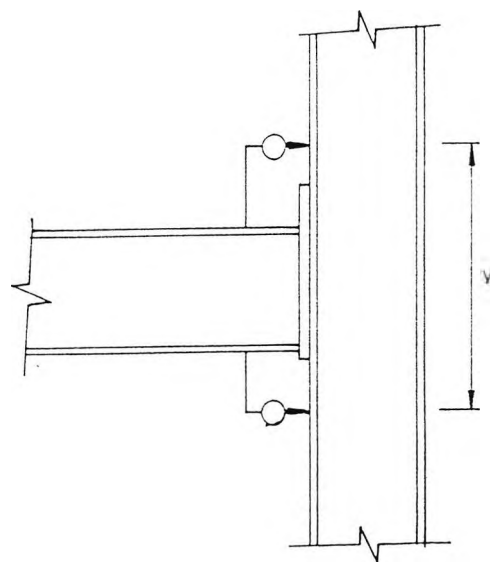


d) External/eave type

Figure 2.1 Types of Specimen for Connection Testing

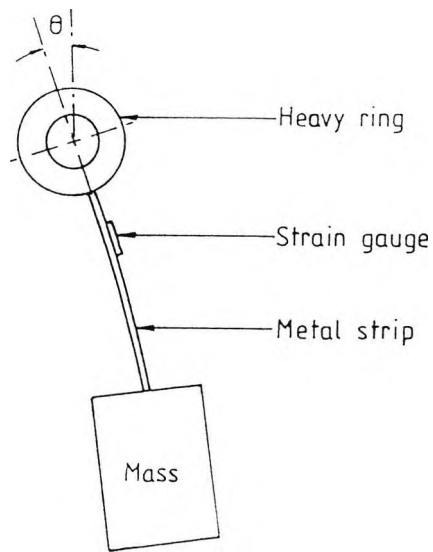


a) Optical arrangement.

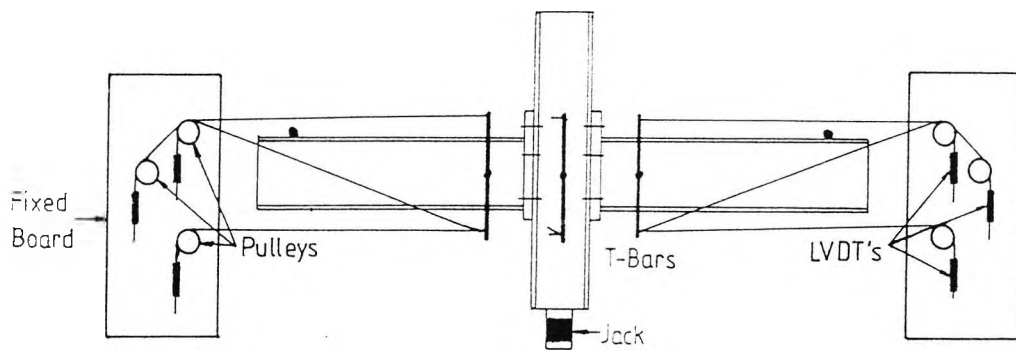


b) Dial gauge arrangement.

Figure 2.2 Surtees and Mann's Method of Connection Rotation Measurement.

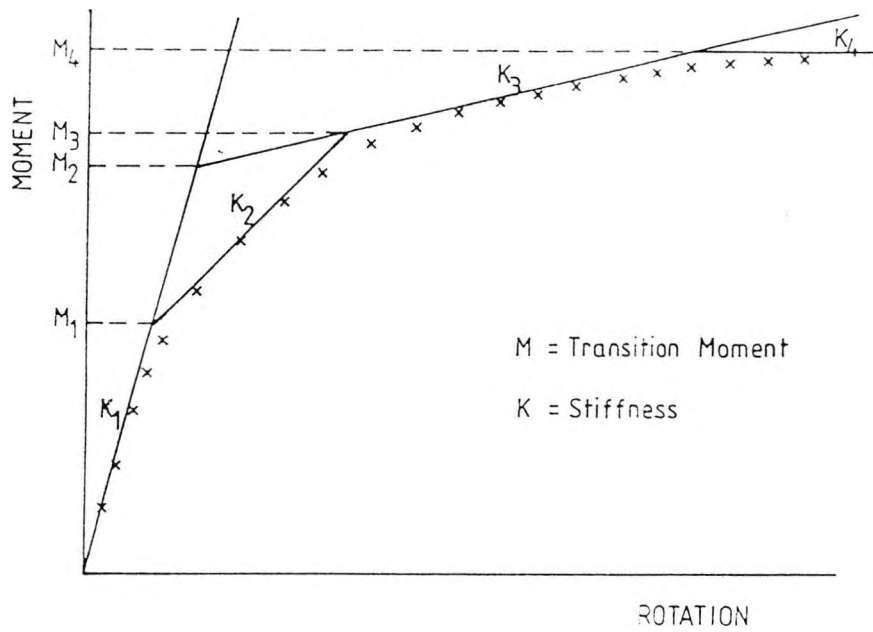


a) Rotation transducer.

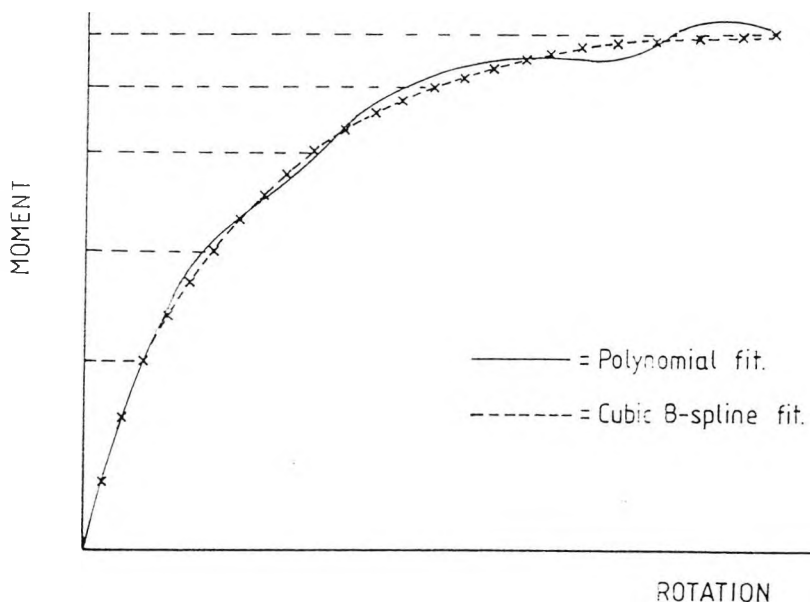


b) Sheffield method.

Figure 2.3 Methods of Rotation Measurement.

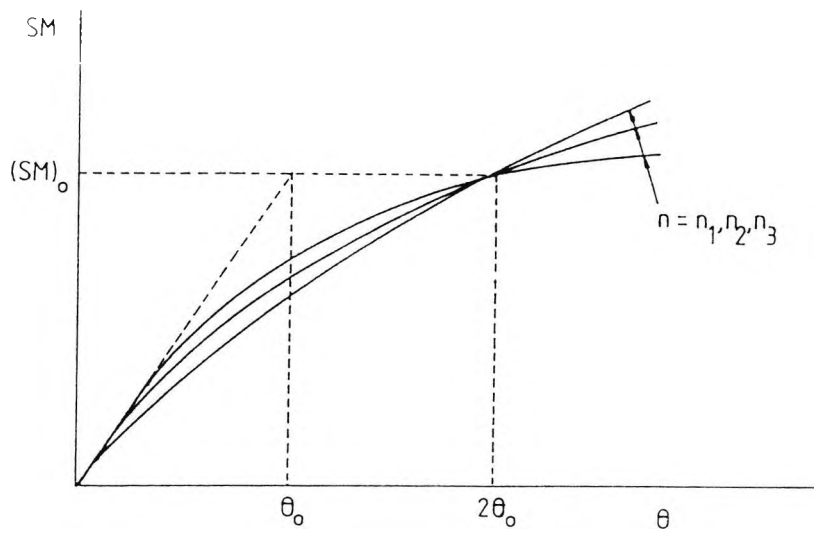


a) Linear based models.

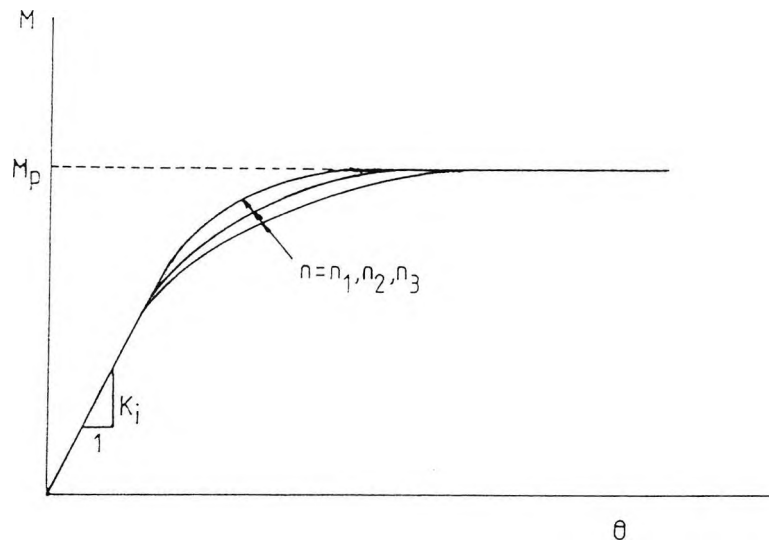


b) Polynomial based models.

Figure 2.4 Models used to Represent Connection Data (1)



c) Ang-Morris model.



d) Colson model.

Figure 2.5 Models used to Represent Connection Data (2)

THEORETICAL DEVELOPMENT

3.1 Introduction.

As discussed in the last chapter the model adopted in this study is the exponential model (equation 2.8) developed for external/eave type extended endplate connections by Yee (13). It is expressed mathematically as

$$M = M_p \left(1 - e^{-\frac{(K_i - K_p + c\theta)\theta}{M_p}} \right) + K_p \theta \quad (3.1)$$

where

- M = Moment at rotation,
- θ = Rotation due to connection
- M_p = Plastic moment of connection
- K_i = Initial stiffness of connection
- K_p = Strain hardening stiffness of connection
- c = Parameter introduced to control the rate of decay of the curve.

This model was chosen since it models the behaviour of endplate connections reasonably well with only a few parameters (Figure 3.1). Three out of four of the parameters are physical parameters. These can be determined by considering the structural behaviour of the connection. This chapter deals with the calculation of two of these three physical parameters, the

moment capacity, M_p , and the initial stiffness of the connection, K_i .

As most experimental work has been concerned with the determination of ultimate strength characteristics of endplate connections, the calculation of the moment capacity of the connection has been fairly well covered. Therefore the author only makes minor modifications to the criteria developed by Yee in the assessment of this parameter. Relatively little work has been carried out on the calculation of the initial stiffness of the extended endplate connection. This is the most important parameter of the model as it controls the amount of moment transferred to the column and the amount of deflection at working load. Due to its importance the author considers the initial stiffness of the connection in some detail in this chapter.

The calculation of the strain hardening stiffness of the endplate connection, or any other connection, is subject to factors which are peculiar to each individual connection. For example, the residual stress distribution within the connection and the rate of loading of the connection. The author feels that for design purposes the strain hardening stiffness of each connection should be assumed to be zero or be empirically determined dependent upon connection size. Therefore, its calculation will not be considered.

The experimental part of this study investigates the behaviour of internal/internal type connections only. However, to

demonstrate the flexibility of the proposed model in dealing with all types of endplate connection, the author outlines the calculation of the parameters for each type of connection.

3.2 Calculation of Initial Stiffness.

3.2.1 Introduction

The load-deflection behaviour of extended endplate connections is extremely complex. This is due to the deflection of the various components of the connection and the interaction between them. If the initial stiffness of the connection is to be determined then some simplification of the connection behaviour needs to be made.

Yee simplified the behaviour of external/eave connections by considering the transfer of load across the connection and then summing the load-deflection behaviour of the individual connection components. This approach will be followed here and is outlined below.

The initial elastic stiffness is defined by Yee as

$$K_i = \left(\frac{dM}{d\theta} \right)_{\theta=0}$$

(3.2)

This can be expressed as

$$K_i \approx \frac{M_0}{\theta_0}$$

(3.3)

where M_0 = Moment of connection near the origin
 θ_0 = Rotation of connection near the origin

It has been established (6) that the beam end moment at the connection can be split up into a couple acting at the beam flange levels. That is

$$M = FD_{bf}$$

(3.4)

where F = Beam flange force
 D_{bf} = Depth between the beam flange centrelines

Yee proposed that the rotation of the connection could be directly related to the deflection of the connection components at the beam flanges by the expression

$$\theta = \frac{\Delta_u + \Delta_l}{D_{bf}}$$

(3.5)

where Δ_u = deflection of components at beam tension flange

Δ_l = deflection of components at beam compression flange

This is shown diagrammatically in Figure 3.2.

By substituting for equations 3.4 and 3.5 into equation 3.3 Yee defined the initial stiffness, K_i

$$K_i \approx \frac{D_{bf}^2}{\Delta_u + \Delta_l} F$$

(3.6)

Thus if the deflection of the various components of the connection at the beam tension and compression flange levels can be found in terms of the flange force, F , then the initial stiffness of the connection can be found based entirely upon the connections initial geometry and physical properties.

Yee split the deflection at the beam tension flange level into the deflections of the individual components contributing to the deflection in that region. The author proposes to split this deflection into two components. The deflection of the endplate/column flange component and the deflection of the column web. The endplate and column flange components are considered together as their behaviour cannot be separated due to their interaction. This is expressed mathematically as

$$\Delta_u = \Delta_{ec} + \Delta_{wt}$$

(3.7)

where Δ_{ec} = deflection of endplate/column flange in the tension region
 Δ_{wt} = deflection of the column web in the tension region.

The deflection at the beam compression flange is simply the deflection due to the compression of the column web, Δ_{cw} as derived by Yee.

The deflection of each of the connection components will now be considered and the derivation of each component's contribution to initial stiffness outlined below.

3.2.2 Deflection of endplate/column flange in the tension region.

3.2.2.1 Introduction

The behaviour of the endplate/column flange component is complex. Simplistically, the flange force is transferred from the endplate to the column flange via the bolts and the contact forces between the endplate and column flange (Figure 3.3). The load is then transferred to the column web by column flange bending.

Difficulties arise in assessing endplate connection behaviour mainly due to the fact that the extent of the tension region and the exact position of the contact areas between the endplate and the column flange are not known. Initially these areas of contact will be unique to each connection and dependent upon the extent of connection lack of fit. Upon loading the initial areas of contact will change and will continue to do so throughout the connection's load history.

Yee calculated the deflection of the endplate/column flange component by assuming that both the endplate and the column flange acted as t-stubs (Figure 3.4) thereby fixing the initial areas of contact. The difference in stiffened and unstiffened connection behaviour was accounted for by changing the orientation of the t-stubs to each other. The biaxial bending of the column flange was taken into account by introducing the concept of the effective length of the flange contributing to bending in the tension region. Good estimates of the initial

connection stiffness for external/eave connections were obtained using this method.

Although good estimates of initial connection stiffness were obtained for eave connections, it was not known if this would be the case with internal connections. The author proposes, therefore, to attempt a more rigorous analysis of the endplate/column flange component. A more rigorous analysis method is justified by the reasons given below.

Firstly, for internal connections, the column flange is restrained above the connection by the rest of the column. The stiffening effect of this restraint is not adequately covered by the concept of the effective length of the flange acting in the tension region. Also, it is not known if the varying position of the contact areas between the endplate and column flange will have a significant effect on the initial stiffness of the connection. Furthermore, more than four bolts are sometimes used around the beam tension flange to enhance the ultimate load carrying capacity of the connection. This could lead to a breakdown of the t-stub analogy in the elastic range. The t-stub method also ignores the restraining effect of the column web in stiffened connections. This could lead to an underestimation of the stiffened connection initial stiffness.

To include an allowance for the above effects in the calculation of initial connection stiffness, the behaviour of the endplate and column flange has to be modelled more closely. Endplate

deflection is mainly one-dimensional and can be accommodated by the use of simple beam theory. Column flange bending is biaxial and, therefore, must be represented by plate theory. Since, the initial elastic behaviour only is required, then simple bending and plate theories can be assumed to be applicable.

The author's procedure for calculating the endplate/column flange deflection in the tension region will now be outlined. The forces acting on the endplate and column flange components are shown in Figure 3.3. The deflection of each component will be calculated in terms of the respective forces acting upon them. These deflections will then be equated by the use of compatibility equations to find the deflection of the whole subassembly in terms of the flange force, F . The deflection will be calculated for the general case of six bolts around the beam tension flange. The connection is symmetrical about the beam web and only one half of the connection under a flange force, F' , will be analysed. Where

$$F' = \frac{F}{2}$$

(3.8)

3.2.2.2 Endplate deflection

In this section, the author derives the deflection at any point on the endplate in terms of the forces acting on the endplate using simple beam theory. The contact forces at the ends of the endplate tension region will also be derived in terms of the same

forces. A free body representation of the endplate in the tension region which defines the dimensions and forces used is shown in Figure 3.5.

By the method given in Lowe (37) the equation of the deflection at any point, x , along the endplate is given by

$$w_e = Ax^3 + Bx^2 + Cx + D - \frac{B_1 z_1^3}{6EI_e} + \frac{F' z_2^3}{6EI_e} - \frac{B_2 z_3^3}{6EI_e} - \frac{B_3 z_4^3}{6EI_e}$$

(3.9)

where $z_1 = (x - a_e)$; $z_2 = (x - a_e - b_e)$; $z_3 = (x - a_e - 2b_e)$; $z_4 = (x - a_e - 2b_e - c_e)$

and the terms only exist if $z > 0$

A, B, C and D are arbitrary constants.

E = Youngs modulus and I_e = Endplate moment of inertia.

Applying the following boundary conditions at the first end of the endplate.

$$\text{At } x = 0 \quad w = w'' = 0$$

(3.10)

$$\therefore B = 0 ; D = 0$$

(3.11)

The other boundary conditions are obtained from the other end of the endplate tension region. In this case, the fixity condition at the end where the tension region of the endplate meets the compression region is assumed to be fixed.

$$\text{i.e. At } x = d_e \quad w = w' = 0$$

(3.12)

where d_e = the depth of endplate assumed to be acting in the tension region.

Applying these boundary conditions (3.12) we obtain

$$Ad_e^3 + Cd_e - \frac{B_1 z_{1d}^3}{6EI_e} + \frac{F' z_{2d}^3}{6EI_e} - \frac{B_2 z_{3d}^3}{6EI_e} - \frac{B_3 z_{4d}^3}{6EI_e} = 0$$

(3.13)

$$3Ad_e^2 + C - \frac{B_1 z_{1d}^2}{2EI_e} + \frac{F' z_{2d}^2}{2EI_e} - \frac{B_2 z_{3d}^2}{2EI_e} - \frac{B_3 z_{4d}^2}{2EI_e} = 0$$

(3.14)

where $z_{1d} = (d_e - a_e)$; $z_{2d} = (d_e - a_e - b_e)$; $z_{3d} = (d_e - a_e - 2b_e)$; $z_{4d} = (d_e - a_e - 2b_e - c_e)$

Solving these two equations gives the values of arbitrary constants, A and C, in terms of B_1 , B_2 , B_3 and F' .

$$A = \frac{1}{12EI_e} (A_1 B_1 + A_2 F' + A_3 B_2 + A_4 B_3)$$

(3.15)

where

$$\begin{aligned}
 A_1 &= -\frac{z_{1d}^3 - 3z_{1d}^2d_e}{d_e^3} \\
 A_2 &= +\frac{z_{2d}^3 - 3z_{2d}^2d_e}{d_e^3} \\
 A_3 &= -\frac{z_{3d}^3 - 3z_{3d}^2d_e}{d_e^3} \\
 A_4 &= -\frac{z_{4d}^3 - 3z_{4d}^2d_e}{d_e^3}
 \end{aligned}
 \tag{3.16}$$

and

$$C = \frac{1}{4EI_e} (C_1B_1 + C_2F' + C_3B_2 + C_4B_3)
 \tag{3.17}$$

where

$$\begin{aligned}
 C_1 &= -\frac{z_{1d}^3 - z_{1d}^2d_e}{d_e} \\
 C_2 &= +\frac{z_{2d}^3 - z_{2d}^2d_e}{d_e} \\
 C_3 &= -\frac{z_{3d}^3 - z_{3d}^2d_e}{d_e} \\
 C_4 &= -\frac{z_{4d}^3 - z_{4d}^2d_e}{d_e}
 \end{aligned}
 \tag{3.18}$$

The deflection at any point x is given by substituting the arbitrary constants in equations (3.11), (3.15) and (3.18) into equation (3.9).

$$\begin{aligned}
 w_e &= \frac{1}{12EI_e} [A_1B_1 + A_2F' + A_3B_2 + A_4B_3]x^3 + \frac{1}{4EI_e} [C_1B_1 + C_2F' + C_3B_2 + C_4B_3] \\
 &\quad + \frac{1}{6EI_e} [-z_1^3B_1 + z_2^3F' - z_3^3B_2 - z_4^3B_3]
 \end{aligned}
 \tag{3.19}$$

The value of the prying force at the end 1 of the endplate, Q_1 , is given by $6AEI_e$. Substituting for A from equation (3.15) gives

$$Q_1 = \frac{1}{2} (A_1 B_1 + A_2 F' + A_3 B_2 + A_4 B_3)$$

(3.20)

By equilibrium, the prying force at the other end of the tension region of the endplate, Q_2 , can be found.

$$Q_2 = (1 - \frac{1}{2}A_2)F' - (1 + \frac{1}{2}A_1)B_1 - (1 + \frac{1}{2}A_3)B_2 - (1 + \frac{1}{2}A_4)B_3$$

(3.21)

The deflection at any point and the prying forces at either end of the endplate tension region are now known in terms of endplate geometry and the bolt and flange forces. The deflections and forces will be used in the derivation of compatibility equations for the endplate/column flange subassembly.

3.2.2.3 Column flange deflection.

In this section the author derives the deflection of any point on the column flange in terms of the forces acting upon it using simple plate theory. The deflections due to these forces acting

individually can be summed to obtain the deflection at any point since only the elastic stiffness of the connection is being determined. The forces acting on the column flange are shown in Figure 3.3.

The deflection at any point, u , due to a load, P , acting at a point, v , is given by

$$w_{uv} = k_{uv}P \quad (3.22)$$

where k_{uv} = flexibility coefficient at u due to load P at point v .

Therefore if the positions of the forces acting on the column flange are given subscripts, 1-5, as denoted in Figure 3.3 then

$$\begin{aligned} w_{CB_1} &= \text{deflection of column flange at boltline 1} \\ &= k_{11}B_1 + k_{12}B_2 + k_{13}B_3 - k_{14}Q_1 - k_{15}Q_2 \\ w_{CB_2} &= \text{deflection of column flange at boltline 2} \\ &= k_{21}B_1 + k_{22}B_2 + k_{23}B_3 - k_{24}Q_1 - k_{25}Q_2 \\ w_{CB_3} &= \text{deflection of column flange at boltline 3} \\ &= k_{31}B_1 + k_{32}B_2 + k_{33}B_3 - k_{34}Q_1 - k_{35}Q_2 \\ w_{CQ_1} &= \text{deflection of column flange at prying force 1} \\ &= k_{41}B_1 + k_{42}B_2 + k_{43}B_3 - k_{44}Q_1 - k_{45}Q_2 \\ w_{CQ_2} &= \text{deflection of column flange at prying force 2} \\ &= k_{51}B_1 + k_{52}B_2 + k_{53}B_3 - k_{54}Q_1 - k_{55}Q_2 \end{aligned} \quad (3.23)$$

The prying forces are known from equations (3.20) and (3.21) in terms of bolt forces, B_1 , B_2 , B_3 and flange force, F' . Therefore the deflection at any point can be determined in terms of these forces. All that remains is to determine the column flange flexibility coefficients for each individual force.

The calculation of these flexibility coefficients can be broken down into three specific cases for both unstiffened and stiffened column flanges. When the column flange is unstiffened, the flange can be considered as an infinitely long cantilever plate under concentrated load. When the column is stiffened, the flange can be considered as a semi-infinite cantilever plate under concentrated load, above the tension stiffener and as a cantilever plate supported on two sides under concentrated load, between the tension and compression stiffeners. The column flange deflection factors for each of these cases will now be given or derived by the author.

3.2.2.3.1 Deflection of an infinitely long cantilever plate under concentrated load.

The deflection of an infinitely long cantilever plate under concentrated load, P , as derived by Jaramillo (38) is given by

$$w = -\frac{Pa_c^2}{8D_c} \left(q_0(\xi, \zeta) e^{-\beta_0 \eta} + 2 \sum_{n=1}^{\infty} (p_n(\xi, \zeta) \sin \alpha_n \eta + q_n(\xi, \zeta) \cos \alpha_n \eta) e^{-\beta_n \eta} \right)$$

(3.24)

Jaramillo's derivation of this equation along with the definition of the various parameters is given in Appendix A.

Briefly

a_c	=	the width of the column flange
D_c	=	the flexural rigidity of the column flange
ξ, η	=	dimensionless variables used to define the position of a point on the flange
ζ	=	a dimensionless variable used to define the position of the force on the flange
α_n, β_n	=	complex roots of the equation used to evaluate infinite integrals by contour integration.

The values of the functions $q_0(\xi, \zeta)$, $p_n(\xi, \zeta)$ and $q_n(\xi, \zeta)$ are given in Appendix A.

A computer program was written by the author to calculate the column flange flexibility coefficients for this and the other cases.

3.2.2.3.2 Deflection of a semi-infinite cantilever plate under concentrated load.

The author derived the deflection, w_1 , of a semi-infinite cantilever plate under concentrated load simply supported at the edge from the infinite case in a similar way to the method of images used by Timoshenko and Woinowsky-Krieger (39) for infinite

plates simply supported on two sides, Figure 3.6. If the simply-supported edge is clamped, the deflection, w_2 , due to the clamping moment can be found by equating the slope of an arbitrary function representing w_2 to the slope of the w_1 function at the simply-supported edge and solving. This solution technique is also outlined by Timoshenko and Woinowsky-Krieger (39) for a simply supported infinite plate.

Firstly a suitable arbitrary function has to be chosen for the clamping moment deflection, w_2 . The author modified the function chosen by Timoshenko and Woinowsky-Krieger to reflect the cantilever case.

Therefore, assuming that

$$w_2 = \sum_{m=1,3,5..}^{\infty} (A_m + B_m y) e^{-\frac{m\pi y}{a_c}} \sin \frac{m\pi x}{2a_c}$$

(3.25)

where x and y refer to the coordinate system outlined in Figure 3.6, A_m and B_m are arbitrary constants and a_c is the width of the column flange.

This function is subject to the boundary conditions at the edge to be fixed.

$$(w_2)_{y=0} = 0 ; -D_c \left(\frac{\partial^2 w_2}{\partial y^2} \right)_{y=0} = f(x)$$

(3.26)

where $f(x)$ is the clamping moment distribution at the fixed edge.

From the first boundary condition ; $A_m = 0$

From the second boundary condition

$$\sum_{m=1,3}^{\infty} B_m \sin \frac{m\pi x}{2a_c} = \sum_{m=1,3}^{\infty} \frac{a_c f(x)}{2m\pi D_c}$$

(3.27)

$$\therefore w_2 = \frac{a_c f(x) y}{2\pi D_c} \sum_{m=1,3}^{\infty} \frac{e^{-\frac{m\pi y}{a_c}}}{m}$$

(3.28)

Deriving the function, w_I , for a semi-infinite cantilever plate under concentrated load simply supported at one edge from the infinite case gives

$$\begin{aligned}
 w_1 = & -\frac{Pa_c^2}{8D_c} \left(q_0(\xi, \zeta) (e^{-\beta_0\eta} - e^{-\beta_0(2\psi - \eta)}) \right. \\
 & + 2 \sum_{n=1}^{\infty} [p_n(\xi, \zeta) (\sin\alpha_n\eta e^{-\beta_n\eta} - \sin\alpha_n(2\psi - \eta) e^{-\beta_n(2\psi - \eta)}) \\
 & \left. + q_n(\xi, \zeta) (\cos\alpha_n\eta e^{-\beta_n\eta} - \cos\alpha_n(2\psi - \eta) e^{-\beta_n(2\psi - \eta)}) \right] \Big)
 \end{aligned}
 \tag{3.29}$$

where $\eta = \frac{y'}{a_c}$; $\psi = \frac{b_c}{a_c}$

y' refers to the coordinate system centring on the point load, P and b_c , defined in Figure 3.6, is the distance of the concentrated load from the supported edge of the plate.

At the simply supported edge $y = 0$, $y' = b_c$, therefore $\eta = \psi$

Therefore differentiating w_I with respect to y and evaluating at $y = 0$ to find the value of the slope of the function at the simply supported edge gives

$$\begin{aligned}
 \left(\frac{\partial w_1}{\partial y} \right)_{y=0} = & -\frac{Pa_c}{8D_c} \left(-2q_0(\xi, \zeta) \beta_0 e^{-\beta_0\psi} + 4 \sum_{n=1}^{\infty} [p_n(\xi, \zeta) (\alpha_n \cos\alpha_n\psi - \beta_n \sin\alpha_n\psi) \right. \\
 & \left. - q_n(\xi, \zeta) (\alpha_n \sin\alpha_n\psi - \beta_n \cos\alpha_n\psi) \right] e^{-\beta_n\psi} \Big)
 \end{aligned}
 \tag{3.30}$$

This will be written for further reference as

$$\left(\frac{\partial w_1}{\partial y}\right)_{y=0} = -\frac{Pa_c}{8D_c}(K_{w'1}) \quad (3.31)$$

Differentiating equation (3.28) with respect to y and substituting for y at $y = 0$ gives

$$\left(\frac{\partial w_2}{\partial y}\right)_{y=0} = \frac{a_c f(x)}{2\pi D_c} \sum_{m=1,3}^{\infty} \frac{1}{m} \quad (3.32)$$

Equating the slopes of both equations and rearranging gives

$$\frac{a_c f(x)}{2\pi D_c} \sum_{m=1,3}^{\infty} \frac{1}{m} = \frac{Pa_c}{8D_c}(K_{w'1}) \quad (3.33)$$

Substituting the left hand side of this equation into equation (3.28) gives

$$w_2 = \frac{Pa_c}{8D_c} (K_{w'1})y \sum_{m=1,3}^{\infty} e^{-\frac{m\pi y}{a_c}} \quad (3.34)$$

The deflection of a semi-infinite cantilever plate clamped at one edge as derived by the author is given by the sum of the equations (3.29) and (3.34).

$$W = W_1 + W_2$$

(3.35)

3.2.2.3.3 Deflection of a cantilever plate fixed at two edges under concentrated load.

The deflection of a cantilever plate simply supported at both sides under concentrated load is derived by the author from the infinitely long cantilever plate case in a similar way to the previous section and considering the loading arrangement shown in Figure 3.7. After choosing a suitably arbitrary function, the value of the deflection, w_2 , due to the clamping moment on each edge can then be found by equating the slopes of the deflection fields at both edges. A different arbitrary function is chosen for the deflection, w_2 , in this case to reflect the effects of the clamping moments on both edges. A modified arbitrary solution for the deflection function, similar to one given in reference 39 for infinite simply-supported plates, is given by

$$w_2 = \sum_{m=1,3}^{\infty} Y_m \sin \frac{m\pi x}{2a_c}$$

(3.36)

where

$$Y_m = A_m \sinh \frac{m\pi y}{a_c} + B_m \cosh \frac{m\pi y}{a_c} + C_m \frac{m\pi y}{a_c} \sinh \frac{m\pi y}{a_c} + D_m \frac{m\pi y}{a_c} \cosh \frac{m\pi y}{a_c} \quad (3.37)$$

where A_m, B_m, C_m, D_m are arbitrary constants

If the coordinate system for w_2 is taken as shown in Figure 3.7.

The boundary conditions at each fixed edge are

$$\begin{aligned} (w_2)_{y=\frac{d_c}{2}, -\frac{d_c}{2}} &= 0 \\ -D_c \left(\frac{\partial^2 w_2}{\partial y^2} \right)_{y=\frac{d_c}{2}} &= f_1(x) \\ -D_c \left(\frac{\partial^2 w_2}{\partial y^2} \right)_{y=-\frac{d_c}{2}} &= f_2(x) \end{aligned}$$

(3.38)

where $f_1(x), f_2(x)$ are functions representing the clamping moment at sides 1 and 2 respectively and d_c is the length of the cantilever plate.

From the first two of these boundary conditions we obtain

$$\begin{aligned} A_m &= -D_m \frac{m\pi d_c}{2a_c} \coth \frac{m\pi d_c}{2a_c} \\ B_m &= -C_m \frac{m\pi d_c}{2a_c} \tanh \frac{m\pi d_c}{2a_c} \end{aligned}$$

(3.39)

Substituting equations (3.39) into (3.35) and (3.36) and applying the other boundary conditions we obtain

$$\begin{aligned} \sum_{m=1,3}^{\infty} C_m \sin \frac{m\pi x}{2a_c} &= -\frac{a_c^2}{\pi^2 D_c} \sum_{m=1,3}^{\infty} \frac{1}{m^2} \frac{f_1(x) + f_2(x)}{4 \cosh \alpha_m} \\ \sum_{m=1,3}^{\infty} D_m \sin \frac{m\pi x}{2a_c} &= \frac{a_c^2}{\pi^2 D_c} \sum_{m=1,3}^{\infty} \frac{1}{m^2} \frac{f_2(x) - f_1(x)}{4 \sinh \alpha_m} \end{aligned} \quad (3.40)$$

where $\alpha_m = \frac{m\pi d_c}{2a_c}$

$$(3.41)$$

If we assume that $\frac{f_1(x) + f_2(x)}{2} = E_{m1}$ and $\frac{f_1(x) - f_2(x)}{2} = E_{m2}$

Then substituting the arbitrary constants into the original equations (3.36,3.37) we obtain

$$\begin{aligned} w_2 &= \frac{a_c^2}{2\pi^2 D_c} \sum_{m=1,3}^{\infty} \frac{1}{m^2} \left[\frac{E_{m1}}{\cosh \alpha_m} \left(\alpha_m \tanh \alpha_m \cosh \frac{m\pi y}{a_c} - \frac{m\pi y}{a_c} \sinh \frac{m\pi y}{a_c} \right) \right. \\ &\quad \left. + \frac{E_{m2}}{\sinh \alpha_m} \left(\alpha_m \coth \alpha_m \sinh \frac{m\pi y}{a_c} - \frac{m\pi y}{a_c} \cosh \frac{m\pi y}{a_c} \right) \right] \end{aligned} \quad (3.42)$$

The deflection of the simply supported plate as outlined in Figure 3.7 is given by

$$\begin{aligned}
 w_1 = & -\frac{Pa_c}{8D_c} \left(q_0(\xi, \zeta) [e^{-\beta_0\eta} - e^{-\beta_0\eta_1} - e^{-\beta_0\eta_2} + e^{-\beta_0\eta_3} + e^{-\beta_0\eta_4} + \dots] \right. \\
 & + 2 \sum_{n=1}^{\infty} \left\{ p_n(\xi, \zeta) [\sin\alpha_n\eta e^{-\beta_n\eta} - \sin\alpha_n\eta_1 e^{-\beta_n\eta_1} - \sin\alpha_n\eta_2 e^{-\beta_n\eta_2} \right. \\
 & \quad \left. + \sin\alpha_n\eta_3 e^{-\beta_n\eta_3} + \sin\alpha_n\eta_4 e^{-\beta_n\eta_4} + \dots] \right. \\
 & \left. + q_n(\xi, \zeta) [\cos\alpha_n\eta e^{-\beta_n\eta} - \cos\alpha_n\eta_1 e^{-\beta_n\eta_1} - \cos\alpha_n\eta_2 e^{-\beta_n\eta_2} \right. \\
 & \quad \left. + \cos\alpha_n\eta_3 e^{-\beta_n\eta_3} + \cos\alpha_n\eta_4 e^{-\beta_n\eta_4} - \dots] \right\} \left. \right)
 \end{aligned}
 \tag{3.43}$$

where

$$\begin{aligned}
 \eta_1 &= 2\psi - \eta \\
 \eta_2 &= 2\delta + \eta \\
 \eta_3 &= 2\psi + 2\delta - \eta \\
 \eta_4 &= 2\psi + 2\delta + \eta
 \end{aligned}$$

$$\tag{3.44}$$

where η and ψ are defined as the previous section

$$\text{and } \delta = \frac{e_c}{a_c}.$$

e_c is defined in Figure 3.7 and the origin of the coordinate system corresponds to the point load, P under consideration.

The expression above is derived for the region of plate between the point load, P , and side 1. For the deflections in the region from P to side 2, η in the expressions (3.44) is negative.

If the above expression (3.43) is differentiated with respect to y and the values at both sides substituted into the equation we obtain

$$\begin{aligned} \left(\frac{\partial w_1}{\partial y}\right)_{y=\frac{d_c}{2}} &= -\frac{Pa_c}{8D_c} \{K_{w'_{11}}\} \\ \left(\frac{\partial w_1}{\partial y}\right)_{y=-\frac{d_c}{2}} &= -\frac{Pa_c}{8D_c} \{K_{w'_{12}}\} \end{aligned}$$

(3.45)

where $\{K_{w'_{11}}\}$ = the function for slope at side 1 for deflection w_1
 $\{K_{w'_{12}}\}$ = the function for slope at side 2 for deflection w_1

If equation (3.42) is differentiated with respect to y and the values at both sides substituted into the equation we obtain

$$\begin{aligned} \left(\frac{\partial w_2}{\partial y}\right)_{y=\frac{d_c}{2}} &= \frac{a_c}{2\pi D_c} \sum_{m=1,3}^{\infty} \frac{1}{m} \left[\frac{E_{m1}}{\cosh\alpha_m} \left(-\frac{\alpha_m}{\cosh\alpha_m} - \sinh\alpha_m \right) \right. \\ &\quad \left. + \frac{E_{m2}}{\sinh\alpha_m} \left(\frac{\alpha_m}{\sinh\alpha_m} - \cosh\alpha_m \right) \right] \\ \left(\frac{\partial w_2}{\partial y}\right)_{y=-\frac{d_c}{2}} &= \frac{a_c}{2\pi D_c} \sum_{m=1,3}^{\infty} \frac{1}{m} \left[\frac{E_{m1}}{\cosh\alpha_m} \left(\frac{\alpha_m}{\cosh\alpha_m} + \sinh\alpha_m \right) \right. \\ &\quad \left. + \frac{E_{m2}}{\sinh\alpha_m} \left(\frac{\alpha_m}{\sinh\alpha_m} - \cosh\alpha_m \right) \right] \end{aligned}$$

(3.46)

Equating the two expressions at each side and rearranging gives

$$\frac{a_c}{2\pi D_c} \sum_{m=1,3}^{\infty} \frac{1}{m} \frac{E_{m1}}{\cosh \alpha_m} = \frac{\frac{Pa_c}{8D_c} (\{K_{w'12}\} - \{K_{w'11}\})}{\sum_{m=1,3}^{\infty} 2 \left(\frac{\alpha_m}{\cosh \alpha_m} + \sinh \alpha_m \right)} = \frac{Pa_c}{8D_c} \{K_{w21}\}$$

$$\frac{a_c}{2\pi D_c} \sum_{m=1,3}^{\infty} \frac{1}{m} \frac{E_{m2}}{\sinh \alpha_m} = \frac{\frac{Pa_c}{8D_c} (\{K_{w'11}\} + \{K_{w'12}\})}{\sum_{m=1,3}^{\infty} 2 \left(\frac{\alpha_m}{\sinh \alpha_m} - \cosh \alpha_m \right)} = \frac{Pa_c}{8D_c} \{K_{w22}\}$$

(3.47)

Substituting equations (3.47) into equation (3.42) gives finally

$$w_2 = \frac{Pa_c^2}{8\pi D_c} \sum_{m=1,3}^{\infty} \frac{1}{m} \left[\{K_{w21}\} \left(\alpha_m \tanh \alpha_m \cosh \frac{m\pi y}{a_c} - \frac{m\pi y}{a_c} \sinh \frac{m\pi y}{a_c} \right) \right. \\ \left. + \{K_{w22}\} \left(\alpha_m \coth \alpha_m \sinh \frac{m\pi y}{a_c} - \frac{m\pi y}{a_c} \cosh \frac{m\pi y}{a_c} \right) \right]$$

(3.48)

The deflection of a clamped cantilever plate under concentrated load as derived by the author is given by

$$w = w_1 + w_2$$

(3.49)

N.B. For brevity, the full derivation of the slope functions at the support points is not given as the equations become cumbersome.

3.2.2.4 Compatibility equations

The deflections of the column flange and endplate at any point have been derived by the author in terms of bolt and flange forces. Compatibility equations are now required to obtain the deflection of the endplate/column flange at the beam tension flange purely in terms of the flange force. The number of equations required is equal to the number of bolts contributing to the endplate tension region structural behaviour. The compatibility equations are formed by considering the deflection of each bolt and equating this to the deflection of the endplate and column flange at that bolt.

If the t-stub analogy as used by Yee is considered, Figure 3.4, it can be seen that the contributions of the column flange and endplate at each boltline can easily be equated to bolt deflection. This is because the deflection of each component is derived relative to datums that are coincident. These datums lie in a plane drawn through the points of contact of the two t-stubs. This contact region is along the top and bottom edges of the t-stubs for a stiffened column arrangement and at the four corners of the t-stubs for a unstiffened column arrangement. The position of these contact regions is fixed.

The derivation of compatibility equations for the combination of a two dimensional plate model and a one dimensional model is not , however, so easy. Figure 3.8 shows that there is a some degree of overlap between the two models. Additionally each model has

a different datum. The column flange model datum is the column flange/column web intersection line or the edge of the root fillet. Whereas the endplate model datum is a line connecting the two contact points of the endplate and column flange. If the points of contact between the column flange and endplate are known then the deflections of each can be related and compatibility equations set up.

Zoetmeijer (7) has already established that the position of the contact points is dependent upon the lack of fit in connections and the relative rigidities of the connected parts by considering the position of the prying forces in t-stub to column flange subassemblages (Figure 3.9). From these results it was proposed by Zoetmeijer that a similar variation in prying force position would take place between endplates and column flanges of differing rigidities. As the variation of prying force with the relative rigidities of t-stubs and column flanges was a postulation based upon experimental observation, the exact position of the prying forces for any combination of endplate and column flange will not be known. It is necessary, therefore, to make some assumption about the position of the prying force before the analysis can proceed.

The author's derivation of the compatibility equation for one bolt will now be outlined. The bolt is the bolt above the tension flange of the beam and the prying force is assumed to act at the corner of the endplate. It should be noted that the derivation is perfectly arbitrary and the contact position could

be assumed to act anywhere between the endplate and column flange. The derivation is outlined in Figure 3.10 which should be consulted. In Figure 3.10, two sections are taken through the endplate/column flange subassembly. The first section is through the top of the endplate, or point of contact, and the second section is through the boltline. These sections are shown superimposed on one another with their deflected shapes greatly exaggerated. From Figure 3.10, it can be seen that the deflection of the column flange contributing to the bolt deflection is given by the deflection of the column flange at the contact point less the deflection of the column flange at the boltline. The compatibility equation can be expressed mathematically by,

$$W_b = W_{eb} + W_{cq} - W_{cb}$$

(3.50)

- where W_{eb} = the deflection of the endplate at the boltline
- W_{cq} = the deflection of the column flange at the contact point
- W_{cb} = the deflection of the column flange at the boltline
- W_b = the deflection of the bolt.

The bolt deflection can be expressed in the form

$$w_b = K_b B$$

(3.51)

where $K_b =$ the stiffness of the bolt (given by Agerskov's (40) derivation in Appendix B)
and $B =$ the appropriate bolt force.

By substituting the appropriate dimensions into the equations of deflection for the column flange (3.23) and endplate (3.19) and then substituting these values into equation (3.50), the author obtained a compatibility equation of the form below.

$$\begin{aligned}
& \left[\frac{1}{12EI_e} (A_1 a_e^3 + 3C_1 a_e) + k_{41} - k_{11} \right. \\
& \qquad \qquad \qquad \left. - (k_{44} - k_{14}) \frac{A_1}{2} + (k_{45} - k_{15}) \left(1 + \frac{A_1}{2} \right) \right] B_1 \\
& + \left[\frac{1}{12EI_e} (A_3 a_e^3 + 3C_3 a_e) + k_{42} - k_{12} \right. \\
& \qquad \qquad \qquad \left. - (k_{44} - k_{14}) \frac{A_3}{2} + (k_{45} - k_{15}) \left(1 + \frac{A_3}{2} \right) \right] B_2 \\
& + \left[\frac{1}{12EI_e} (A_4 a_e^3 + 3C_4 a_e) + k_{43} - k_{13} \right. \\
& \qquad \qquad \qquad \left. - (k_{44} - k_{14}) \frac{A_4}{2} + (k_{45} - k_{15}) \left(1 + \frac{A_4}{2} \right) \right] B_3 \\
& + \left[\frac{1}{12EI_e} (A_2 a_e^3 + 3C_2 a_e) - (k_{44} - k_{14}) \frac{A_2}{2} + (k_{45} - k_{15}) \left(1 - \frac{A_2}{2} \right) \right] F' \\
& = K_b B_1
\end{aligned}$$

(3.52)

All the above terms have previously been defined.

Compatibility equations can be similarly constructed at boltlines 2 and 3 assuming a position for the prying force at the other end of the tension region of the endplate.

All the terms in the coefficients of the forces are known in terms of connection geometry only. Solving all three compatibility equations gives the bolt forces in terms of flange force, F' . If it is assumed that $B_1 = \lambda_1 F'$, $B_2 = \lambda_2 F'$ and $B_3 = \lambda_3 F'$ then the appropriate value of the deflection of the endplate and column flange can be found by back substituting into equations (3.19) and (3.23) respectively.

For the endplate, at the beam tension flange level, $x = a_e + b_e$.

Therefore, the endplate deflection is defined as,

$$w_{ep} = \frac{1}{12EI_e} \left[(A_1 \lambda_1 + A_3 \lambda_2 + A_4 \lambda_3 + A_2) (a_e + b_e)^3 + 3 (C_1 \lambda_1 + C_3 \lambda_2 + C_4 \lambda_3 + C_2) (a_e + b_e) - 2 \lambda_1 b_e^3 \right] F'$$

(3.53)

This deflection is relative to the 'datum' defined by the contact points between the column flange and endplate. The deflection of the column flange at these contact points needs to be known. Therefore, the deflections at the prying force positions are

$$w_{cO_1} = \left[(k_{41} - k_{44} \frac{A_1}{2} + k_{45} (1 + \frac{A_1}{2})) \lambda_1 + (k_{42} - k_{44} \frac{A_3}{2} + k_{45} (1 + \frac{A_3}{2})) \lambda_2 + (k_{43} - k_{44} \frac{A_4}{2} + k_{45} (1 + \frac{A_4}{2})) \lambda_3 - (k_{44} \frac{A_2}{2} - k_{45} (1 - \frac{A_2}{2})) \right] F'$$

$$w_{cO_2} = \left[(k_{51} - k_{54} \frac{A_1}{2} + k_{55} (1 + \frac{A_1}{2})) \lambda_1 + (k_{52} - k_{54} \frac{A_3}{2} + k_{55} (1 + \frac{A_3}{2})) \lambda_2 + (k_{53} - k_{54} \frac{A_4}{2} + k_{55} (1 + \frac{A_4}{2})) \lambda_3 - (k_{54} \frac{A_2}{2} - k_{55} (1 - \frac{A_2}{2})) \right] F'$$

(3.54)

The contribution of the column flange to the overall deflections is the average value of these two deflections at the beam tension flange level.

Therefore,

$$W_{cf} = W_{c\phi_1} - \frac{a_e + b_e}{d_e} (W_{c\phi_1} - W_{c\phi_2})$$

(3.55)

where a_e , b_e and d_e are defined in Figure 3.5

If F' is substituted for the full flange force, equation (3.8) then, the deflection of the endplate/column flange subassembly in the tension region is given by

$$\Delta_{ec} = \frac{W_{ep} + W_{cf}}{2} F'$$

(3.56)

It should be stated that the deflection due to the bolt is included in this value.

3.2.3. Deflection of column web at the beam tension flange.

In this section the deflection of the column web in the tension region is considered. The deflection of the column web at the beam tension flange can be split up into two possible sources. Firstly, the deflection of the web in pure tension and secondly,

the deflection of the web in shear. In this experimental study, the connections are balanced internal connections, therefore, the deflection due to shear in the web is negligible. From experimental observation (discussed later) the author found that deflection due to pure tension is also negligible. To give a complete picture of how moment-rotation curves can be found for all connection types, however, the calculation of the shear deflection component of the initial stiffness as derived by Yee and further modified by the author to include all endplate connection types will be outlined below.

Yee calculated the shear deflection component by assuming that the eave connection acted as a short column stub (Figure 3.11(a)). In an external/internal connection this is not the case but the author postulates that an approximation can be made by assuming that the column acts as a fixed beam of twice the depth of the beam (Figure 3.11(b)). The deflection in this case can be found in the same manner as the eave case by the method of unit loads which is given as follows.

$$\Delta_s = \int_0^1 \frac{Mm}{EI_c} dx + k \int_0^1 \frac{VV'}{GA_c} dx$$

(3.57)

where M = the moment due to the applied load
 V = the shear force due to the applied load
 m = the moment due to a unit load acting at the section where the deflection is desired.

- $v' =$ the shear force due to a unit load acting at the section where the deflection is desired
 $I_c =$ the moment of inertia of the connection
 $A_c =$ the cross-sectional area of the section
 $E =$ Young's modulus
 $G =$ the shear modulus
 $k =$ a factor dependent on the form of the section

For deep sections, compared to their spans, the deflection due to the moment is small when compared with shear and can be neglected. For an external connection the value of the shear force, V , is equal to the flange force, F . Therefore, evaluating equation (3.57) gives:

For an eave connection,

$$\Delta_s = \frac{kL}{GA_c} F$$

(3.58)

For an internal connection,

$$\Delta_s = \frac{kL}{4GA_c} F$$

(3.59)

Roark and Young (41) state that good approximations for I-sections can be obtained by assuming $k = 1$ and A_c is the cross-sectional area of the web, A_{cw} , only. Therefore, substituting these values, $G = \frac{E}{2(1 + \nu)}$ and the appropriate length of the

column assumed to be acting into equations (3.58) and (3.59) we obtain

$$\Delta_s = \frac{2(1 + \nu)(D_b - t_{bf})}{ED_c t_{cw}} F \text{ for an eave connection} \quad (3.60)$$

and
$$\Delta_s = \frac{(1 + \nu)(D_b - t_{bf})}{ED_c t_{cw}} F \text{ for an internal connection} \quad (3.61)$$

where D_b = the depth of the beam
 t_{bf} = the beam flange thickness
 D_c = the depth of the column between root fillets
 t_{cw} = the column web thickness

These equations have been derived for external connections where the full flange force, F , is acting across the web. However, for unbalanced internal connections there will be an out of balance shear force across the connection. The author will now consider the out-of-balance shear force.

The out of balance shear force, F_u , is demonstrated in Figure 3.12 and is given by

$$F_u = F_A - F_B \text{ where } F_A > F_B \quad (3.62)$$

Therefore, relating the flange force on either side of the connection to the moment on that side of the connection gives,

$$F_u = \frac{M_A}{D_{bA}} - \frac{M_B}{D_{bB}}$$

(3.63)

where D_{bA} = the depth of beam A, etc.

If a factor, α , is introduced to relate the out of balance shear force to the flange force on the side of the connection under consideration. Then,

$$\alpha = \frac{F_u}{F}$$

(3.64)

For example, if side A is considered, then

$$\alpha = 1 - \frac{M_B}{M_A} \frac{D_{bA}}{D_{bB}}$$

(3.65)

Therefore the author expresses the deflection due to shear generally as

$$\Delta_s = \alpha k_t \frac{(1 + \nu) (D_b - t_{bf})}{ED_c t_{cw}} F$$

(3.66)

where k_c is a constant depending on connection type
($k_c = 1$ for an internal connection and $k_c = 2$ for
an eave connection)
and α is a constant depending upon the unbalanced
moment across the connection.
($\alpha = 1$ for an external connection and $\alpha = 0$ for
a balanced internal connection)

It should be noted that α will be negative for the connection on
the side of the lesser of the unbalanced moments.

The value of the shear deformation is unaffected by the placement
of tension, compression and backing plate stiffeners. If a shear
stiffener is used, however, then the effect of can be accounted
for by the use of compatibility conditions similar to those
derived by Yee (13).

3.2.4. Deflection of the column web in the compression region

The deflection of the column web in the compression region of
unstiffened connections is given by the formula derived by Yee
i.e

$$\Delta_{cw} = \frac{1 - \nu^2}{Et_{cw}} F$$

(3.67)

Yee assumed that the deflection of the column web in the
compression region of stiffened connections was negligible. The

author's experimental evidence (discussed later) shows that this is not the case. The author proposes that an approximate measure of the deflection in the compression region can be obtained by assuming that the stiffener is in pure compression (see Figure 3.13). This assumption will be valid for the initial stages of loading.

In pure compression the stress in any part of the stiffener is given by,

$$\sigma = \frac{F}{A_s}$$

(3.68)

where A_s = the area of the stiffener

The strain in the stiffener is given by,

$$\epsilon = \frac{\sigma}{E}$$

(3.69)

The deflection of the stiffener is given by,

$$\Delta_{sc} = l_s \epsilon$$

(3.70)

where l_s is the length of the stiffener = D_c

This is the deflection of the whole stiffener under the load system given in Figure 3.13. The deflection contributing to the deflection on either side of the balanced connection is half this value. Therefore, substituting equations (3.68) and (3.69) into (3.70) the author derives the deflection of the compression stiffener as,

$$\Delta_{sc} = \frac{D_c}{4 t_s b_s E} F$$

(3.71)

where t_s = the thickness of the stiffener
 b_s = the width of one stiffener (see fig. (3.13))

Therefore,

$$\Delta_l = \Delta_{cw} \quad (\text{for unstiffened connections})$$

$$\Delta_l = \Delta_{sc} \quad (\text{for stiffened connections})$$

3.2.5. Summary

Summarising, the author has extended Yee's calculation of initial stiffness to include all extended endplate connection types classified by position in the steel framework. Additionally the author has rigorously derived the deflection of the endplate and column flange in the tension region to place its derivation for unstiffened and stiffened column flanges on a more rational basis. The author has demonstrated that the model chosen can easily be adapted to account not only for different geometric

configurations but also for different load conditions at the connection. This could only have been done by choosing a physically based model in which the parameters have some engineering significance.

3.3 Calculation of Plastic Moment (M_p)

3.3.1 Introduction

Strength criteria of extended endplate connections are well established. Therefore only a brief outline of the criteria previously used to determine the plastic moment will be given here. Plastic moment will be calculated by the relationship given by Surtees and Mann (7) which is,

$$M_p = F_p D_{bf}$$

(3.72)

where F_p = the flange force at the plastic moment capacity of the connection
 D_{bf} = the depth of the beam section between the beam flanges

3.3.2 Endplate failure

The endplate yield line mechanism of Surtees and Mann (7) as modified by Whittaker and Walpole and outlined by Yee (13) will be used in this study and is shown in Figure 3.14. It is,

$$F_p = \sigma_{yep} t_{ep}^2 \left[\frac{2W_{ep}}{(C_v - t_{bf} - 2ll)} + \frac{2\kappa D_{bf}}{(A_h - t_{bw} - 2ll)} \right]$$

(3.73)

where

- ll = weld leg length
- σ_{ycp} = endplate yield stress
- κ = a factor used to control the depth of the yield line mechanism
- t_{ep} = endplate thickness
- W_{ep} = endplate width
- C_v = vertical bolt gauge
- t_{bf} = beam flange thickness
- A_h = horizontal bolt gauge
- t_{bw} = beam web thickness

3.3.3. Column flange failure in the tension region.

For unstiffened column flanges two yield line mechanisms need to be checked. The lowest value gives the failure force for column flange bending. Both yield line mechanisms were derived by Packer and Morris (8). These are shown in Figure 3.15. They give values of F_p below,

$$F_{p1} = \sigma_{yc} t_{cf}^2 \left[3.14 + \frac{0.5 C_v}{(m + n)} \right] + \frac{4 B_u n}{(m + n)} \quad (3.74)$$

$$F_{p2} = \sigma_{yc} t_{cf}^2 \left[3.14 + \frac{2n + C_v - d_{bh}}{m} \right] \quad (3.75)$$

where σ_{yc} = the column flange yield stress

- t_{cf} = the column flange thickness
 m, n = dimensions defined in Figure 3.14
 B_u = the ultimate bolt load
 d_{bh} = the diameter of the bolt hole

For stiffened connections the following formulae are used

For a backing plate stiffener derived by Zoetmeijer (7),

$$F_p = (\sigma_{yc} t_{cf}^2 + 0.5 \sigma_{yp} t_{bp}^2) \frac{C_v + 4m + 1.25n}{m} \quad (3.76)$$

- where σ_{yp} = the backing plate yield stress
 t_{bp} = the backing plate thickness

For a tension stiffener derived by Packer and Morris (8),

$$F_p = t_{cf}^2 \sigma_{yc} \left[\frac{n}{v} + \frac{n}{m} + \frac{n - 0.5 d_{bh}}{\left(\frac{1}{v} + \frac{1}{m} \right)} + \pi + \pi \sec^2 \left(\tan^{-1} \left(\frac{2}{\pi} \ln \frac{v}{m} \right) \right) \right] \quad (3.77)$$

where v, m and n are defined in Figure 3.16

3.3.4. Column web shear failure.

The column web shear failure force derived by Yee (13) is given by,

$$F_p = \alpha \frac{\sigma_{yc} t_{cw} D_c}{\sqrt{3}}$$

(3.78)

where α is defined in equation (3.65) and σ_{yc} , t_{cw} and D_c are as defined previously.

3.3.5. Column web buckling failure.

The buckling force of the flange on the column web in the compression region is given by the Chen and Newlin (42) semi-empirical formula,

$$F_p = 10700 \frac{t_{cw}^3 \sqrt{\sigma_{yc}}}{D_c}$$

(3.79)

where $[\sigma_{yc}]$ units are N/mm^2

$[t_{cw}]$ units are mm

$[D_c]$ units are mm

$[F_p]$ units are N

3.3.6. Column web crippling failure.

The column web crippling failure is given by the formula

$$F_p = \sigma_{yc} t_{cw} (t_{bf} + 1l + 2t_{ep} + 5k) \quad (3.80)$$

where $k = t_{cf} + \text{column root radius, } r_k$.

This is defined by Witteveen and given by Yee (13).

3.3.7. Bolt failure.

Yee (13) used bolt failure as a criteria for establishing the plastic moment of the connection. The author feels that as bolt failure is sudden it should not be used as the plastic moment of the connection. Indeed, if the proposed prediction curves are used as design aids bolt failure cannot be used as a failure criterion as it is excluded by BS5950 (1). However, the author proposes that bolt failure should be checked using the formula given by Surtees and Mann (6) allowing for a 33% increase in bolt load due to prying forces.

$$F_p = 3\sigma_{bo}A_{bo} \quad (3.81)$$

where σ_{bo} = the ultimate yield stress of a bolt

A_{bo} = the area of the threaded portion of a bolt

3.3.8. Section failure.

Clearly the connection cannot transmit more moment than the plastic moment capacity of the sections it joins and, therefore, the plastic moment capacity of each section should be checked. For internal balanced connections the beam section failure only should be the limiting case as the column theoretically carries no moment. For unbalanced connections, the unbalanced moment should be checked against the plastic moment capacity of the column, if the column is the weaker section.

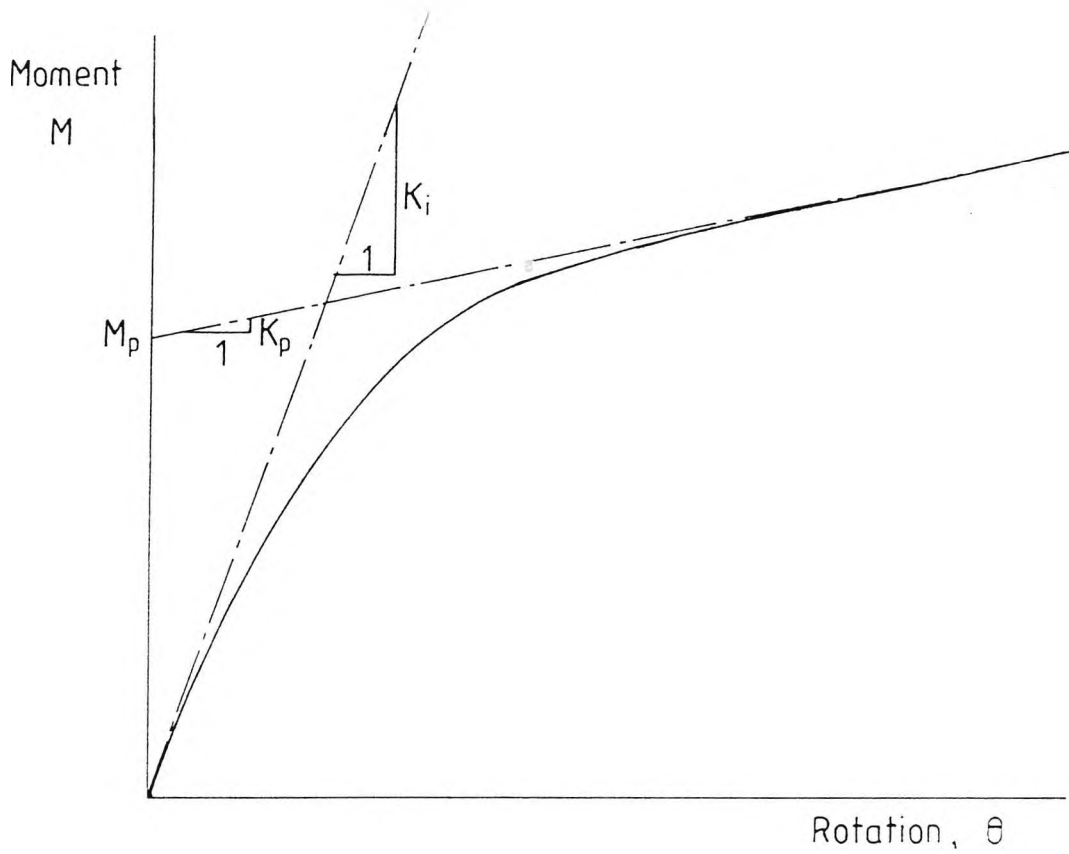
$$M_p = Z_p \sigma_y$$

(3.82)

where Z_p = the plastic modulus of the section
 σ_y = the yield stress of the section

3.4 Summary of Theoretical Development

The initial stiffness and plastic moment capacity parameters for the moment-rotation model have been derived or given for most types of extended endplate connection. In particular the initial deflection behaviour of the endplate and column flange in the tension region has been considered very carefully and placed on a more rational basis. For completeness the deflection of the other connection components have been given and modified to include all types of extended endplate connection so that the flexibility of the Yee connection model can be demonstrated.



$$M = M_p \left(1 - \exp \left(- \frac{(K_i - K_p + c\theta)\theta}{M_p} \right) \right) + K_p \theta$$

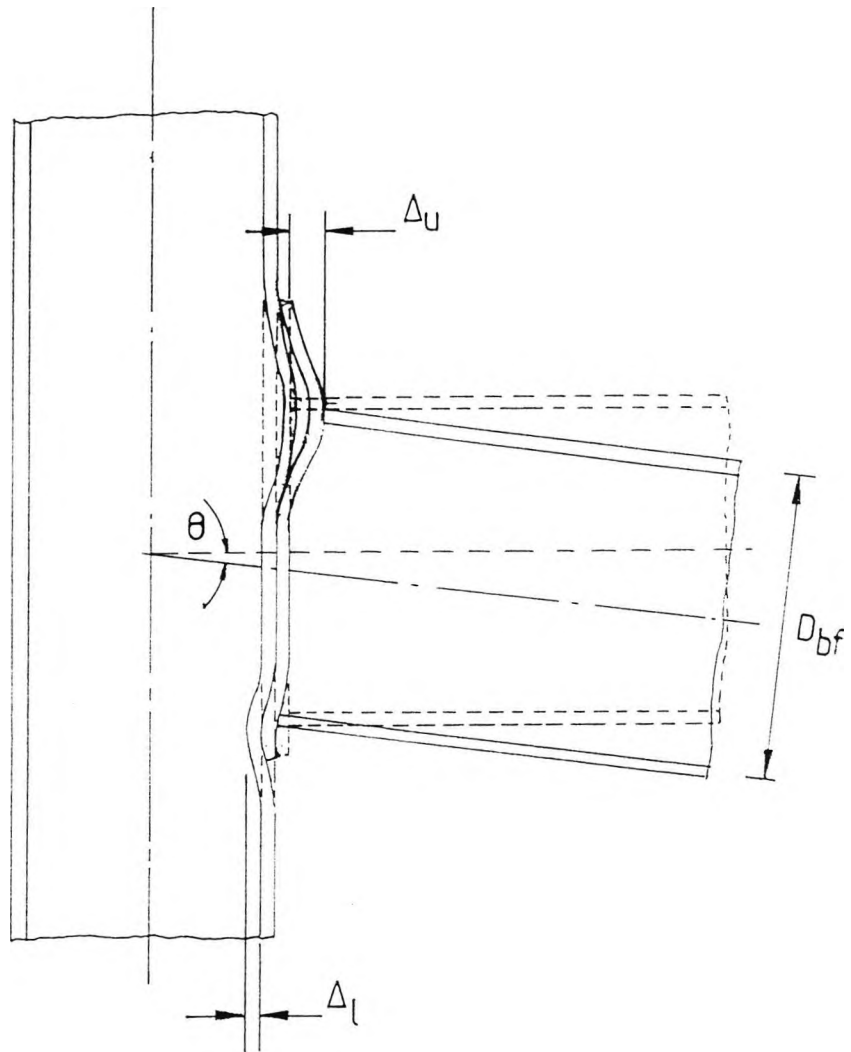
M_p = Plastic Moment.

K_i = Initial Elastic Stiffness.

K_p = Strain Hardening Stiffness.

c = Rate of Decay Parameter.

Figure 3.1 Moment-Rotation Model



$$\theta = \frac{(\Delta_U + \Delta_L)}{D_{bf}}$$

Figure 3.2 Connection Rotation expressed in terms of the Deflection at the Beam Flange Levels.

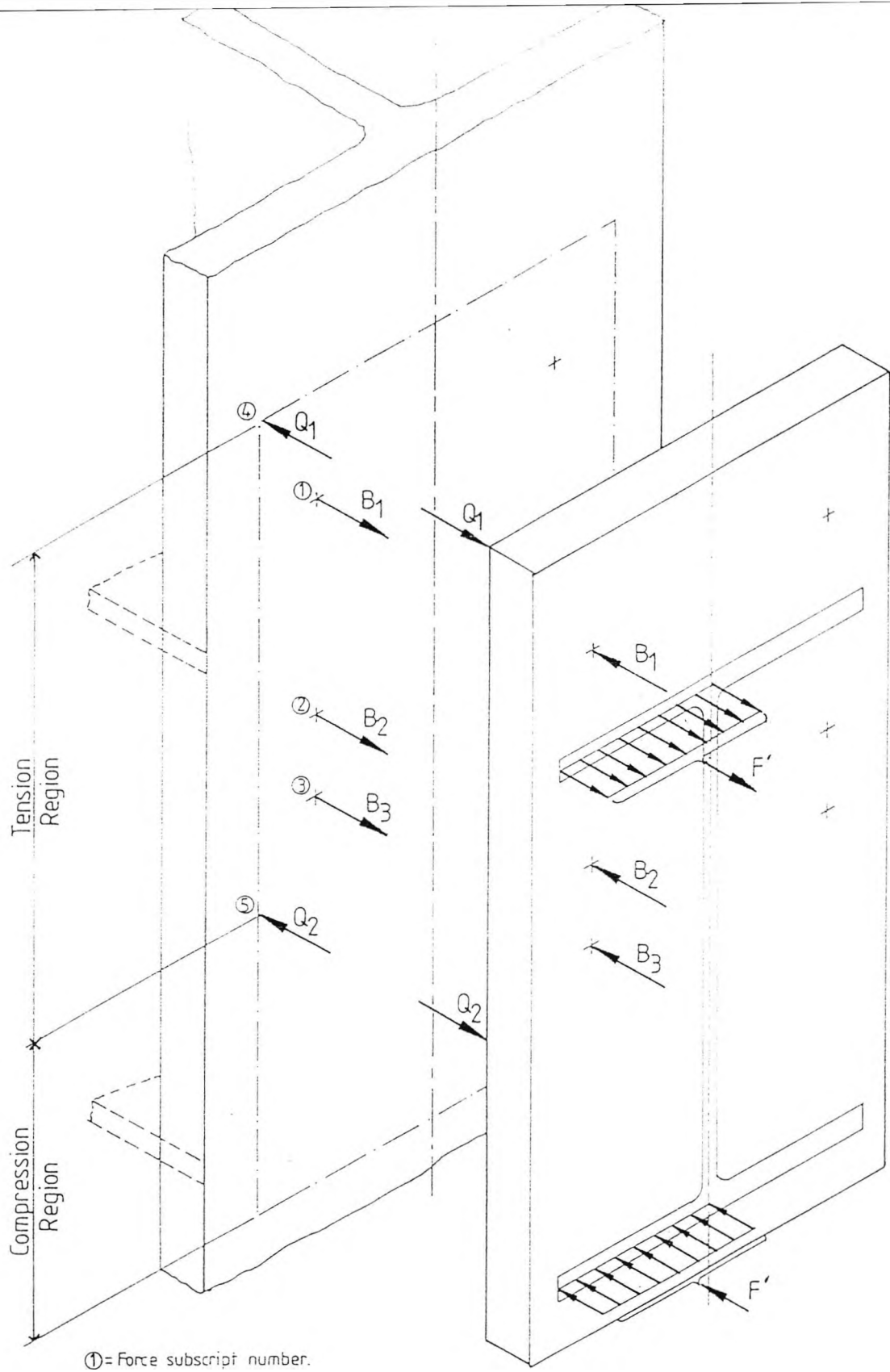
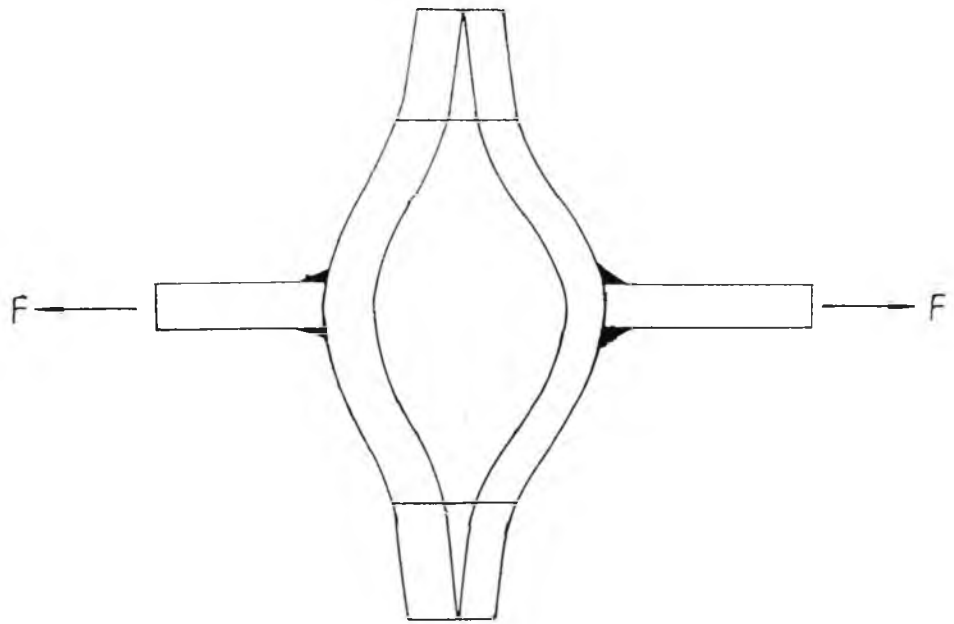
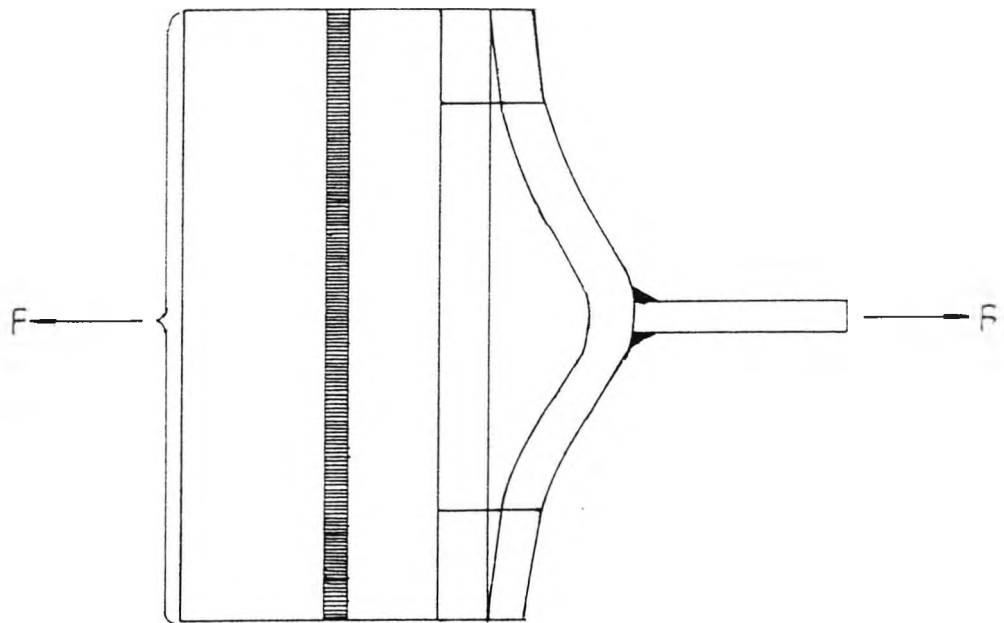


Figure 3.3 Force Interaction between the Column Flange and Endplate.

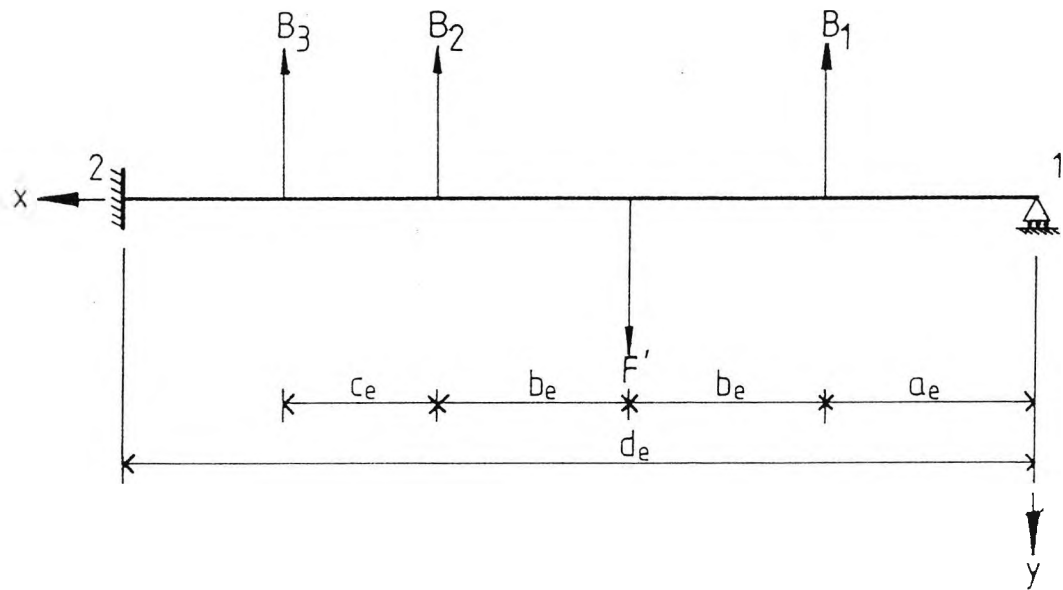


a) Stiffened column arrangement.



b) Unstiffened column arrangement.

Figure 3.4 Column Flange and Endplate Modelled using the T-stub Analogy.



$B_1, B_2, B_3 = \text{Bolt Forces}$
 $F' = \text{Flange Force} / 2$

Figure 3.5 Free Body Diagram of the Tension region of the Endplate.

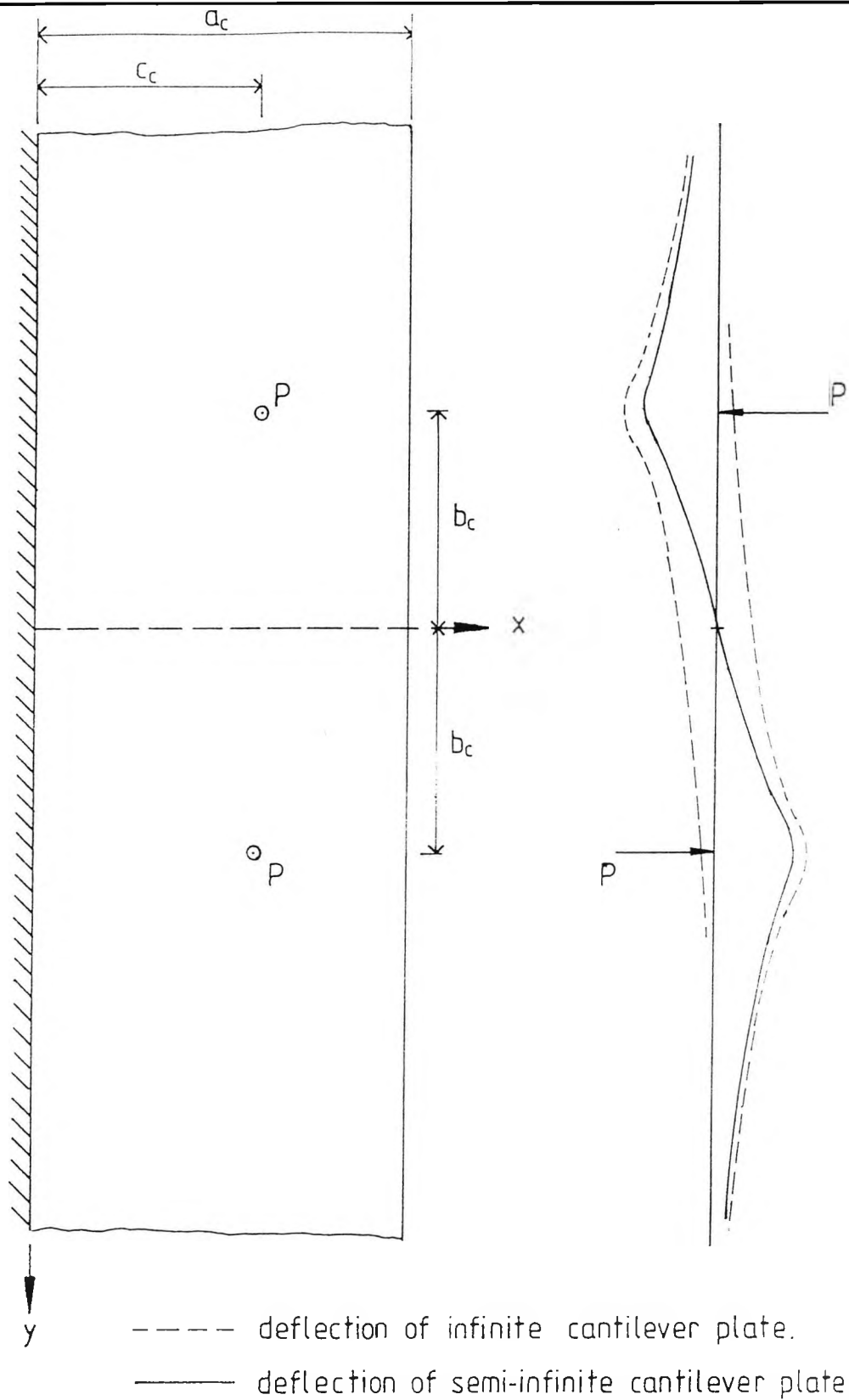


Figure 3.6 Derivation of the Deflection of a Semi-infinite Cantilever Plate Simply Supported at the Edge under Concentrated load.

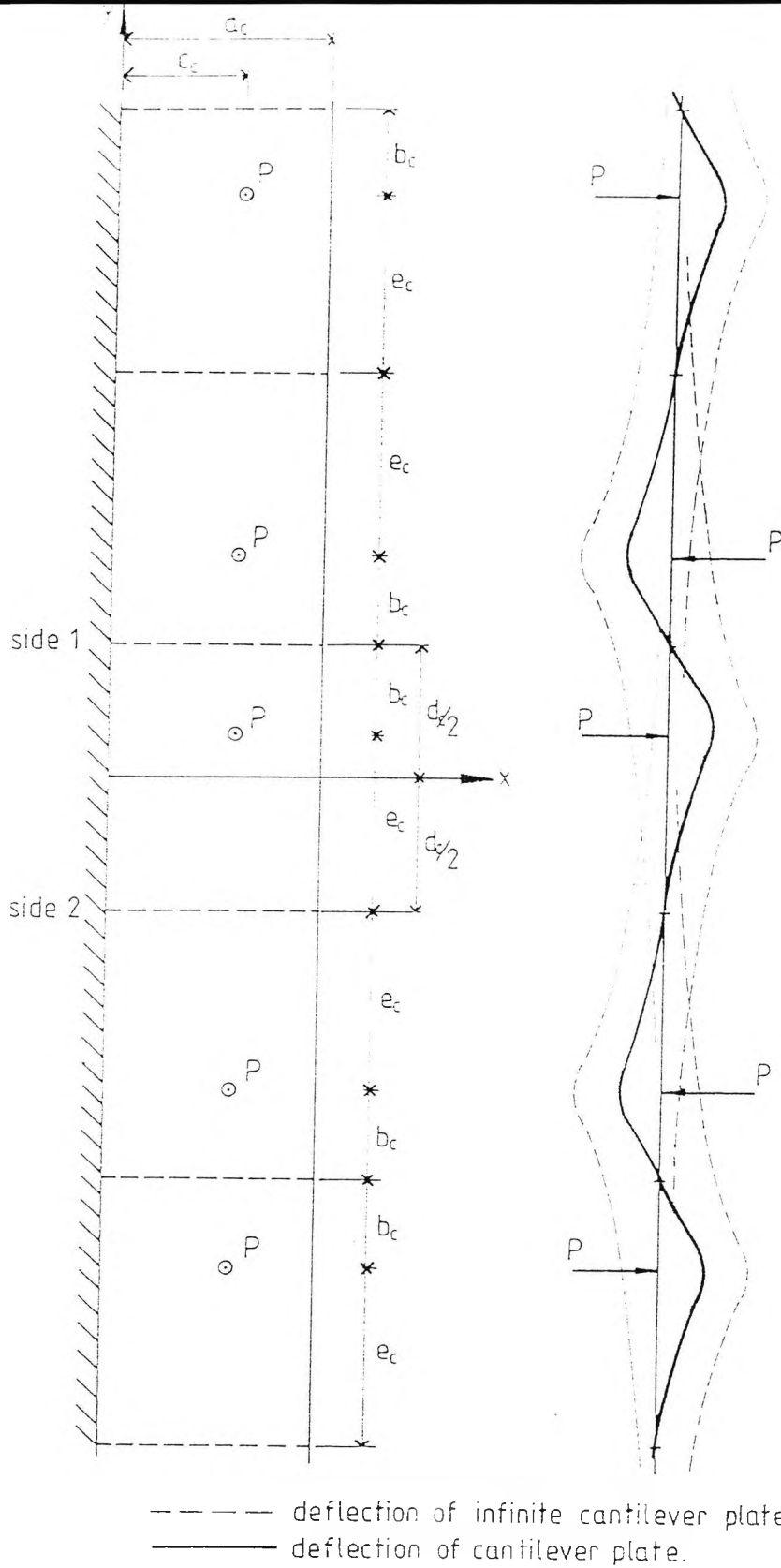


Figure 3.7 Derivation of the Deflection of a Cantilever Plate Simply Supported at each Side under Concentrated Load.

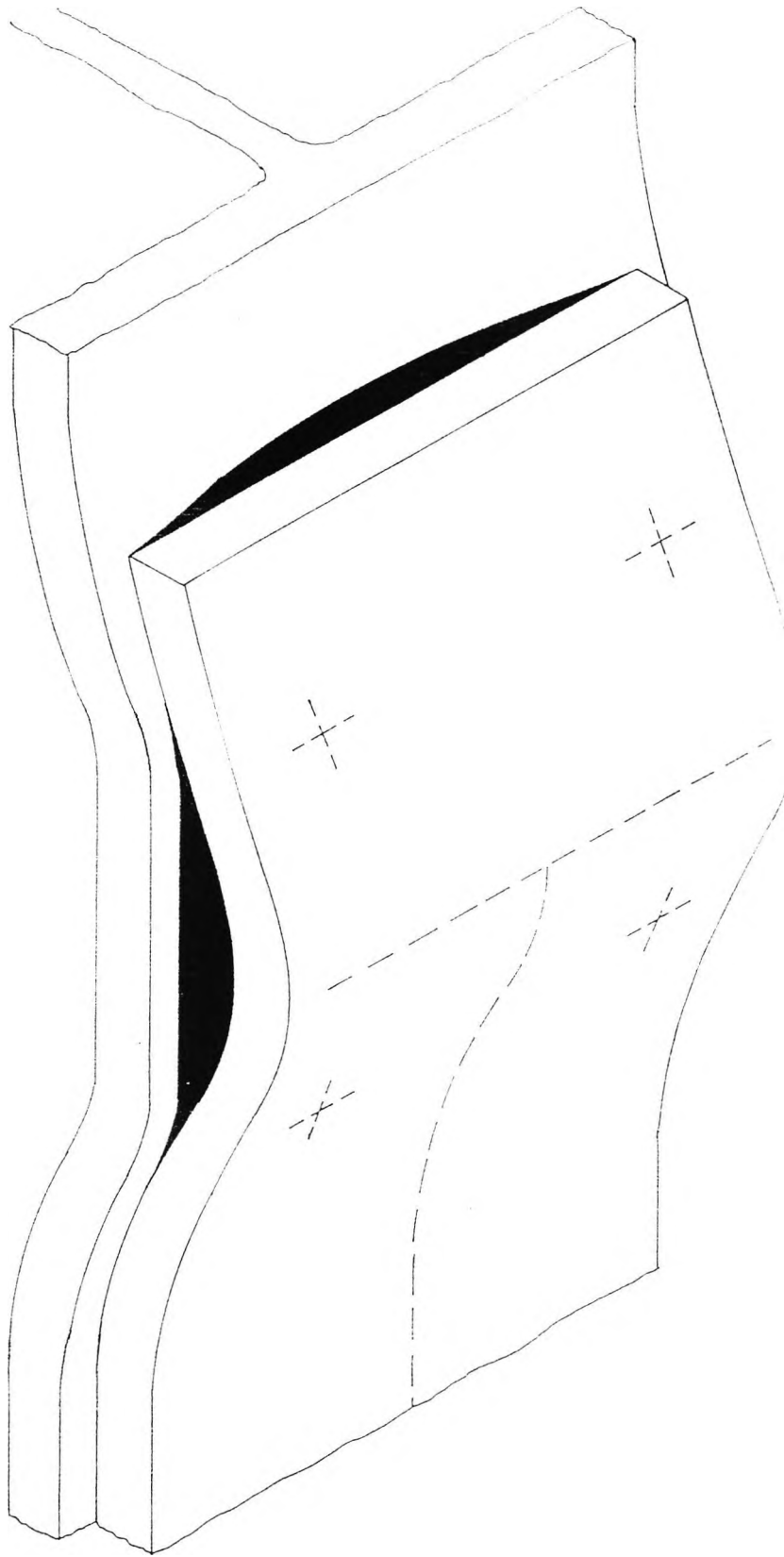
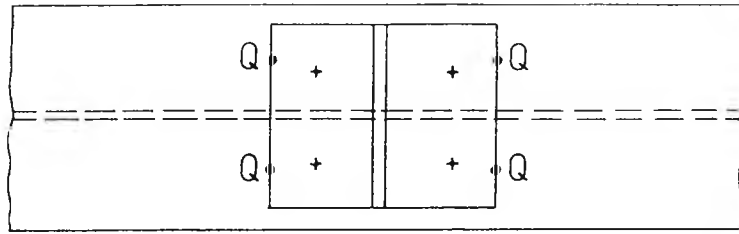
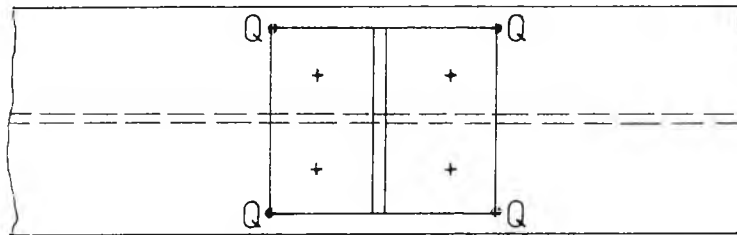


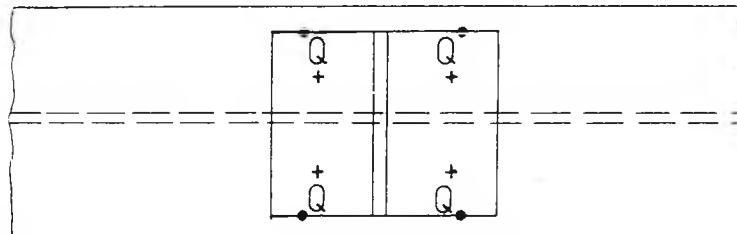
Figure 3.8 Exaggerated Deflection of One-dimensional Endplate and Two-dimensional Column Flange Models.



a) Column flange rigidity \gg T-stub rigidity.

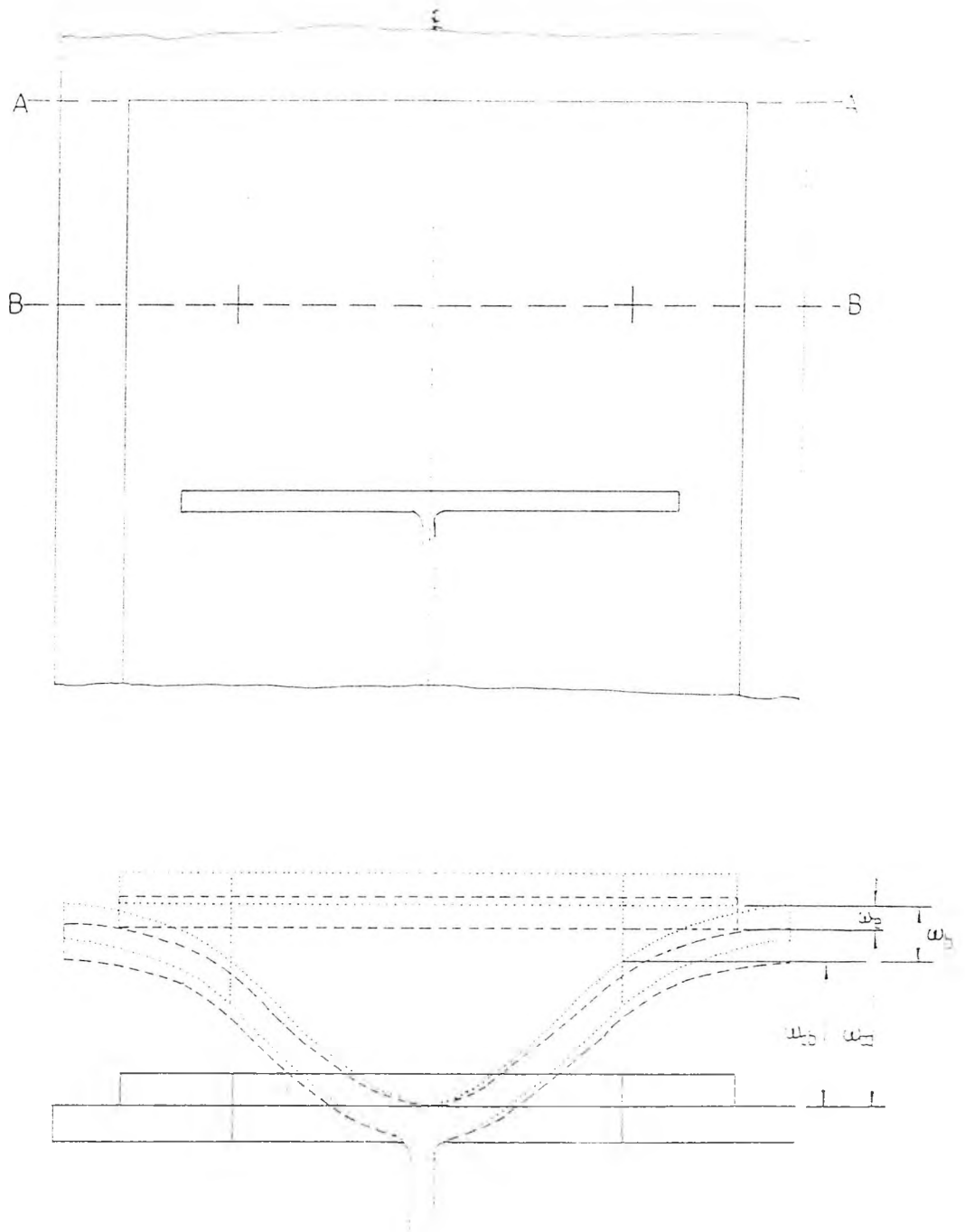


b) Column flange rigidity \approx T-stub rigidity.



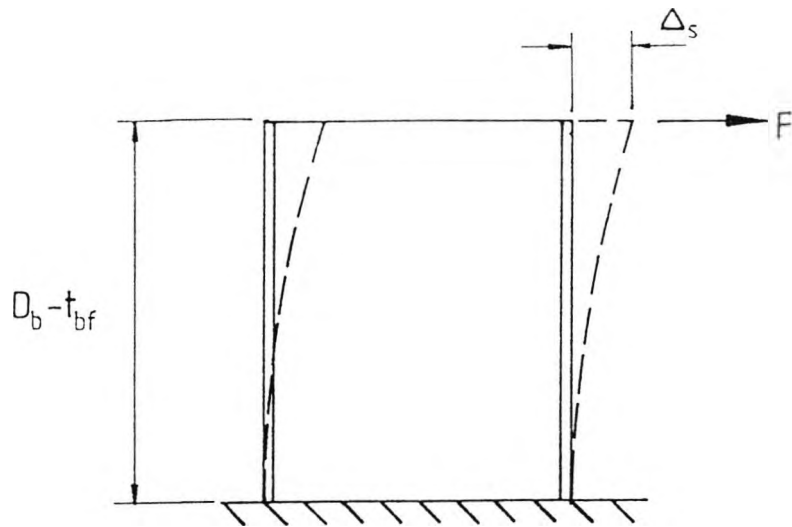
c) Column flange rigidity \ll T-stub rigidity.

Figure 3.9 Variation in Location of Prying Force with changing Relative Rigidity of Column Flange and T-stub.

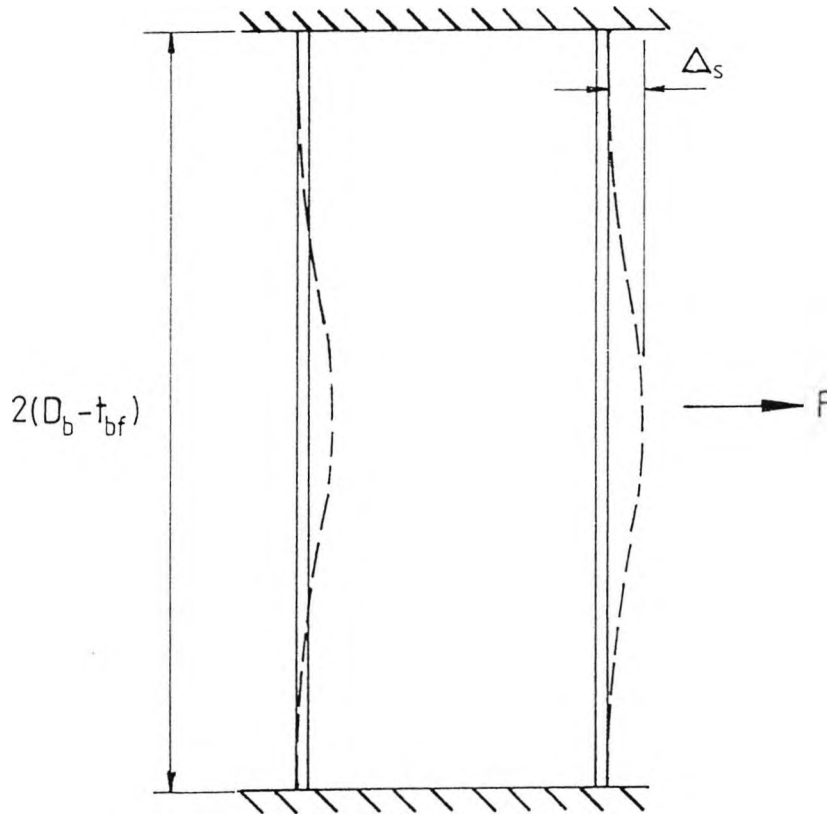


- ω_{cq} = deflection of column flange at contact point.
- ω_{cb} = deflection of column flange at boltline.
- ω_e = deflection of endplate at boltline.
- ω_b = deflection of bolt.
- = deflected shape at section A-A
- = deflected shape at section B-B

Figure 3.10 Derivation of the Compatibility Equation.

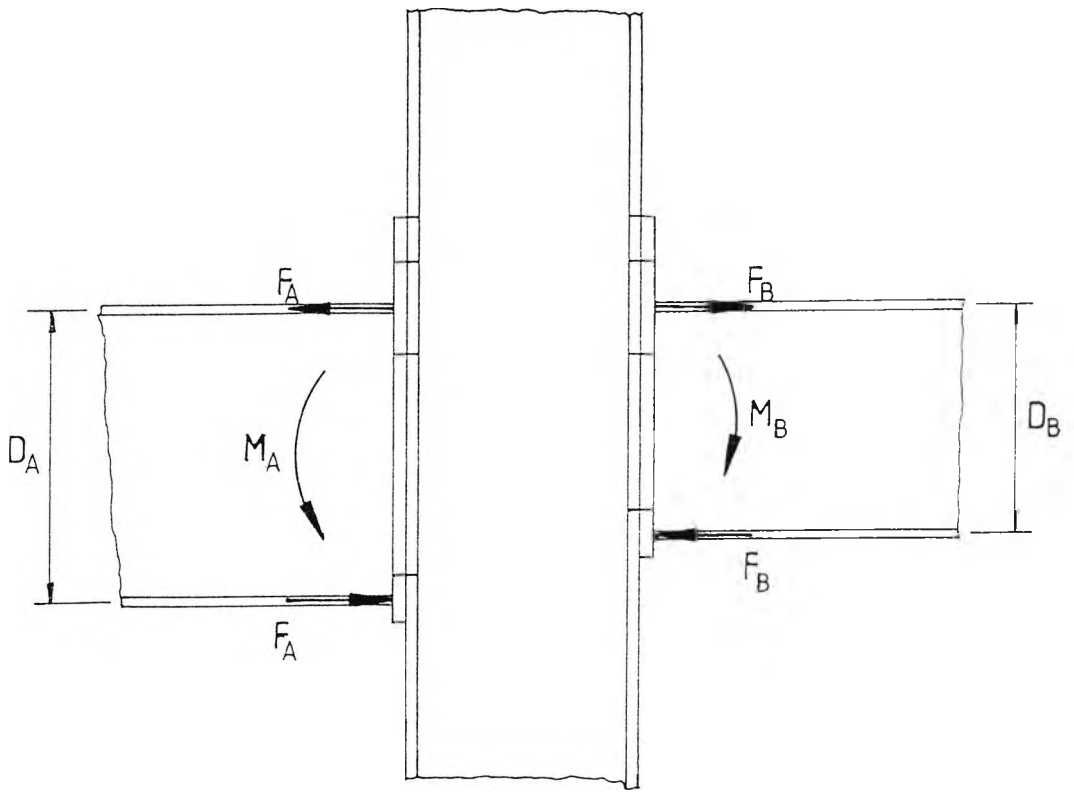


a) Eave connection.



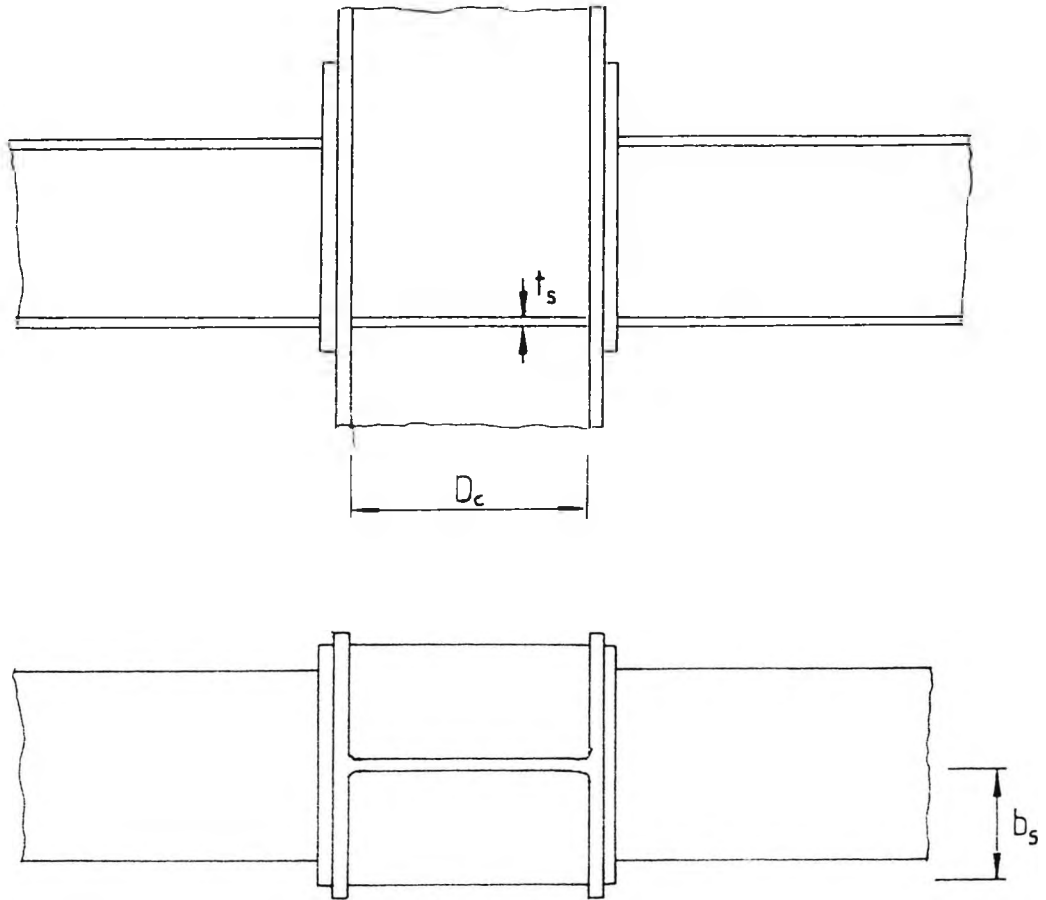
b) Internal connection.

Figure 3.11 Shear Deformation of the Column Web.

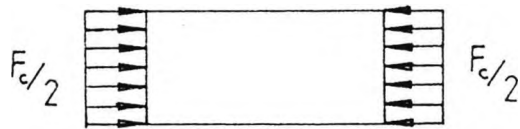


$$F_U = F_A - F_B$$

Figure 3.12 Unbalanced Internal Connection.

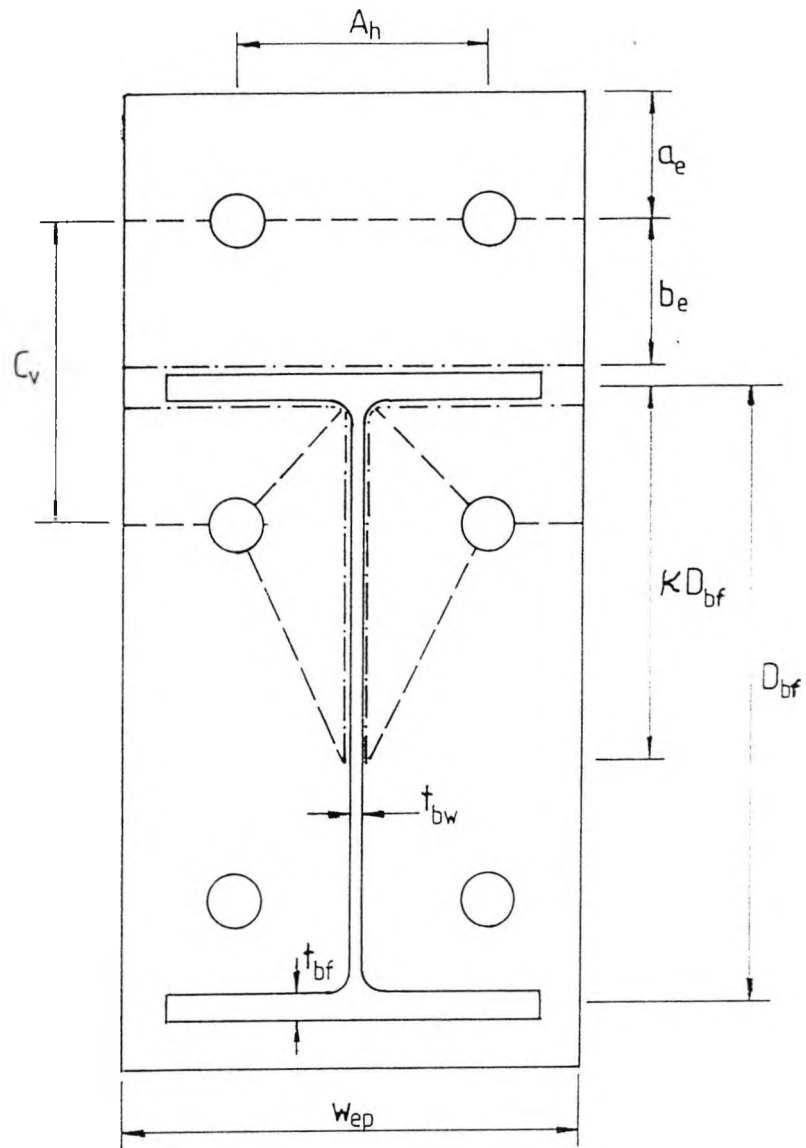


a) Dimensions of Compression Stiffener.



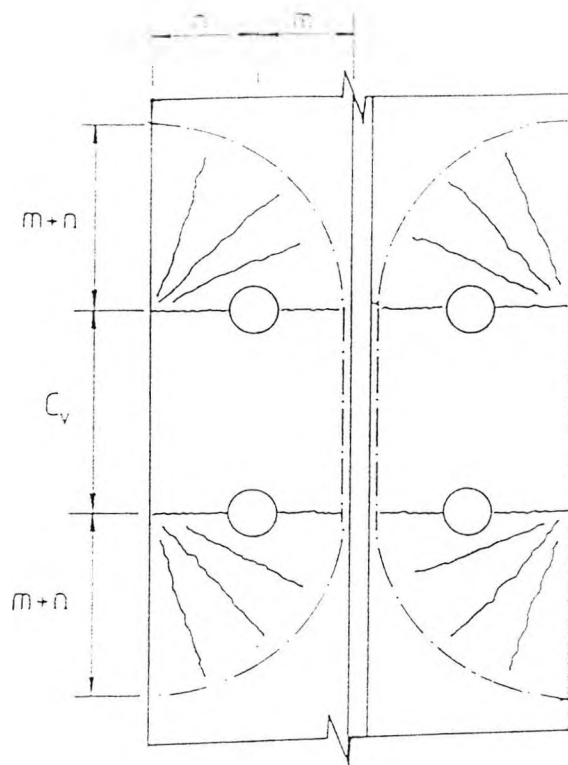
b) Assumed Load on Stiffener.

Figure 3.13 Derivation of Compression Stiffener Deflection.

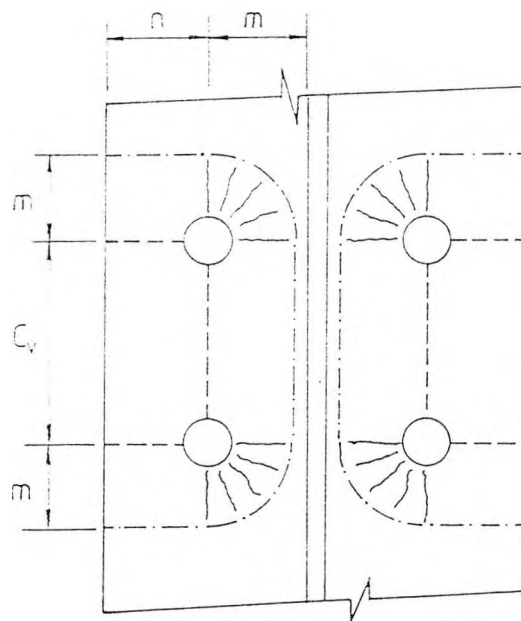


--- Sagging yield line
 - - - Hogging yield line

Figure 3.14 Endplate Yield Line Mechanism (Reference 13).



a) Mechanism 1



b) Mechanism 2

— · — · — Hogging yield line
 - - - - - Sagging yield line

Figure 3.15 Unstiffened Column Flange Yield Line Mechanism (Reference 8).

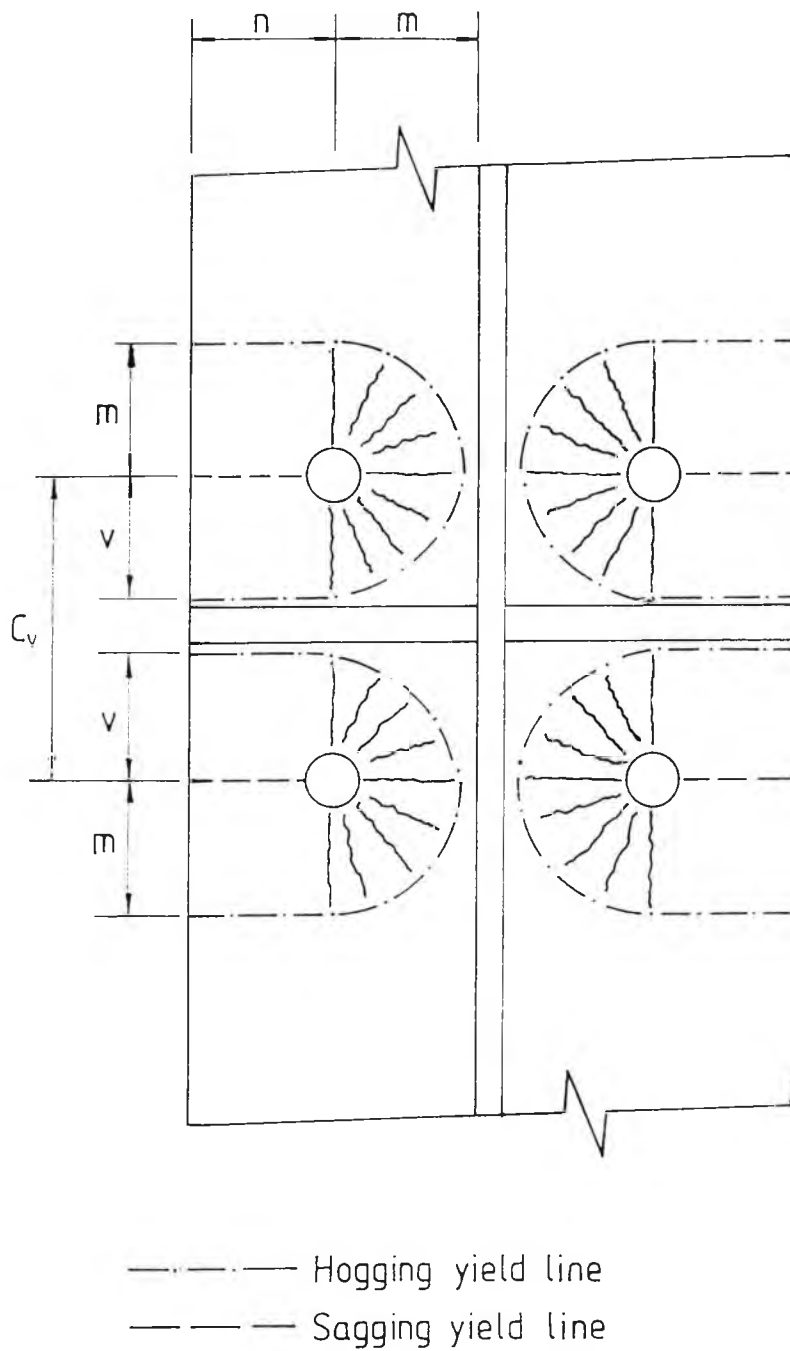


Figure 3.16 Stiffened Column Flange Yield Line Mechanism (Reference 8).

CHAPTER 4

EXPERIMENTAL STUDY

4.1 Introduction

A full-scale testing programme was carried out to assess the validity of the proposed model. The programme could also help formulate a new solution by providing valuable feedback if the proposed model deviated significantly from the actual connection behaviour. The literature review has indicated that most previous tests have been carried out to establish strength criteria. In tests where moment-rotation characteristics have been presented, only overall connection rotation has been measured. This test programme attempted the assessment of the contribution of each component of the connection to the overall rotation.

In this chapter, a description of the specimens tested, the test rig, instrumentation and test procedure will be given. This will be followed by a summary of each test series.

4.2 Test specimens

The types of specimen available for testing are shown in Figure 2.1. It is difficult to incorporate all types of specimen into a test programme due to the differing load and restraint

conditions required for each case. Therefore the internal/internal type of specimen (type (a)) only was investigated. This type of specimen was chosen as it reduced the number of factors affecting moment-rotation behaviour to manageable proportions. Shear deflection is negligible in balanced connections and, with the column being free, there is no axial load in the column. Theoretically, this should leave rotation dependent on column flange/endplate deflection and column web compression only.

Since the majority of endplate tests have been concerned with stiffened connections, unstiffened connections have been investigated in this study. Some stiffened connection tests were also carried out to examine the assumptions made in the derivation of the stiffened column flange model in the tension region.

Previous combinations of beam-column sections tested are shown in Table 4.1. Test specimens were chosen to avoid duplication of test data on similar size test specimens. If Table 4.1 is consulted it can be seen that there is a lack of moment-rotation data on larger sizes of connection. It was proposed that as large a beam section as possible be tested, within the limitations of the equipment available in the laboratory.

The main limitations were that the maximum size jack was 90 tonne and that a maximum lever arm of 1.5m was preferred to prevent lateral instability of the specimen. The maximum size beam that could be tested (after applying a suitable factor of safety) was

a 457 x 191 UB for grade 43A mild steel. The other connection sizes chosen are given in Table 4.1.

Once specimen sizes had been chosen, connections were designed to carry the plastic moment of the beam using a method outlined in Horne and Morris (43). A typical design calculation is given in Appendix C. High strength friction grip bolts were used to reduce bolt sizes and to minimize deflection due to slip between the column flange and endplate. The largest size connection had six bolts around the tension flange to assess the effect of this on the overall connection behaviour.

The tests were split into four series. These are outlined in Table 4.2. The first series consisted of eight tests on the smallest connection size (254 x 146 UB / 203 x 203 UC). These tests were carried out to examine the effect of the most important variables on the moment-rotation data. Six of these tests were unstiffened and two tests were stiffened.

The first test, A1, was a pilot test to decide which was the best method of rotation measurement. It failed prematurely due to tension bolt failure. On inspection it was discovered that the bolts used were sub-standard. All bolts for the following tests were changed and test A8 is a repeat of test A1.

Five unstiffened tests (A2-A5, A8) were carried out to examine the effect of varying endplate and column flange thickness around a design value (A8). The two lighter column sections were tested

stiffened so that the effect of tension and compression stiffeners on the moment-rotation curve could be ascertained.

Test series B and C were carried out to see if the method of prediction was unaffected by the size of the connection. Each series consisted of two tests, one stiffened and the other unstiffened. The final test (D1) was carried out to determine whether the method could successfully predict the moment-rotation behaviour of a small beam connecting into a large column. This test was unstiffened.

The specimens were fabricated in the structures laboratory. All specimens were constructed in grade 43A mild steel. The dimensions of the endplate profile for each series of tests is given in Table 4.3. For each series of tests, one endplate was used as a template for the fabrication of the rest. The column flanges were then drilled using each endplate as a template to ensure good fit. The endplates were then welded to the beam ends. Column compression and tension stiffeners, where required, were welded in position at the beam tension and compression flange levels. Stiffeners were also placed in the beam at the support points of the specimen.

Tensile specimens were taken from each batch of steel used and a summary of the results is given in Table 4.4.

4.3 Test Rig

Once the specimen sizes had been decided, a suitable test rig had to be chosen in which the specimens could be loaded to failure. Due to the unsuitability of testing vertically due to the size of the plinths required to support the specimens, it was decided to build a horizontal reaction frame. The rig shown in Figure 4.1 is similar to one that was built at Sheffield University (14) but larger due to size of the specimens to be tested. The rig consists of 432 x 102 rolled steel channels (R.S.C.s) welded back to back and separated with 254 x 89 R.S.C.s. The frame was supported by buffers, which consisted of 356 x 368 UC welded to 20mm thick plate and bolted to the strong floor using 75mm diameter Macalloy steel bars. The arms of the test rig were also bolted through the floor using the same bars via 20mm thick plates welded to the bottom of the frame.

The ends of the beams of the specimen were supported on rollers and load cells in the arms of the test frame, and the column was loaded from a central point. This meant that all the load was contained within the frame. The frame was securely bolted to the floor in case it failed for any reason.

4.4 Instrumentation

4.4.1 Rotation and deflection measurement

The most important measurement to be taken in any moment-rotation test is the rotation due to the connection. Therefore, the best method of measuring connection rotation was carefully considered.

Previous methods used to measure connection rotation (section 2.2) use some sort of magnification device to amplify deflections or some sort of transducer calibrated to measure rotation directly. These devices are usually offset and, therefore, contain some degree of beam or column flexure.

The amount of flexure due to the beam or column is difficult to obtain and hence a method which measures connection rotation directly is preferable. As the specimens in this study were tested horizontally, some methods of measurement were automatically excluded, namely certain transducers which depend on gravity. Optical methods were also excluded due to the limited space around the test rig. A further problem was that, for internal/internal type connections, the area in which deflection measurements were taken was moving relative to the only fixed datums, the floor and the test rig. This effectively left amplification of deflections by means of rotation arms offset from the connection or some method of measuring the actual deflections of the connection within the required tolerance.

It was proposed to measure the connection deformation using a photogrammetry technique so that an overall picture of the actual connection deformation could be obtained. The first test (A1) was conducted using this technique and the results are given in Appendix D. Connection rotation in the initial stages of loading could not be measured within the required tolerance. In fact, the rotation in the initial stages of loading was of the same order as the standard error of each reading. Therefore, a more precise method of measuring deflection was needed.

The possibility of measuring connection rotation using the same method as that proposed in the theoretical development (Eqn. (3.5)) was investigated for the photogrammetric results. The endplate deflection at the beam tension and compression flange levels was divided by their distance apart and averaged on both sides of the connection. Reasonable correlation between initial and expected connection rotation was obtained. However, these results were based upon deflections which had a standard error an order of magnitude too high. Deflections would need to be measured to a greater degree of accuracy.

It was decided to measure the deflections of the endplate, column flange and column web using a series of linear displacement transducers. These were mounted from a measuring frame which sat on the column web of the specimen. In this way the connection rotation was deduced from deflection measurements and the deflection of the various components could be directly related to it. The measuring frame was bolted to the column web away

from the area of interest. This ensured that deflections at each transducer position were measured relative to the moving column centreline.

The measuring frame is shown in Figure 4.2. It is fully adjustable and was able to fit all specimen sizes. Transducers had a maximum extension of 10mm and were used as they were light and small (Figure 4.3). Each transducer was individually calibrated thus ensuring that deflection could be measured to $\pm 0.01\text{mm}$. This was deemed to be sufficiently precise for rotation measurements. A few transducers were calibrated several times to ensure repeatability of measurement. The frame enabled each transducer to be positioned anywhere on the column flange or endplate to within 2mm. The transducers were wired into a data logging system so that all the readings could be taken simultaneously (Figure 4.4).

The transducers on the measuring frame were positioned solely to monitor endplate and column flange deflection at the edge of the endplate. It was also necessary to monitor the deflection of the column web. This was achieved by mounting a transducer at either end of a perspex rod of sufficient length that, when placed just above the column root radius, the rod was held between the two column flanges by the spring force of the transducers (Figure 4.5). The average of the two transducer readings gave the deflection of the column web relative to the column centreline. For the majority of tests there were 32 transducers on each specimen. This was the maximum allowed by the logging system.

The position of each transducer is shown diagrammatically in Figure 4.6. There were 24 transducers at the edge of the endplate and at the same level on the column flange, and there were 8 transducers at 4 positions on the column web.

The second test (A2) was used to check the suitability of the transducer method of rotation measurement. Rotation was also measured by dial gauges bearing on extension arms offset from the connection, by monitoring the central deflection of the specimen and by the photogrammetric method used in the first test. The photogrammetry method required the transducers on the column web to be omitted as they hindered the sight of the photogrammetric targets on the column web. Unfortunately, due to a camera malfunction, the results of the photogrammetric analysis of this test were invalid. However, good agreement was obtained between the rotation measurements deduced from the offset dial gauge readings, the transducer deflections and the central deflection. It was decided to adopt all three methods of measurements for subsequent tests so that further comparisons could be made.

The method of deducing rotation measurements from the central deflection of the specimen is outlined in Appendix E along with the calculation of rotation due to offset flexure.

4.4.2 Load measurement

The load at each support point was monitored using two calibrated load cells, shown in Figure 4.7. Each was connected to a simple Wheatstone bridge arrangement and output readings were average values of the three strain gauges around the perimeter. The load was transferred to the load cells using two simple roller bearings, one fixed and the other free.

4.4.3 Strain gauge measurements.

The first test (A1) was fully strained gauged (45 strain gauges being used) to assess which strain gauge position would be useful for detecting the yield points of each component of the connection. The number of strain gauges was reduced to twenty one for the second test as many of the gauges were relatively unstrained in the first test. For subsequent tests the beam flanges only were strain gauged as the yielding of the components of the connection could be detected from load and transducer deflection readings. The plots of beam flange strain gauge readings versus load are given in Appendix F.

4.5 Test procedure

An outline of the test procedure for each test will now be given. Firstly, the prefabricated parts of the specimen, the column and the beam arms were assembled. The column section was clamped upright to the test rig. The first beam arm was then offered up to the column section and bolted. While the first beam was still supported, the second beam was similarly bolted. Each bolt was then pretensioned, an endplate at a time, using load indicating washers and a feeler gauge to ensure uniformity of pretension. The specimen was then laid flat on the floor.

The specimen was lifted and placed in the test rig. While the crane supported the specimen at the level of the jack, rollers were placed under the column section. These rollers ran on a plate which was packed up so that the column web was level with the centre of the jack. The plate was lightly oiled to minimize out-of-plate movement of the specimen.

The load cells and roller bearings were held in position by wooden blocks as the specimen was pushed tight up against them. The free roller was held in position by threaded screws until the specimen was ready to be loaded. The jack was packed up behind to ensure that the maximum travel was available.

While the specimen was in this position, the rotation arms were welded into position, offset 220mm from the connection. The

transducer measuring frame was then placed on the column web and bolted in place. The transducers were fixed in the desired position (Figure 4.8). The specimen was ready for testing.

The initial test set up is shown in Figure 4.9. At the start of each test, the specimen was subject to as small a load as possible to just hold it in position. Then the blocks supporting the load cells and roller bearings were removed so that the specimen was held up by the rollers under the column section, the jack and the support points only.

All the transducers and dial gauges were zeroed. The first load increment was applied and the specimen was allowed to settle. Load and transducer readings were then taken simultaneously. The dial gauge readings for the measurement of offset rotation were taken as close together as possible. This became increasingly difficult at large loads due to the appreciable creep that was present in the specimen. This procedure was repeated until failure occurred or no further readings could be taken.

In practice, it was difficult to monitor the specimens all the way up to failure due to the fear of damaging the transducers. Each transducer has a maximum travel of 10mm and was set up approximately in the middle of its range, giving a maximum deflection measurement of ± 5 mm. Sudden failure of any part of the connection, particularly bolt failure, could have damaged a whole row of transducers. At this stage each test was stopped and the transducers were removed before failure was reached.

4.6 Summary of tests.

4.6.1 Test series A

It has been mentioned in the previous section that each test was curtailed before ultimate failure of the connection due to possible damage to the instrumentation. The specimen in each test, however, (with the exception of A1) entered the strain hardening phase of the moment-rotation curve, the plastic moment capacity of the beam having been reached. The rotation of each connection at the end of each test was typically between 15×10^{-3} and 20×10^{-3} radians. The specimen sizes used in each test are outlined in Table 4.2.

4.6.1.1 Test A1

Test A1 was carried out to assess the feasibility of using photogrammetry to determine the rotation of the connection and the relative contributions of the various components that make up the connection to that rotation. It was decided to have relatively large load increments initially to minimise the number of photographic plates needed. Thus the initial load increments equated to a connection moment of approximately 35 kNm per load step. The design moment of the connection was 128 kNm. The connection failed between 111 kNm and 140 kNm due to bolt failure above the tension flange of beam 2. On inspection it was revealed that bolt stripping had taken place due to ordinary black bolts being used. Re-testing was not possible due to

significant plastic deformation of the endplate and column flanges (Figure 4.10).

4.6.1.2. Test A2

Subsequent tests were carried out with the correct bolts and using the measuring frame to determine displacements. A disadvantage of using the measuring frame was that it made direct observation of the connection specimen difficult (Figure 4.9). However, it was possible to deduce the separation of the column flange and endplate more accurately by observation of the transducer readings. Separation was deemed to have occurred when a gap of 0.05mm appeared between the endplate and column flange at the same point. The analysis of the transducer results was quicker than the photogrammetric method and more load increments could be taken. Therefore, initial load increments for the rest of test series A equated to a connection moment of approximately 15 kNm.

The deflection profiles of the endplate and column flange were similar for each unstiffened test throughout the loading range. The profiles for test A2 are shown in Figures 4.11 and 4.12. Separation occurred at 84 kNm for endplate 1 and at 76 kNm for endplate 2. The test was stopped at 139 kNm. Deformation of the column web in the compression region was clearly visible on removal of the measuring frame.

4.6.1.3 Test A3

This specimen behaved as expected. Separation occurred at 129 kNm for endplate 1 and slightly earlier at 115 kNm for endplate 2. Each side of the connection specimens behaved nearly identically in each test. The maximum moment reached in test A3 was 161 kNm when the test was stopped due to excessive endplate deflection. The deflected endplate profile at failure is shown in Figure 4.13.

4.6.1.4. Test A4

Separation occurred at 140 kNm for endplate 1 and at 130 kNm for endplate 2. Separation was expected to occur later than the other tests in the series due the relatively smaller deflections of the thicker endplate. The ultimate moment reached was 150 kNm when the test was stopped due to the excessive deflection of the endplate and column flange in the tension region.

4.6.1.5. Test A5

In contrast, separation occurred in both endplates at 92 kNm for this thinner endplate test. The ultimate moment reached was 140.5 kNm and the test was stopped due to excessive endplate deflection (see Figure 4.14).

4.6.1.6. Test A6

This was the first of the stiffened tests carried out. The stiffeners were not full depth for this test series and subsequently some column flange deflection in the tension and compression region was measured when none was expected. Although this could have been due to the necessity of offsetting the transducers from the stiffener positions (see Figure 4.15).

Separation, as expected, occurred almost immediately. The ultimate moment reached was 153 kNm at which the deflected shape of the column flange and endplate can be seen in Figure 4.15.

4.6.1.7. Test A7

The ultimate moment reached in test A7 was 167 kNm. Separation at failure is shown in Figure 4.16. The deflection of the column flange was negligible compared with the deflection of the endplate.

4.6.1.8. Test A8

This was the design test around which the other unstiffened tests were varied. It performed as expected with separation occurring around 120 kNm. The ultimate moment reached was 160 kNm and the deflection at failure is shown in Figure 4.17.

4.6.2. Test series B.

The design moment for these larger tests was 246 kNm. Instrumentation for this test series was the same as tests A3 to A8. The load increments were increased initially to approximately 30 kNm. The ultimate rotation reached in each test was around 15×10^{-3} and 9×10^{-3} radians for tests B1 and B2 respectively. Specimen sizes are outlined in Table 4.3.

4.6.2.1. Test B1

Each endplate in this test behaved differently, separation occurring at 109 kNm for endplate 1 and at 205 kNm for endplate 2. The ultimate load reached was 247 kNm when sudden failure occurred due to beam tension weld fracture (Figure 4.18). The transducers were undamaged since the endplate remained bolted to the column flange. A cross-section of the weld was taken (Figure 4.19). The measured throat thickness was approximately 11mm against a design thickness of 12mm. The presence of slag inclusions in the welds on both side of the tension flange could be the reason for failure.

4.6.2.2. Test B2

This stiffened test was carried out with full depth stiffeners to examine the column flange deflection near the stiffeners. Separation occurred immediately upon loading. The ultimate load reached was 297 kNm when the test was unloaded due to excessive

deflection. The transducers were left in place on unloading to examine the unloading stiffness of the connection. Deflection of the thick endplate and the column flange can be seen in Figure 4.20.

4.6.3. Test Series C

These were the largest specimens tested. The design moment was 456 kNm and was almost achieved in both tests. Both these tests were ended prematurely. Test C1 was curtailed due to instability of the column flange in the compression region. This was due to the specimen being too short in the compression region. When the test rig was designed it was envisaged that the load cells would be of the pressure pad variety and thus only around 100mm thick. It was subsequently discovered that due to the loads carried (up to 50 tonnes) a more substantial load cell was needed. These load cells were 200mm long. This led to the specimen being shortened in the compression region (see Figure 4.21).

This did not matter for the stiffened test as the stiffener restrained the column flange in the compression region. This test was stopped as the design load of the test rig was being reached.

The load increments for this test were 37 kNm in terms of connection moment initially and the maximum rotations recorded were in the region of only 7 to 8 x 10⁻³ radians.

4.6.3.1. Test C1

This specimen failed due to instability of the column flange in the compression region. Separation did not occur until 320 kNm and the ultimate moment reached was 410 kNm. The excessive deflection of the column flange in the compression region is demonstrated in the relevant component deflection versus load graph (Figure 5.36).

4.6.3.2. Test C2

Separation occurred almost immediately upon loading for this stiffened test. The maximum moment reached was 460 kNm, but if the moment-rotation curve for this specimen is consulted (Figure 5.11), it can be seen that the plastic plateau of the moment-rotation curve is not reached. The rotation of the specimen on unloading was measured to examine the unloading stiffness of the specimen. On unloading the deflection of the column flange was found to be negligible.

4.6.4. Test D1

This final test was carried out to examine the behaviour of a small beam framing into a large column. Initially the load increments were the same as the majority of the test series A tests. Separation occurred at 98 kNm and 124 kNm respectively for endplates 1 and 2. The ultimate moment reached was 163 kNm and the moment-rotation curve was well into its plastic plateau.

This test was stopped due to the dial gauges reaching the end of their travel. The deflection was almost solely due to endplate deflection as can be seen at failure (Figure 4.22). The maximum rotation reached was 11.5×10^{-3} radians.

4.7 Summary of Test Programme

A test program of 13 full scale tests on internal/internal unstiffened and stiffened connection specimens of various sizes was carried out. Connection rotation was carefully considered. Four separate methods of connection rotation measurement were used in all the tests. For the majority of the tests rotation was derived from transducer, offset dial gauge and central specimen deflection readings. The smaller connection tests behaved as expected. The larger connection specimen tests (test series C) were not so successful due to column flange instability and the limit of the test rig being reached.

UC UB	152x152	203x203	254x254	305x305	Misc.
203x133		5			
254x102	8,14,18	5			
254x146		6 ●		●	
305x102			7 ■		
305x127		5			
305x165		5	16		13 305x165UB
356x127		4,5,9,10 ■ ■			
356x171		5,12 ○	●		
406x140			6,9 ■		
406x178					13 457x191UB
457x152			6,10 ■		
457x191				13 ●	13 457x191UB
533x210			10 ■		
610x229				11	

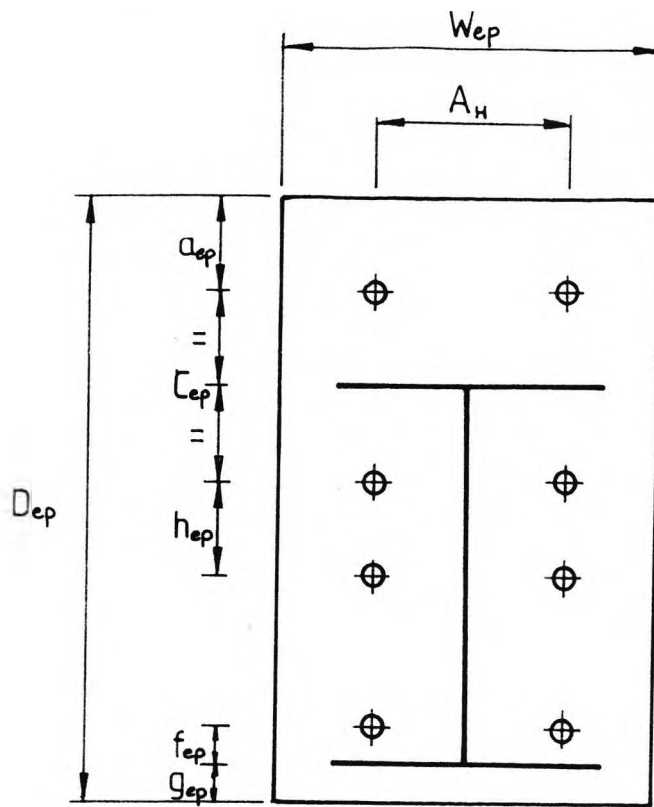
Key

- US/AUS/EEC equivalent sections
- Fabricated column
- Specimens in this study
- 9 Reference No.

Table 4.1. Sizes of Previous Endplate Specimens.

Test No.	Type	Column	Beam	Endplate Thickness mm
A1	Unstiffened	203x203x71	254x146x37	20
A2	Unstiffened	203x203x60	254x146x37	20
A3	Unstiffened	203x203x86	254x146x37	20
A4	Unstiffened	203x023x71	254x146x37	25
A5	Unstiffened	203x203x71	254x146x37	15
A6	Stiffened	203x203x60	254x146x37	20
A7	Stiffened	203x203x71	254x146x37	20
A8	Unstiffened	203x203x71	254x146x37	20
B1	Unstiffened	254x254x89	356x171x51	25
B2	Stiffened	254x254x89	356x171x51	25
C1	Unstiffened	305x305x137	457x191x74	25
C2	Stiffened	305x305x137	457x191x74	25
D1	Unstiffened	305x305x137	254x146x37	20

Table 4.2. Definition of Test Specimens.



D_{bo} = Bolt Diameter

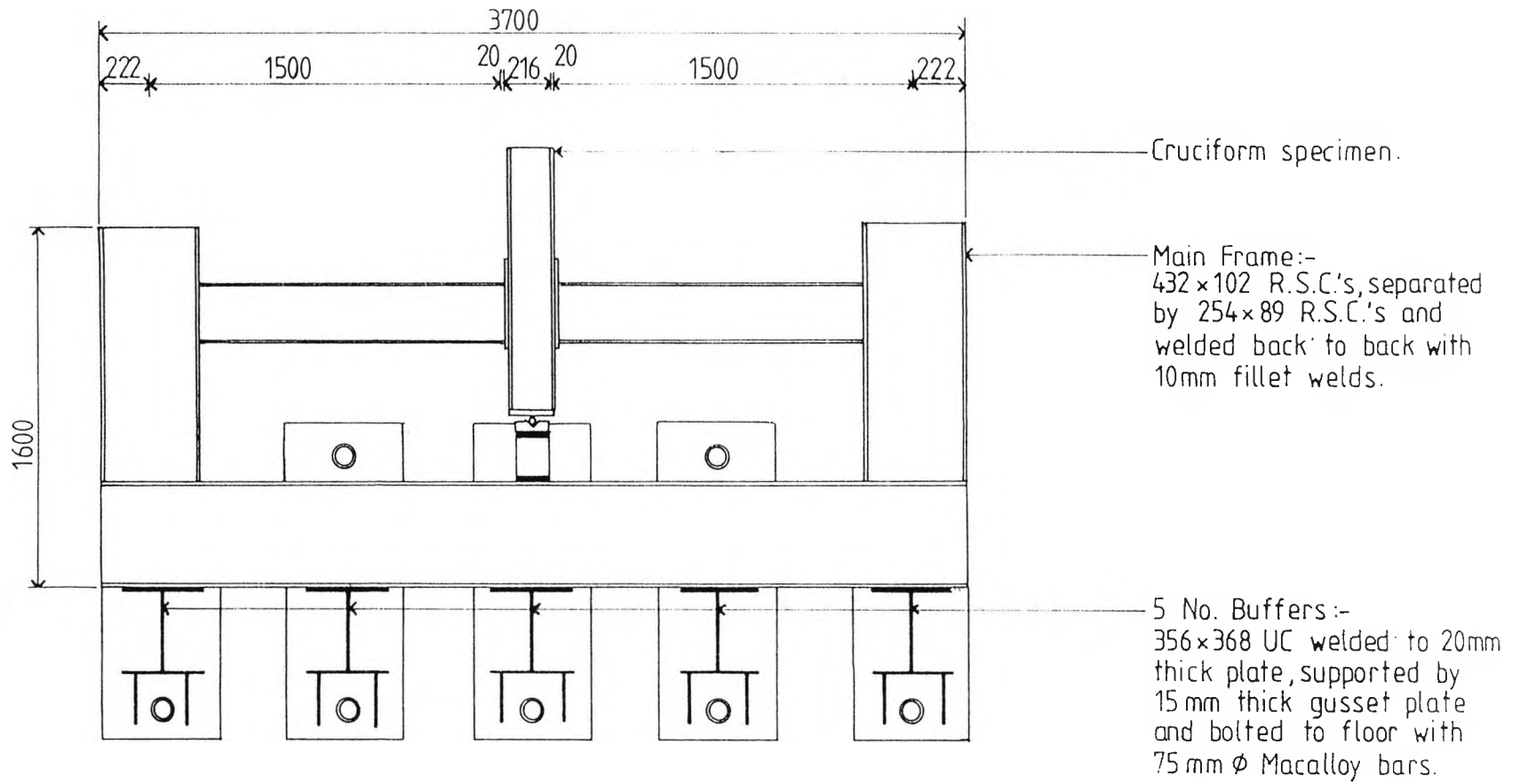
Dimension mm	Test Series		
	A/D	B	C
W_{ep}	180	200	220
A_H	100	110	120
a_{ep}	50	55	60
c_{ep}	120	130	140
D_{cp}	380	490	600
f_{cp}	50	50	50
g_{ep}	20	20	20
h_{cp}	-	-	70
D_{bo}	20	22	24

Table 4.3 Dimensions of Endplates.

Section	0.2% Proof Stress N/mm²	Youngs Modulus N/mm²
203x203x60 UC	275	224,000
203x203x71 UC	276	222,000
203x203x86 UC	287	219,000
254x146x37 UB	294	214,000
254x254x89 UC	268	216,000
356x171x51 UB	286	205,000
305x305x137 UC	275	218,000
457x191x74 UB	285	209,000
180x15 Plate	294	221,000
180x20 Plate	291	230,000
180x25 Plate	275	208,000
200x25 Plate	265	229,000
220x25 Plate	304	211,000

Table 4.4 Summary of Tensile Test Specimens.

Figure 4.1 Test Rig Layout.



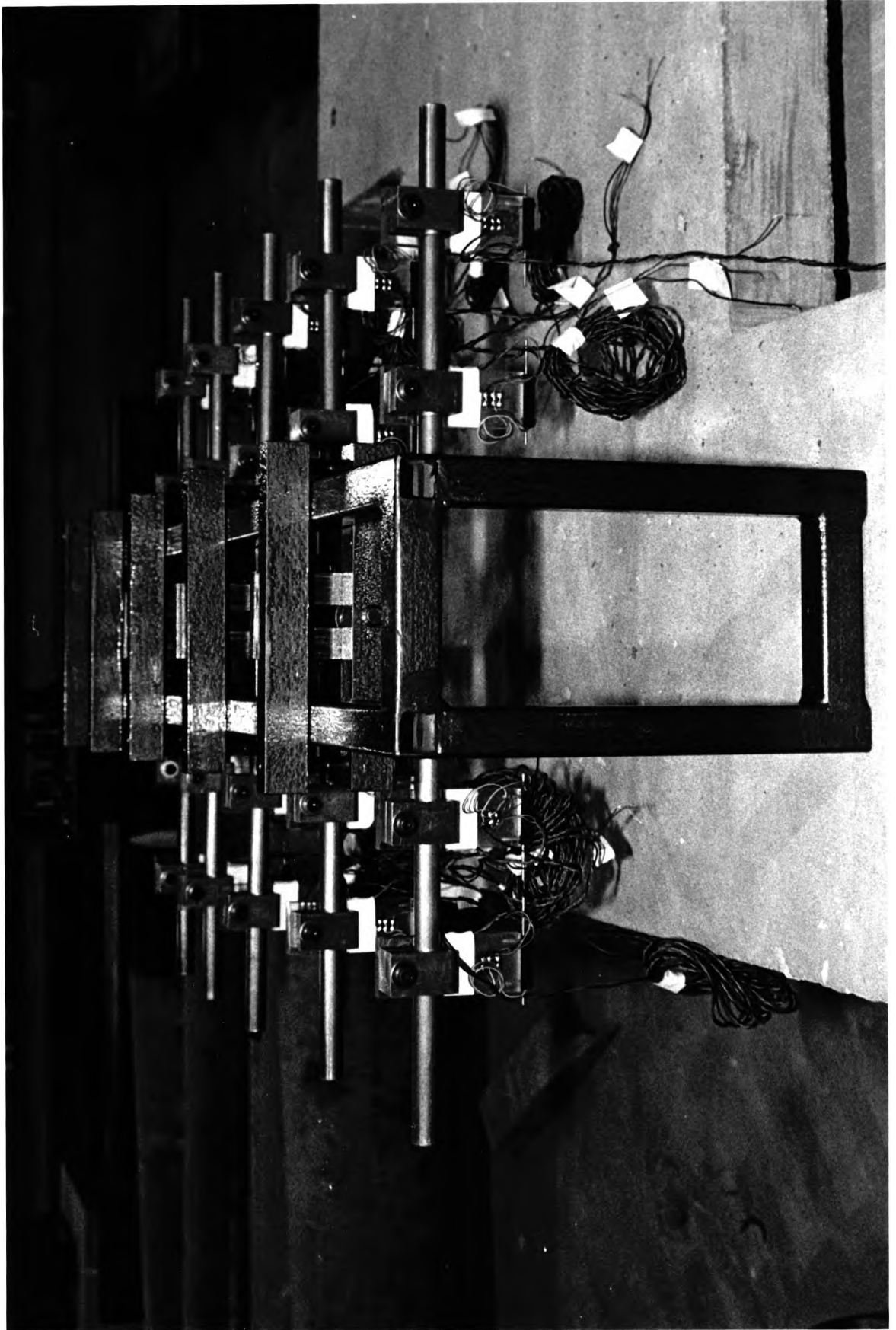


Figure 4.2 Transducer Measuring Frame.

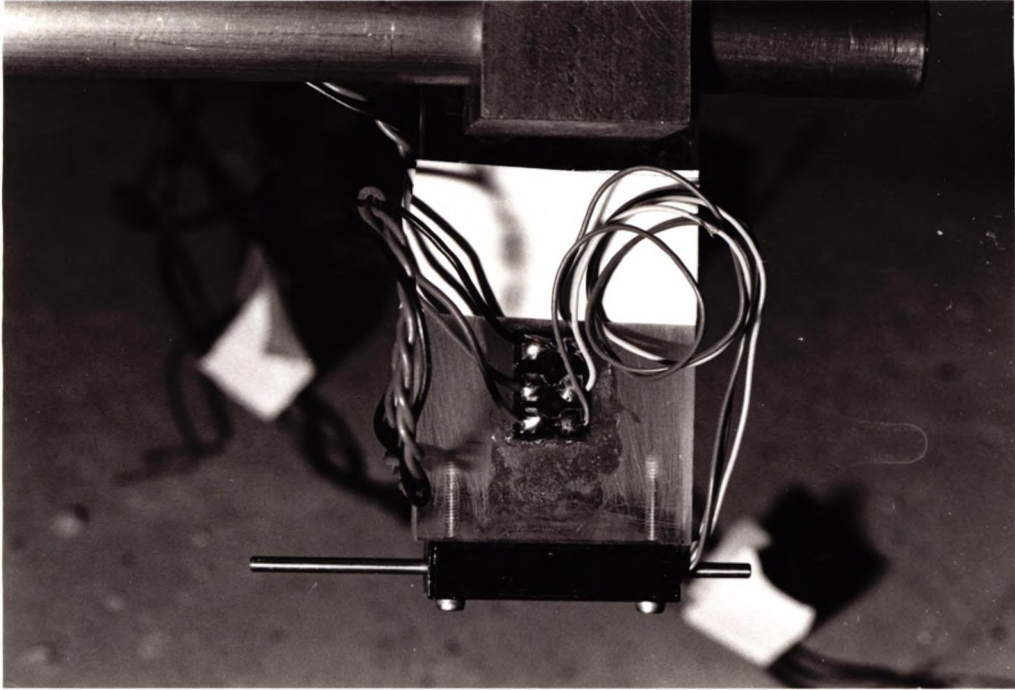


Figure 4.3 Transducer and Mounting.



Figure 4.4 Data Logging System.

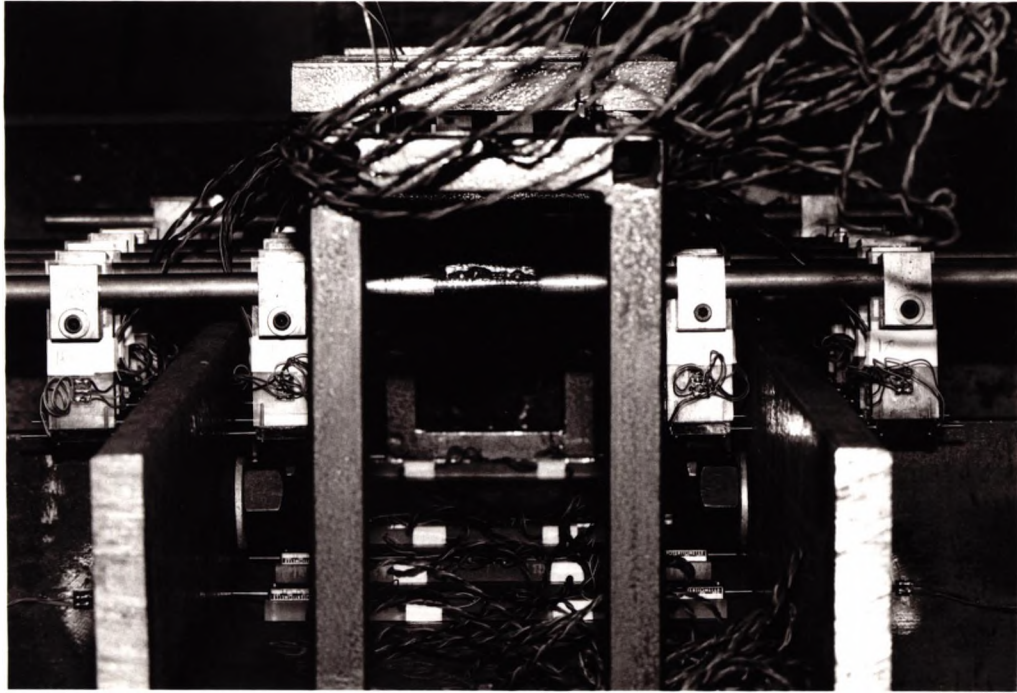


Figure 4.5 Column Web Transducer Placement.

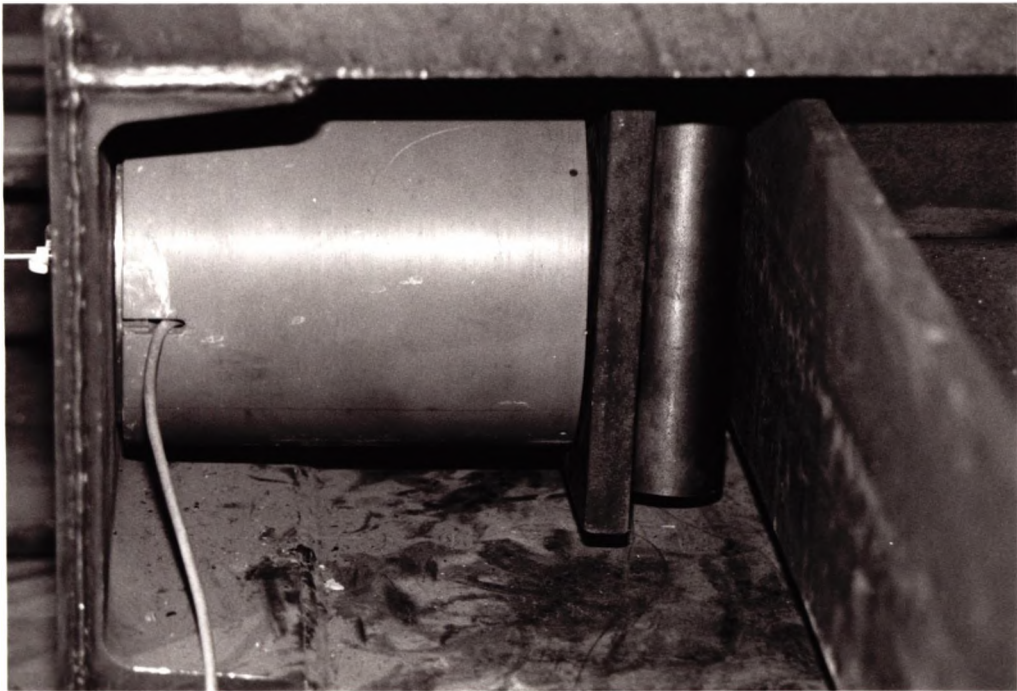
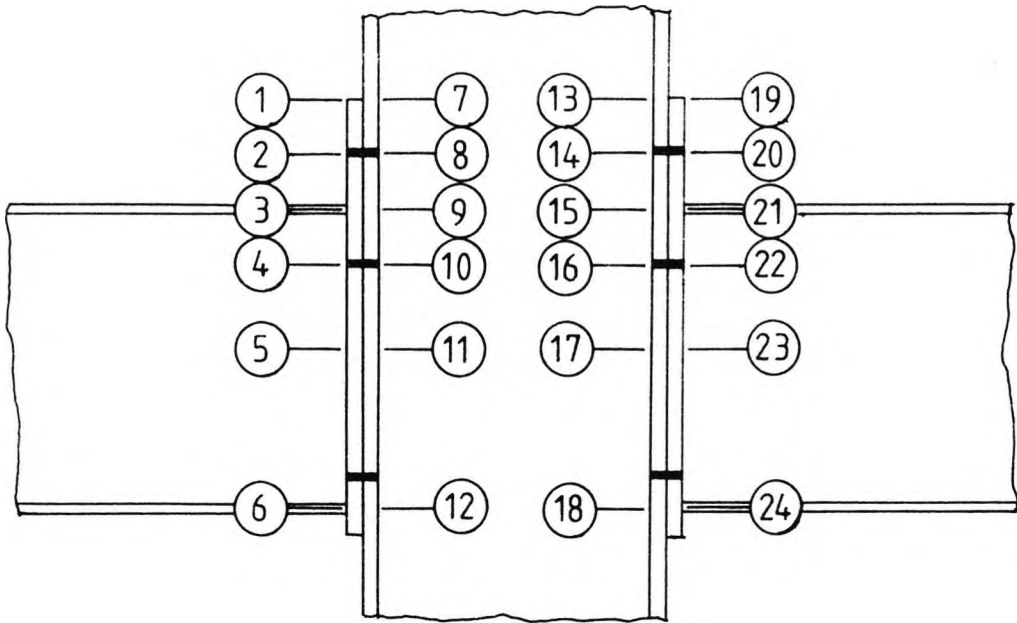
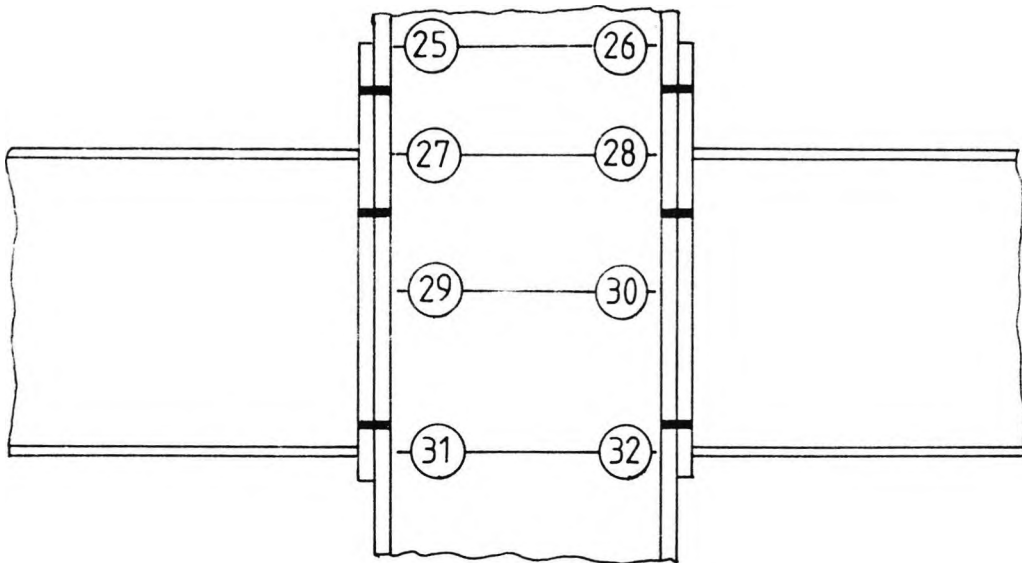


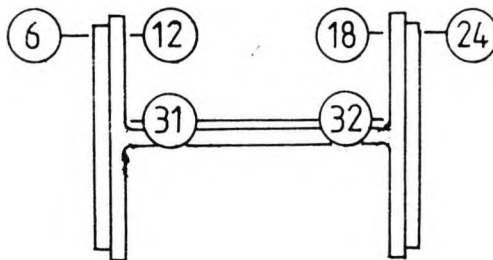
Figure 4.7 Load Cell and Roller Arrangement.



a) Endplate / Column Flange.



b) Column Web.



c) Cross-section

Figure 4.6 Transducer Positions.

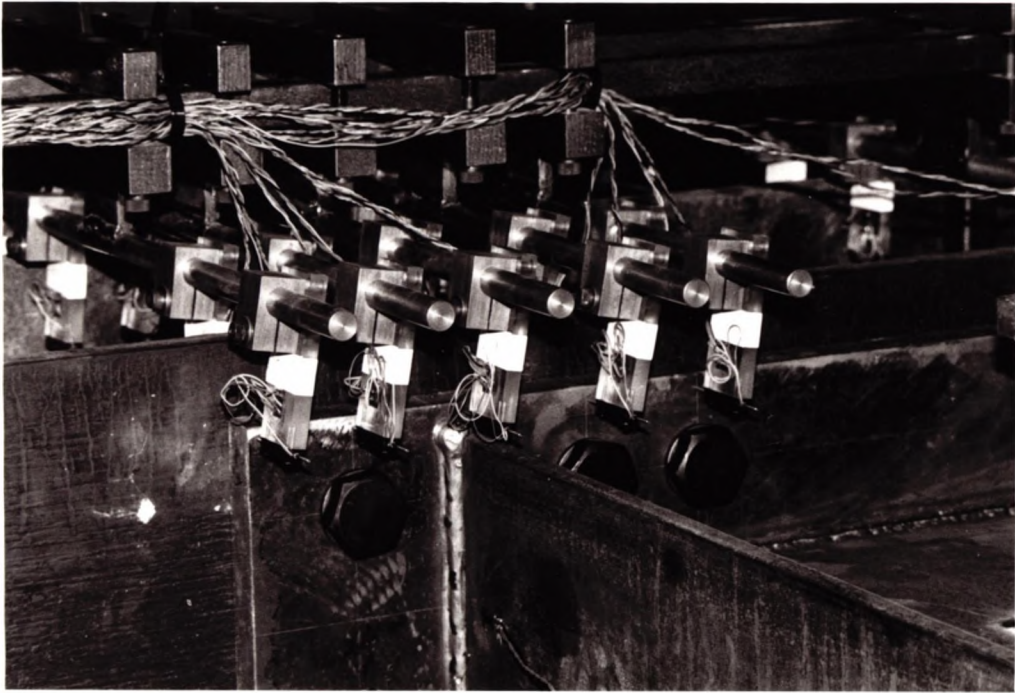


Figure 4.8 Placement of Endplate Transducers.



Figure 4.10 Deformation of Endplate at Failure (Test A1).

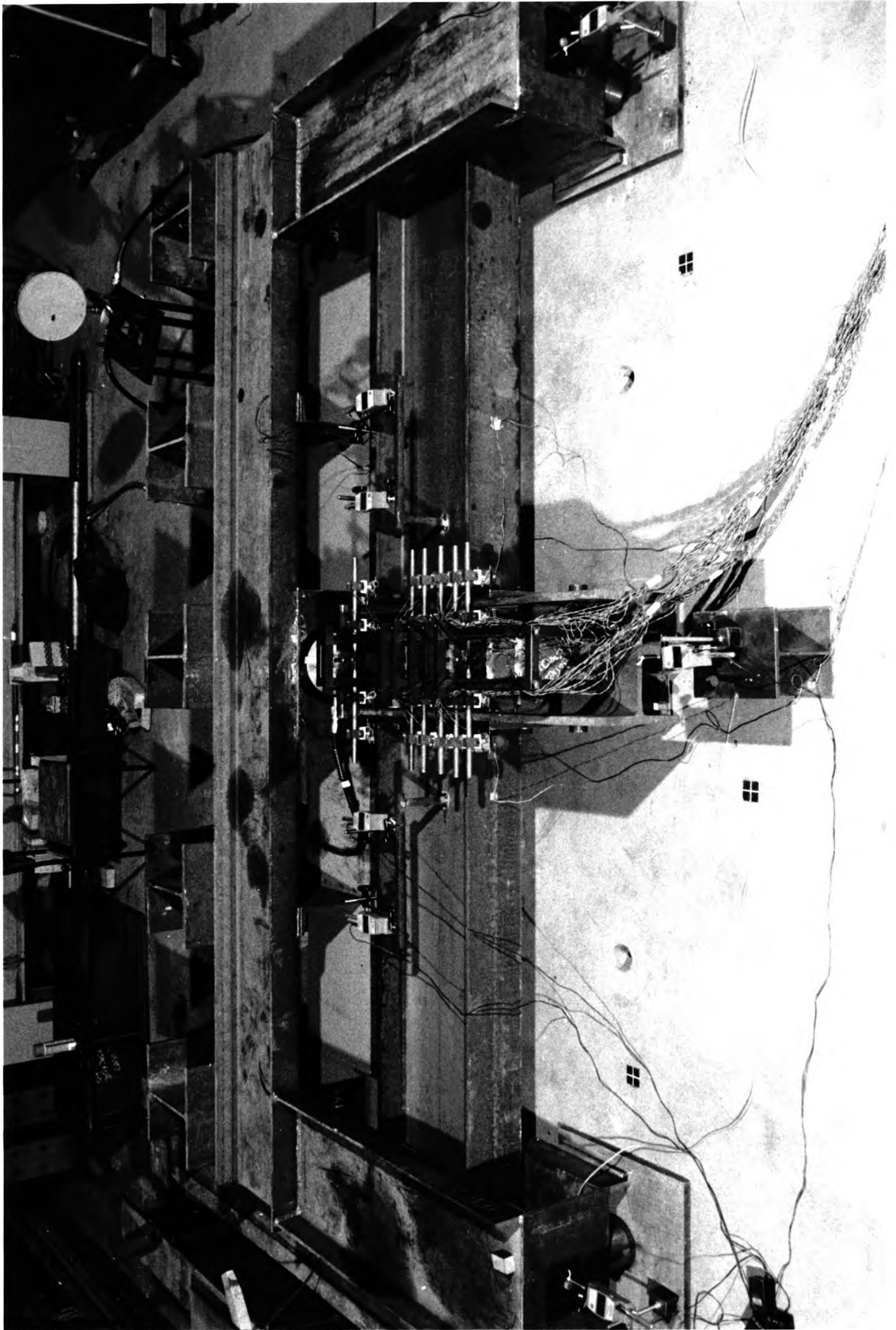
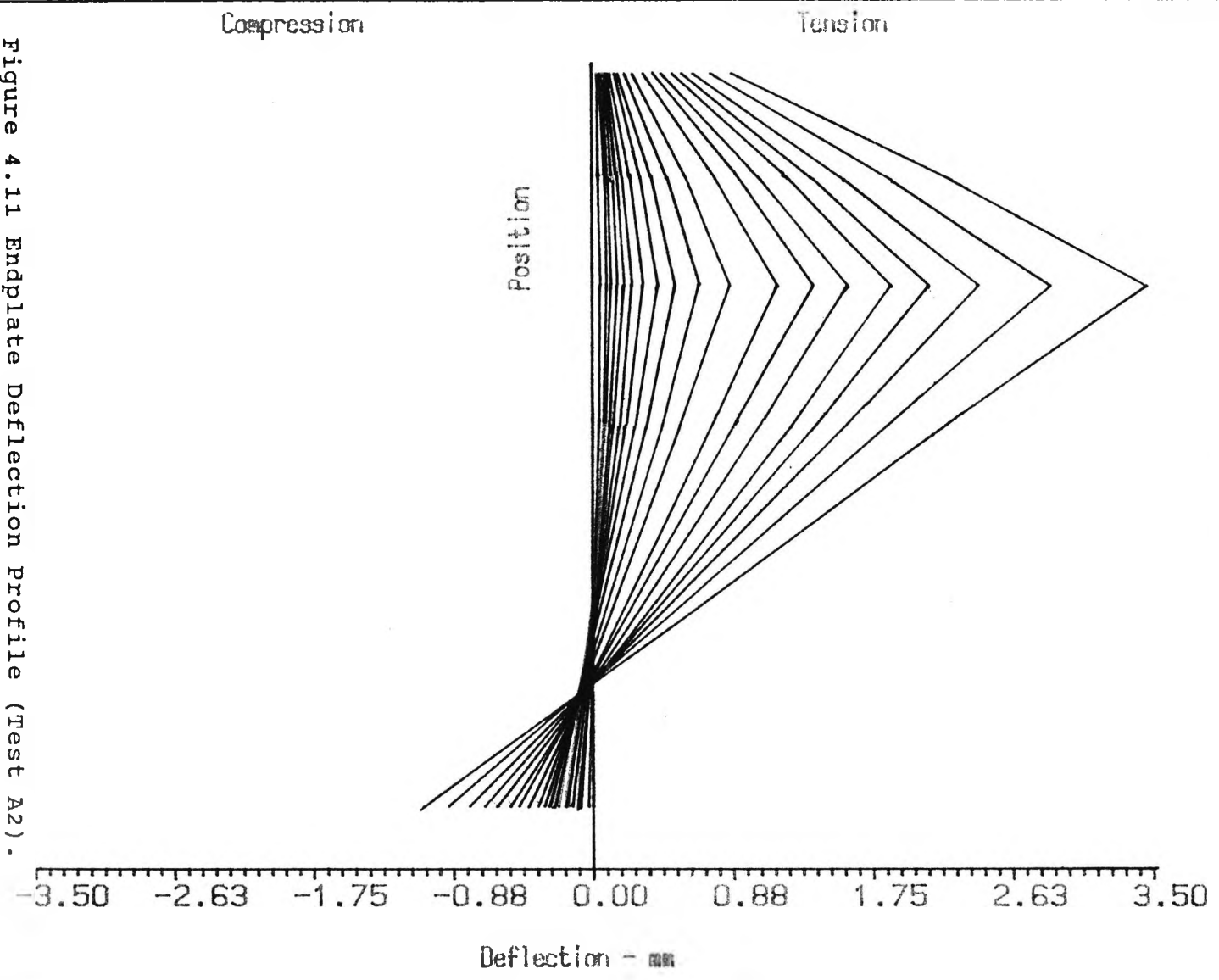


Figure 4.9 Test Set-up.

Figure 4.11 Endplate Deflection Profile (Test A2).



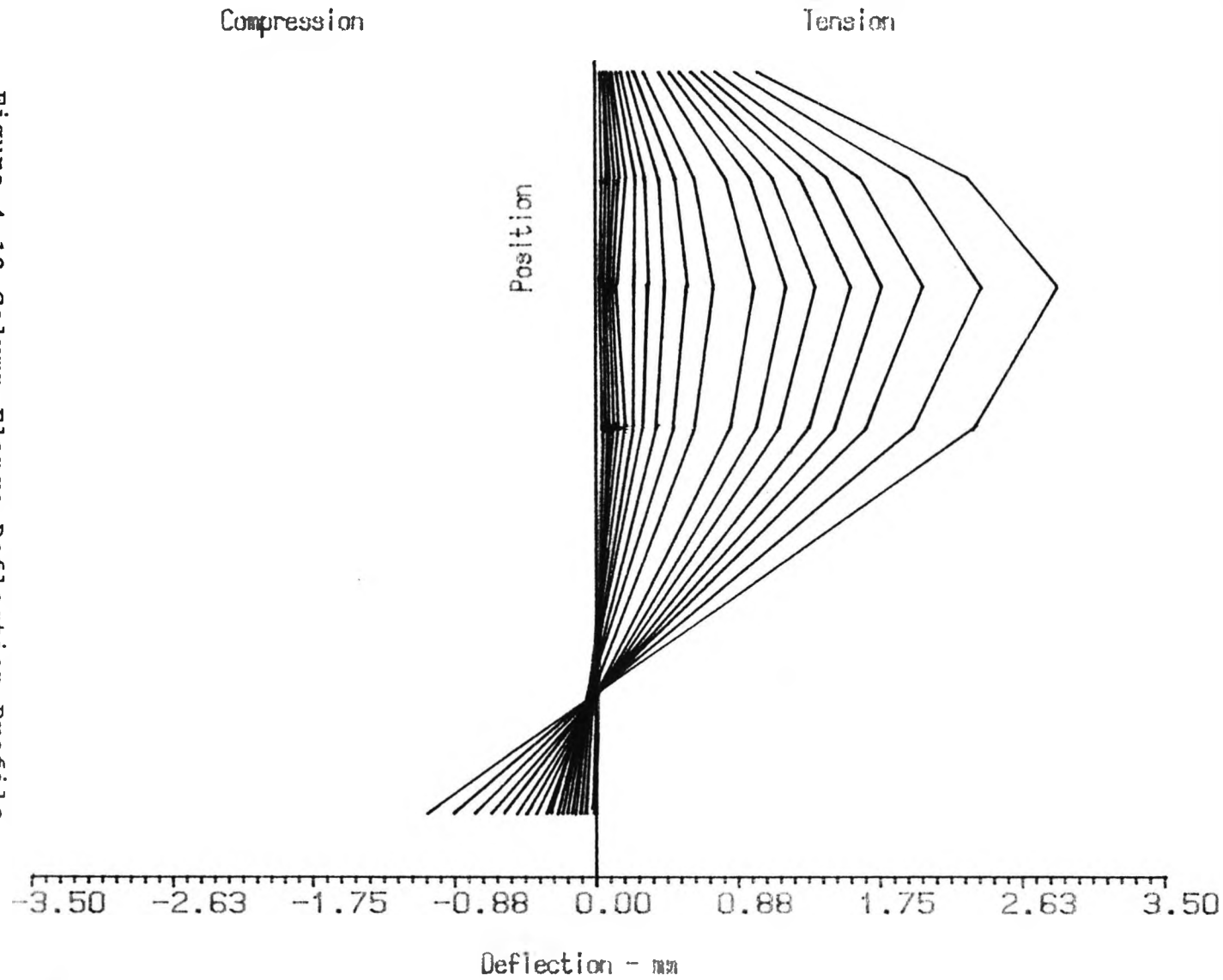
Connection Type :-
Unstiffened
Internal
Beam Size -254x146 UB37
Column Size -203x203 UC60
4 M20 Tension Bolts
Grade HSFG -Pretensioned
Endplate Thickness = 20 mm

ENDPLATE DEFLECTION

Test A2

Figure 4.12 Column Flange Deflection Profile.

138



Connection Type :-
Unstiffened
Internal
Beam Size -254x146 UB37
Column Size -203x203 UC60
4 M20 Tension Bolts
Grade HSFG -Pretensioned
Endplate Thickness = 20 mm

COLUMN FLANGE
DEFLECTION

Test A2

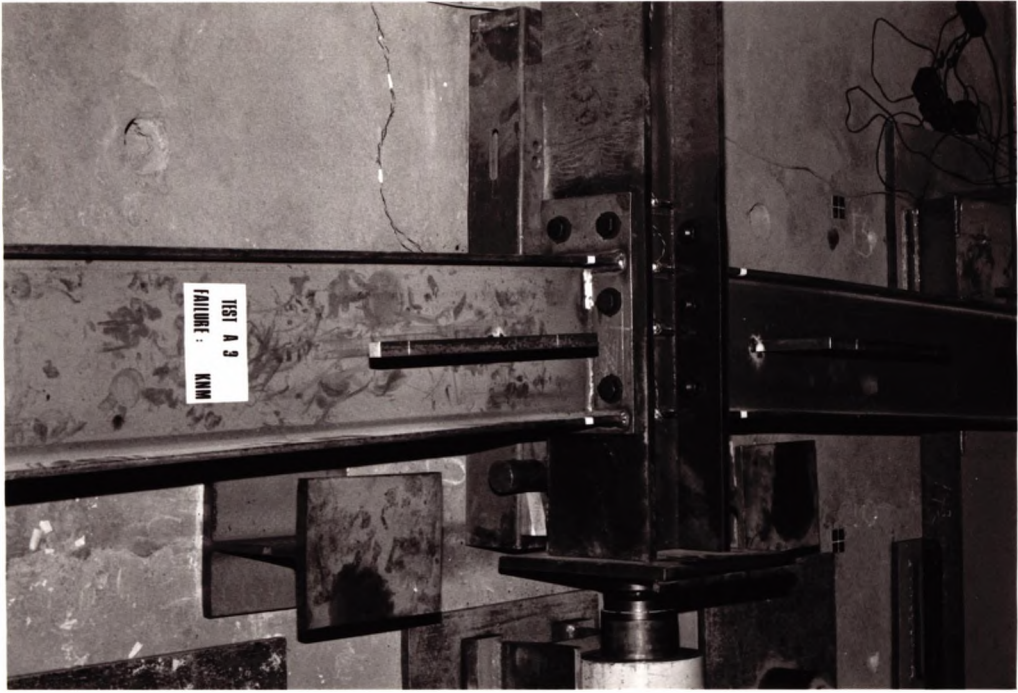


Figure 4.13 Lateral Deflection at Failure (Test A3).

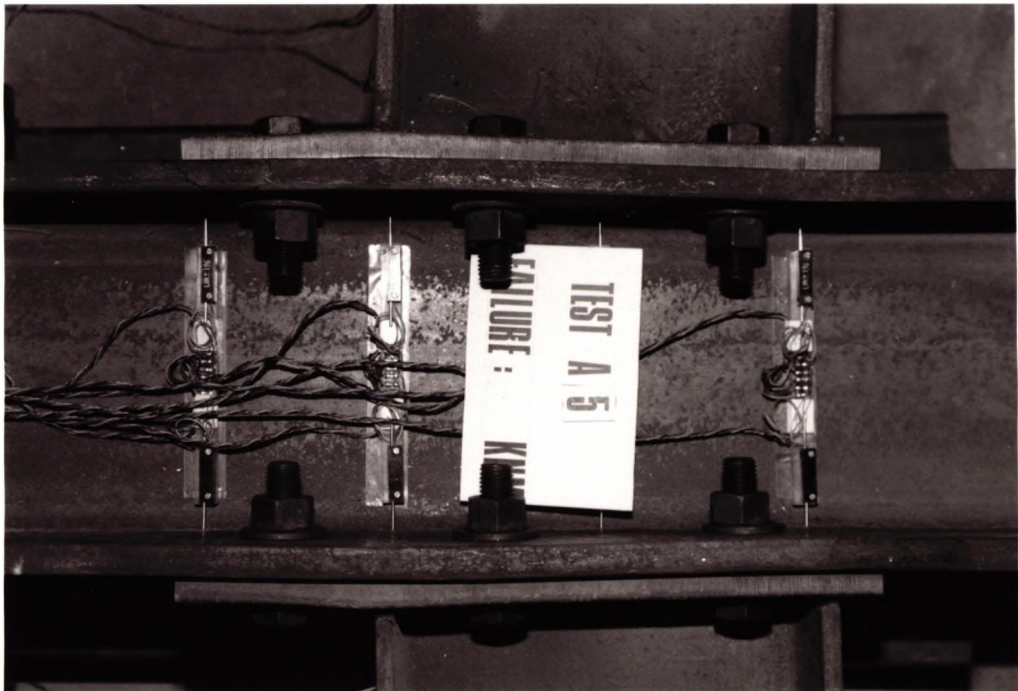


Figure 4.14 Endplate Deflection at Failure (Test A5)

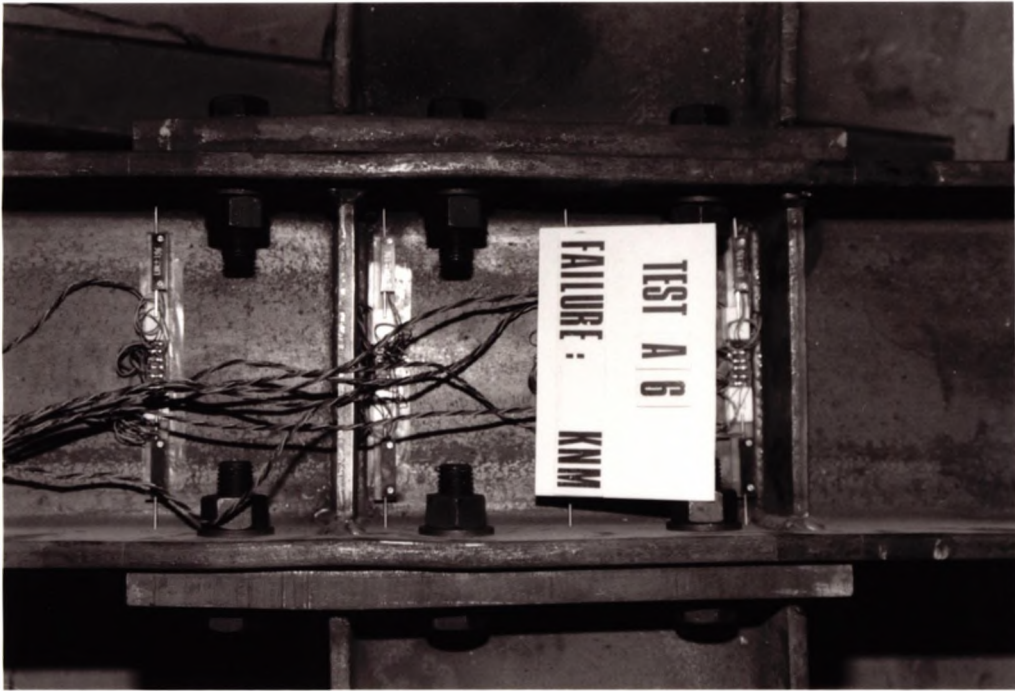


Figure 4.15 Separation of Endplate and Column Flange (Test A6)

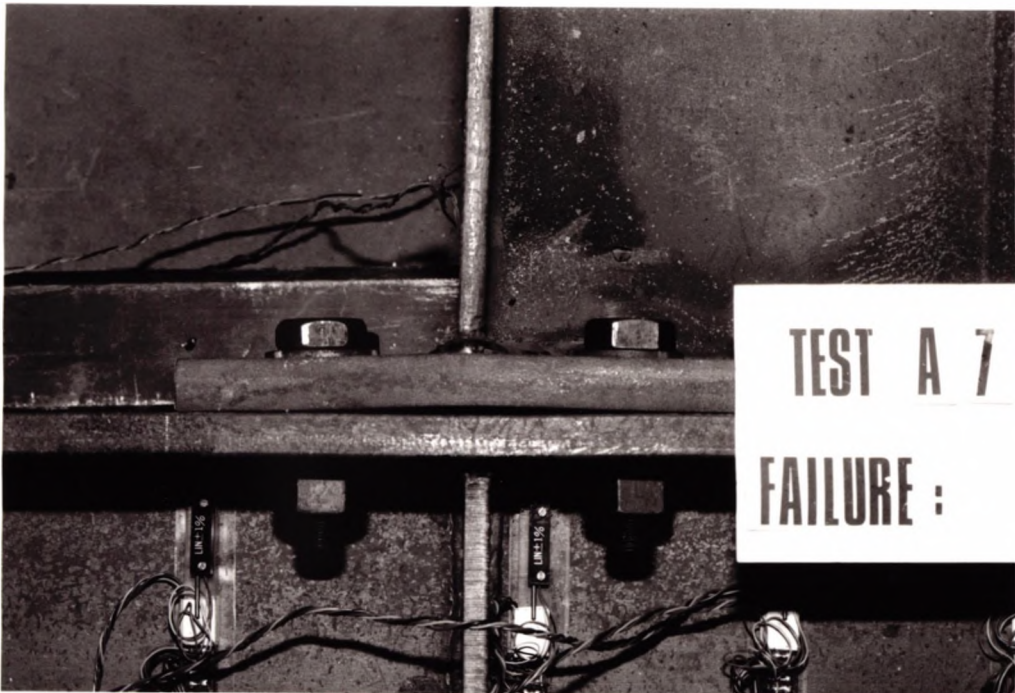


Figure 4.16 Separation at Failure.



Figure 4.17 Deflection of Test A8 at Failure.



Figure 4.18 Beam Tension Flange Weld Failure (Test B1).



Figure 4.19 Weld Cross-section showing Slag Inclusion (Test B1).



Figure 4.20 Deflection of Endplate and Column Flange at Failure (Test B2).



Figure 4.21 Proximity of Endplate to Specimen End (Test C1).



Figure 4.22 Endplate Deflection at Failure (Test D1).

CHAPTER 5

COMPARISON AND DISCUSSION OF RESULTS

5.1 Introduction.

In this chapter the results of the test program will be presented, compared with each other and then discussed. Firstly, the various methods of rotation measurement will be compared. One or a combination of the methods will be chosen to represent the moment-rotation of the connections for comparison with the predicted moment-rotation curves. Next, the underlying trends in each series of moment-rotation curves will be examined to check if the expected behaviour of each test relative to every other test in the series is obtained. Then the contribution of each component of the connection to overall rotation will be examined and discussed for each test. The predicted curves will be contrasted with the actual curves obtained and the appropriate conclusions will be drawn. Finally the predicted method will be compared with the results of similar tests from other sources.

5.2. Comparison of the Methods of Rotation Measurement.

Before presenting the results, an outline of the calculation of rotation from the test results is given. The rotation from the transducer measurements was measured in two ways. Firstly, rotation was taken as the endplate deflection at the beam tension flange transducer position plus the endplate deflection at the

beam compression flange transducer position divided by the distance between the transducer readings. Rotation was also taken as the endplate deflection at the beam tension flange transducer position plus the deflection at the column web transducer position in the compression region divided by the distance between the transducer readings.

The rotation value measured at the offset position was obtained by dividing the difference in the two dial gauge readings by their distance apart on the rotation arms. Rotation was also deduced from the central deflection of the test specimen using the method outlined in Appendix E. This is the specimen central deflection less the deflection of a simply supported beam of the same span as the specimen divided by the span length. For this purpose the span is the length of the two beams i.e the width of the column is omitted from the total specimen span.

The test curves obtained from each method of measurement are presented for each test in Figures 5.1 to 5.12. These curves are adjusted to allow for initial bedding down of the test specimen. This initial bedding down, outlined below, is demonstrated by the deflection profiles of the endplate and column flange for test D1 (Figures 5.13 and 5.14). All tests behaved similarly.

The endplate was expected to have a positive deflection at the tension flange and a negative deflection at the compression flange. Initially, the endplate and column flange had a constant compression deflection for each profile (see Figures 5.13 and

5.14). After this initial settlement the endplate and column flange began to take up their expected deflection profiles.

The initial settlement (approximately 0.25mm, in this case) was due to bedding down of the specimen at the support points. These support points are a fixed and free roller bearing respectively to make the test arrangement determinate. This arrangement allowed some initial movement at low loads. The moment-rotation behaviour of a connection in a real frame would not behave in this manner due to the restraining effect of the rest of the framework. Therefore, the initial settlement was extracted from the test measurements to give a more accurate representation of connection behaviour in real frameworks. This demonstrates the importance of considering the behaviour of test specimens carefully to ensure that the data obtained is representative of real structural behaviour.

The curves were adjusted by taking the increment at which all initial settlement was deemed to have occurred (increment 2, in this case) and making this the starting point for rotation measurements. The initial stiffness of the curve was then taken as the stiffness between this starting increment and the next increment. This initial stiffness value was then projected back to the origin to give adjusted moment-rotation curves. This procedure was adopted for all methods of rotation measurement so that a comparison between the various methods could be made.

In comparing the methods of rotation measurement several trends occurred. Firstly, the transducer rotation measurements were in agreement with one another. This was because the major contributor to overall rotation was tension deflection which was common to both methods of measurement. Generally, the rotation measured offset from the connection was greater than the rotation from other methods of measurement. It was always greater than the rotation measured by the transducers. The rotation extracted from the central deflection readings usually fell between the transducer and dial gauge methods of measurement. It was nearer the transducer deduced readings initially and nearer the latter method in the final stages of loading. This was expected as the method of determining rotation from deflection readings assumed elastic behaviour which was obviously not the case in the later stages of loading. A few anomalies did occur using this method of measurement, notably during the test with the larger beam and column sections. Generally, the central deflection method can give a good indication of the initial stiffness of a connection using test data which only presents load-deflection measurements.

An initial estimate of the offset stiffness can be made using the theory derived to extract rotation data from deflection readings (Appendix E). The initial value of offset stiffness for a 220mm offset for each test series is given in Table 5.1(a). If this value of stiffness is subtracted from the value of initial stiffness given by the dial gauge readings, an indication of the initial connection stiffness is given. It can be seen from Table

5.1(b) that the initial stiffness derived using this method lies between the initial stiffnesses obtained using the transducer readings.

The difference in the two transducer methods of measurement lies in the deflection in the compression region. The deflection at the endplate edge was always greater than the deflection at the column flange/web junction. This could be due to one of two explanations which may be given with the use of Figure 5.15. The first case is bending of the endplate and column flange about the column web, and the second case is skew deflection of the column flange. Since the specimens were supported out of plane, it is thought that the former explanation is the more likely. Rotation measurements used for the rest of this discussion will be the average rotation given by the two sets of transducer readings. This is consistent with the initial connection stiffness obtained by the dial gauge readings.

The difference in the rotation measurements at both sides of the connection was monitored during each test. The difference between the two sets of readings was negligible for both transducer methods of measurement. Therefore, average values of rotation and connection moment at both sides of the connection are presented in this thesis.

Summarising, the average of the transducer methods of measurement will be used in this thesis for the connection rotation. The transducer method is chosen as it has the advantage of being a

direct measurement of connection deformation. That is, offset stiffness does not have to be subtracted from the rotation measurements. It is also possible to directly relate the deflections of the various components at the beam flange levels to the connection rotation.

5.3. Comparison of moment-rotation curves obtained.

Before the moment-rotation behaviour of each connection is studied in depth the curve obtained for each specimen in each test series is inspected to examine its relative behaviour to each other specimen curve in the series. Two criteria will be used to judge if each connection has behaved as expected. A comparison of the initial stiffnesses of each connection in a particular group and a comparison of actual plastic moment obtained by each test connection with the plastic design moment for that connection.

The moment-rotation curves for the unstiffened connections in test series A are given in Figure 5.16. The general trend expected was that the curves for tests A3 (larger column section) and A4 (thicker endplate) should be above the 'design' connection curve, test A8. Tests A2 (smaller column section) and A5 (thinner endplate) should fall below the test A8 curve. This general trend was obtained.

The initial stiffnesses for the unstiffened connections in test series A fell into a very narrow range, 50000 - 70000 kNm/rad.

This may seem a substantial range, but near the rigid axis of the moment-rotation axes a small change in slope manifests itself as a large change in the numerical value of initial stiffness. The effect of an increase in initial stiffness over this range on frame behaviour will be discussed in the next chapter.

The main difference in the curves lies in the points at which each starts to decay. The three connections which were designed to carry the plastic moment of the beam (128 kNm) all behave similarly and all attain the plastic moment of the beam before excessive deviation from elastic behaviour occurs. The two connections in which component sizes were reduced from the design value also attain the plastic moment of the beam, but this was due to the strain hardening stiffness of each connection. Both curves begin to decay substantially before the plastically designed connection curves. These facts indicate that the design criteria used can accurately predict failure moment. An increase in component size does not result in a substantially stronger connection. This is expected as beam section failure is the failure criterion for an adequately designed connection.

The effect of increasing and decreasing endplate and column flange thickness around the 'design' value is outlined more clearly in Figures 5.17 and 5.18 respectively. In both cases the initial stiffness of the 'design' connection (test A8) is similar to the initial stiffness of the oversized connection (tests A3 and A4). Test A8 can also be compared with test D1, which had a much larger column section (Figure 5.19). Again the

initial stiffness of test A8 is similar to that obtained in test D1. This indicates that the test A8 connection was slightly stiffer than expected when compared with the other connection curves.

The moment-rotation curves for the stiffened connections in test series A are shown in Figure 5.20. The initial stiffness of the test A7 curve is greater than the test A6 curve, which was expected. What is surprising, though, is that the plastic moment obtained by the test A7 curve is far greater than the test A6 curve. This is most likely due to strain hardening in the beam as the yield stresses of the different UC's are similar (see Table 4.4).

The stiffened connections are compared with their relevant unstiffened connections in Figures 5.21 and 5.22. The stiffening appears to have little effect on the initial stiffness of each connection. The plastic moment obtained in each test is affected by the stiffening although the plastic moments of tests A7 and A8 were expected to be similar as the beam plastic moment was expected to be the failure criterion for both connections. The fact that the plastic moment of test A7 is significantly greater than that of test A8 is further indication that strain hardening took place in test A7.

The stiffened connections in test series B and C both outperform their relevant unstiffened connections (Figures 5.23 and 5.24). This was expected although the moment-rotation curve for the

unstiffened test C connection was substantially lower due to column compression flange instability. The stiffening in both cases had an effect on initial stiffness. Both stiffened connections were monitored on unloading. The final test points on unloading are the isolated points in figures 5.23 and 5.24. Each test had an unloading stiffness approximately equal to the initial stiffness of the connection.

An overall view of all the unstiffened and stiffened connections in all the test series is given in Figures 5.25 and 5.26 respectively. The range of initial stiffness over all the connections tested is 50,000 to 260,000 kNm/rad. It can be seen that all connections vary significantly from the rigid assumption.

Summarising, the initial stiffness for a particular size of connection falls within a narrow range despite changing the geometry of the connection. The design criteria used for the plastic moment of the connection are satisfactory. Overall the connections behaved as expected.

5.4 Component contributions to rotation

By adopting the transducer method of rotation measurement it is possible to relate the deflections at the beam tension and compression flanges directly to rotation measurement. From equation (3.5)

$$\theta = \frac{\Delta_u + \Delta_l}{D_{bf}}$$
$$\Delta_u = \Delta_{ep} + \Delta_{cf}$$
$$\Delta_l = \Delta_{wc}$$

(5.1)

If the relative deflections are plotted against beam end moment then the relative contribution of each component at any given load can be seen. These plots are given in Figures 5.27 to 5.38 for each test. While these plots give a good visual indication of which component is contributing most to connection rotation in any particular test, they do not give a good indication of the contributions of the components for comparison between different tests.

Recalling the theory, it can be seen that the deflections are derived as a function of the beam flange forces (equation (3.55)). If the deflection of any component is divided by the beam flange force, an indication of the flexibility of each component is given for comparison with other tests.

From equation (3.4)

$$F = \text{Beam flange force} = \frac{M}{D_{bf}}$$

(5.2)

The flexibility of each component is given by

$$f_a = \frac{\Delta_a D_{bf}}{M}$$

(5.3)

where f_a = the flexibility of component a

The component deflections that contribute to overall deflection are now defined. The tension region deflection is given by the transducer reading at the endplate/beam flange junction. This is made up of endplate, column flange and, possibly, column web tension deflection. The difficulty of defining where column flange deflection ends and endplate deflection starts has been outlined in Chapter 3. This difficulty is due to the overlapping of the column flange and endplate deflections (see Figure 3.8). The theoretical model calculates the column flange contributions at the assumed contact points between the column flange and endplate. In reality, these could be anywhere due to the initial lack of fit of the column and endplate. After initial settlement of the specimen, however, the approximate position of the contact points should be known. The contact points should be near the endplate corner above the tension flange and near the endplate

edge between the beam centreline and the tension bolt below the tension flange. The column flange deflection will be taken as the average of the column deflection at position 7 (Figure 4.6) and the column flange between the beam centreline and the second bolt (positions 10 and 11). The deflection will be calculated theoretically at the same assumed points for comparison purposes.

The contribution of the column web in the tension region was found to be negligible for all tests (less than 0.2mm at ultimate load). Tension deflection was, therefore, assumed to be made up of endplate and column flange deflection only. Endplate deflection was taken as the total tension deflection less the assumed column flange deflection.

The deflection in the compression region is due to the column web and the column flange deflection. For comparison purposes both these deflections have been plotted in Figures 5.27 to 5.38. It should be noted that column flange deflection includes column web deflection. All deflection values are average values of the corresponding values on either side of the connection.

Before discussion of the component contributions of each test it would be beneficial to give a qualitative view of the overall load-deflection behaviour of the extended endplate connection. Firstly, the mechanism of the load transfer between the various components of the connection will be considered. For convenience it is best to regard the load as being transferred in two separate regions, tension and compression. In reality the

boundary between the two regions will be indistinct. Secondly, the load deflection behaviour will be discussed throughout the load history of the connection.

The moment at the end of the beam can be considered as a couple acting at the two beam flanges. In the tension region this flange force is transferred to the column flange in two ways. Firstly via the bolts and endplate bending and secondly directly by prying action. The majority of load is transferred through the bolts to the column flange. Column flange bending leads to direct transfer of load into the column web from bending moment and shear force action at the column web root fillet.

Load transfer in the compression region is a lot simpler. The flange force acts directly onto the endplate at the beam compression flange level. Load is dissipated through the endplate, column flange and root fillet to the column web. From experimental observation some load is transferred to the column web via the endplate and column flange bending (see Figure 5.15).

The load-deflection behaviour of the connection can be split into three distinct parts. An initial elastic stage, a transitional stage and a strain hardening stage. The initial elastic stiffness of the connection is governed by the endplate/column flange deflection in the tension region along with column web compression (for internal connections). The deflection of the endplate/column flange component is governed initially by component geometry and the regions of contact between the

endplate and the column flange. Experimental observations show that even in the elastic portion, connection behaviour deviates from a linear path. This is due to the contact positions between the endplate and column flange changing in the initial loading period. From their initial state the endplate and column flange gradually bend into the deflected shape shown in Figure 3.8. The regions of contact between the endplate and column flange move away from the beam tension flange to the extremities of the endplate. This leads to the connection stiffness decreasing while material behaviour remains essentially elastic. This has been explained by some observers as a gradual change in the centre of rotation of the connection.

The transitional stage starts with yielding in the weakest component of the connection. As this component yields it sheds moment to the unyielded parts of the connection. This increased load on the other components leads in turn to them yielding and the connection reaching its plastic or strain hardening phase.

The strain hardening phase is reached when one component has fully yielded. The strain hardening stiffness is simply the contributions due to the strain hardening component of this section plus the stiffness of any unyielded components of the connection. This phase lasts until fracture occurs in some part of the connection. It should be noted that it is assumed, in this study, that bolts and welds have adequate strength and, therefore, failure of either does not occur.

The above description of the load-deflection behaviour is obtained from theoretical and experimental observation. The component contributions to connection rotation of each test will be discussed within this framework.

The component flexibilities which may be used as a measure of contribution to initial stiffness and the component contribution deflections at yield are shown in Tables 5.2 and 5.3 respectively. From Appendix G, it can be seen that the precision of estimating each flexibility contribution (equation (5.3)) is of the order of $\pm 0.06 \times 10^{-6}$ mm/N while the precision of the deflection readings are ± 0.01 mm. The values of flexibility of each component, therefore, are given to two decimal places only. Some values are of the same order as the initial precision of these measurements and therefore their accuracy must be questioned. However, the flexibility contributions are useful as they give an overall view of the relative contributions of each component to connection stiffness.

The deflection values in Table 5.3 are taken at the start of yield in the beam section. From the strain gauge versus load readings in Appendix F, it can be seen that beam yield starts at a consistent value of 135 kNm for test series A and D. Unfortunately the two unstiffened connections in test series B and C did not reach beam failure. The values for these test series are taken at the final measurement or beam yield, whichever is the lower.

The component contribution versus load relationships presented in Figures 5.27 to 5.38 can be split into two types. These usually correspond to whether tests are unstiffened or stiffened. Test D1, although unstiffened, falls into the latter category as the column section is much stiffer than the beam or endplate. In each type of test there is considerable deflection of one or more of the connection components before initial yield of the beam. This is evident even in connections which are designed not to yield before the plastic moment of the beam.

In unstiffened tests all components tend to yield gradually throughout the loading period, test A8 (Figure 5.33) being a typical example. This makes it difficult to ascertain which component begins to yield first. The gradual yielding behaviour is probably due to the changing interaction between the components of the connections as outlined previously. Stiffened connections behave differently to unstiffened connections in that the only component that decays significantly is the endplate deflection. The other components deflect, but only linearly with load. This is expected as the stiffeners strengthen the column by offering an alternative load path into the column in the tension region and by offering restraint against out of plane instability in the compression region. The exception to this is test A6 where column flange tension deflection decays with load. This could be due to the stiffeners not being the full depth in this connection specimen.

If the contributions to initial stiffness are consulted (Table 5.2), it can be seen that it is difficult to establish a trend in the endplate and column flange contributions to deflection in the tension region. For example, it was expected that the much thicker endplate test(A4) would result in a much reduced endplate contribution than the much thinner endplate test(A5). The same trend was expected of the test with differing column sizes. That this is not the case must be due to

- a) the assumptions made regarding the endplate and column flange contact positions in order to maintain consistency in the analysis of the results of each test
- and b) the interaction between the endplate and column flange in the tension region masking the expected trends.

Due to the difficulty of separating the endplate and column flange contributions to the initial tension region contribution, this quantity will be considered alone to see if any trends can be determined. The value of the initial tension region flexibility is also included in Table 5.2. If the results for test series A are considered, it can be seen that the expected trends do occur. Test A3 (thicker column flange) is less flexible than test A2 (thinner column flange) and test A4 (thicker endplate) is less flexible than test A5 (thinner endplate). The stiffened connections are both less flexible than the unstiffened connections tests A2-A5. The only anomaly occurs in the results for test A8 which as mentioned previously is a lot stiffer initially than expected.

The column web compression contributions are also given in Table 5.2. These results are more consistent with each other than the tension region contributions especially the contribution of the column web alone. This is due to the load path into the compression region being fixed while the deflections in the tension region are subject to varying and unknown initial contact conditions.

For unstiffened connections each component contribution decays gradually from the initial conditions (see Figures 5.27-5.30, 5.33, 5.34 and 5.36). It was expected that each component curve would decay at varying rates depending on component stiffness. The trends here do show some consistency in that deflection component curves for test A3 (Figure 5.28) decay at a slower rate than those of tests A2 and A8 (Figures 5.27 and 5.33) and that deflection component curves for test A4 (Figure 5.29) decay at a slower rate than those of test A5 (Figure 5.30).

At yield it can be seen that by far the biggest contributor to deflection is tension region deflection, typically between 70 and 90% of total deflection at yield (Table 5.3). If test series A results are considered the deflections at yield are as expected relative to each other. Tests A2 and A5 (thinner column flange and endplate respectively) deflections are greater than test A8 deflection, while tests A3 and A4 (thicker column flange and endplate respectively) deflections are lower. Each stiffened connection deflection (tests A6 and A7) is less than its relevant unstiffened connection deflection (test A2 and A8 respectively).

Test series B, C and D also behave as expected, the unstiffened deflections being far greater than the stiffened connections.

Overall it is evident that it is difficult to break connection behaviour down into component behaviour, especially in the tension region in the initial stages of loading. However, the overall behaviour will still be able to be reasonably predicted as the local variation in component stiffness will be averaged out across the connection by the associated redistribution of the load.

5.5 Comparison of the method of prediction with the experimental results.

5.5.1 Introduction

The comparison of the method of prediction with the experimental results can be split into two parts. Firstly, a comparison of the model parameters calculated and the components which make up those parameters with the results obtained and secondly, a comparison of the overall prediction method with the overall behaviour. Before a comparison of either can be carried out, it would be useful to know the model parameters which give the best fit to each experimental curve.

5.5.2 Curve fitting of experimental results

The effect of varying each parameter in the model on the overall moment-rotation behaviour is outlined in Figure 5.39. A fuller description of the effect of each parameter is given in Yee's thesis (13). The 'best' fit curves for each test, which were found on an iterative basis, are shown in Figures 5.40 to 5.51 along with the parameters used. The initial stiffness value corresponds to the initial value found from the test results. The plastic moment and strain hardening stiffness are then adjusted until the best fit possible is obtained. Once these parameters have been found the semi-empirical factor, c , is introduced if needed.

The parameter, c , was introduced by Yee as it was noticed that even if the initial stiffness of the connection derived from the experimental results was input to the model the curve still decayed too rapidly. Yee introduced a linear factor which increased the initial stiffness with rotation. Therefore, the effective initial stiffness at any rotation value was given by

$$K' = K_i + c\theta$$

(5.4)

The need for Yee's adjustment of initial stiffness with rotation can be explained by referring back to the component contribution curves. The model is obtained by assuming that the stiffness of the curve decays exponentially between two predetermined values,

which are the initial and strain hardening stiffnesses of the connection. If the contributions of the various components to total deflection and hence stiffness are observed in Figures 5.27 to 5.38, it can be seen that each component contribution decays at substantially different rates. Therefore the parameter, c , can be considered as being introduced to control these varying rates of decay.

Satisfactory results were obtained by Yee using the above approach but if the Figures 5.40 to 5.51 are consulted one of the limitations of this model can be seen. The initial stiffness of the curve is modelled correctly and so is the strain hardening phase. However, the transition phase is difficult to obtain precisely. Here an averaging of the curve in the transition phase is adopted for some curves by adjusting the c parameter. This can be seen typically in the 'best' fit curves for tests A2, A5, A7 and A8 (Figures 5.40, 5.43, 5.45 and 5.46 respectively).

The fact that a linear relationship affecting the change of initial stiffness in the connection cannot model the transition phase precisely would indicate that a higher order relationship is required. The added complexity introduced to the model along with any additional semi-empirical parameter would offset any benefit gained by modelling the transition phase more precisely.

Overall, a reasonable fit to most moment-rotation curves was obtained using the four parameter model. The worst fit was test C2 where the strain hardening phase of the connection was not

reached. The comparison of the four parameters obtained for each model from the experimental curve with the parameters predicted by the theoretical model will now be discussed.

5.5.3 Comparison of the theoretical model with the 'best' fit curves.

5.5.3.1 Initial stiffness

5.5.3.1.1 Initial stiffness derived by the 'rigorous' method

The initial stiffness of the connection can be compared on two levels. The theoretical contributions of each component to the initial stiffness can be compared with the experimentally obtained results and the predicted overall stiffness can be compared with the experimentally obtained overall stiffness. The former could give an indication of which component deflection factor under contributes or over contributes to theoretical initial stiffness.

It was mentioned in the previous section (5.4) that the experimental individual component contributions in the tension region did not exhibit the expected trends. It would be useful to assess the individual component contributions obtained theoretically to see if changing contact between the column flange and endplate could explain these results.

The theoretical endplate and column flange components in the tension region were assessed for changing contact position. There are an infinite number of combinations of contact positions for the endplate and column flange. To reduce these, only contact positions around the edge of the endplate were considered. These assumed contact positions are shown in Figure 5.52 along with a definition of the factors used to describe them.

The changes in component contribution and initial stiffness (assuming compression components are constant) with varying contact position are given in Tables 5.4 to 5.17 for each test. Referring to Figure 5.52, the cases examined for each test are

- a) varying contact position along the top of the endplate (varying r) with varying depth of the tension region (varying f_k)
- and b) varying the contact position down the top side of the endplate (varying a_{ep}) with constant depth of the tension region.

Test series C was analysed using a four and a six bolt model for the connection. The values given in Tables 5.4 to 5.17 are flexibility values which are defined in section 5.4.

It is assumed that if the contact position is changed across the width of the endplate (varying r) then it changes for both contact points. A change in contact point between the top edge

of the endplate and the boltline above the tension flange is achieved by simply reducing the ' a_{ep} ' dimension of the endplate (see Figure 5.52).

If Tables 5.4 to 5.17 are examined it can be seen that as the point of contact below the beam tension flange moves down the endplate (increasing f_k) the stiffness decreases. Most of this decrease is due to an increase in endplate flexibility over column flange flexibility. This is borne out in the experimentally obtained component contribution versus moment relationships where endplate deflection decays more rapidly than column flange deflection.

It can also be seen that although the overall tension region contribution does not vary that much with changing contact position, the ratio of column flange contribution to endplate contribution can vary quite rapidly. For example in, Table 5.4(b), reducing a_{ep} from 50mm to 30mm results in a change in overall tension contribution of 4% but the corresponding change in the ratio of endplate to column flange contribution is from 1.5:1 to 1:1.5 respectively. Therefore, varying contact position can easily account for the results obtained in Table 5.2.

If the variation of initial stiffness with the assumed contact positions is observed it can be seen that for each test there will be a particular configuration where the flexibility of the endplate/column flange subassembly is a minimum. These contact

points are not necessarily at the extremities of the endplate i.e. at the corner position. The minimum flexibility of the subassembly occurs when the value of f_k is a minimum. This minimum value is the distance below the beam tension flange to just below the first boltline (see figure 5.52). With f_k maintained at a minimum, parameters 'r' and a_{ep} can be varied until the minimum flexibility is found.

The parameters, r and a_{ep} were varied and the results obtained are outlined in Tables 5.4 to 5.17. From these results the overall trend of varying the relevant parameters on initial connection stiffness can be obtained. It should be noted that the exact position of minimum initial connection flexibility will be somewhere between the parameter values considered in tables 5.4 to 5.17. Generally, for unstiffened connections the maximum initial connection stiffness occurs when $r = 1.0$ and a_{ep} lies somewhere between 0.5 and 1.0 times its full value. For stiffened connections, the maximum initial stiffness occurs when parameter, r , lies somewhere between 0.8 and 1.0 with a_{ep} equal to its' full value.

This behaviour agrees with the behaviour observed by Zoetmeijer (7) (Figure 3.9) in his work with t-stubs and column flanges of varying relative rigidities. For t-stubs less stiff than the column flange, the prying force was positioned on the top of the t-stub and for t-stubs stiffer than the column flange, the prying force was positioned between the top of the t-stub and the first boltline at the side of the t-stub.

This behaviour also concurs with theoretical work carried out by Ioanniddes (10) who conducted a series of finite element studies to predict the behaviour of endplate and column flange interaction. Ioanniddes joined two plate models with springs between all coincident node points. By applying an appropriate load, Ioanniddes iterated until the contact configuration of the two plates was achieved. These configurations for a "thin" and "thick" endplate are shown in Figure 5.53. It can be seen that the contact positions obtained agree with the positions assumed to give minimum flexibility in this study.

If Tables 5.13-5.14 and 5.16-5.17 are consulted the difference in calculating initial stiffness utilising a four or six bolt model can be seen. Small differences in stiffness for this size of connection result in large numerical differences and, therefore, there is little difference between the four and six bolt models. The stiffening effect of the extra bolt is offset by the added flexibility of the extra length of endplate assumed to be acting in the tension region. It is considered, therefore, that a four bolt model will still be valid for initial stiffness calculations of connections with six bolts around the beam tension flange. This is reasonable since the extra layer of bolts is added for extra strength near the plastic moment of the beam and, therefore, would have little initial effect.

The experimental values for the overall tension region contribution along with the minimum theoretical tension region contribution from Tables 5.4-5.17 is given in Table 5.18.

Generally, the theoretical model tends to overestimate overall initial tension flexibility, although some results showed good agreement, notably tests A3, A4, B1 and B2. None of the results show good agreement on the basis of individual contributions to tension deflection for the reasons outlined previously. The six bolt model for test series C shows marginally better results than the four bolt one, although it should be noted that the results of test C1 are dubious because of the column flange instability in the compression region.

In the compression region, the individual contributions of the web and flange are given in Table 5.19 along with the theoretical web compression. Also included in the table is the theoretical value for web compression for stiffened connections based upon the theory outlined in section 3.2.4. It is apparent that much better agreement is obtained between experimental and theoretical column web behaviour than experimental and theoretical tension region behaviour. This is due to knowledge of the exact compression contact region.

The column flange compression component is a lot more difficult to obtain theoretically. All load is assumed to pass directly into the column web. In reality some load must pass into the column web via column flange bending. The exact load distribution across the section will not be known, but the majority of the compression flange force should pass into the much stiffer web. Therefore, it is proposed to ignore column flange deflection theoretically in the compression region. The effect

of this will be offset by the slight overestimation of the theoretical tension component.

Summarising, the theoretical web compression deflection contribution to initial stiffness compares well with experimentally obtained values. The theoretical tension region component tends to overestimate tension deflection. From the comparison of the theoretical and experimental results, the tension component will be assumed to be that defined by contact points at minimum f_k below the tension flange and at the corner of the endplate above the tension flange i.e. assuming that $r = 1.0$ and a_{ep} is its full geometrical value. This contact position is chosen because the overall effect of the contact position on the overall initial stiffness has little effect for the stiffness range of the extended endplates considered in this study. This will be demonstrated in chapter six when the effect of changes in the initial stiffness in the extended endplate connection stiffness range on overall frame behaviour will be examined.

If these assumptions are applied to the theoretical model to calculate initial stiffness for each test then the values shown in Table 5.20 are obtained. These show reasonable agreement with the experimentally obtained values. It should be noted that the theoretically obtained compression flexibility is included for stiffened tests. Overall, the theoretical stiffness is in good agreement with the experimentally obtained values due to overestimation in the theoretical tension deflection offsetting underestimation in the theoretical compression deflection. The

underestimation in theoretical compression deflection is due to neglecting column flange deflection.

5.5.3.1.2 Comparison of the initial connection stiffness derived by the 'rigorous' method with Yee's method.

The initial stiffnesses derived by Yee's t-stub method are also presented in Table 5.20. It can be seen that there is little difference between the theoretical stiffness obtained using this method and the more rigorous method adopted in this study. If the two methods are compared on a component by component basis, there is good agreement between tension deflection components overall for unstiffened connections. Yee's method overestimates tension component deflection for stiffened connections and this is due to neglecting the stiffening effect of the column web in this region. This is offset by the assumption that compression web deflection is negligible for stiffened connections.

The rigorous method of initial stiffness calculation takes a lot more computational effort than the t-stub approach. This is due solely to the calculation of the individual column flange factors. The expression for the unstiffened column flange factor is outlined in Appendix A. This expression is iterated ten times for convergence for unstiffened column flange factors. For each four bolt connection 16 column flange factors are required. The expression is, therefore, calculated a minimum of 160 times. For stiffened column flange factors, derived in sections 3.2.2.3.2 and 3.2.2.3.3, over 50 iterations are required for convergence.

This is due to the introduction of the first derivative of the deflection expression and the subsequent reduction in power of the damping terms in the denominator of the relationship.

A flow diagram for the calculation of the parameters for the model used in this study is outlined in Appendix H. If the initial stiffness portion of this diagram is consulted, it can be seen that approximately 90% of the computer run time is used to calculate the column flange factors. This time could be reduced considerably by having a data file from which the appropriate column flange factors could be extracted or derived. Only factors for the infinite case need to be stored as the stiffened flange can be estimated by assuming that the column flanges are simply supported at the stiffener positions. This neglects the first derivative part of the deflection factor expression with little effect on the overall stiffness of the connection.

Overall the t-stub approach gives just as good an estimate of initial stiffness as the rigorous method especially if the effect of a small change in initial stiffness on overall frame behaviour is considered (see Chapter six). Since the t-stub model is a lot simpler it would be wise to adopt this approach. The rigorous method is useful however since it is perfectly general and can explain many things about the initial behaviour of connections in the tension region. It might also be possible to use the method to assess the column flange stiffness of other connection types with alternative tensile bolting arrangements. The

feasibility of this depends on whether a consistent load transfer mechanism exists through the connection and whether sufficient compatibility equations are available for the calculation of all the unknowns.

5.5.3.2 Strain hardening stiffness

The strain hardening stiffness of the connection is not as easy to calculate as initial stiffness. This is due to the nature of strain hardening which is dependent on the rate of loading, the yield stress of the material and other, mainly geometrical, considerations. Yee assumed that the strain hardening stiffness of unstiffened connections is due mostly to the column web and that the strain hardening stiffness of stiffened connections is negligible. If Figures 5.1 to 5.12 are consulted it can be seen that internal/internal stiffened connections do possess some strain hardening stiffness. In stiffened connections the beam usually fails first, a plastic hinge forming at the end of the beam. If rotation is measured offset along the beam, the connection appears to have little stiffness at yield due to the plastic hinge between the offset point and the connection. As connection rotation is measured at the connection in this study the strain hardening stiffness of stiffened connections can be obtained. This is another advantage of the transducer based method of measurement.

The strain hardening stiffness of the test connections A2 to D1 falls within the narrow range 1400 kNm/rad to 3000kNm/rad. It

is difficult to judge whether the particular strain hardening value varies with the size of connection as some of the larger connections did not fully reach the strain hardening range. Hence, an average value of strain hardening stiffness is used in this method of prediction. Although it might be more conservative to assume that each connection has zero strain hardening stiffness, it is felt that this approach is valid as it gives a better fit to the curve in its transition phase. The transition phase is of most interest to analysts or designers who might use prediction curves as it is likely to be within the range of the design moment of the beam.

5.5.3.3 Plastic moment

The theoretical plastic moment compares well with the experimental results as most of the previous work on this type of connection has been carried out to specifically obtain this parameter. However, the accuracy of any prediction depends upon the assumed yield stress. The yield stress to be adopted for a design of a framework would be that given in BS5950 (1), depending on the type of section and grade of material. For this reason BS5950 values for yield stress are used for all theoretical plastic moment calculations. The yield stress values obtained from the tensile test specimens are summarised in Table 4.4. The range of values obtained fall within acceptable limits of the nominal yield stresses.

The difference in theoretical and experimental plastic moment is shown in Table 5.21. The experimental values given are those that give the 'best' fit to the curve as outlined in section 5.5.2. It should be noted that these might not be the actual plastic moment of the connection due to the assumptions of the model (see Figure 5.39). The actual yield stresses obtained from tensile specimens for each test series are shown in Table 4.4. The theoretical plastic moment capacities using these values are also given in Table 5.21 for comparison purposes.

Overall theoretical values of plastic moment based on both nominal and actual yield stresses compare well with the experimentally obtained values. This is not surprising though it should be borne in mind that factors such as residual stresses and the effects of welds have not been taken into account. In addition, only three types of failure were examined in this test series as most of the test connections were designed to carry the plastic moment of the beam.

5.5.3.4 Rate of decay parameter

Yee introduced the parameter, c , to model the transition phase of the connection curve more accurately. The author feels that this parameter actually accounts for the different rates of yielding of each component of the connection. This will vary from test to test due to the effects of residual stresses, etc., and, therefore, the author considers that it is best to ignore this parameter altogether for internal connections. The effect

of neglecting the c parameter with the benefit of reducing the model to one of three parameters will be discussed in the next chapter.

5.5.4 Comparison of the predicted curves with the experimentally obtained curves.

The predicted curves based upon the above assumptions are compared with the experimentally obtained curves in Figures 5.54 to 5.65. All predicted curves (except test A4) deviate from the experimentally obtained curves to some extent. Most curves compare favourably initially followed by underestimation of the stiffness in the transition phase. In the later stages of loading deviation from experimental curves is more pronounced. This is expected due to the assumptions adopted in selecting strain hardening stiffness. In a few stiffened connections (A7, B2, C2), this is due to an underestimation of the plastic moment of the connection. Test C1 is the only test in which the predicted curve overestimates connection behaviour over the loading range. This is due to the previously mentioned problems during testing.

5.5.5 Summary

The predicted curves show good agreement with the experimentally obtained curves although they are based on only three parameters. The criteria by which this good fit is judged will be discussed in the next chapter. Overall, the initial stiffness of the

connection is well predicted using the derived method. However, the much simpler t-stub model predicts overall behaviour just as well. The rigorous method is useful, though, for examining the effects of varying contact position on connection stiffness and places column flange tension stiffness for unstiffened and stiffened connections on a more rational basis. Values for strain hardening stiffness are assumed for each connection size due to the presence of unknown factors which will vary from test to test. The predicted plastic moment values show good agreement with experimentally obtained values whether based upon BS5950 design or actual yield stresses. Finally, the parameter, c , is neglected as it will have little effect on frame behaviour. This reduces the model to three parameters for internal/internal type connections.

5.6 Comparison of the method of prediction with other existing results.

It would be beneficial to compare the method of prediction with other existing test data. However, as described in the literature review actual connection rotation results are not always presented. Data from over 90 tests was collected in total. From the majority of these tests plastic moment is the only useful parameter that can be identified. Initial stiffness can be derived from some test results but its validity, as seen earlier, is not guaranteed. A comparison of predicted plastic moment and initial stiffness with existing experimental results is presented in Tables 5.22 and 5.23 respectively. The method

of prediction will be compared more fully with results given by Davison (14) and Moore and Sims (18).

The comparison of experimental and theoretical plastic moment is shown in Table 5.22. Theoretical values of plastic moment are based upon BS5950 design yield stresses. Despite a few anomalies overall agreement is good. This is not surprising as most of the experiments were used to derive the respective yield criteria.

No previous tests have measured connection rotation directly. Therefore, initial stiffnesses of most tests cannot be compared with the method of prediction. However, an estimate of connection behaviour can be obtained by including offset stiffness in the predicted value of initial stiffness. This is done for Davison's, Moore and Sims and Yee's tests. Yee's tests are not discussed here as they are adequately covered in Yee's own thesis (13). Where raw load-deflection results are presented, an estimate of initial stiffness can be made using the method outlined in Appendix E. This method can be erratic as outlined in previous sections. A comparison of predicted and theoretical initial stiffness, taking into account the above points, is given in Table 5.23. Overall agreement between predicted and theoretical methods is seen to be variable. Generally, agreement is better with the results of more recent tests where the exact method of measurement is known.

The comparison of the Davison and the Moore and Sims tests with the predicted moment-rotation curves is shown in Figures 5.66 and

5.67 respectively. Both these curves are offset rotation values. An allowance for the offset stiffness has been included in the predicted initial stiffness value for each connection. These tests form a useful comparison as they have been performed on the same connection size. The difference in the three tests being that test 3 (Moore and Sims) is unstiffened, test 4 (Moore and Sims) is stiffened by backing plates and test JT/13B (Davison) employs a more conventional stiffening system. In all three tests a reasonable fit is obtained. It is assumed that the connection stiffened with the backing plate has the same initial stiffness as the unstiffened connection. The author deems this to be valid due to the column flange deriving most of its stiffness from the column web root fillet junction.

Summarising, acceptable agreement between theoretical and experimental parameters has been obtained for most tests. However, these observations are based upon estimates of connection parameters due to results having to be derived from experimental data.

Series	Beam Size	Offset Stiffness K_m kNm/rad
A	254x146UB37	51000.0
B	356x171UB51	132000.0
C	457x191UB74	311000.0

Table 5.1(a) Values of Offset Stiffness for each Test Series.

Test	Offset Readings kNm/rad	Offset Readings - Offset Stiffness kNm/rad	Transducer Readings Flange Compression kNm/rad	Transducer Readings Web Compression kNm/rad
A2	26300.	54000.	52000.	-
A3	30600.	76000.	67000.	72000.
A4	27800.	61000.	46000.	67000.
A5	25600.	51000.	41000.	63000.
A6	26500.	55000.	60000.	70000.
A7	33400.	97000.	73000.	100000.
A8	28400.	64000.	57000.	78000.
B1	49900.	80000.	69000.	123000.
B2	64700.	127000.	79000.	160000.
C1	114000.	180000.	190000.	260000.
C2	128000.	218000.	230000.	296000.
D1	33400.	97000.	61000.	87000.

Table 5.1(b) Comparison of the Initial Connection Stiffness Measured from Offset and Transducer Readings.

Test	Tension Region Contribution (10^{-6} m/kN)			Compression Region Contribution (10^{-6} m/kN)		
	Total	Endplate	Column Flange	Total	Column Web	Column Flange
A2	0.63	0.33	0.30	0.54	-	0.54
A3	0.49	0.25	0.24	0.43	0.29	0.56
A4	0.45	0.33	0.12	0.67	0.45	0.88
A5	0.53	0.35	0.18	0.70	0.43	0.96
A6	0.45	0.32	0.13	0.49	0.42	0.56
A7	0.38	0.30	0.08	0.33	0.21	0.44
A8	0.35	0.26	0.09	0.57	0.42	0.71
B1	0.50	0.36	0.14	0.83	0.46	1.20
B2	0.48	0.42	0.06	0.63	0.25	1.00
C1	0.49	0.19	0.30	0.42	0.27	0.56
C2	0.47	0.31	0.16	0.29	0.19	0.38
D1	0.32	0.26	0.06	0.55	0.38	0.71

Table 5.2 Contribution of the Various Connection Components to Initial Stiffness in terms of Flexibility.

Test	Tension Region Deflection (mm)			Compression Region Deflection (mm)		
	Total	Endplate	Column Flange	Total	Column Web	Column Flange
A2	2.84	2.00	0.84	0.90	-	0.90
A3	0.79	0.58	0.21	0.24	0.17	0.31
A4	0.97	0.60	0.37	0.35	0.29	0.41
A5	2.25	1.79	0.46	0.66	0.44	0.88
A6	1.52	1.26	0.26	0.20	0.18	0.21
A7	0.67	0.61	0.06	0.19	0.10	0.27
A8	1.11	0.90	0.21	0.45	0.37	0.53
B1	3.64	2.50	1.14	1.07	0.91	1.23
B2	1.23	1.06	0.17	0.22	0.17	0.26
C1	2.20	1.40	0.80	1.70	1.16	2.24
C2	1.43	1.16	0.27	0.25	0.21	0.29
D1	0.67	0.60	0.07	0.24	0.20	0.27

Table 5.3 Deflections of the Various Connection Components at Yield.

Relative Rigidity Factor r	Tension Region Depth Factor, f_k					
	0.25		0.35		0.50	
1.0	0.8598		0.9768		1.0696	
	0.5074	0.3524	0.6492	0.3276	0.8128	0.2568
	44924		41314		38836	
0.8	0.8676		1.0095		1.0971	
	0.4811	0.3865	0.6098	0.3997	0.7847	0.3124
	44668		40403		38157	
0.6	0.9106		1.0802		1.1442	
	0.4854	0.4252	0.6750	0.4052	0.8599	0.2843
	43282		38569		37049	

a) Effect of varying relative rigidity factor, r , and depth of tension region factor, f_k .

Endplate dimension a_{cp}					
50 mm		30 mm		10 mm	
0.8598		0.8282		0.8324	
0.5074	0.3524	0.3302	0.4980	0.3414	0.4910
44924		46012		45871	

b) Effect of varying endplate dimension, a_{cp} , (constant $r=1, f_k=0.25$)

Key to Results.

Total Tension Region Contribution (10^{-6} m/kN)	
Endplate Contribution	Column Flange Contribution
Initial Stiffness (kNm/rad)	

Table 5.4 Effect of Theoretically Changing Contact Position on the Tension Region Contribution to Initial Stiffness (Test A2).

Relative Rigidity Factor r	Tension Region Depth Factor, f_k					
	0.25		0.35		0.50	
1.0	0.5031		0.5337		0.5914	
	0.4417	0.0614	0.4988	0.0349	0.5914	0.0000
	71133		68645		64399	
0.8	0.5040		0.5334		0.5948	
	0.4106	0.0934	0.4523	0.0811	0.5456	0.0492
	71053		68664		64164	
0.6	0.5195		0.5546		0.6101	
	0.4009	0.1186	0.4464	0.1082	0.5500	0.0604
	69774		67040		63112	

a) Effect of varying relative rigidity factor, r , and depth of tension region factor, f_k .

Endplate dimension a_{ep}					
50 mm		30 mm		10 mm	
0.5031		0.4928		0.5347	
0.4417	0.0614	0.4560	0.0368	0.4852	0.0495
71133		72004		68559	

b) Effect of varying endplate dimension, a_{ep} , (constant $r=1, f_k=0.25$)

Key to Results.

Total Tension Region Contribution (10^{-6} m/kN)	
Endplate Contribution	Column Flange Contribution
Initial Stiffness (kNm/rad)	

Table 5.5 Effect of Theoretically Changing Contact Position on the Tension Region Contribution to Initial Stiffness (Test A3).

Relative Rigidity Factor r	Tension Region Depth Factor, f_k					
	0.25		0.35		0.50	
1.0	0.4778		0.5385		0.5859	
	0.2661	0.2117	0.3444	0.1941	0.4350	0.1509
	66100		61968		59079	
0.8	0.4864		0.5569		0.6007	
	0.2560	0.2304	0.3294	0.2275	0.4256	0.1751
	65486		60811		58231	
0.6	0.5169		0.5913		0.6241	
	0.2660	0.2509	0.3674	0.2239	0.4682	0.1559
	63379		58764		56941	

a) Effect of varying relative rigidity factor, r , and depth of tension region factor, f_k .

Endplate dimension a_{ep}					
50 mm		30 mm		10 mm	
0.4778		0.4619		0.4630	
0.2661	0.2117	0.2594	0.2025	0.2530	0.2100
66100		67285		67200	

b) Effect of varying endplate dimension, a_{ep} , (constant $r=1, f_k=0.25$)

Key to Results.

Total Tension Region Contribution (10^{-6} m/kN)	
Endplate Contribution	Column Flange Contribution
Initial Stiffness (kNm/rad)	

Table 5.6 Effect of Theoretically Changing Contact Position on the Tension Region Contribution to Initial Stiffness (Test A4).

Relative Rigidity Factor r	Tension Region Depth Factor, f_k					
	0.25		0.35		0.50	
1.0	1.0325		1.1299		1.2113	
	0.9724	0.0601	1.1299	0.0000	1.2113	0.0000
	41048		38487		36578	
0.8	1.0194		1.1257		1.2159	
	0.8911	0.1283	1.0066	0.1191	1.1294	0.0865
	41420		38591		36447	
0.6	1.0256		1.1685		1.2463	
	0.8383	0.1873	1.0020	0.1665	1.1360	0.1103
	41243		37559		35815	

a) Effect of varying relative rigidity factor, r , and depth of tension region factor, f_k .

Endplate dimension a_{ep}					
50 mm		30 mm		10 mm	
1.0325		1.0052		1.1130	
0.9724	0.0601	1.0052	0.0000	1.1130	0.0000
41048		41829		38906	

b) Effect of varying endplate dimension, a_{ep} , (constant $r=1, f_k=0.25$)

Key to Results.

Total Tension Region Contribution (10^{-6} m/kN)	
Endplate Contribution	Column Flange Contribution
Initial Stiffness (kNm/rad)	

Table 5.7 Effect of Theoretically Changing Contact Position on the Tension Region Contribution to Initial Stiffness (Test A5).

Relative Rigidity Factor r	Tension Region Depth Factor, f_k					
	0.25		0.35		0.50	
1.0	0.6674		0.7265		0.7745	
	0.5141	0.1533	0.6700	0.0565	0.7745	0.0000
	90019		82690		77558	
0.8	0.6650		0.7219		0.7704	
	0.4750	0.1900	0.5965	0.1254	0.7063	0.0641
	90337		83217		77977	
0.6	0.6663		0.7421		0.7870	
	0.4525	0.2138	0.5761	0.1660	0.6847	0.1023
	90154		80956		76336	

a) Effect of varying relative rigidity factor, r , and depth of tension region factor, f_k .

Endplate dimension a_{cp}					
50 mm		30 mm		10 mm	
0.6674		0.6567		0.6942	
0.5141	0.1553	0.5152	0.1415	0.5030	0.1912
90019		91473		86545	

b) Effect of varying endplate dimension, a_{cp} , (constant $r=1, f_k=0.25$)

Key to Results.

Total Tension Region Contribution (10^{-6} m/kN)	
Endplate Contribution	Column Flange Contribution
Initial Stiffness (kNm/rad)	

Table 5.8 Effect of Theoretically Changing Contact Position on the Tension Region Contribution to Initial Stiffness (Test A6).

Relative Rigidity Factor r	Tension Region Depth Factor, f_k					
	0.25		0.35		0.50	
1.0	0.5245		0.5718		0.6027	
	0.4776	0.0469	0.5718	0.0000	0.6027	0.0000
	114538		105065		99673	
0.8	0.5209		0.5619		0.5940	
	0.4377	0.0832	0.5272	0.0347	0.5912	0.0028
	115328		106914		101135	
0.6	0.5213		0.5678		0.6008	
	0.4142	0.1071	0.4981	0.0717	0.5619	0.0389
	115235		105428		99980	

a) Effect of varying relative rigidity factor, r , and depth of tension region factor, f_k .

Endplate dimension a_{cp}					
50 mm		30 mm		10 mm	
0.5245		0.5200		0.5663	
0.4776	0.0469	0.4899	0.0301	0.4973	0.0690
114538		115513		106082	

b) Effect of varying endplate dimension, a_{cp} , (constant $r=1, f_k=0.25$)

Key to Results.

Total Tension Region Contribution (10^{-6} m/kN)	
Endplate Contribution	Column Flange Contribution
Initial Stiffness (kNm/rad)	

Table 5.9 Effect of Theoretically Changing Contact Position on the Tension Region Contribution to Initial Stiffness (Test A7).

Relative Rigidity Factor r	Tension Region Depth Factor, f_k					
	0.25		0.35		0.50	
1.0	0.6252		0.6999		0.7586	
	0.4724	0.1528	0.5865	0.1134	0.6896	0.0690
	56881		53122		50501	
0.8	0.6288		0.7127		0.7604	
	0.4402	0.1886	0.5355	0.1772	0.6423	0.1281
	55265		50665		48834	
0.6	0.6561		0.7547		0.7992	
	0.4341	0.2220	0.5603	0.1944	0.6688	0.1304
	55265		50665		48834	

a) Effect of varying relative rigidity factor, r , and depth of tension region factor, f_k .

Endplate dimension a_{ep}					
50 mm		30 mm		10 mm	
0.6252		0.6074		0.6352	
0.4724	0.1528	0.4776	0.1298	0.4882	0.1470
56881		57858		56342	

b) Effect of varying endplate dimension, a_{ep} , (constant $r=1, f_k=0.25$)

Key to Results.

Total Tension Region Contribution (10^{-6} m/kN)	
Endplate Contribution	Column Flange Contribution
Initial Stiffness (kNm/rad)	

Table 5.10 Effect of Theoretically Changing Contact Position on the Tension Region Contribution to Initial Stiffness (Test A8).

Relative Rigidity Factor r	Tension Region Depth Factor, f_k					
	0.17		0.25		0.35	
1.0	0.5262		0.6209		0.6908	
	0.2896	0.2366	0.4355	0.1854	0.5349	0.1559
	124773		113444		106323	
0.8	1.1943		0.6365		0.7129	
	0.2754	0.9189	0.4081	0.2284	0.5108	0.2021
	73221		111774		104259	
0.6	0.8281		0.6796		0.7505	
	0.3045	0.5236	0.4265	0.2531	0.5540	0.1965
	94657		107411		100923	

a) Effect of varying relative rigidity factor, r , and depth of tension region factor, f_k .

Endplate dimension a_{ep}					
55 mm		35 mm		15 mm	
0.5262		0.5089		0.5061	
0.2896	0.2366	0.2860	0.2229	0.2838	0.2223
124773		127083		127473	

b) Effect of varying endplate dimension, a_{ep} , (constant $r=1, f_k=0.17$)

Key to Results.

Total Tension Region Contribution (10^{-6} m/kN)	
Endplate Contribution	Column Flange Contribution
Initial Stiffness (kNm/rad)	

Table 5.11 Effect of Theoretically Changing Contact Position on the Tension Region Contribution to Initial Stiffness (Test B1).

Relative Rigidity Factor r	Tension Region Depth Factor, f_k					
	0.17		0.25		0.35	
1.0	0.4107		0.4926		0.5333	
	0.2916	0.1191	0.4501	0.0425	0.5333	0.0000
	288231		240384		222033	
0.8	0.7880		0.4911		0.5319	
	0.2808	0.5072	0.4138	0.0773	0.4980	0.0339
	150266		241088		222609	
0.6	0.5608		0.4993		0.5437	
	0.2827	0.2781	0.3978	0.1015	0.4825	0.0612
	211107		237150		217784	

a) Effect of varying relative rigidity factor, r , and depth of tension region factor, f_k .

Endplate dimension a_{ep}					
55 mm		35 mm		15 mm	
0.4107		0.4033		0.4168	
0.2916	0.1191	0.2924	0.1109	0.2892	0.1276
288231		293615		284105	

b) Effect of varying endplate dimension, a_{ep} , (constant $r=1, f_k=0.17$)

Key to Results.

Total Tension Region Contribution (10^{-6} m/kN)	
Endplate Contribution	Column Flange Contribution
Initial Stiffness (kNm/rad)	

Table 5.12 Effect of Theoretically Changing Contact Position on the Tension Region Contribution to Initial Stiffness (Test B2).

Relative Rigidity Factor r	Tension Region Depth Factor, f_k					
	0.15		0.25		0.35	
1.0	0.3749		0.4512		0.4828	
	0.2940	0.0809	0.4119	0.0393	0.4577	0.0251
	281352		253575		243635	
0.8	0.3763		0.4590		0.4919	
	0.2748	0.1015	0.3776	0.0814	0.4290	0.0629
	278791		251053		240877	
0.6	0.3938		0.4801		0.5093	
	0.2781	0.1157	0.3861	0.0940	0.4399	0.0694
	273941		244425		235869	

a) Effect of varying relative rigidity factor, r , and depth of tension region factor, f_k .

Endplate dimension a_{ep}					
60 mm		40 mm		20 mm	
0.3749		0.3667		0.3745	
0.2940	0.0809	0.2982	0.0685	0.3069	0.0676
281352		284708		281526	

b) Effect of varying endplate dimension, a_{ep} , (constant $r=1, f_k=0.15$)

Key to Results.

Total Tension Region Contribution (10^{-6} m/kN)	
Endplate Contribution	Column Flange Contribution
Initial Stiffness (kNm/rad)	

Table 5.13 Effect of Theoretically Changing Contact Position on the Tension Region Contribution to Initial Stiffness (Test C1 - 4 bolts).

Relative Rigidity Factor r	Tension Region Depth Factor, f_k					
	0.15		0.25		0.35	
1.0	0.3103		0.3733		0.3899	
	0.2971	0.0132	0.3733	0.0000	0.3899	0.0000
	631557		524976		502672	
0.8	0.3134		0.3686		0.3854	
	0.2818	0.0316	0.3686	0.0000	0.3854	0.0000
	625238		531688		508493	
0.6	0.3171		0.3704		0.3872	
	0.2745	0.0426	0.3615	0.0089	0.3872	0.0000
	618100		529102		506183	

a) Effect of varying relative rigidity factor, r , and depth of tension region factor, f_k .

Endplate dimension a_{ep}					
60 mm		40 mm		20 mm	
0.3103		0.3077		0.3271	
0.2971	0.0132	0.3033	0.0044	0.3144	0.0127
631557		636362		604695	

b) Effect of varying endplate dimension, a_{ep} , (constant $r=1, f_k=0.15$)

Key to Results.

Total Tension Region Contribution (10^{-6} m/kN)	
Endplate Contribution	Column Flange Contribution
Initial Stiffness (kNm/rad)	

Table 5.14 Effect of Theoretically Changing Contact Position on the Tension Region Contribution to Initial Stiffness (Test C2 - 4 bolts).

Relative Rigidity Factor r	Tension Region Depth Factor, f_k			
	0.35		0.50	
1.0	0.4825		0.4922	
	0.4563	0.0262	0.4612	0.0310
	243711		240795	
0.8	0.4931		0.5024	
	0.4352	0.0579	0.4468	0.0556
	240560		237817	
0.6	0.5094		0.5164	
	0.4405	0.0689	0.4577	0.0587
	235827		233837	

a) Effect of varying relative rigidity factor, r , and depth of tension region factor, f_k .

Endplate dimension a_{ep}					
60 mm		40 mm		20 mm	
0.4825		0.4762		0.4971	
0.4563	0.0262	0.4646	0.0116	0.4848	0.0123
243711		245635		239380	

b) Effect of varying endplate dimension, a_{ep} , (constant $r=1, f_k=0.35$)

Key to Results.

Total Tension Region Contribution (10^{-6} m/kN)	
Endplate Contribution	Column Flange Contribution
Initial Stiffness (kNm/rad)	

Table 5.15 Effect of Theoretically Changing Contact Position on the Tension Region Contribution to Initial Stiffness (Test C1 - 6 bolts).

Relative Rigidity Factor r	Tension Region Depth Factor, f_k			
	0.35		0.50	
1.0	0.3784		0.3783	
	0.3784	0.0000	0.3783	0.0000
	517888		518333	
0.8	0.3798		0.3801	
	0.3798	0.0000	0.3801	0.0000
	516025		515589	
0.6	0.3839		0.3843	
	0.3826	0.0013	0.3830	0.0013
	510437		509886	

a) Effect of varying relative rigidity factor, r , and depth of tension region factor, f_k .

Endplate dimension a_{ep}					
60 mm		40 mm		20 mm	
0.3784		0.3821		0.4139	
0.3784	0.0000	0.3821	0.0000	0.4139	0.0000
517888		512968		473596	

b) Effect of varying endplate dimension, a_{ep} , (constant $r=1, f_k=0.35$)

Key to Results.

Total Tension Region Contribution (10^{-6} m/kN)	
Endplate Contribution	Column Flange Contribution
Initial Stiffness (kNm/rad)	

Table 5.16 Effect of Theoretically Changing Contact Position on the Tension Region Contribution to Initial Stiffness (Test C2 - 6 bolts).

Relative Rigidity Factor r	Tension Region Depth Factor, f_k					
	0.25		0.35		0.50	
1.0	0.4369		0.4711		0.4911	
	0.4193	0.0176	0.4711	0.0000	0.4911	0.0000
	79190		75799		73914	
0.8	0.4360		0.4684		0.4921	
	0.3971	0.0389	0.4517	0.0167	0.4829	0.0092
	79293		76036		73821	
0.6	0.4404		0.4768		0.4995	
	0.3851	0.0553	0.4408	0.0360	0.4783	0.0212
	78823		75232		73150	

a) Effect of varying relative rigidity factor, r , and depth of tension region factor, f_k .

Endplate dimension a_{ep}					
50 mm		30 mm		10 mm	
0.4369		0.4336		0.4866	
0.4193	0.0176	0.4336	0.0000	0.4855	0.0011
79190		79541		74329	

b) Effect of varying endplate dimension, a_{ep} , (constant $r=1, f_k=0.25$)

Key to Results.

Total Tension Region Contribution (10^{-6} m/kN)	
Endplate Contribution	Column Flange Contribution
Initial Stiffness (kNm/rad)	

Table 5.17 Effect of Theoretically Changing Contact Position on the Tension Region Contribution to Initial Stiffness (Test D1).

Test	Experimental Tension Region Contribution (10^{-6} m/kN)	Theoretical Tension Region Contribution (10^{-6} m/kN)
A2	0.63	0.83
A3	0.49	0.49
A4	0.45	0.46
A5	0.53	1.02
A6	0.45	0.66
A7	0.38	0.52
A8	0.35	0.60
B1	0.50	0.51
B2	0.48	0.40
C1	0.49	0.37/0.48*
C2	0.47	0.30/0.38*
D1	0.32	0.43

* Theoretical contribution calculated using 6 bolt model

Table 5.18 Tension Region Contribution to Initial Stiffness.

Test	Column Web Compression (10^{-6} m/kN)	Column Flange Compression (10^{-6} m/kN)	Theoretical Column Web Compression (10^{-6} m/kN)
A2	-	0.54*	0.48
A3	0.29	0.27	0.34
A4	0.45	0.43	0.43
A5	0.43	0.56	0.43
A6	0.42	0.14	0.26**
A7	0.21	0.23	0.26**
A8	0.42	0.29	0.43
B1	0.46	0.74	0.42
B2	0.25	0.75	0.20**
C1	0.27	0.29	0.32
C2	0.19	0.19	0.19**
D1	0.38	0.33	0.32

* Column Web and Column Flange Compression

** Theoretical Stiffener Deflection

Table 5.19 Compression Contribution to Initial Stiffness.

Test	Theoretical Initial Stiffness kNm/rad	Experimental Initial Stiffness kNm/rad	Yee (13) Initial Stiffness kNm/rad
A2	45000.	50000.	41000.
A3	71000.	70000.	69000.
A4	66000.	60000.	62000.
A5	41000.	50000.	39000.
A6	59000.*	65000.	56000.+
A7	68000.*	85000.	81000.+
A8	57000.	65000.	53000.
B1	113000.	100000.	107000.
B2	164000.*	125000.	151000.+
C1	253000.	220000.	242000.
C2	325000.*	260000.	422000.+
D1	79000.	85000.	73000.

* Including compression zone flexibility.
+ Neglecting compression zone flexibility.

Table 5.20 Comparison of the Predicted and Experimental Initial Stiffness.

Test	Theoretical Plastic Moment Nominal Yield kNm	Theoretical Plastic Moment Actual Yield kNm	Theoretical Failure Mode	Experimental Plastic Moment kNm
A2	113.	117.	CWC	112.
A3	128.	142.	BS	125.
A4	128.	142.	BS	122.
A5	111.	123.	EP	115.
A6	128.	142.	BS	120.
A7	128.	142.	BS	135.
A8	128.	142.	BS	127.
B1	207.	209.	CWC	205.
B2	237.	256.	BS	285.
C1	420.	436.	CWC	370.
C2	440.	473.	BS	460.
D1	128.	142.	BS	135.

Key to Failure Modes.

CWC - Column Web Compression Failure.

BS - Beam Section Failure.

EP - End Plate Failure.

Table 5.21 Comparison of Theoretical and Experimental Plastic Moment.

Reference	Test	M_p Experimental kNm	M_p Theoretical kNm	Notes
Sherborne (4)	A1	159.	130.	
	A2	240.	290.	Stiffened
	A3	270.	290.	Stiffened
	B1	260.	290.	Stiffened
	B2	260.	290.	Stiffened
Bailey (5)	1	254.	223.	
	2	139.	116.	
	3	160.	142.	
	4	264.	186.	Stiffened
	5	230.	166.	Stiffened
	6	429.	316.	Stiffened
	7	301.	220.	Stiffened
	8	111.	81.	Stiffened
	9	82.	81.	Stiffened
	10	213.	186.	Stiffened
	11	152.	166.	Stiffened
	12	305.	220.	Stiffened
	13	320.	316.	Stiffened
Surtees and Mann (7)	C1	165.	111.	
	C2	335.	330.	Stiffened
	C3	393.	330.	Stiffened
	C4	356.	330.	Stiffened
	C5	329.	330.	Stiffened
	C6	558.	665.	Stiffened
Packer and Morris (8)	J1	60.	72.	
	J2	50.	59.	
	J3	40.	79.	

Table 5.22 Comparison of Theoretical Plastic Moment with Existing Test Data Plastic Moment(1).

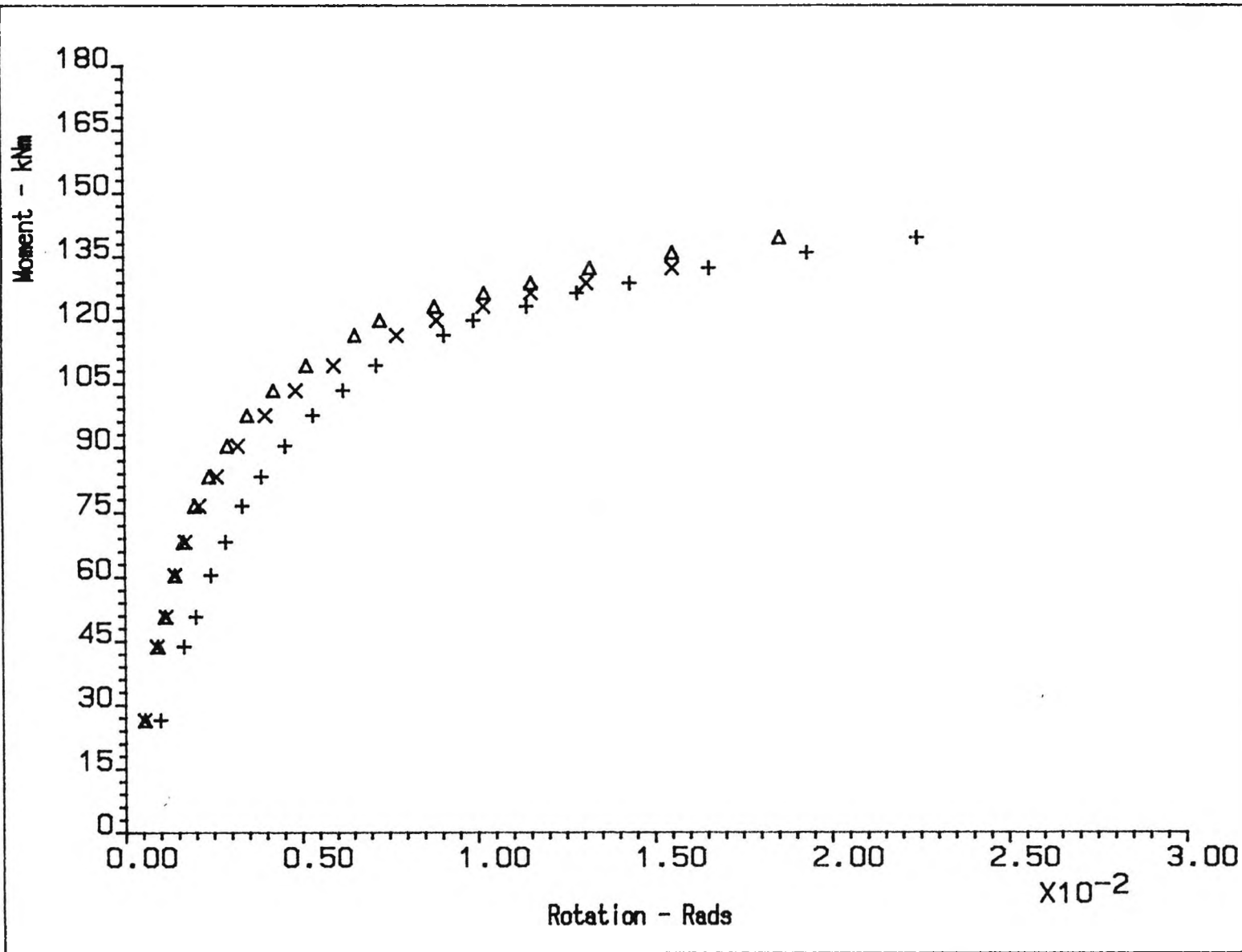
Reference	Test	M_p Experimental kNm	M_p Theoretical kNm	Notes
Dews (9)	1	79.	72.	US Sections
	2	72.	58.	
	3	119.	81.	
Ioaniddes (10)	1	68.	73.	US Sections
	2	170.	147.	
	3	209.	196.	
	4	90.	74.	
	5	185.	147.	
	6	220.	196.	
Davison (14)	JT13B	45.	55.	Stiffened
Jenkins Tong and Prescott (16)	4	120.	100.	Stiffened
	9	174.	156.	Stiffened
	10	232.	246.	Stiffened
	14	245.	246.	Stiffened
	15	128.	100.	Stiffened
	18	204.	246.	Stiffened
	22	120.	167.	Stiffened
	23	174.	167.	Stiffened
	27	120.	167.	Stiffened
	28	135.	167.	Stiffened
Moore and Simms (18)	J3	34.	27.	
	J4	41.	37.	Stiffened

N.B. All theoretical plastic moment capacities are derived using nominal yield stresses

Table 5.22 Comparison of Theoretical Plastic Moment with Existing Test Data Plastic Moment(2).

Reference	Test	Experimental Initial Stiffness kNm/rad	Theoretical Initial Stiffness kNm/rad	Notes
Sherborne (4)	A1	86000.	78000.	Experimental stiffness derived from load-deflection readings
	A2	155000.	179500.	
	A3	223000.	179858.	
	B1	223000.	111000.	
	B2	245000.	93000.	
Surtees and Mann (7)	C1	36000.	45000.	Accuracy of moment-rotation curves unknown
	C2	48000.	76000.	
	C3	91000.	76000.	
	C4	42000.	92000.	
	C5	58000.	92000.	
	C6	109000.	168000.	
Packer and Morris	J1	36000.	37000.	Experimental stiffness derived from load-deflection readings
	J2	29000.	24000.	
	J3	14000.	11000.	
Davison (14)	JT13B	16000.	17000.	Offset stiffness added to theoretical stiffness
Moore and Simms (18)	J3	6000.	10000.	Offset stiffness added to theoretical stiffness
	J4	7000.	10000.	

Table 5.23 Comparison of Theoretical Initial Stiffness with Existing Test Data Initial Stiffness.



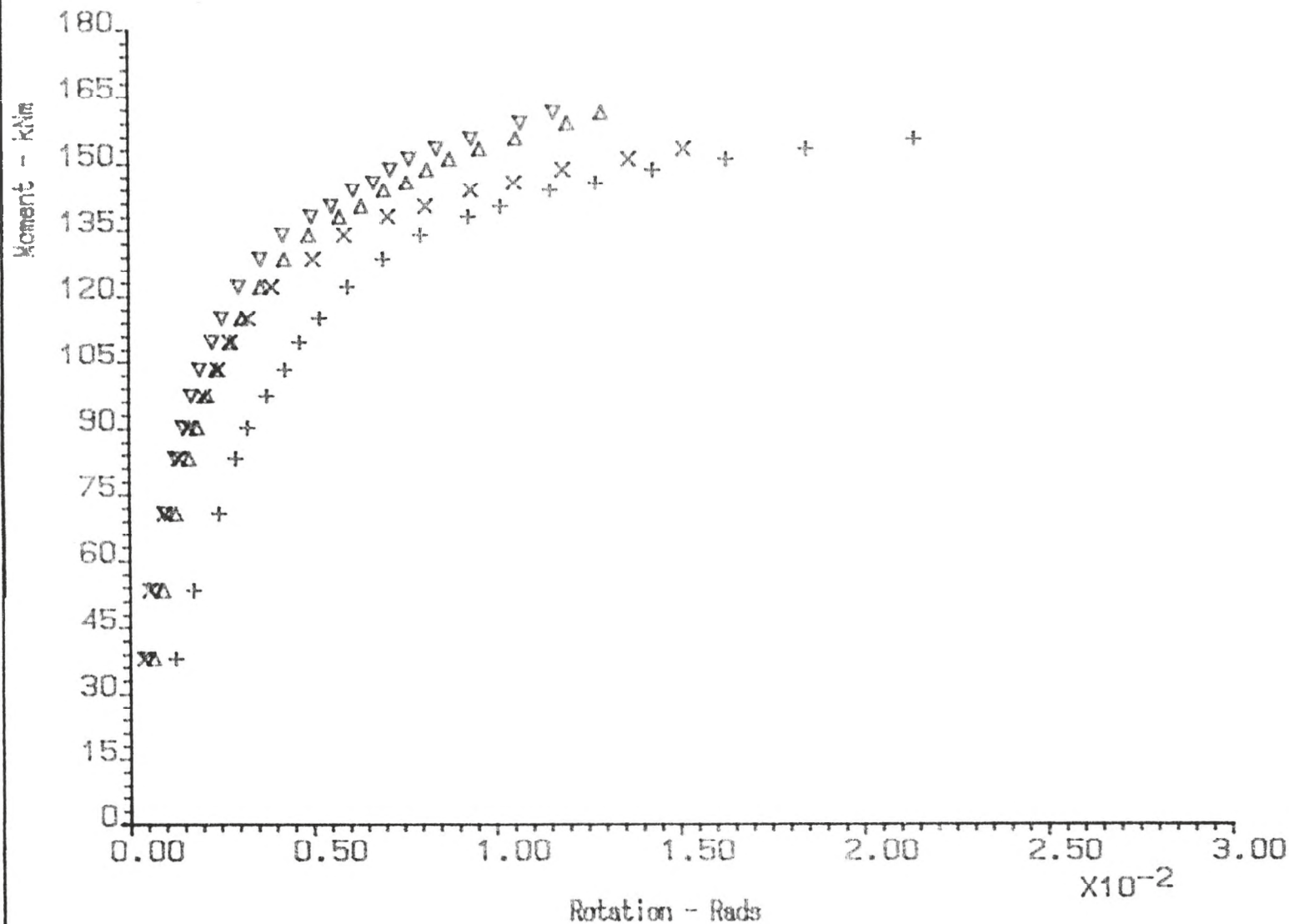
Connection Type :-
 Unstiffened
 Internal
 Beam Size -254x146 UB37
 Column Size -203x203 UC60
 4 M20 Tension Bolts
 Grade HSFG -Pretensioned
 Endplate Thickness = 20mm

Δ = endplate/endplate
 + = dial gauge
 x = central deflection

Figure 5.1

COMPARISON OF METHODS
 OF ROTATION MEASUREMENT.

Test A2



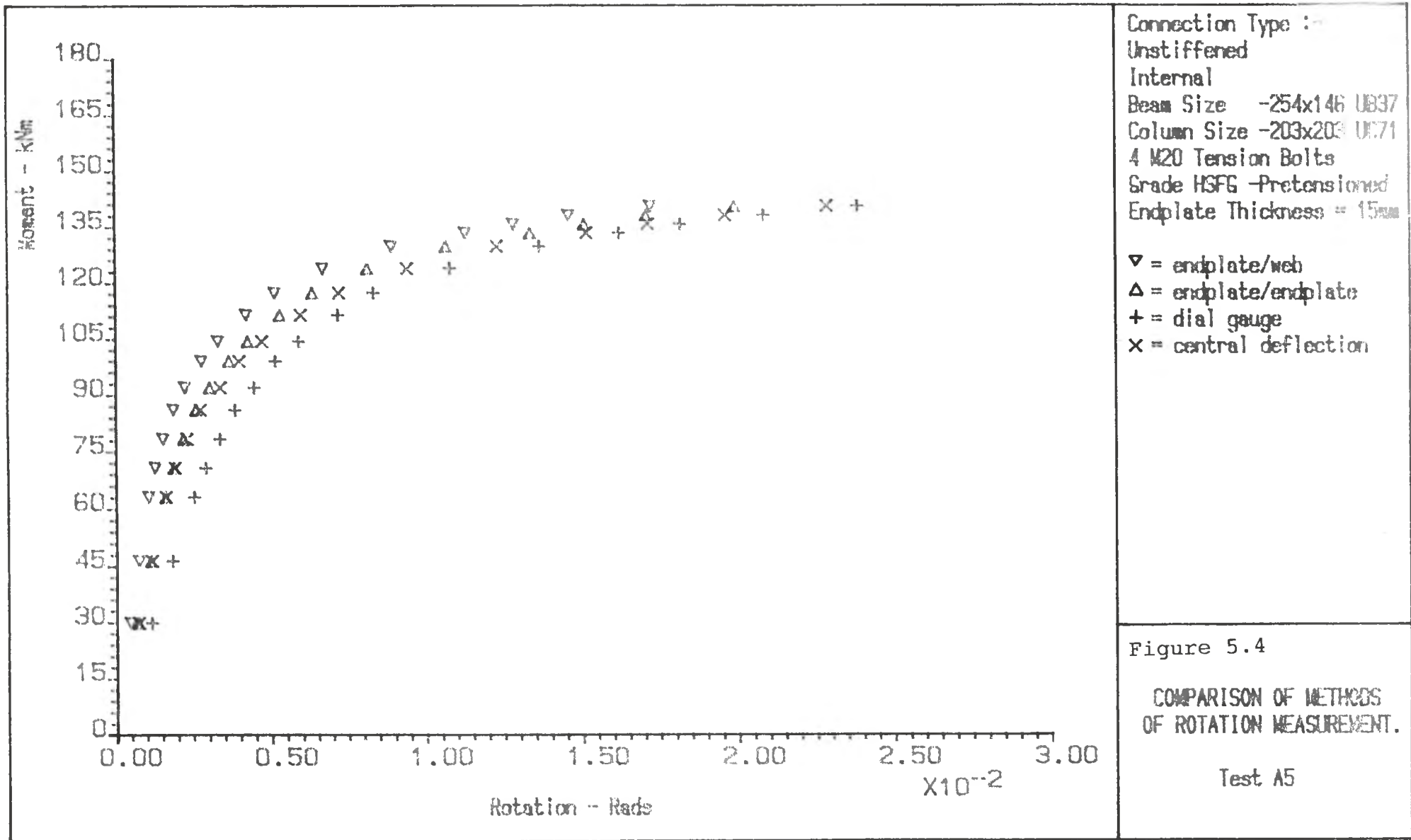
Connection Type :-
 Unstiffened
 Internal
 Beam Size -254x146 UB37
 Column Size -203x203 UC86
 4 M20 Tension Bolts
 Grade HSFG -Pretensioned
 Endplate Thickness = 20mm

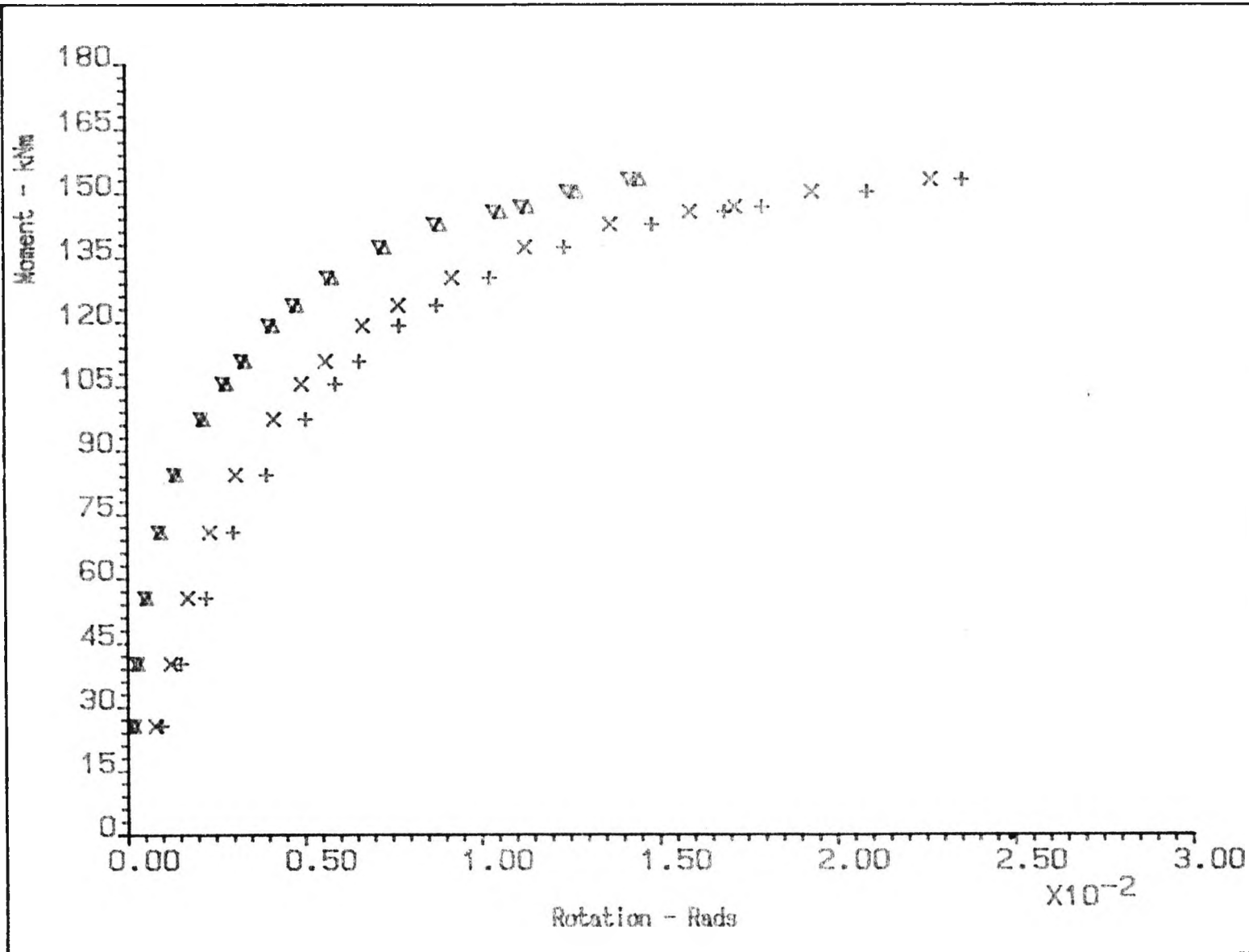
∇ = endplate/web
 Δ = endplate/endplate
 + = dial gauge
 x = central deflection

Figure 5.2

COMPARISON OF METHODS
 OF ROTATION MEASUREMENT.

Test A3





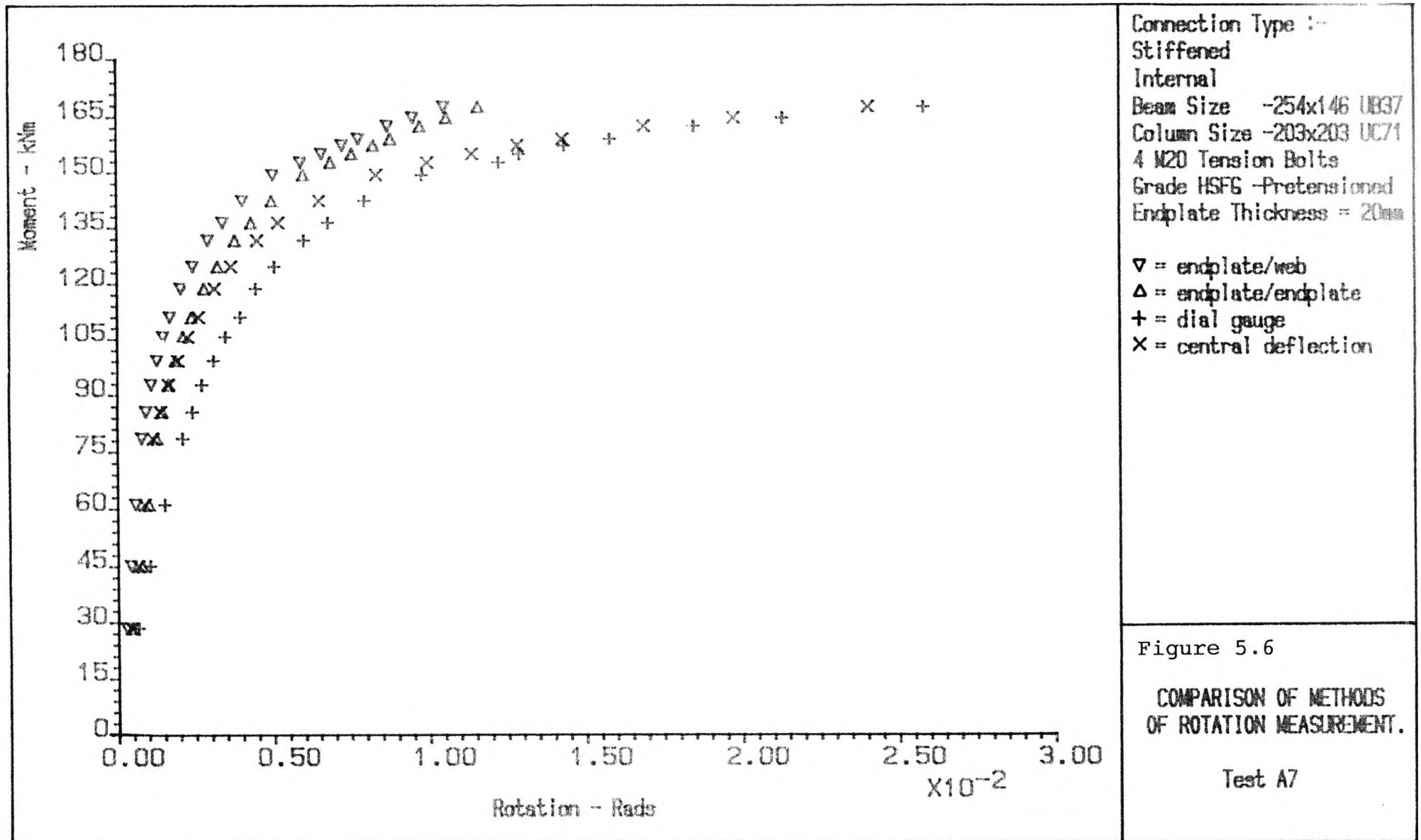
Connection Type :-
 Stiffened
 Internal
 Beam Size -254x146 UB37
 Column Size -203x203 UC60
 4 M20 Tension Bolts
 Grade HSFG -Pretensioned
 Endplate Thickness = 20mm

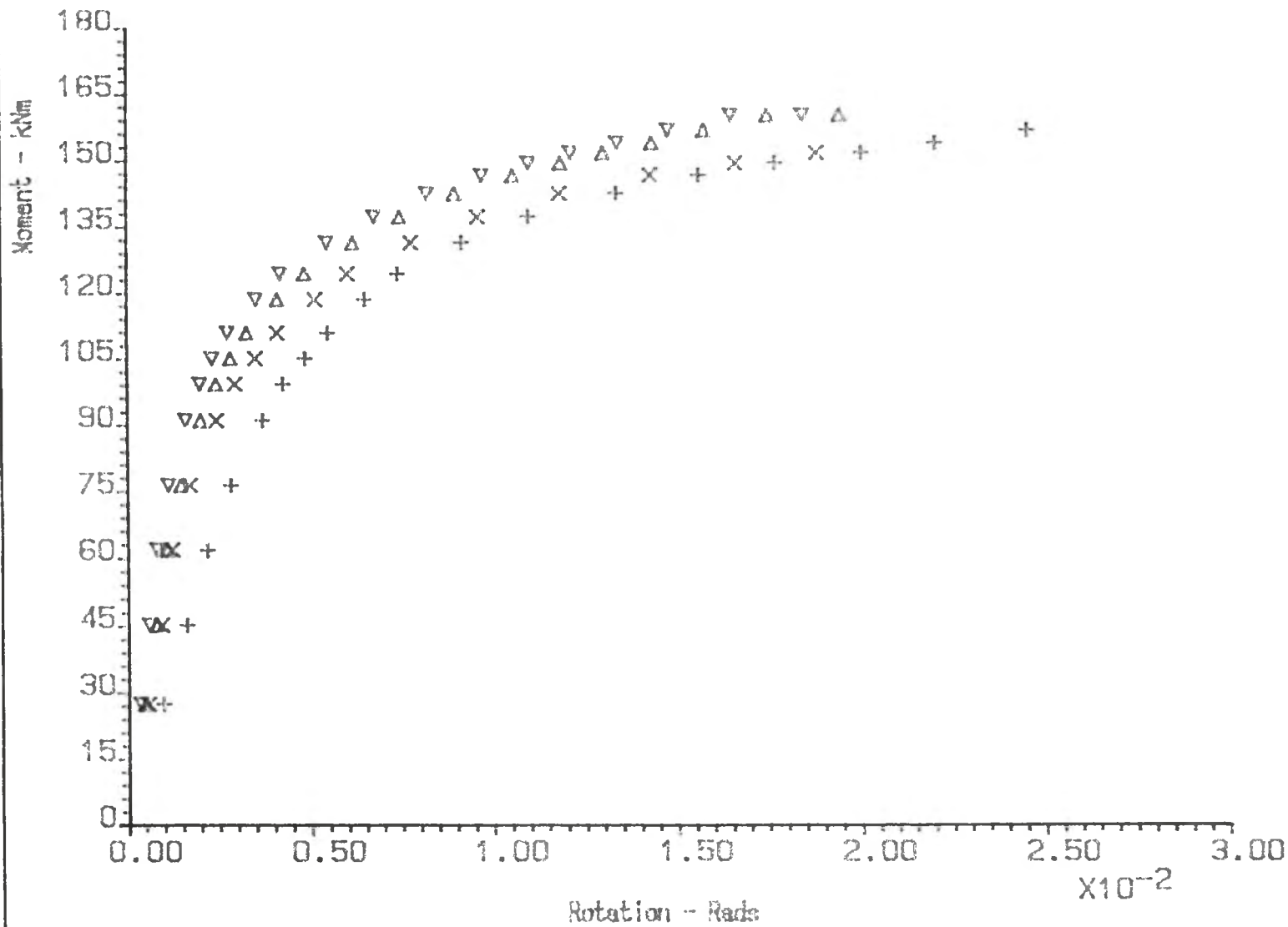
▽ = endplate/web
 △ = endplate/endplate
 + = dial gauge
 x = central deflection

Figure 5.5

COMPARISON OF METHODS
 OF ROTATION MEASUREMENT.

Test A6





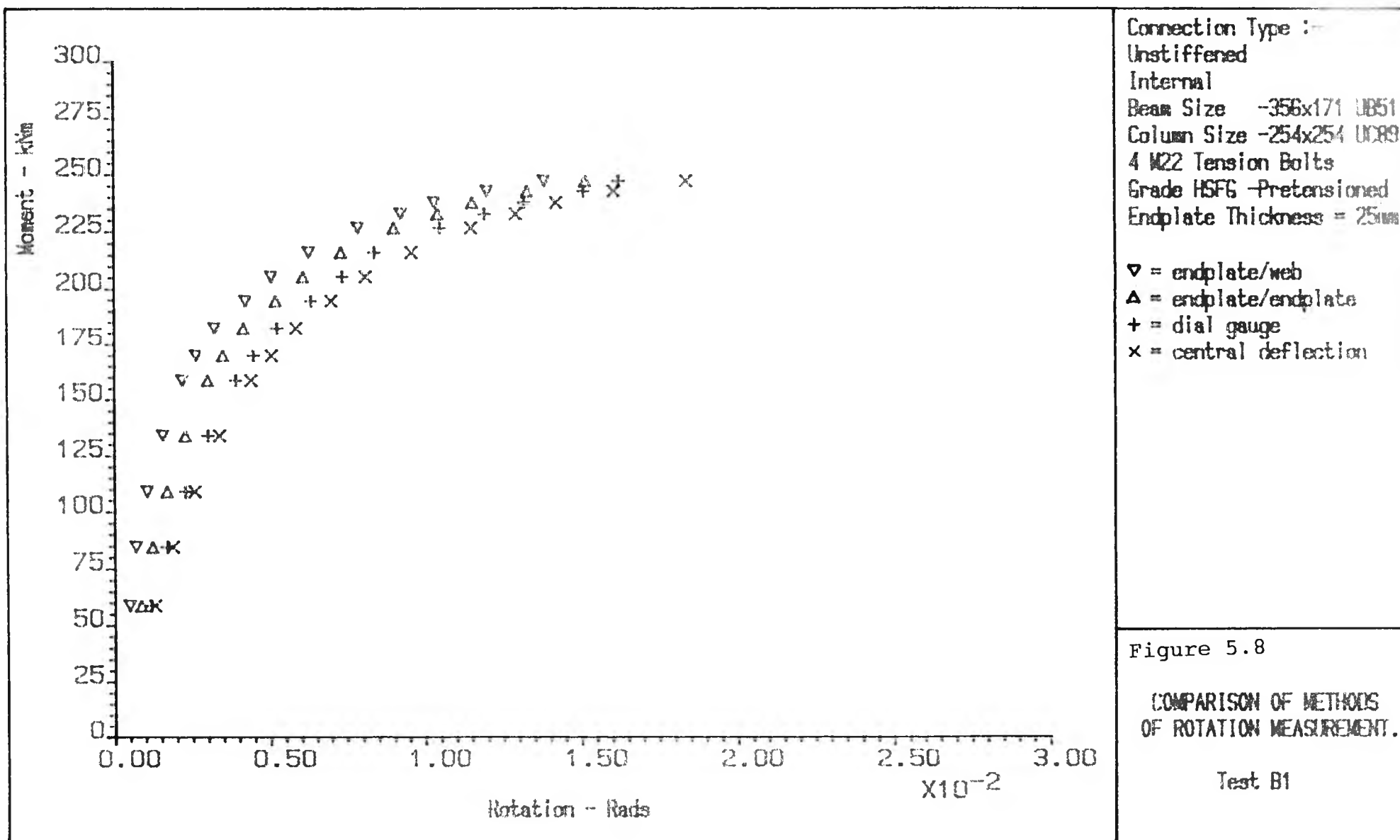
Connection Type :
 Unstiffened
 Internal
 Beam Size -254x146 UB37
 Column Size -203x203 UC71
 4 M20 Tension Bolts
 Grade HSFG -Pretensioned
 Endplate Thickness = 20mm

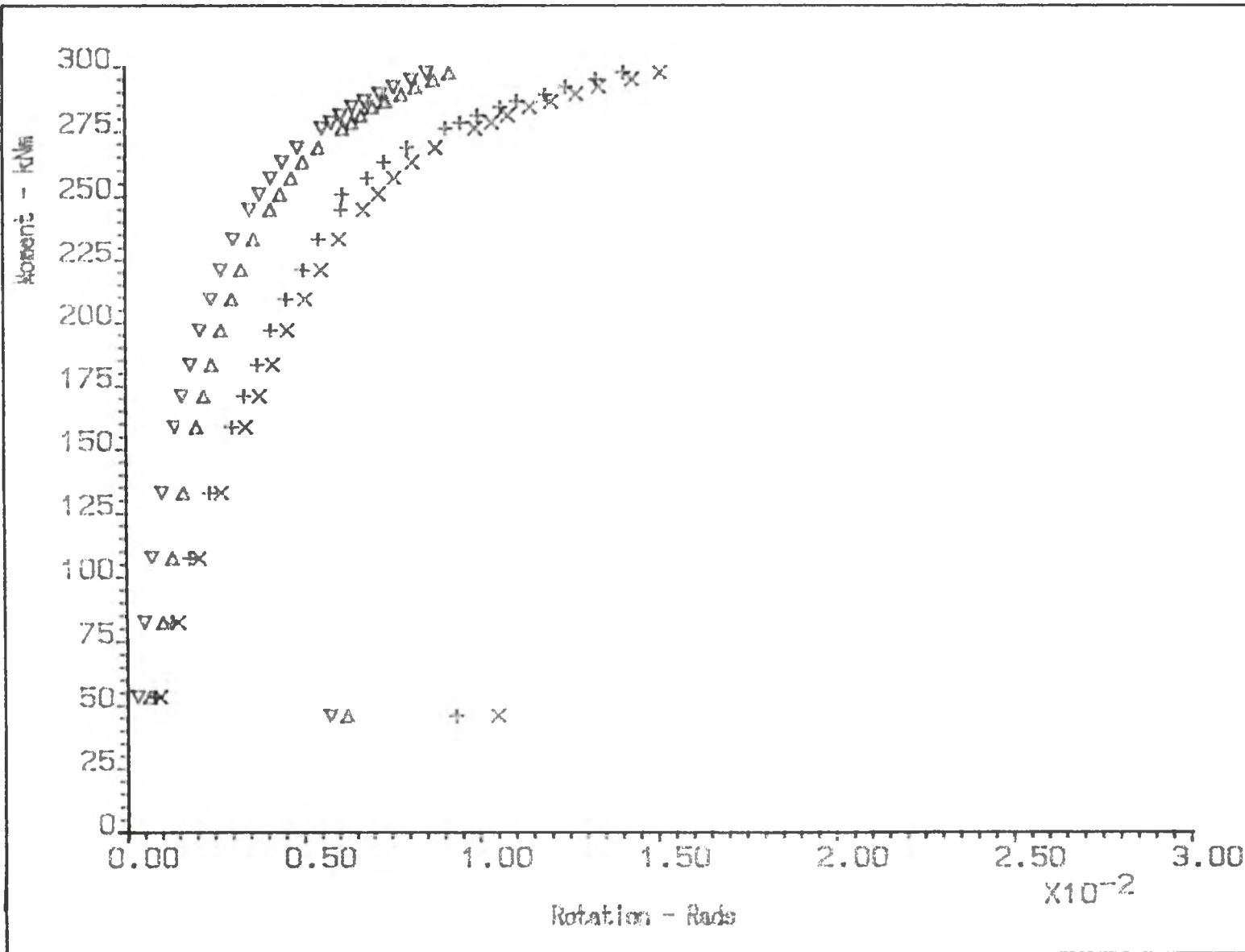
∇ = endplate/web
 Δ = endplate/endplate
 + = dial gauge
 X = central deflection

Figure 5.7

COMPARISON OF METHODS
 OF ROTATION MEASUREMENT.

Test A8





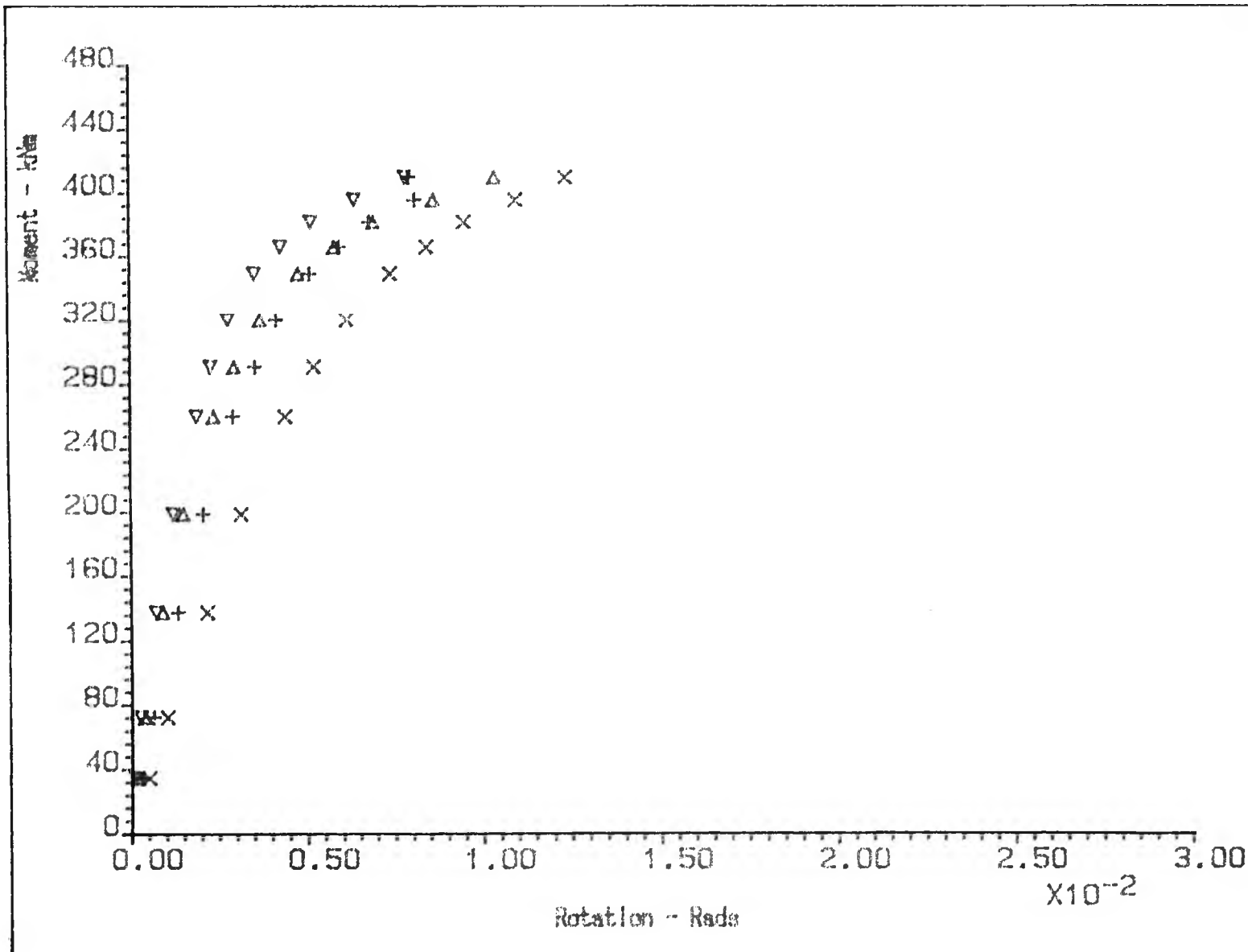
Connection Type :-
 Stiffened
 Internal
 Beam Size -356x171 UB51
 Column Size -254x254 UC89
 4 M22 Tension Bolts
 Grade HSFG -Pretensioned
 Endplate Thickness = 25mm

∇ = endplate/web
 Δ = endplate/endplate
 + = dial gauge
 x = central deflection

Figure 5.9

COMPARISON OF METHODS
 OF ROTATION MEASUREMENT.

Test B2



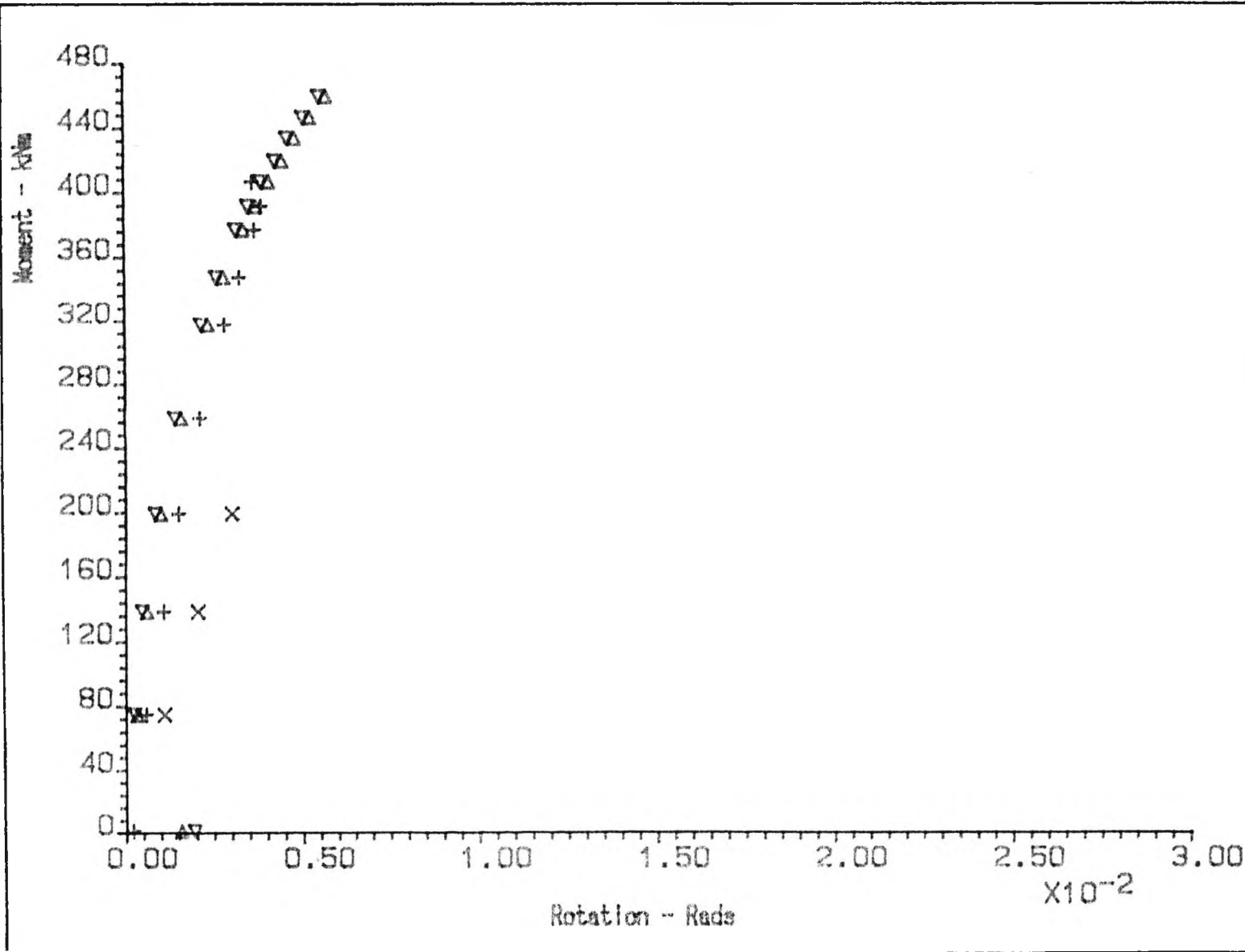
Connection Type :-
 Unstiffened
 Internal
 Beam Size -457x191UB74
 Column Size -305x305x137
 6 M24 Tension Bolts
 Grade HSFG -Pretensioned
 Endplate Thickness = 25mm

∇ = endplate/web
 Δ = endplate/endplate
 + = dial gauge
 x = central deflection

Figure 5.10

COMPARISON OF METHODS
 OF ROTATION MEASUREMENT.

Test C1



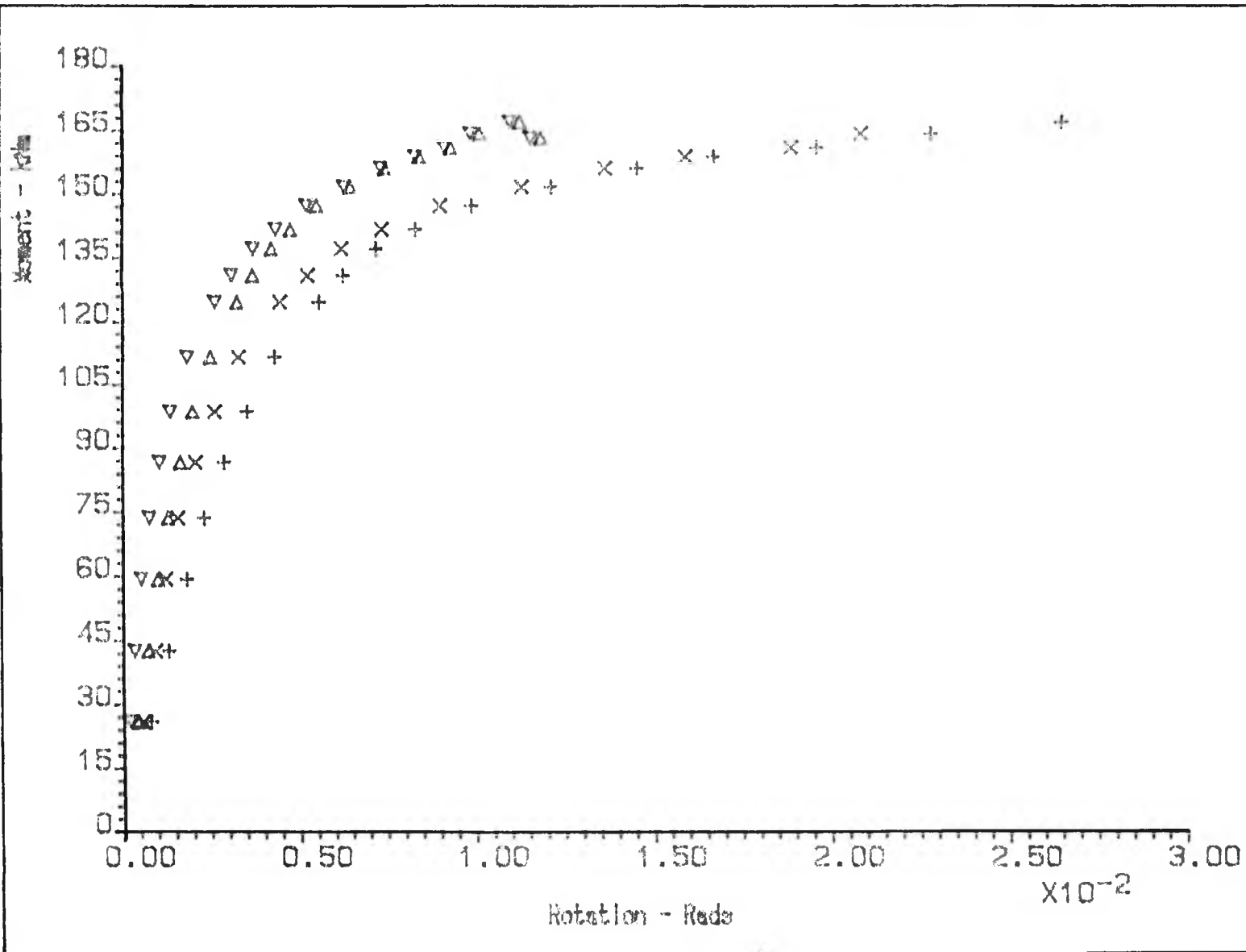
Connection Type :-
 Stiffened
 Internal
 Beam Size -457x191UB74
 Column Size -305x305UC137
 6 M24 Tension Bolts
 Grade HSFG -Pretensioned
 Endplate Thickness = 25mm

▽ = endplate/web
 △ = endplate/endplate
 + = dial gauge
 × = central deflection

Figure 5.11

COMPARISON OF METHODS
 OF ROTATION MEASUREMENT.

Test C2



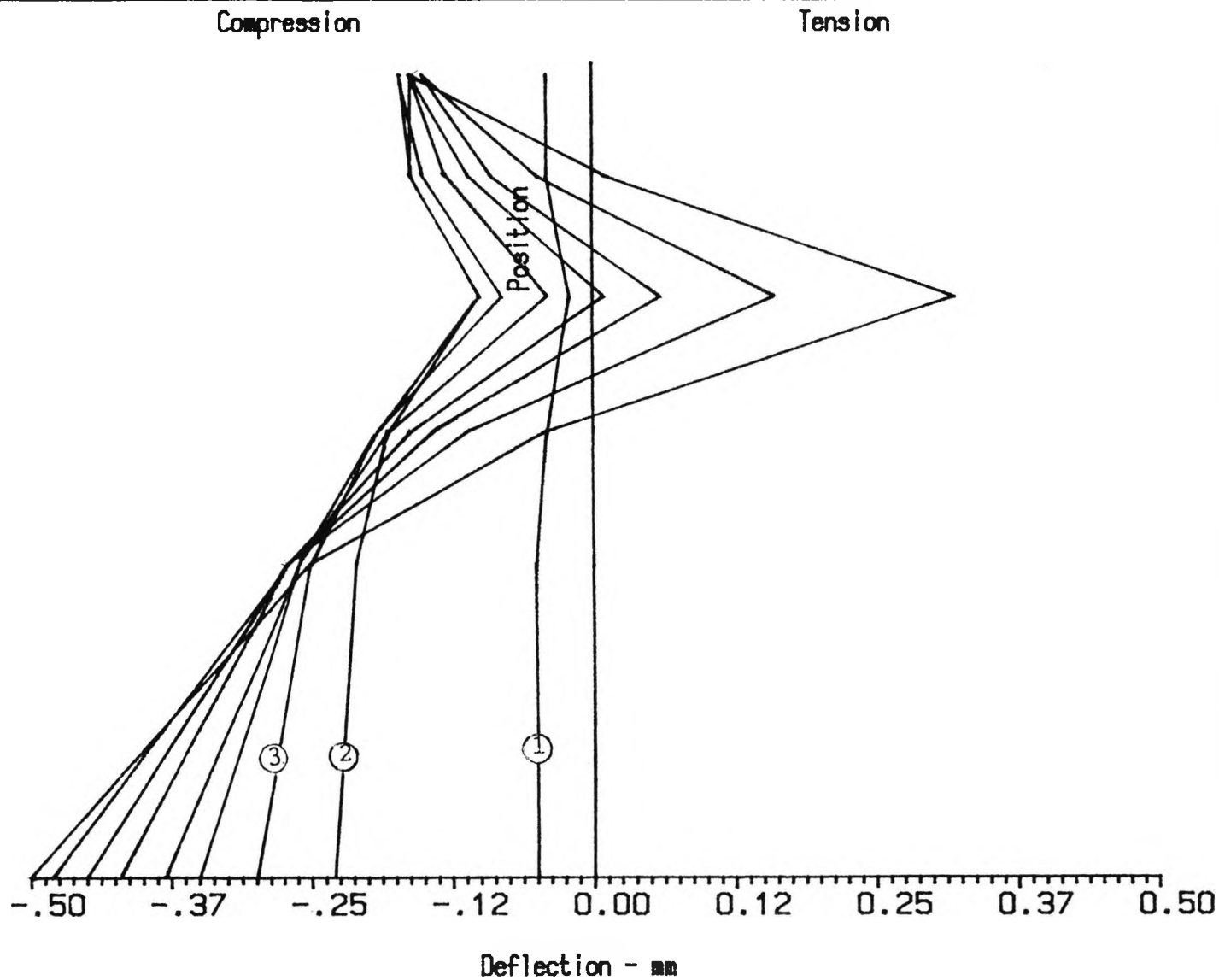
Connection Type :-
 Unstiffened
 Internal
 Beam Size -254x146UB37
 Column Size -305x305UC137
 4 M20 Tension Bolts
 Grade HSFG -Pretensioned
 Endplate Thickness = 20mm

▽ = endplate/web
 △ = endplate/endplate
 + = dial gauge
 x = central deflection

Figure 5.12

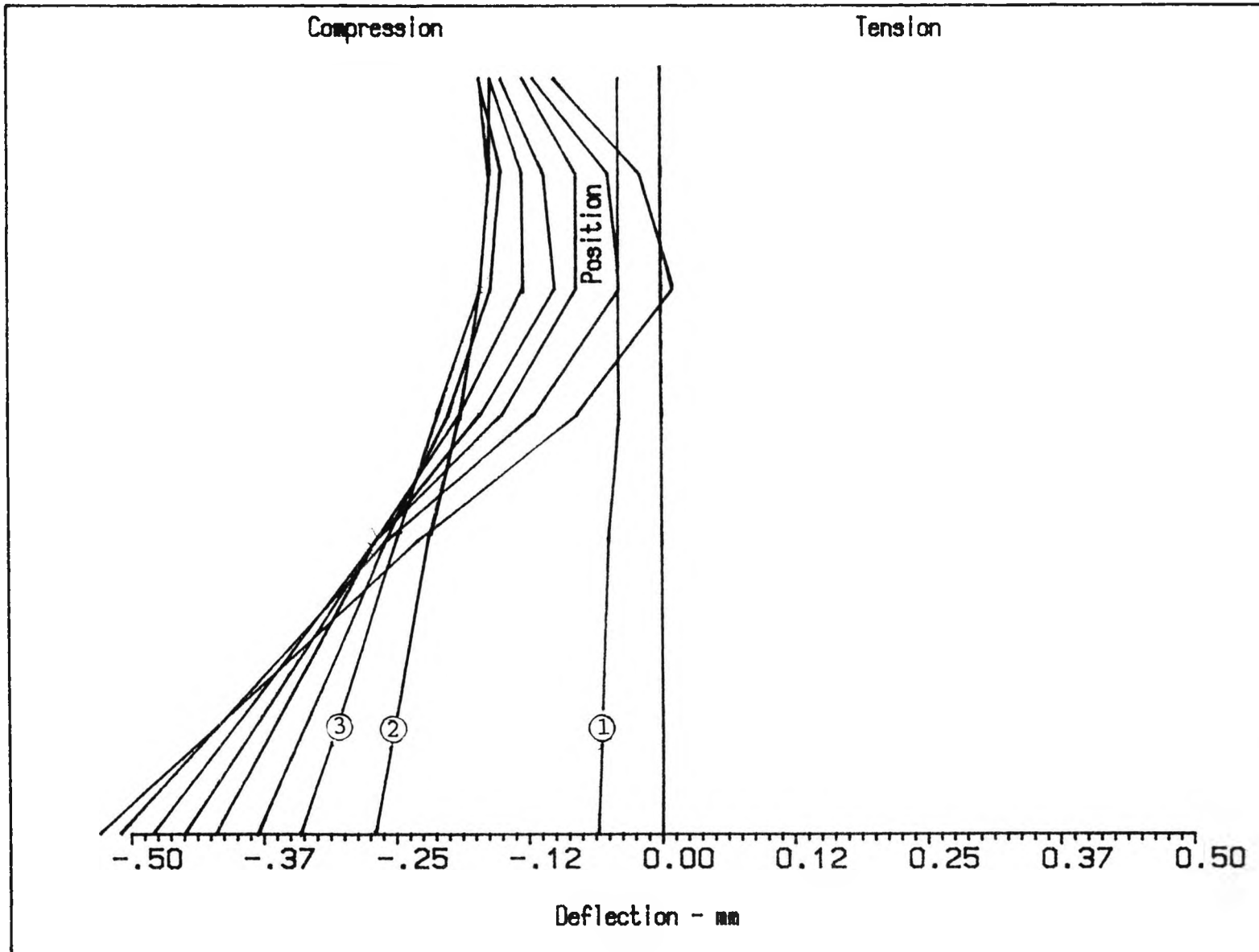
COMPARISON OF METHODS
 OF ROTATION MEASUREMENT.

Test D1



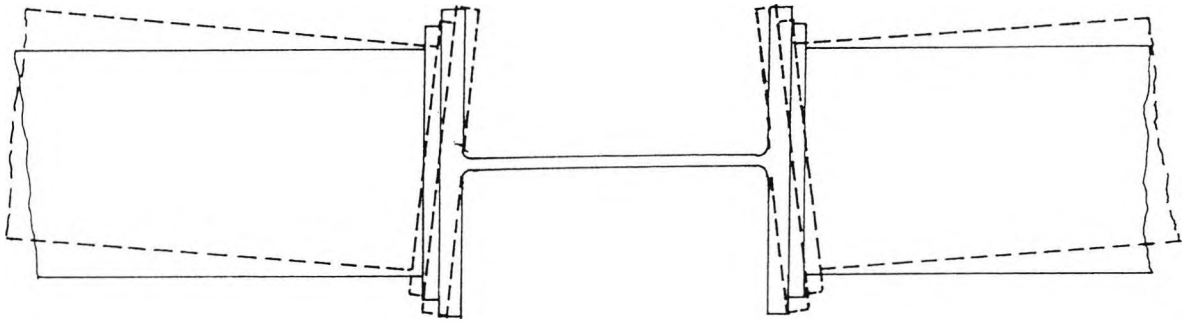
Connection Type :-
Unstiffened
Internal
Beam Size -254x102UB37
Column Size -305x305UC137
4 M20 Tension Bolts
Grade HSFG -Pretensioned
Endplate Thickness = 20 mm

Figure 5.13
ENDPLATE DEFLECTION
Test D1

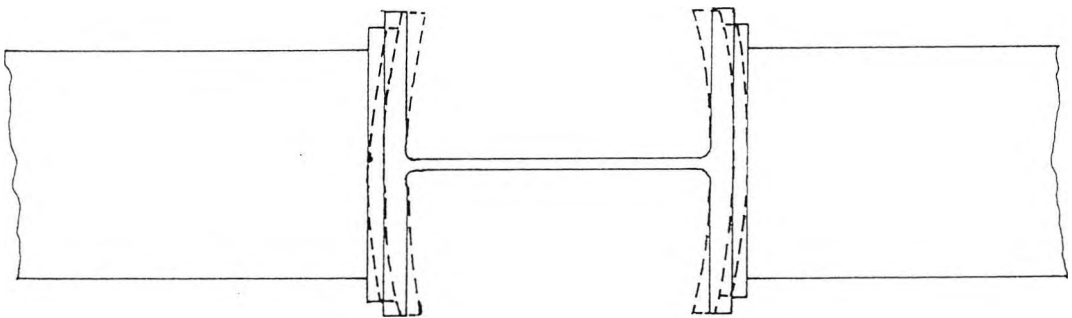


Connection Type :-
Unstiffened
Internal
Beam Size -254x102UB37
Column Size -305x305UC137
4 M20 Tension Bolts
Grade HSF8 -Pretensioned
Endplate Thickness = 20 mm

Figure 5.14
COLUMN FLANGE
DEFLECTION
Test D1

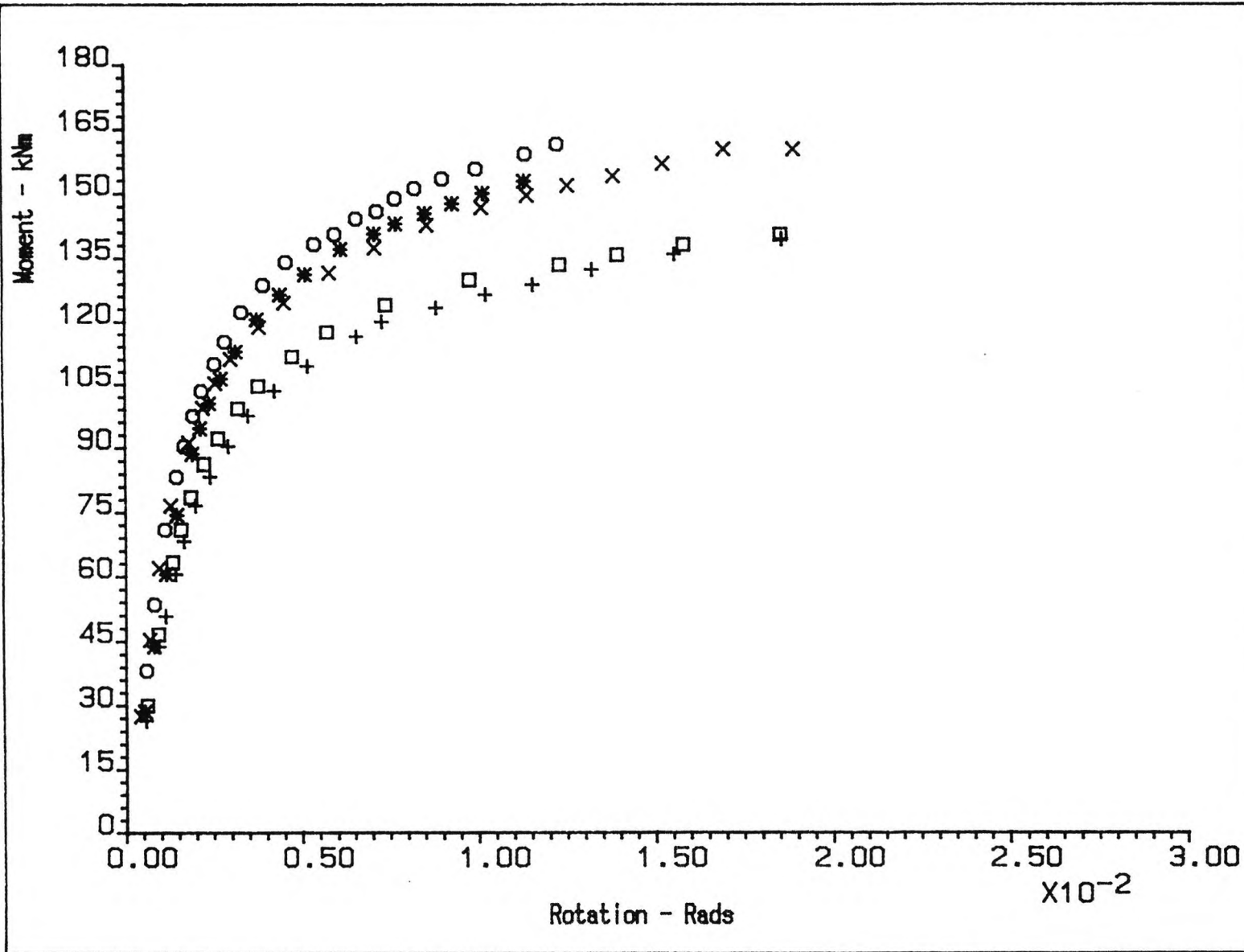


a) Skew Deflection of Column Flange.



b) Bending Deflection of Column Flange.

Figure 5.15 Column Flange Deflection in the Compression Region.



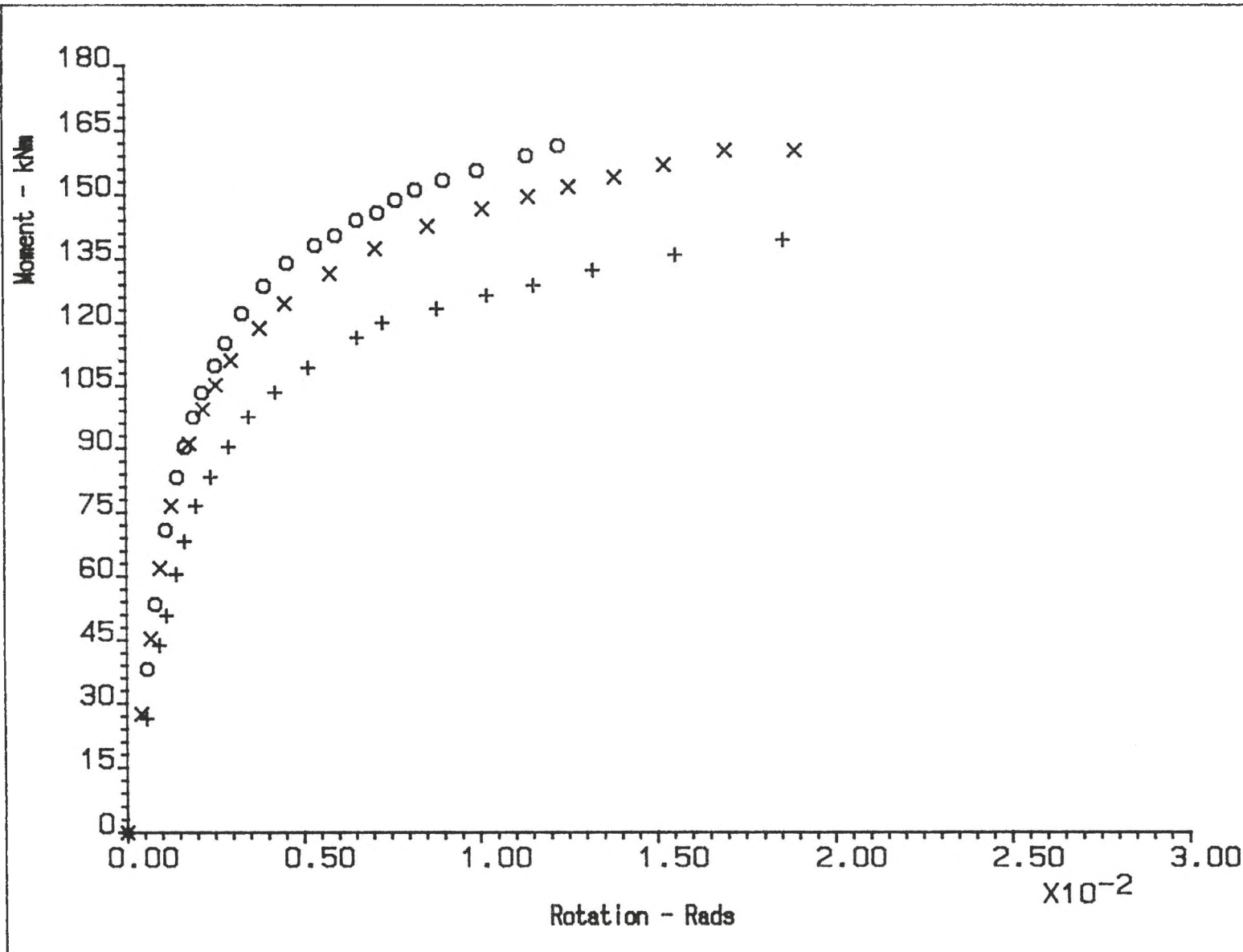
Connection Type :-
 Unstiffened
 Internal
 Beam Size -254x146 UB37
 Column Size -203x203 UC
 4 M20 Tension Bolts
 Grade HSFG -Pretensioned

× = Test A8
 + = Test A2
 ○ = Test A3
 * = Test A4
 □ = Test A5

Figure 5.16

COMPARISON OF MOMENT-
 ROTATION DATA.

Series A.



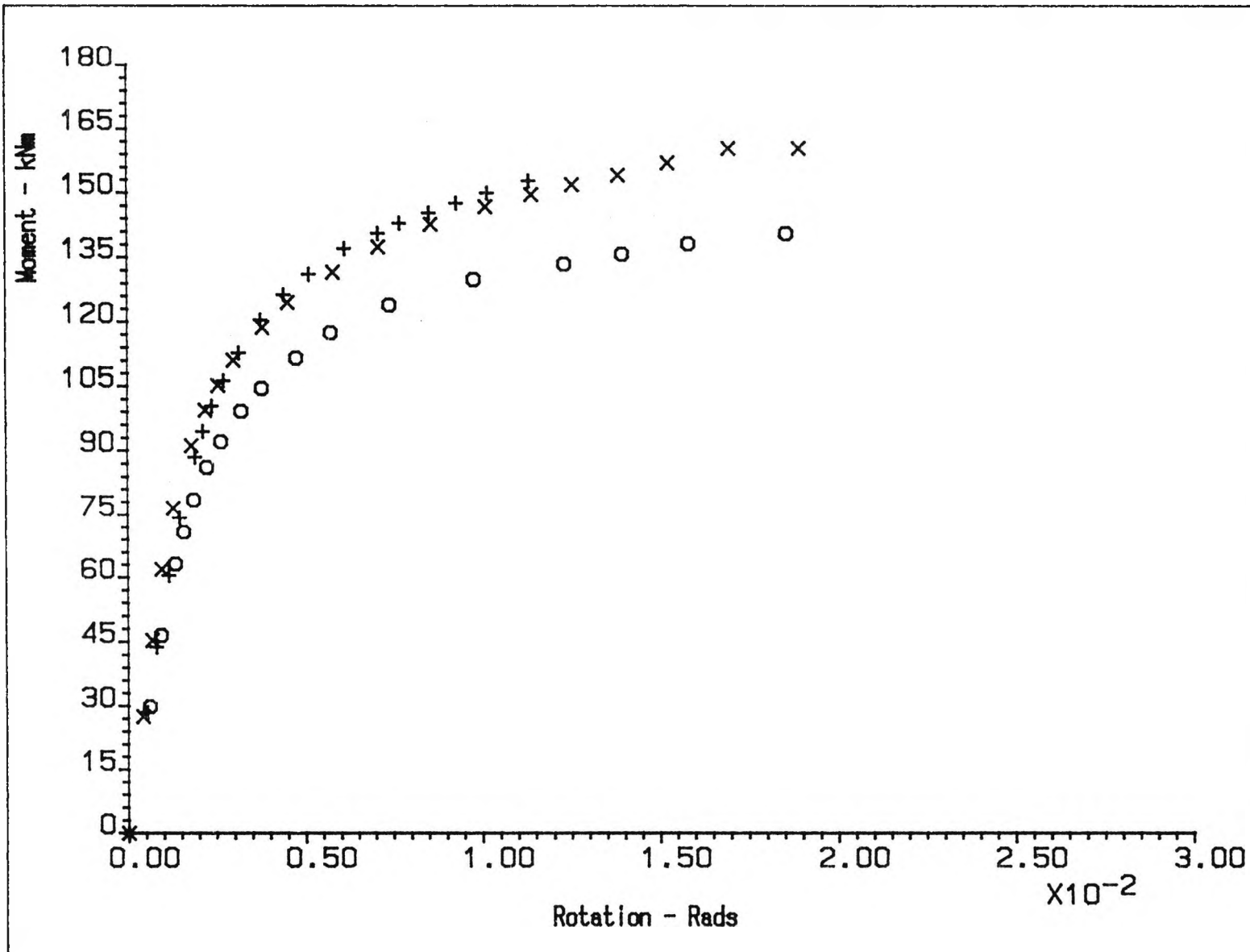
Connection Type :-
 Unstiffened
 Internal
 Beam Size -254x146 UB37
 Column Size -203x203 UC
 4 M20 Tension Bolts
 Grade HSFG -Pretensioned
 Endplate Thickness = 20mm

x = Test A8 ($t_{cf}=17.3\text{mm}$)
 + = Test A2 ($t_{cf}=14.2\text{mm}$)
 o = Test A3 ($t_{cf}=20.5\text{mm}$)

Figure 5.17

COMPARISON OF MOMENT-
 ROTATION DATA.

Series A



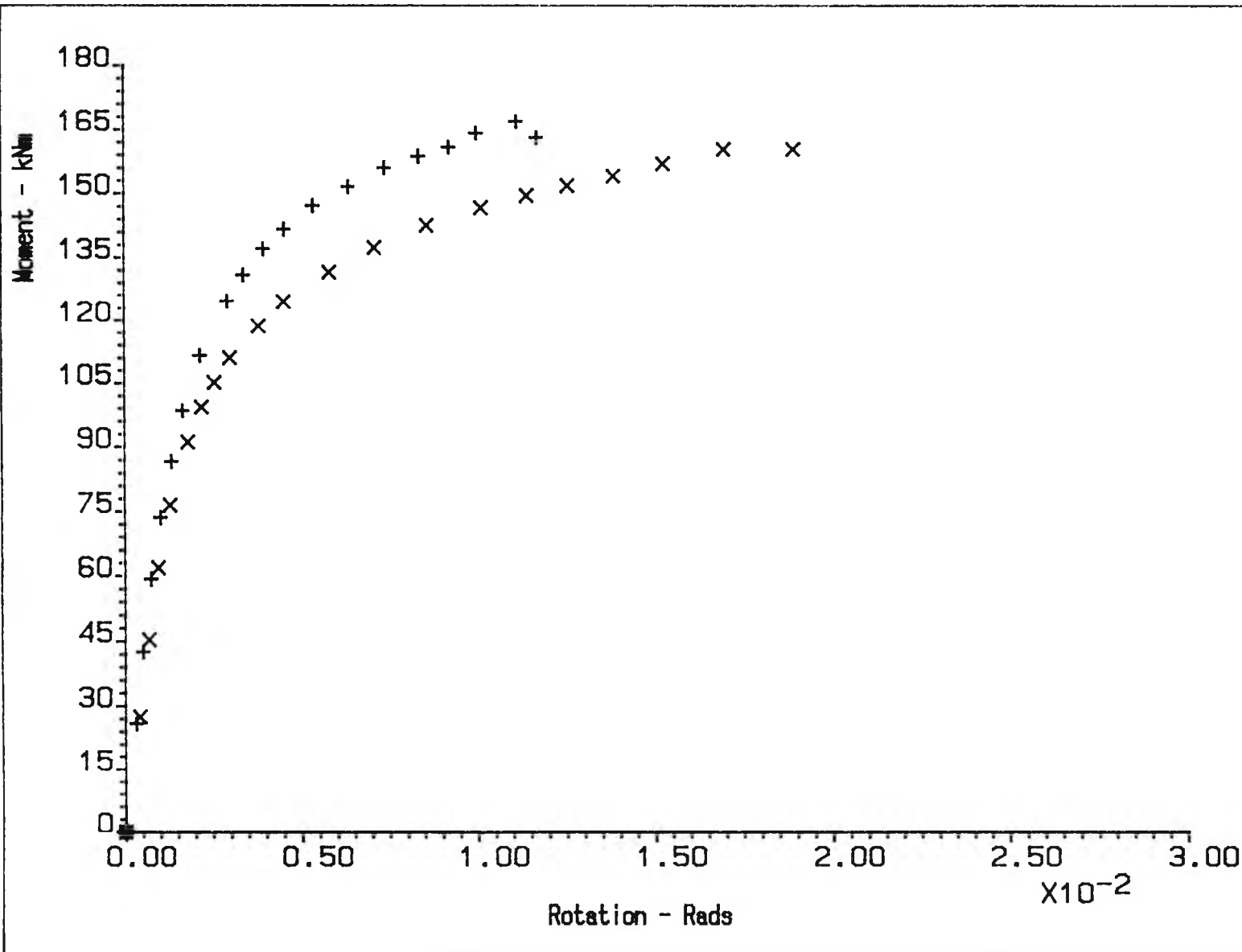
Connection Type :-
 Unstiffened
 Internal
 Beam Size -254x146 UB37
 Column Size -203x203 UC71
 4 M20 Tension Bolts
 Grade HSFG -Pretensioned

x = Test A8 ($t_{ep}=20.\text{mm}$)
 + = Test A4 ($t_{ep}=25.\text{mm}$)
 o = Test A5 ($t_{ep}=15.\text{mm}$)

Figure 5.18

COMPARISON OF MOMENT-
 ROTATION DATA.

Series A



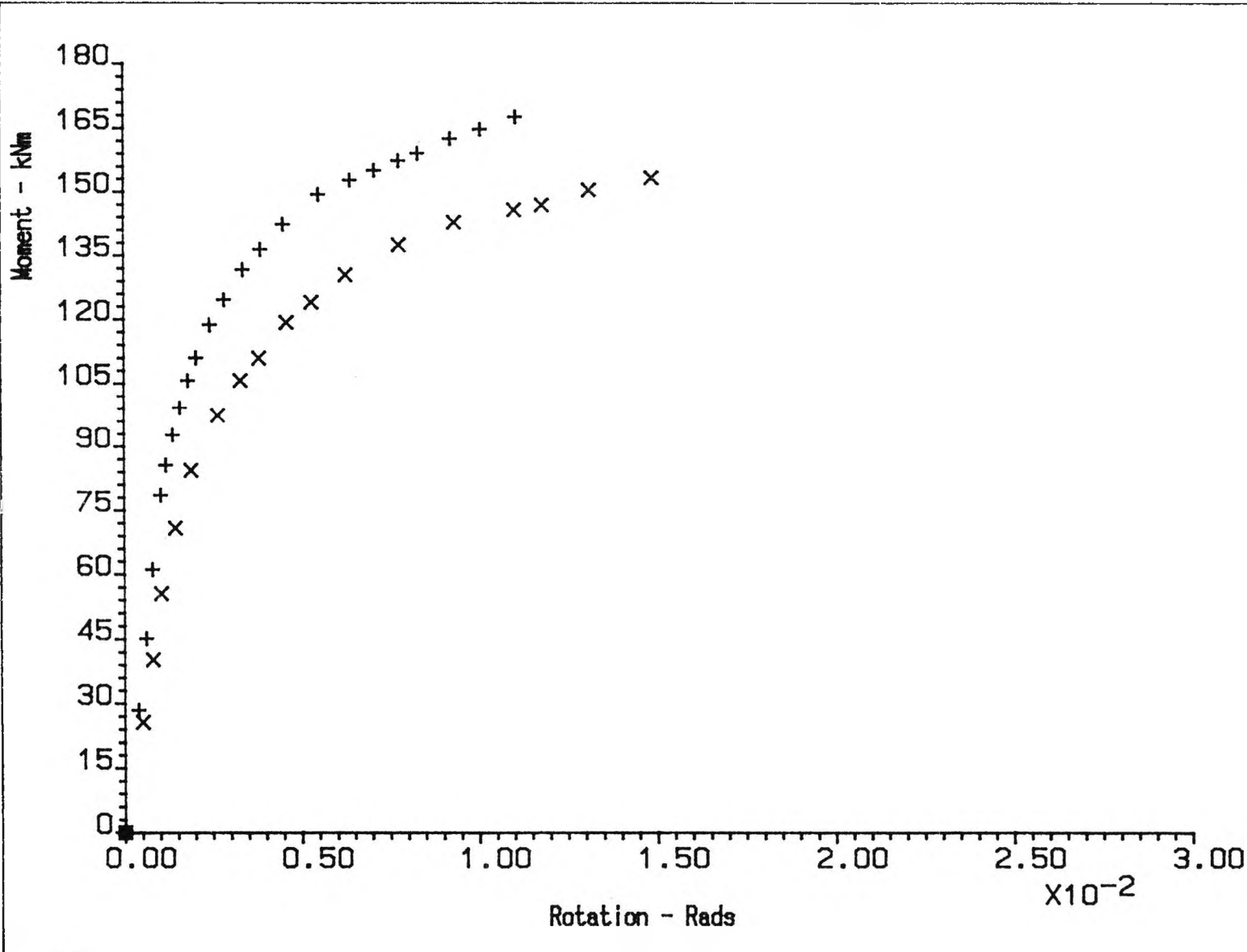
Connection Type :-
 Unstiffened
 Internal
 Beam Size -254x146 UB37
 4 M20 Tension Bolts
 Grade HSFG -Pretensioned
 Endplate Thickness = 20mm

x = Test A8 (203x203UC71)
 + = Test D1 (305x305UC137)

Figure 5.19

COMPARISON OF MOMENT-
 ROTATION DATA.

Series A & D



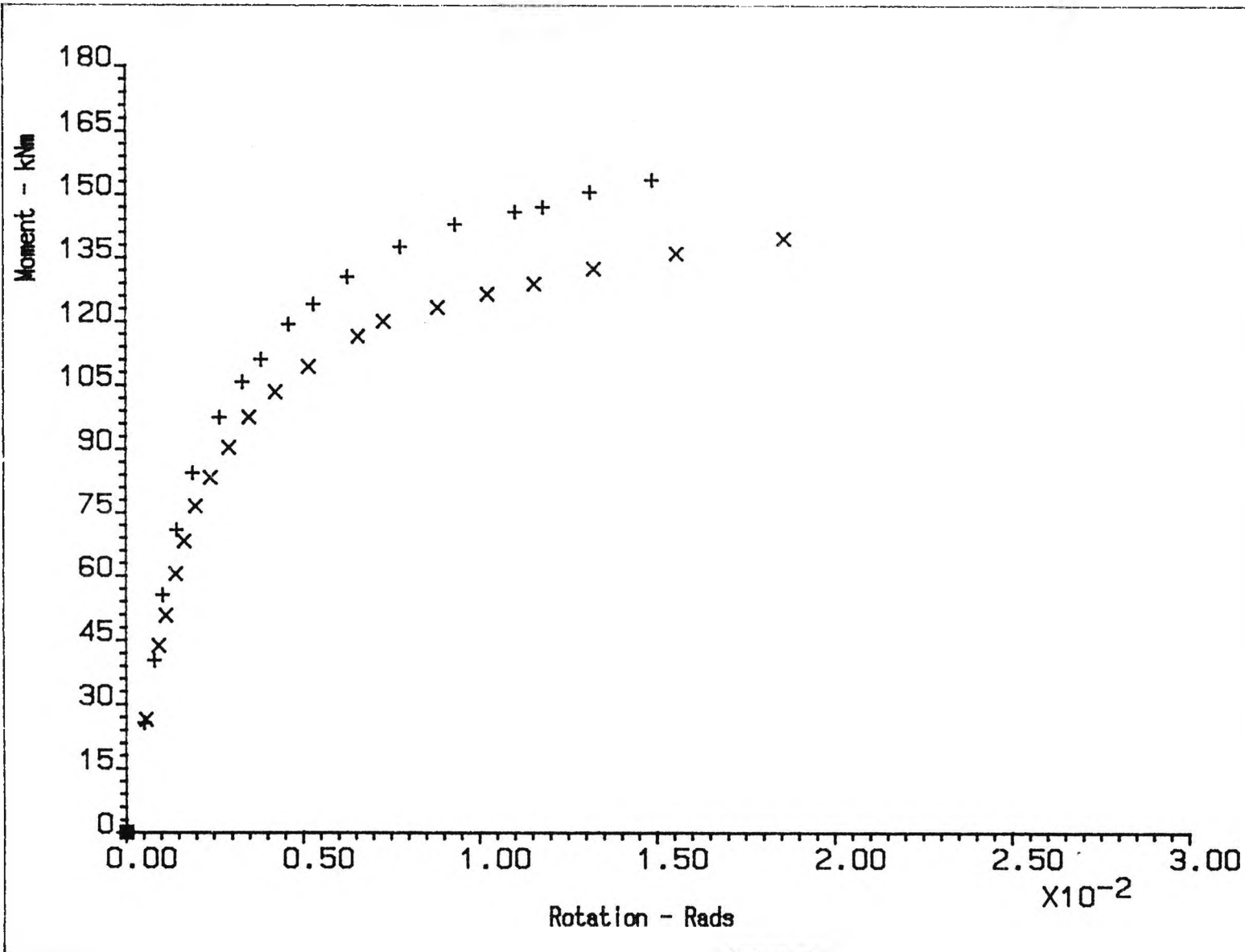
Connection Type :-
 Stiffened
 Internal
 Beam Size -254x146 UB37
 Column Size -203x203 IC
 4 M20 Tension Bolts
 Grade HSFG -Pretensioned
 Endplate Thickness = 20mm

x = Test A6 ($t_{cf}=14.2\text{mm}$)
 + = Test A7 ($t_{cf}=17.3\text{mm}$)

Figure 5.20

COMPARISON OF MOMENT-
 ROTATION DATA.

Series A



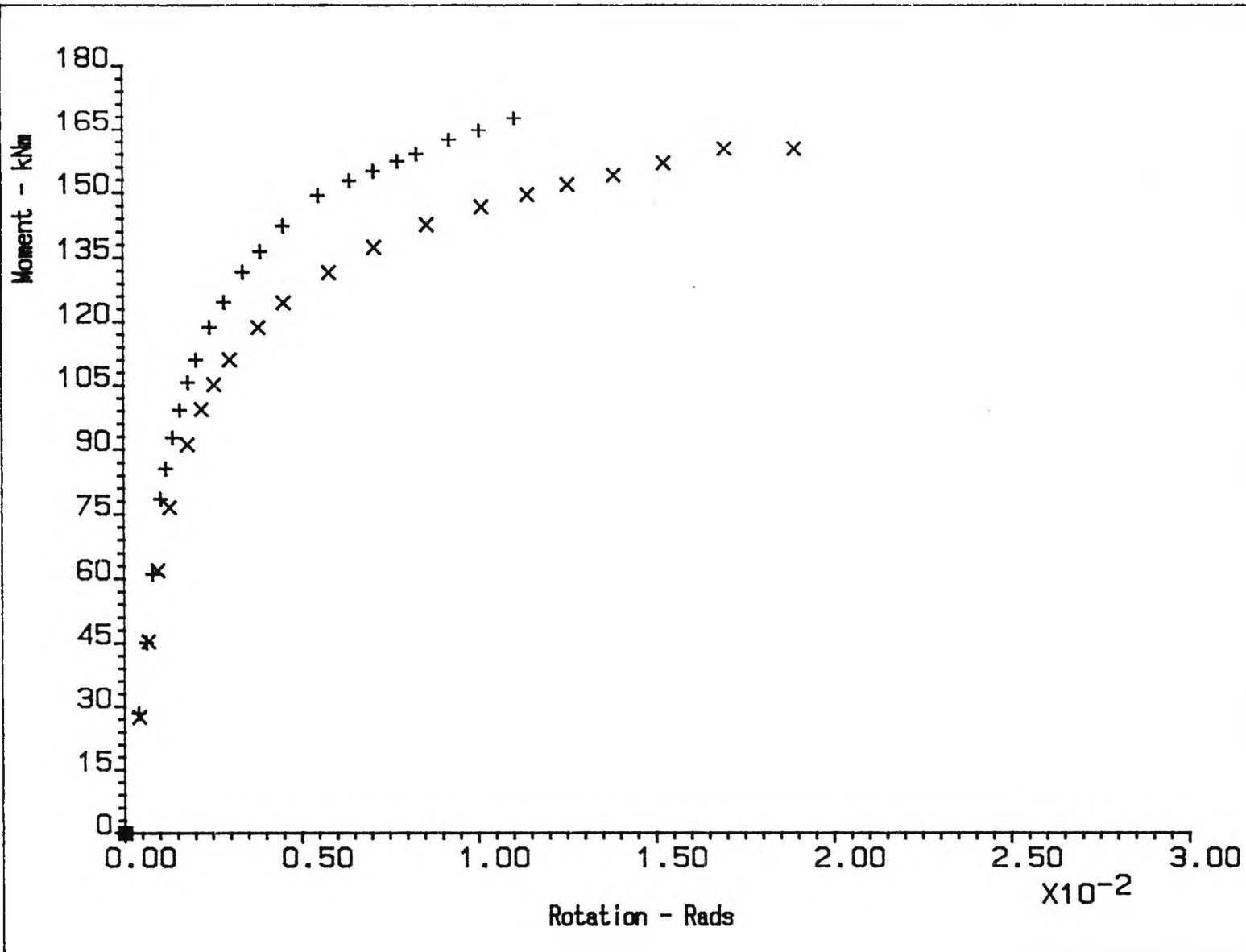
Connection Type :-
 Internal
 Beam Size -254x146 UB37
 Column Size -203x203 UC60
 4 M20 Tension Bolts
 Grade HSFG -Pretensioned
 Endplate Thickness = 20mm

x = Test A2 (unstiffened)
 + = Test A6 (stiffened)

Figure 5.21

COMPARISON OF MOMENT-
 ROTATION DATA.

Series A



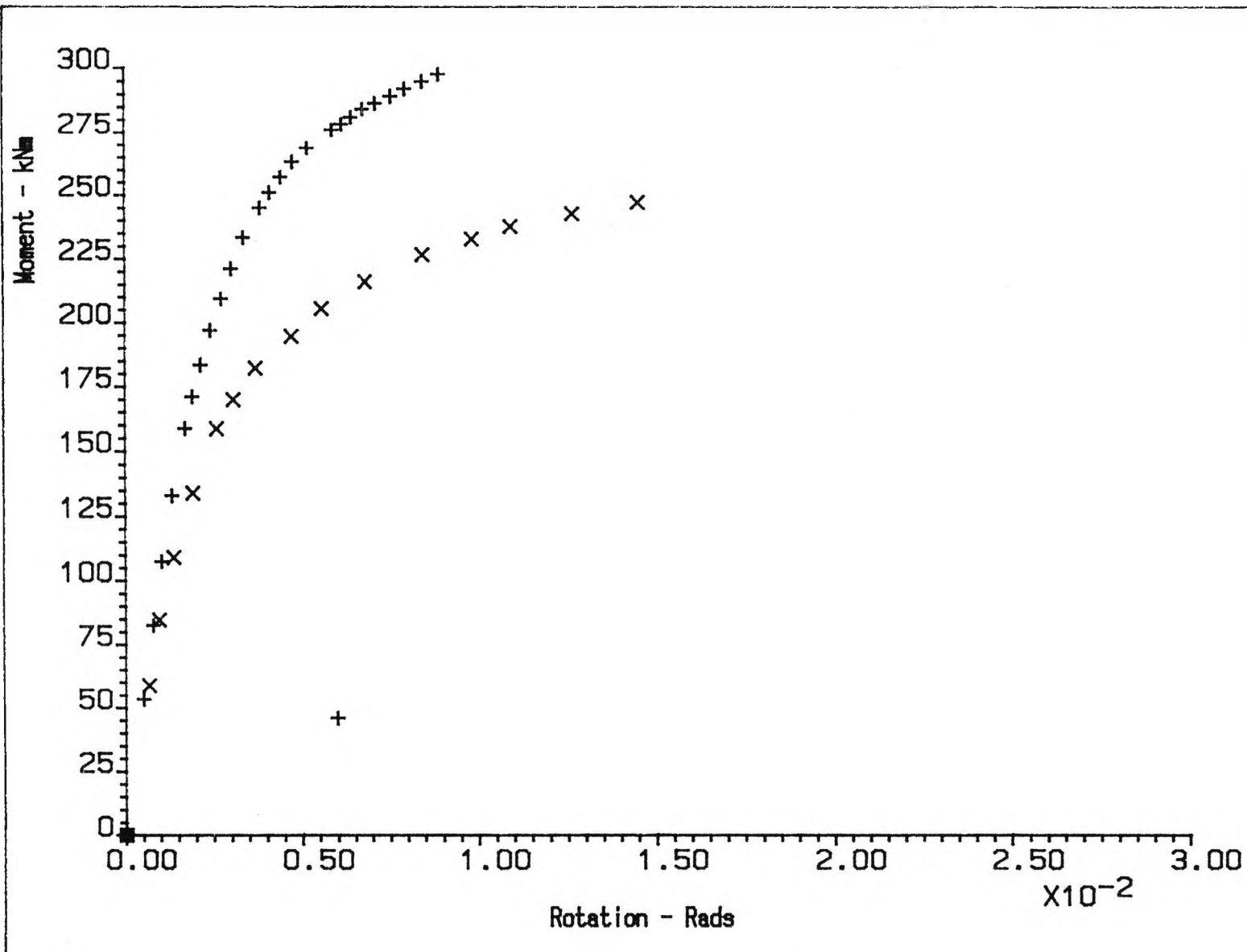
Connection Type :-
 Internal
 Beam Size -254x146 UB37
 Column Size -203x203 UC71
 4 M20 Tension Bolts
 Grade HSFG -Pretensioned
 Endplate Thickness = 20mm

x = Test A8 (unstiffened)
 + = Test A7 (stiffened)

Figure 5.22

COMPARISON OF MOMENT-
 ROTATION DATA.

Series A



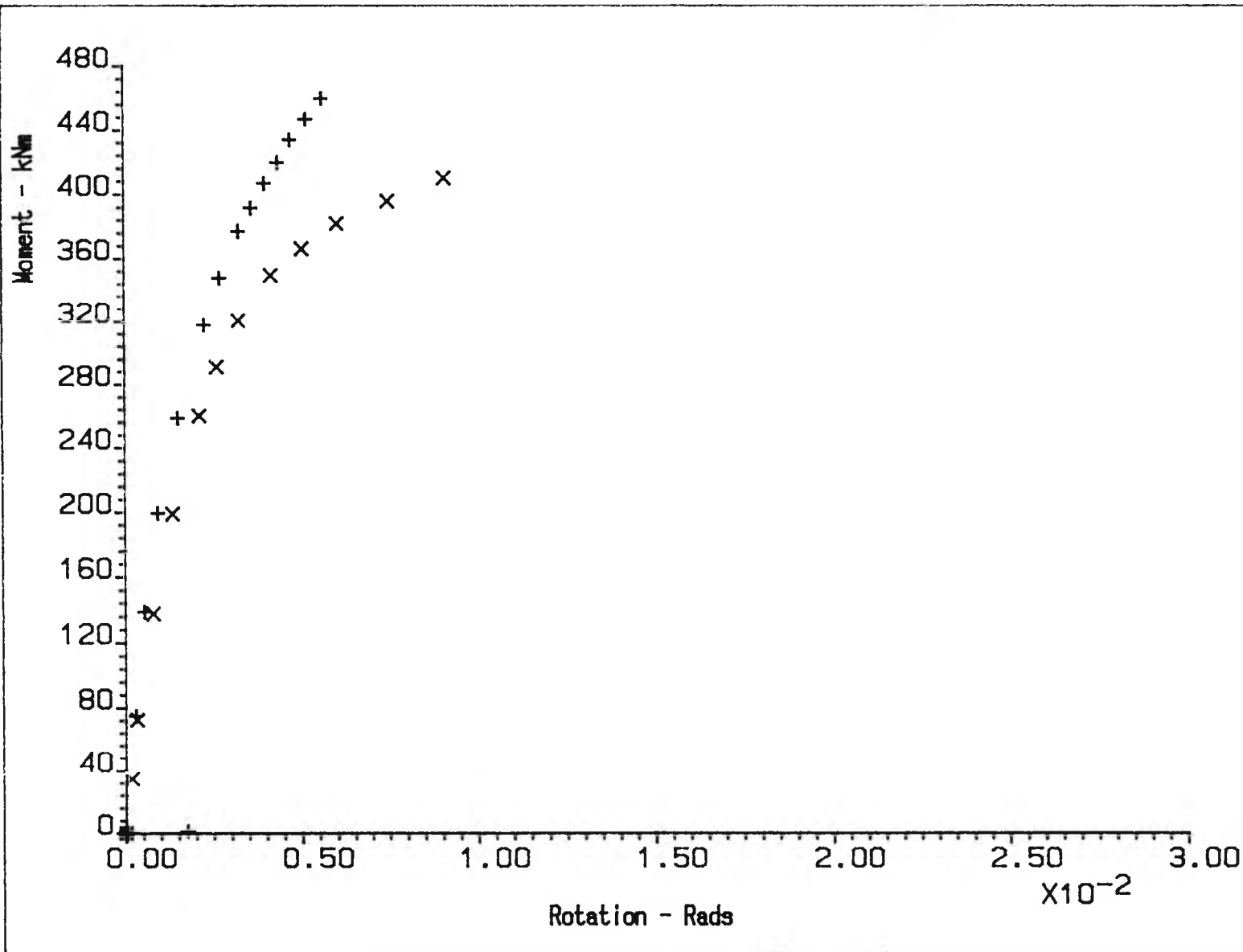
Connection Type :-
 Internal
 Beam Size -356x171 UB51
 Column Size -254x254 UC89
 4 M22 Tension Bolts
 Grade HSFG -Pretensioned
 Endplate Thickness = 25mm

x = Test B1 (unstiffened)
 + = Test B2 (stiffened)

Figure 5.23

COMPARISON OF MOMENT-
 ROTATION DATA.

Series B



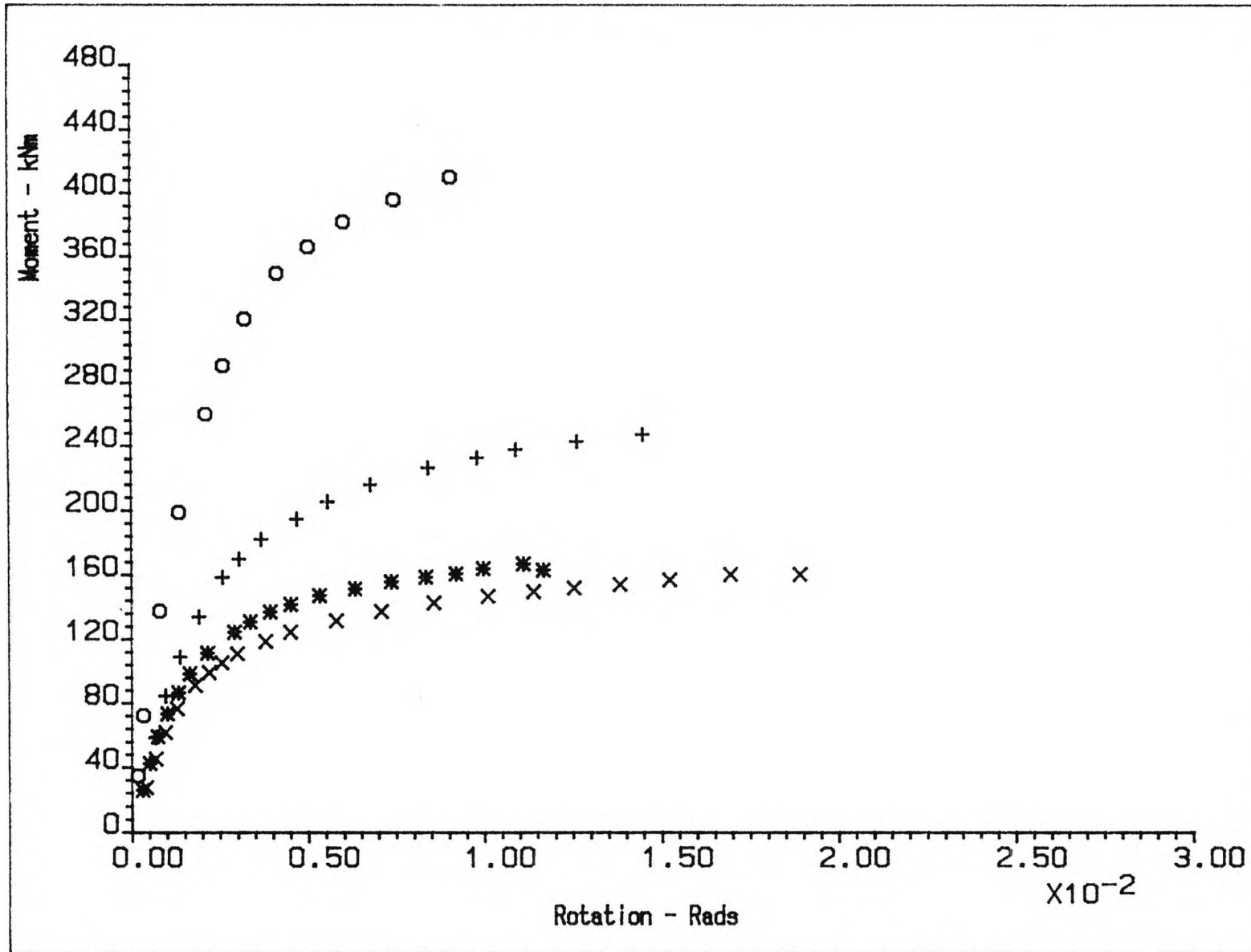
Connection Type :-
 Internal
 Beam Size -457x191UB74
 Column Size -305x305UC137
 6 M24 Tension Bolts
 Grade HSFG -Pretensioned
 Endplate Thickness = 25mm

x = Test C1 (unstiffened)
 + = Test C2 (stiffened)

Figure 5.24

COMPARISON OF MOMENT-
 ROTATION DATA.

Series C



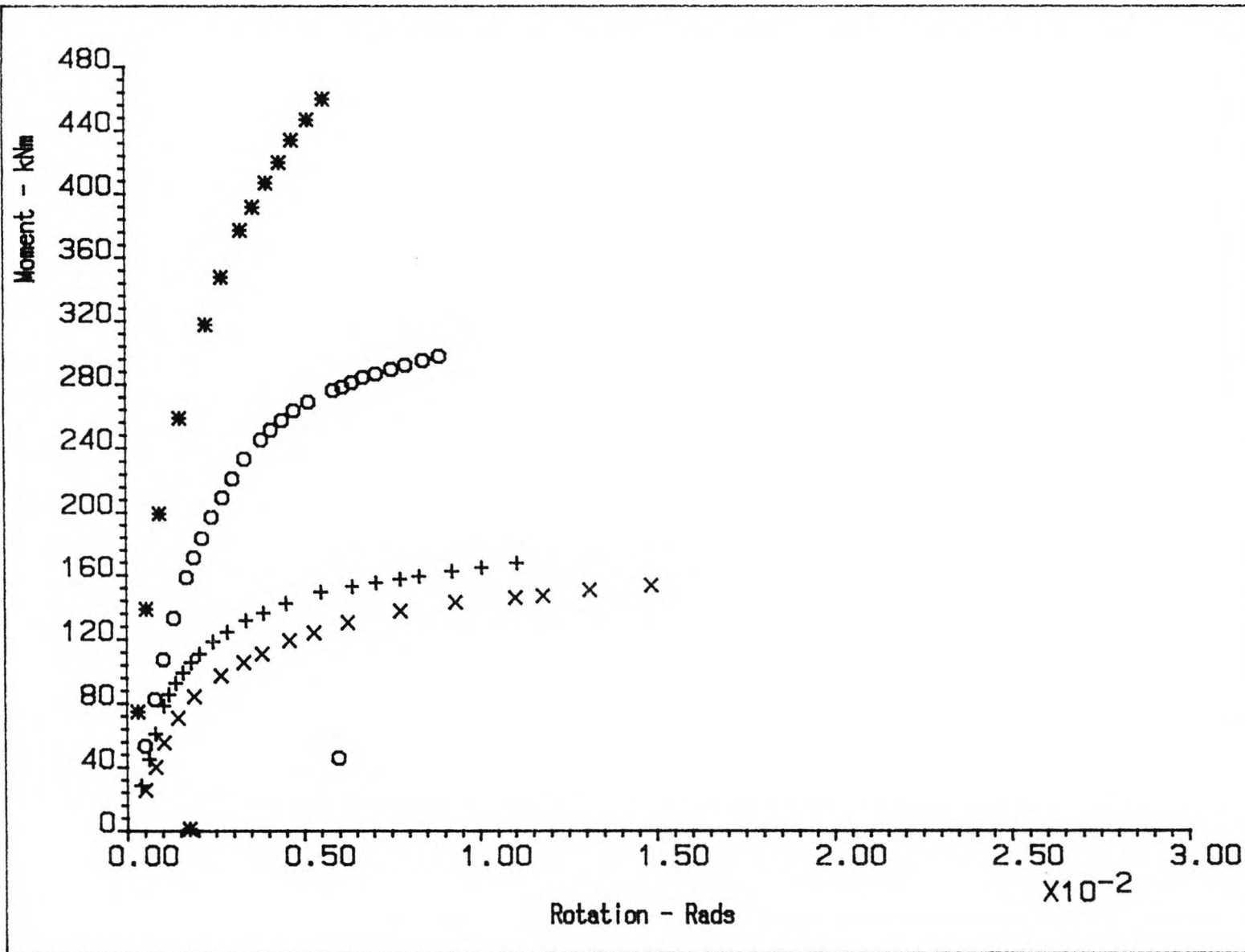
Connection Type :-
Unstiffened
Internal

x = Test A8
+ = Test B1
o = Test C1
* = Test D1

Figure 5.25

COMPARISON OF MOMENT-
ROTATION DATA.

Design connections



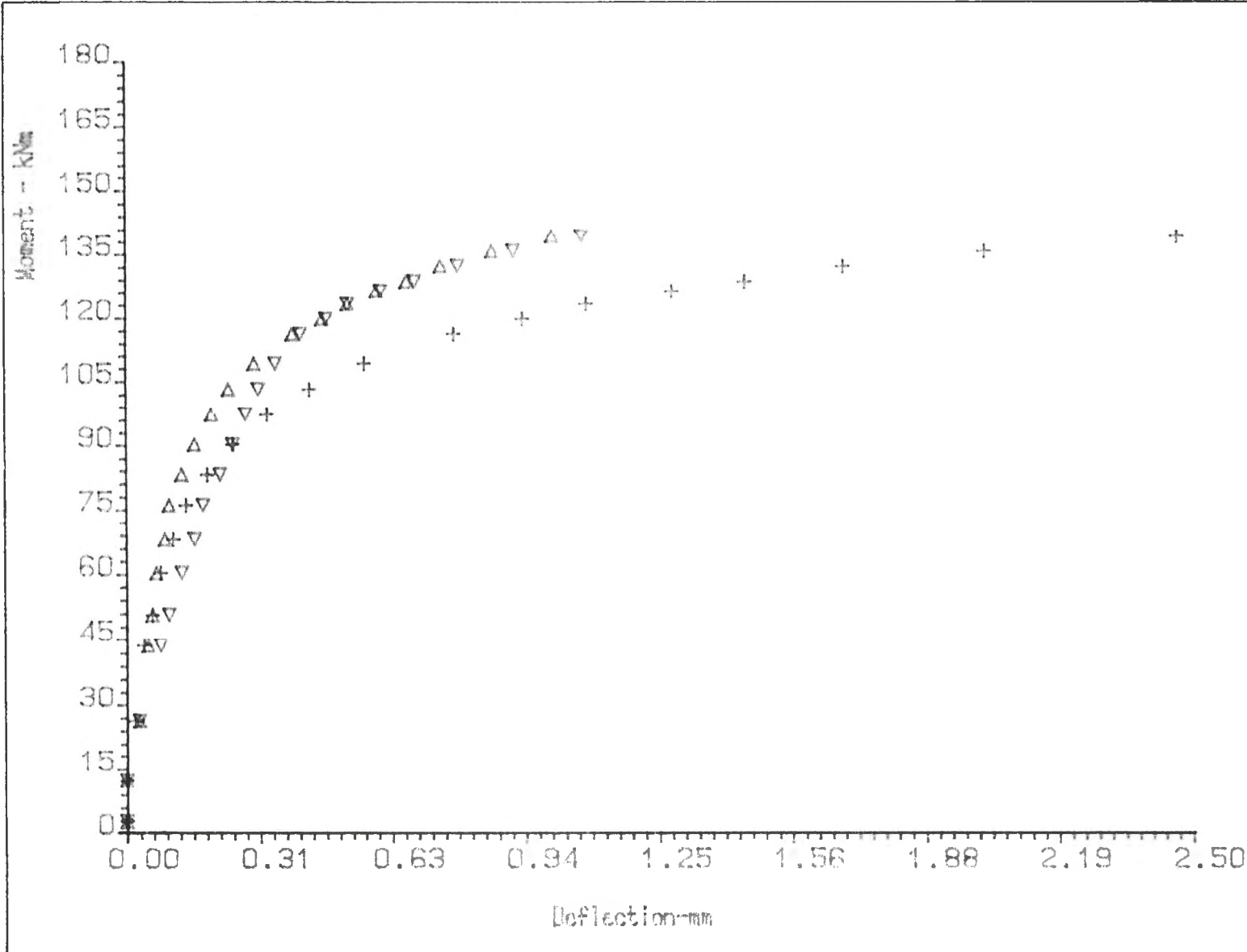
Connection Type :-
Stiffened
Internal

x = Test A6
+ = Test A7
o = Test B2
* = Test C2

Figure 5.26

COMPARISON OF MOMENT-
ROTATION DATA.

Stiffened connections



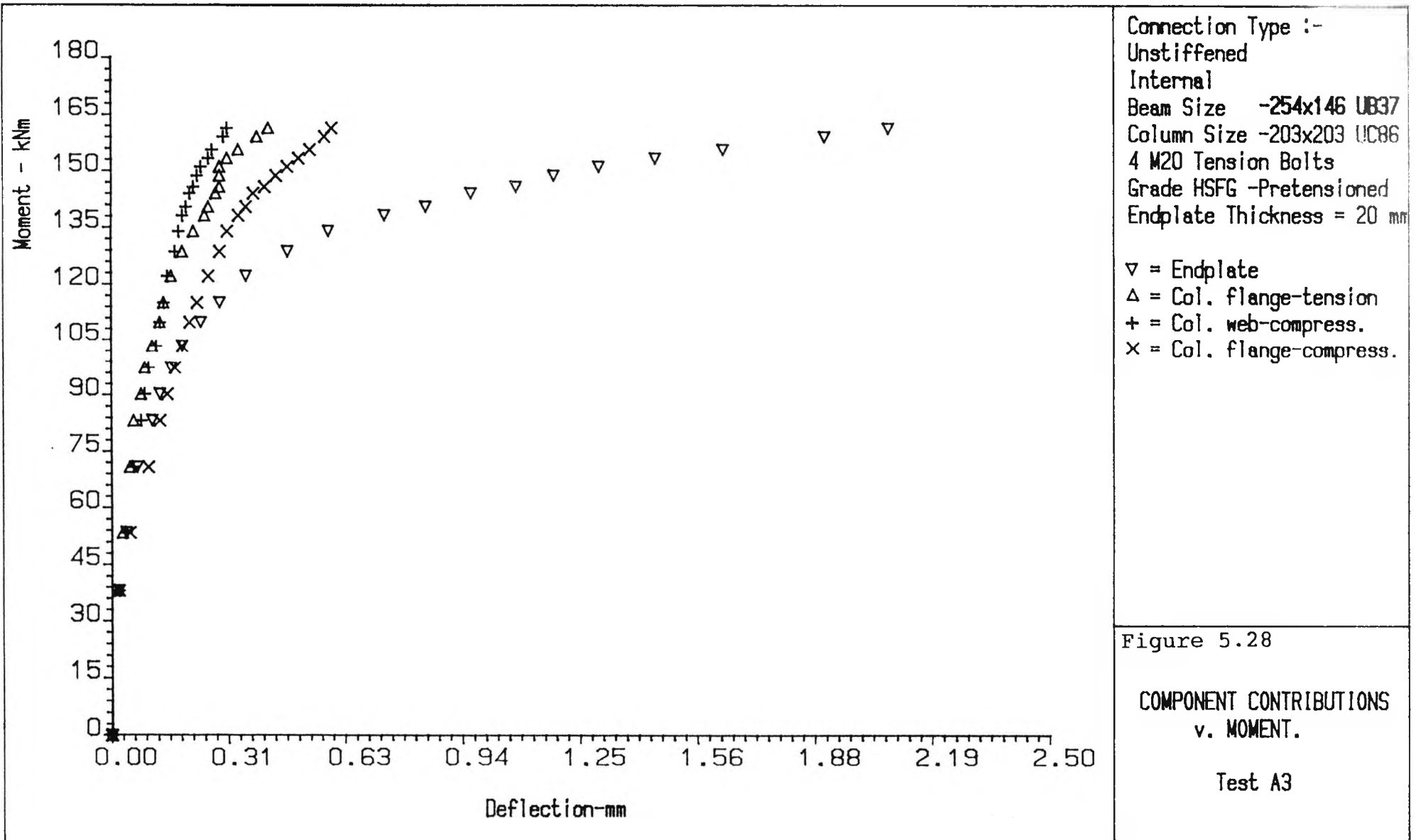
Connection Type :-
 Unstiffened
 Internal
 Beam Size -254x146 UB37
 Column Size -203x203 UC60
 4 M20 Tension Bolts
 Grade HSFG -Pretensioned
 Endplate Thickness = 20mm

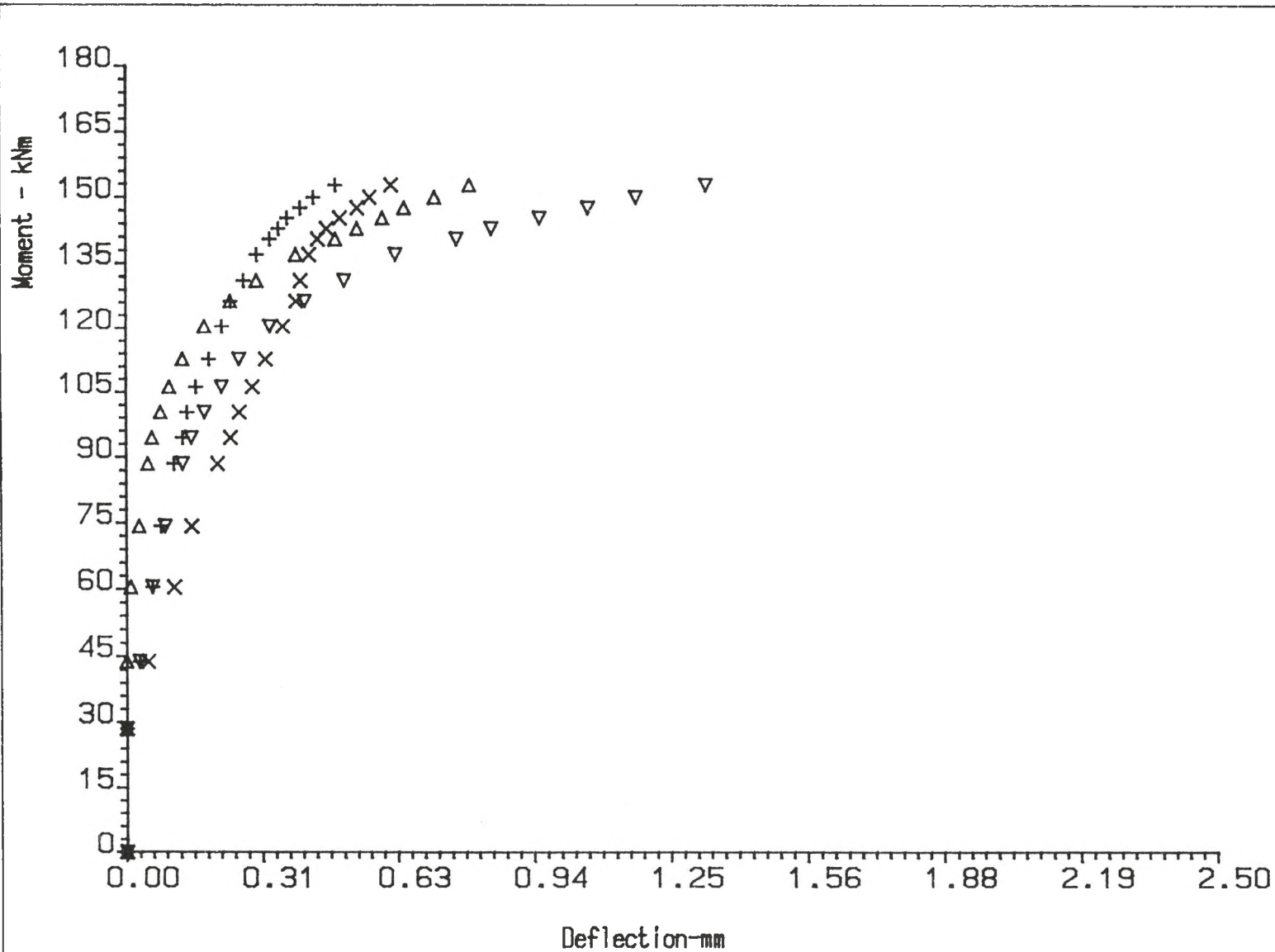
+ = Endplate
 Δ = Col. flange-tension
 ∇ = Col. flange-compress.

Figure 5.27

COMPONENT CONTRIBUTIONS
 v. MOMENT.

Test A2





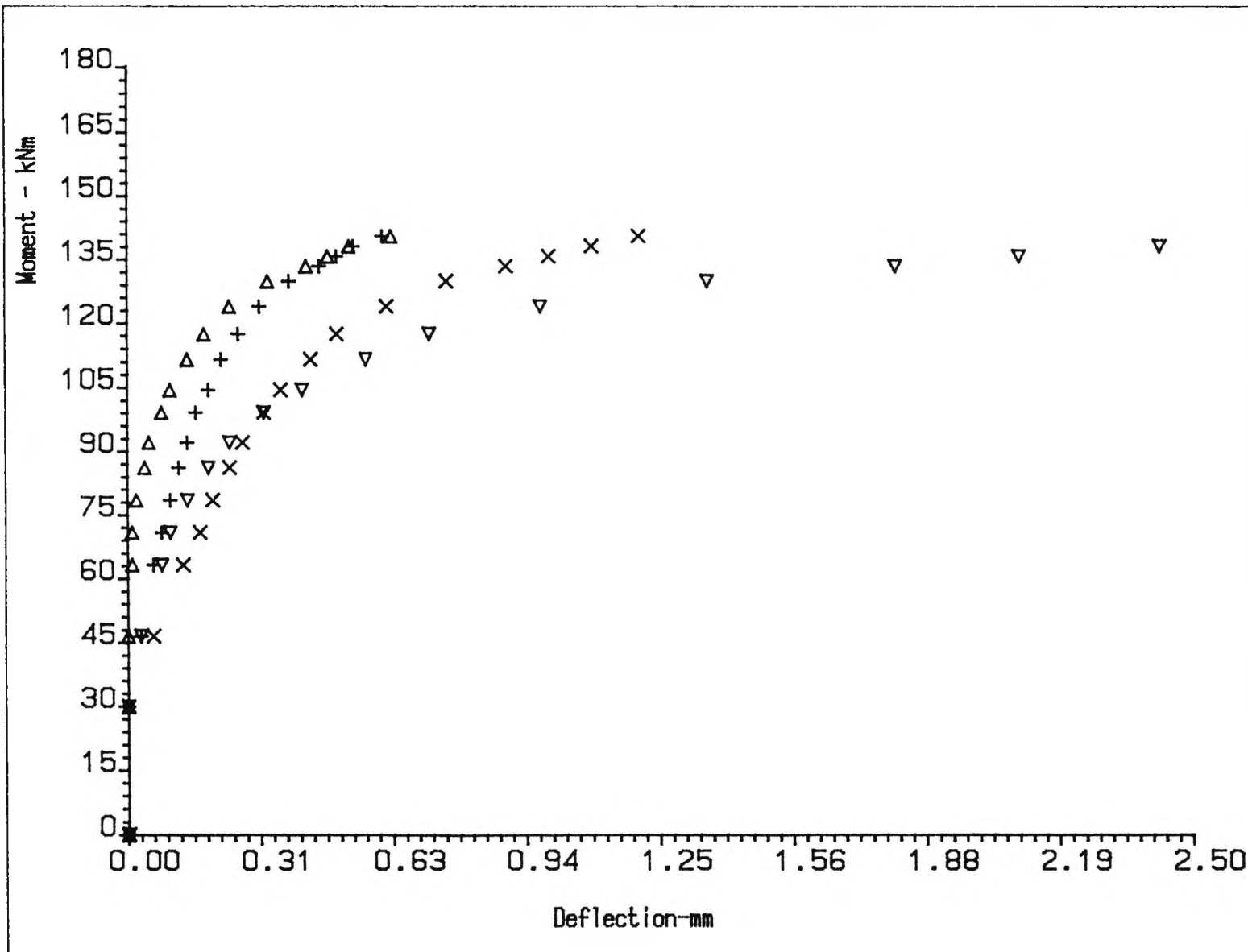
Connection Type :-
 Unstiffened
 Internal
 Beam Size -254x146 UB37
 Column Size -203x203 UC71
 4 M20 Tension Bolts
 Grade HSFG -Pretensioned
 Endplate Thickness = 25 mm

▽ = Endplate
 △ = Col. flange-tension
 + = Col. web-compress.
 × = Col. flange-compress.

Figure 5.29

COMPONENT CONTRIBUTIONS
 v. MOMENT.

Test A4



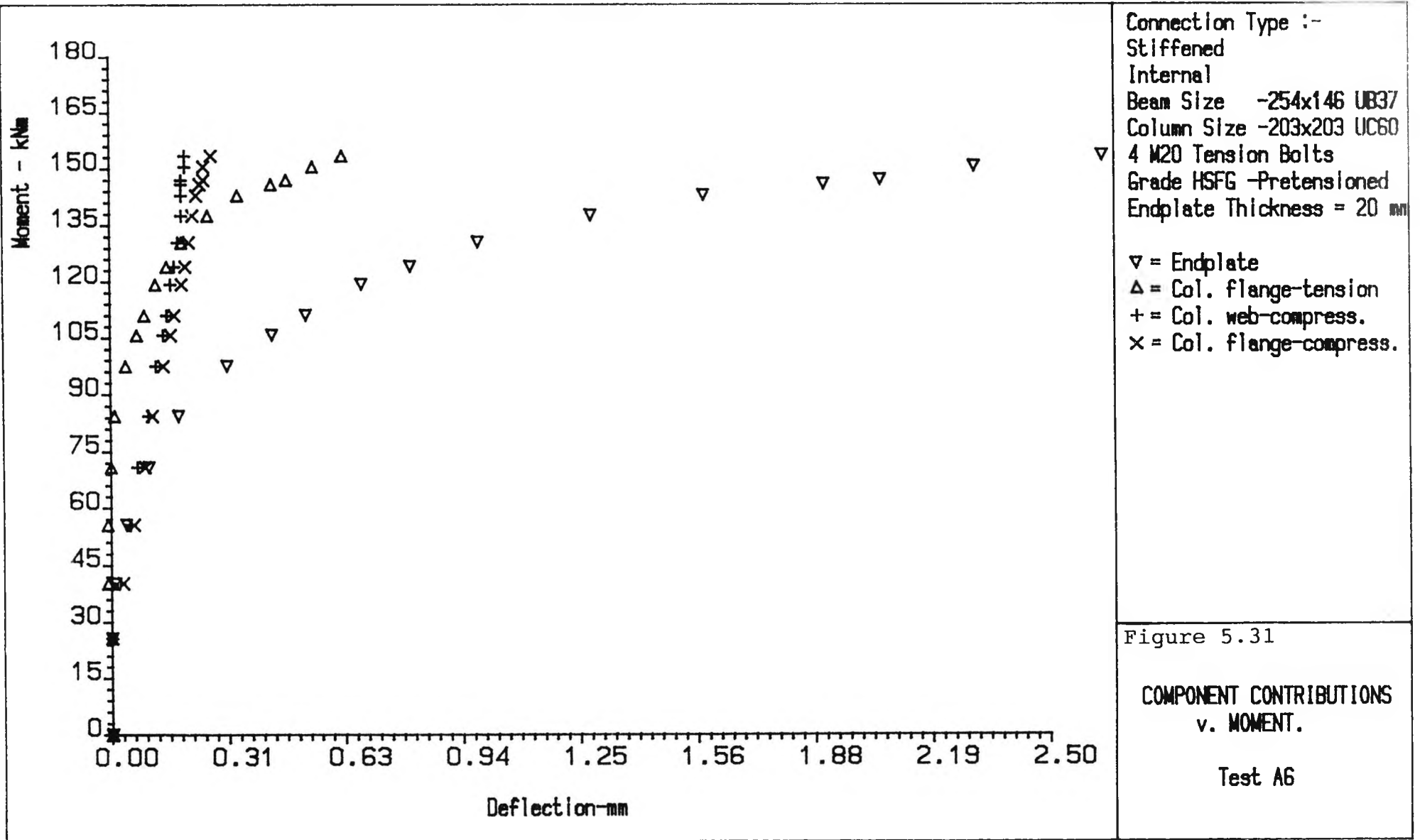
Connection Type :-
 Unstiffened
 Internal
 Beam Size -254x146 UB37
 Column Size -203x203 UC71
 4 M20 Tension Bolts
 Grade HSFG -Pretensioned
 Endplate Thickness = 15 mm

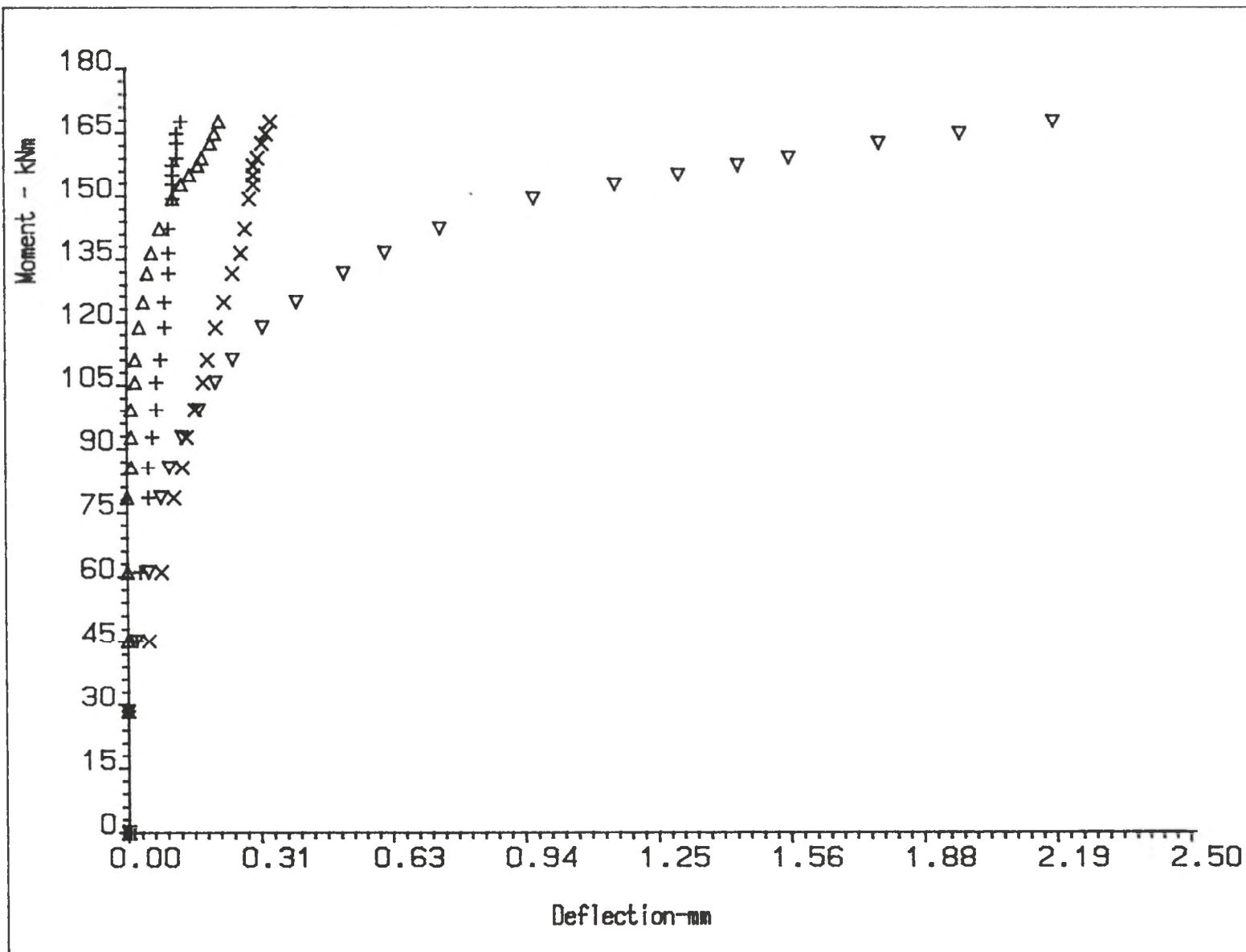
▽ = Endplate
 △ = Col. flange-tension
 + = Col. web-compress.
 × = Col. flange-compress.

Figure 5.30

COMPONENT CONTRIBUTIONS
 v. MOMENT.

Test A5





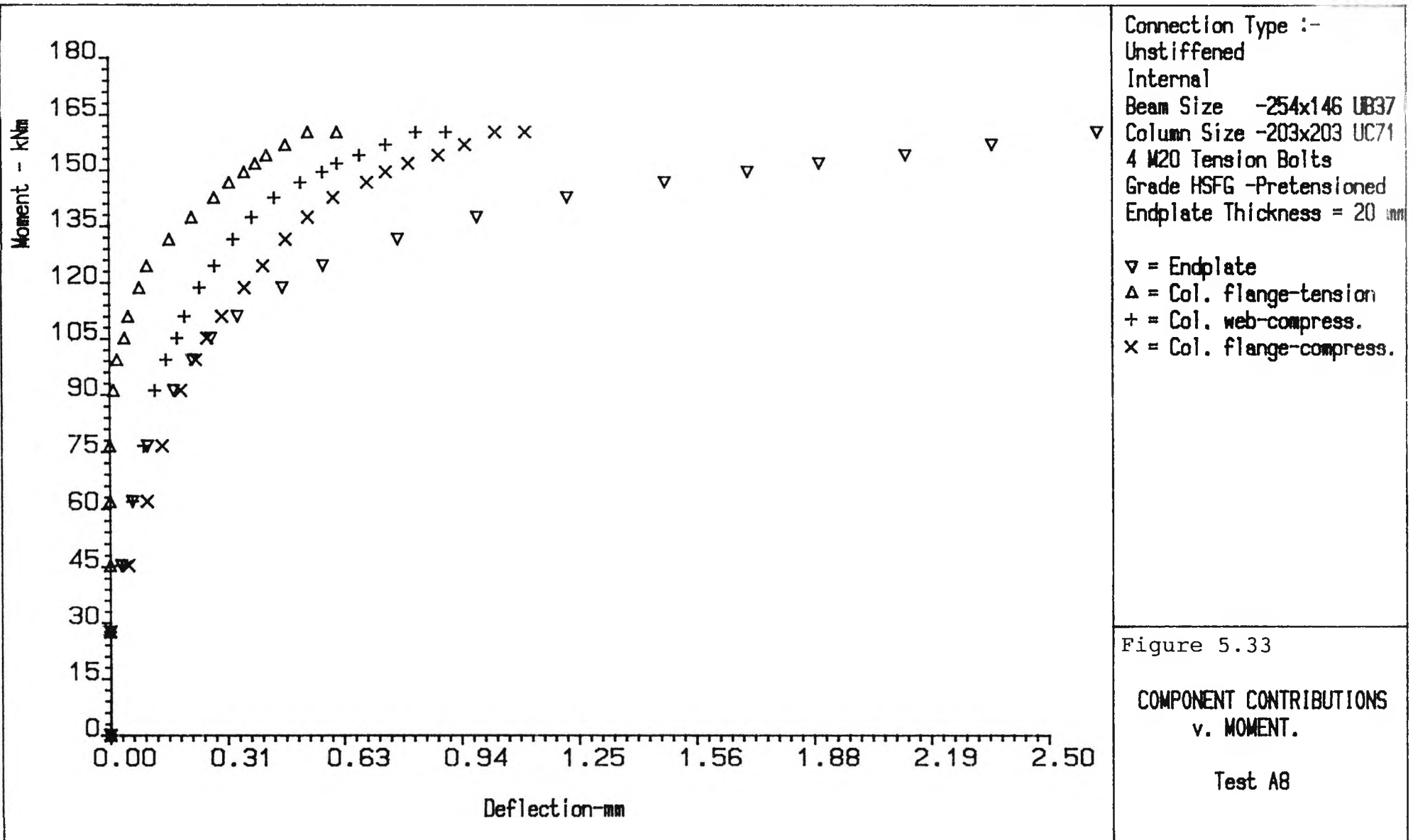
Connection Type :-
 Stiffened
 Internal
 Beam Size -254x146 UB37
 Column Size -203x203 UC71
 4 M20 Tension Bolts
 Grade HSFG -Pretensioned
 Endplate Thickness = 20 mm

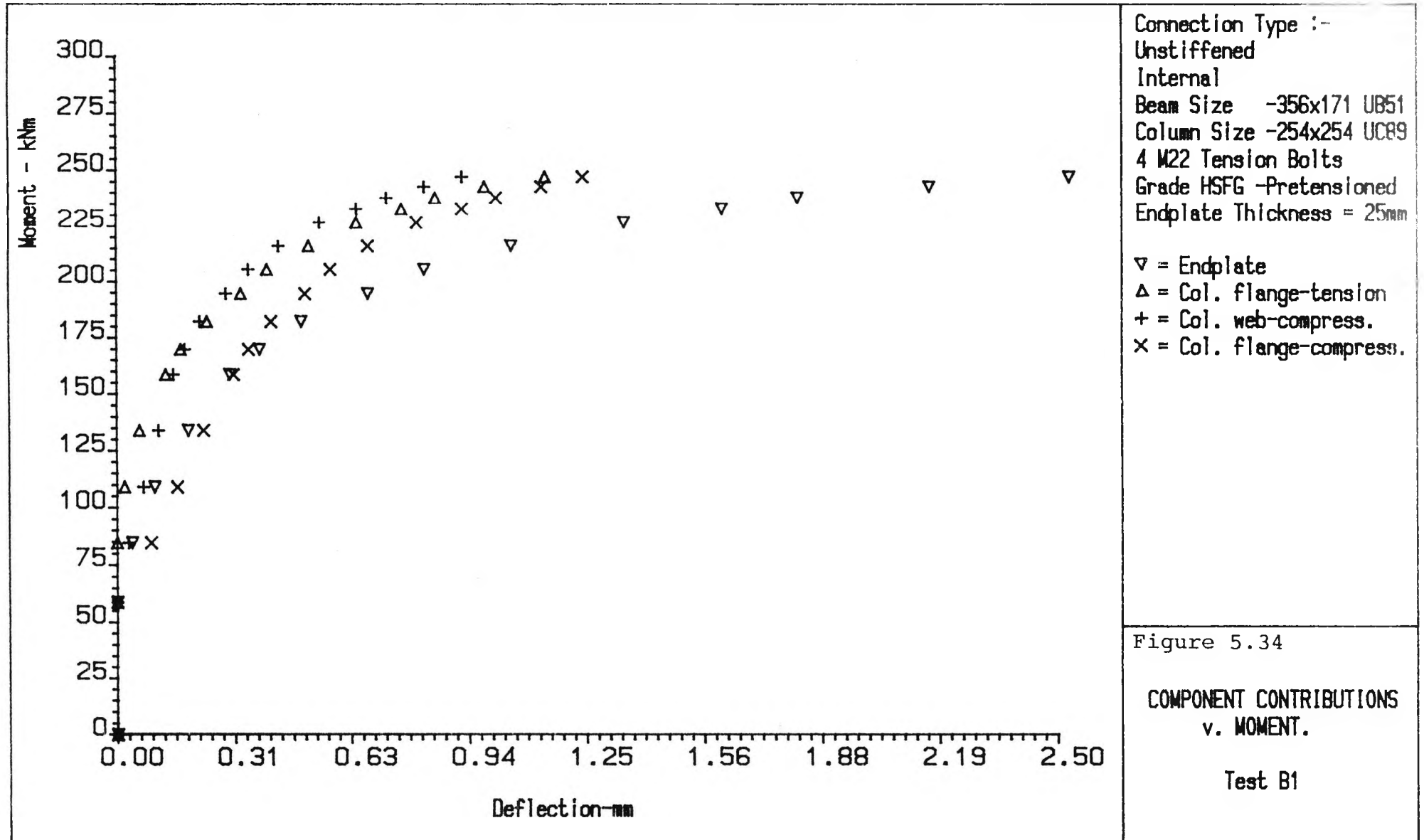
▽ = Endplate
 △ = Col. flange-tension
 + = Col. web-compress.
 × = Col. flange-compress.

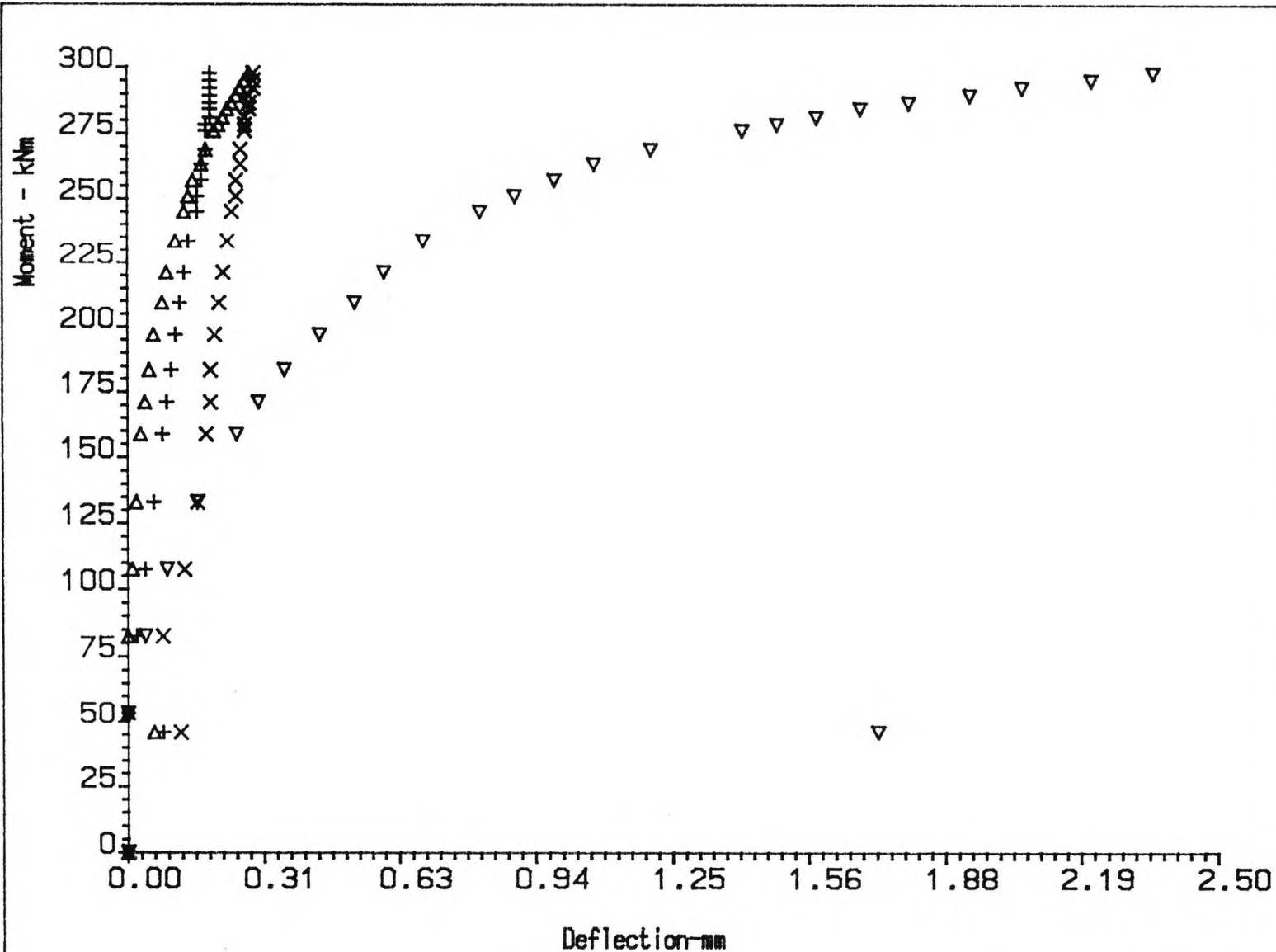
Figure 5.32

COMPONENT CONTRIBUTIONS
 v. MOMENT.

Test A7







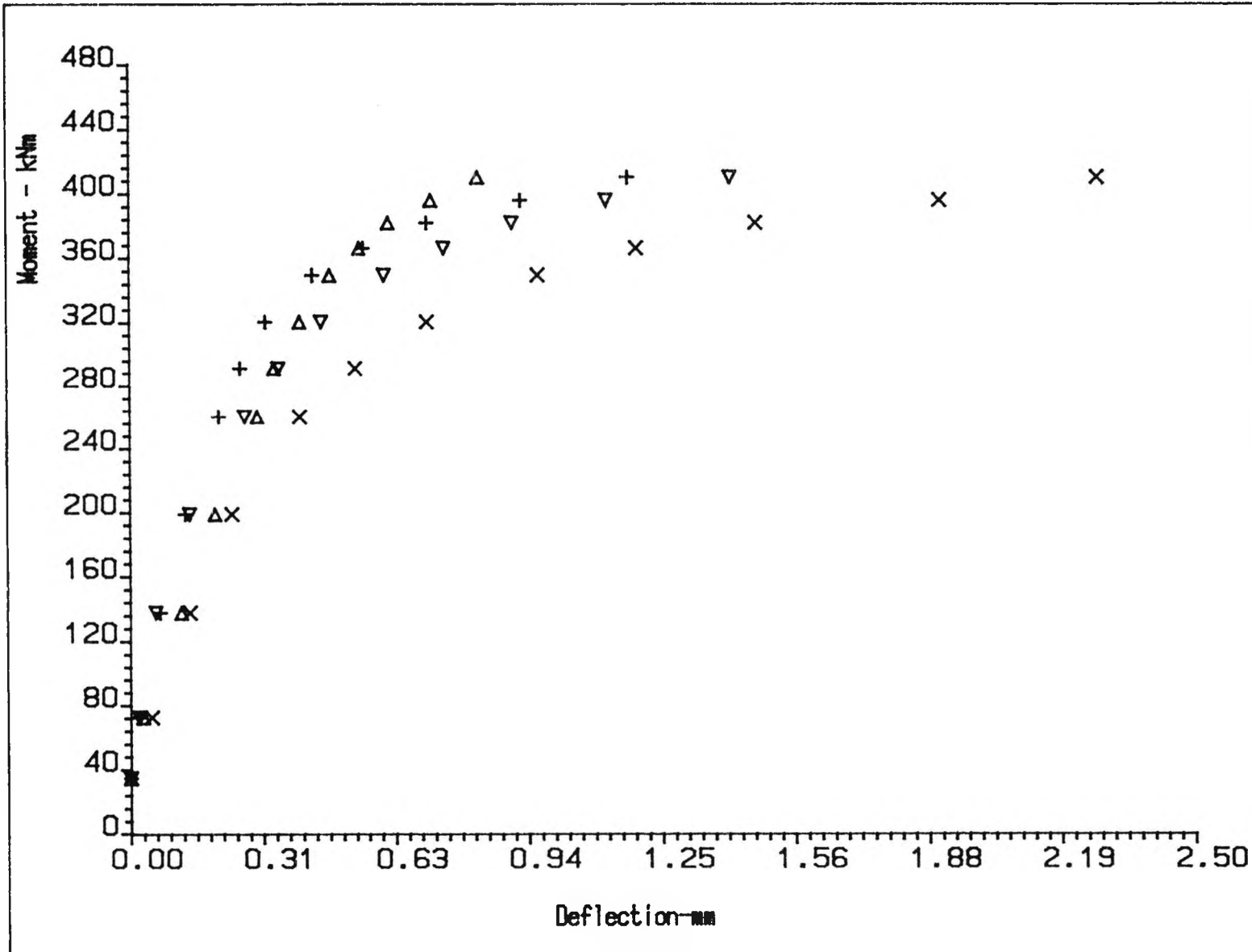
Connection Type :-
 Stiffened
 Internal
 Beam Size -356x171 UB51
 Column Size -254x254 UC89
 4 M22 Tension Bolts
 Grade HSFG -Pretensioned
 Endplate Thickness = 25mm

▽ = Endplate
 Δ = Col. flange-tension
 + = Col. web-compress.
 X = Col. flange-compress.

Figure 5.35

COMPONENT CONTRIBUTIONS
 v. MOMENT.

Test B2



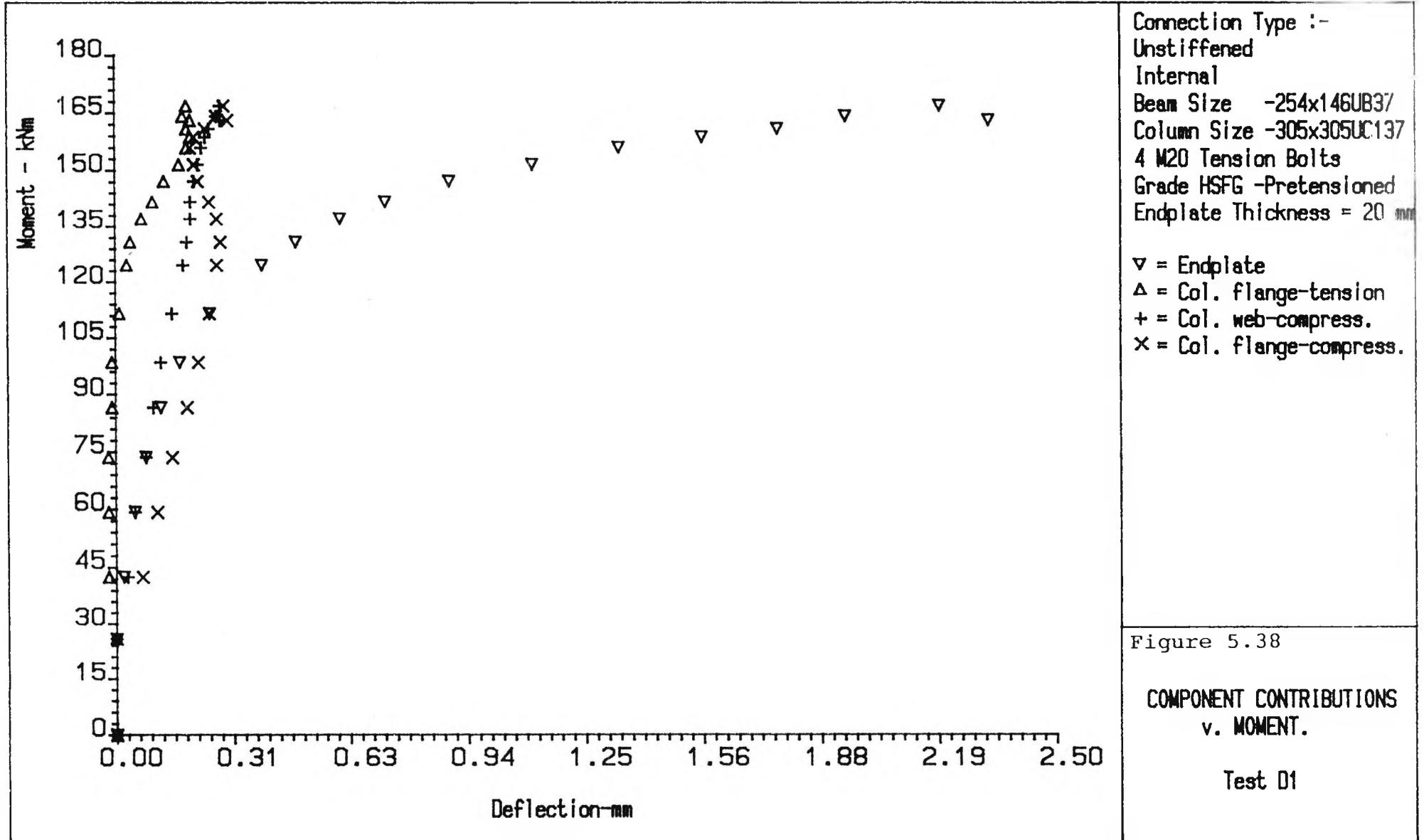
Connection Type :-
 Unstiffened
 Internal
 Beam Size -457x191UB74
 Column Size -305x305UC137
 6 M24 Tension Bolts
 Grade HSFG -Pretensioned
 Endplate Thickness = 25mm

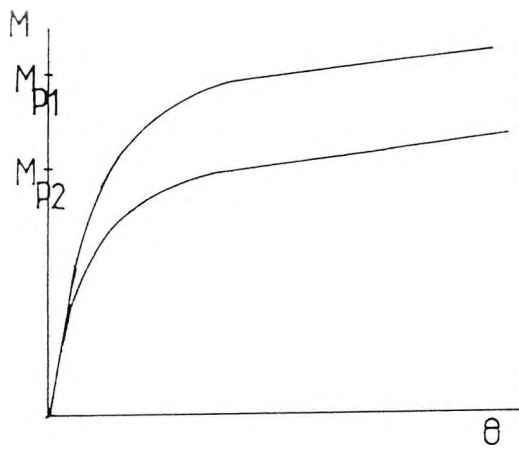
▽ = Endplate
 △ = Col. flange-tension
 + = Col. web-compress.
 x = Col. flange-compress.

Figure 5.36

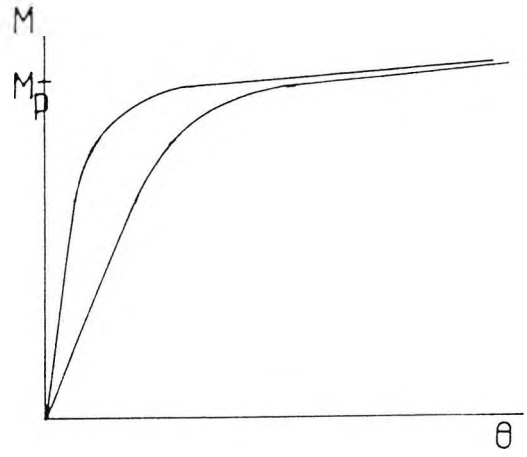
COMPONENT CONTRIBUTIONS
 v. MOMENT.

Test C1

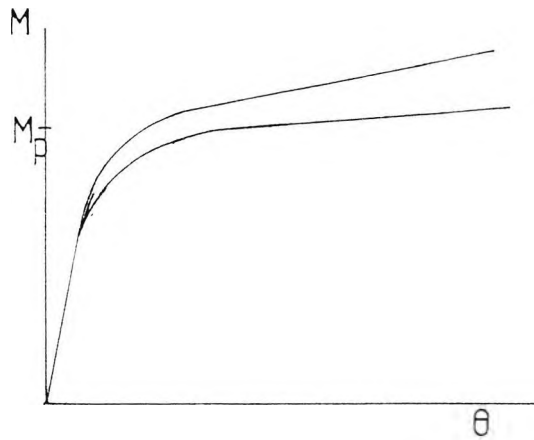




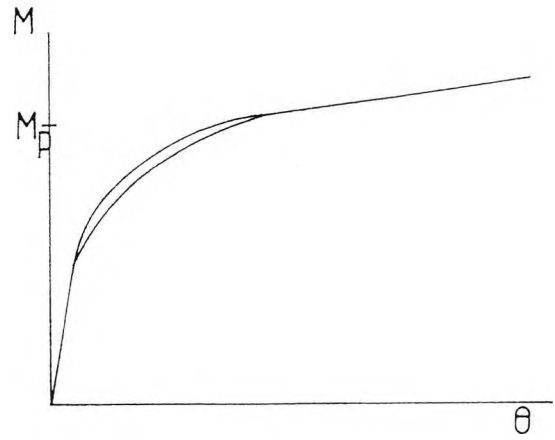
a) Effect of changing M_p



b) Effect of changing K_i

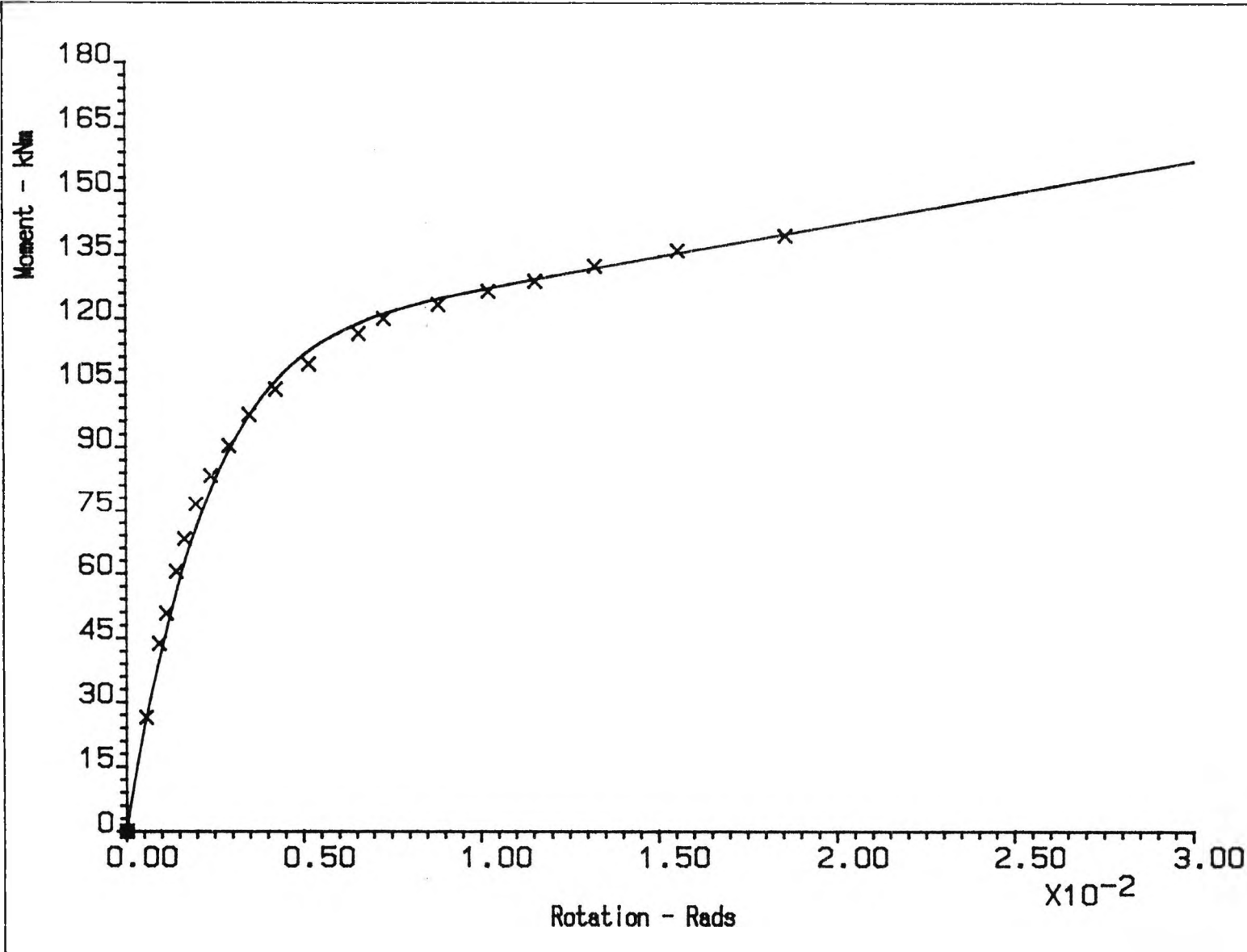


c) Effect of changing K_p



d) Effect of changing c

Figure 5.39 Effect of Varying Model Parameters on Moment-Rotation Behaviour.



Connection Type :-
 Unstiffened
 Internal
 Beam Size -254x146 UB37
 Column Size -203x203 UC60
 4 M20 Tension Bolts
 Grade HSFG -Pretensioned
 Endplate Thickness = 20mm

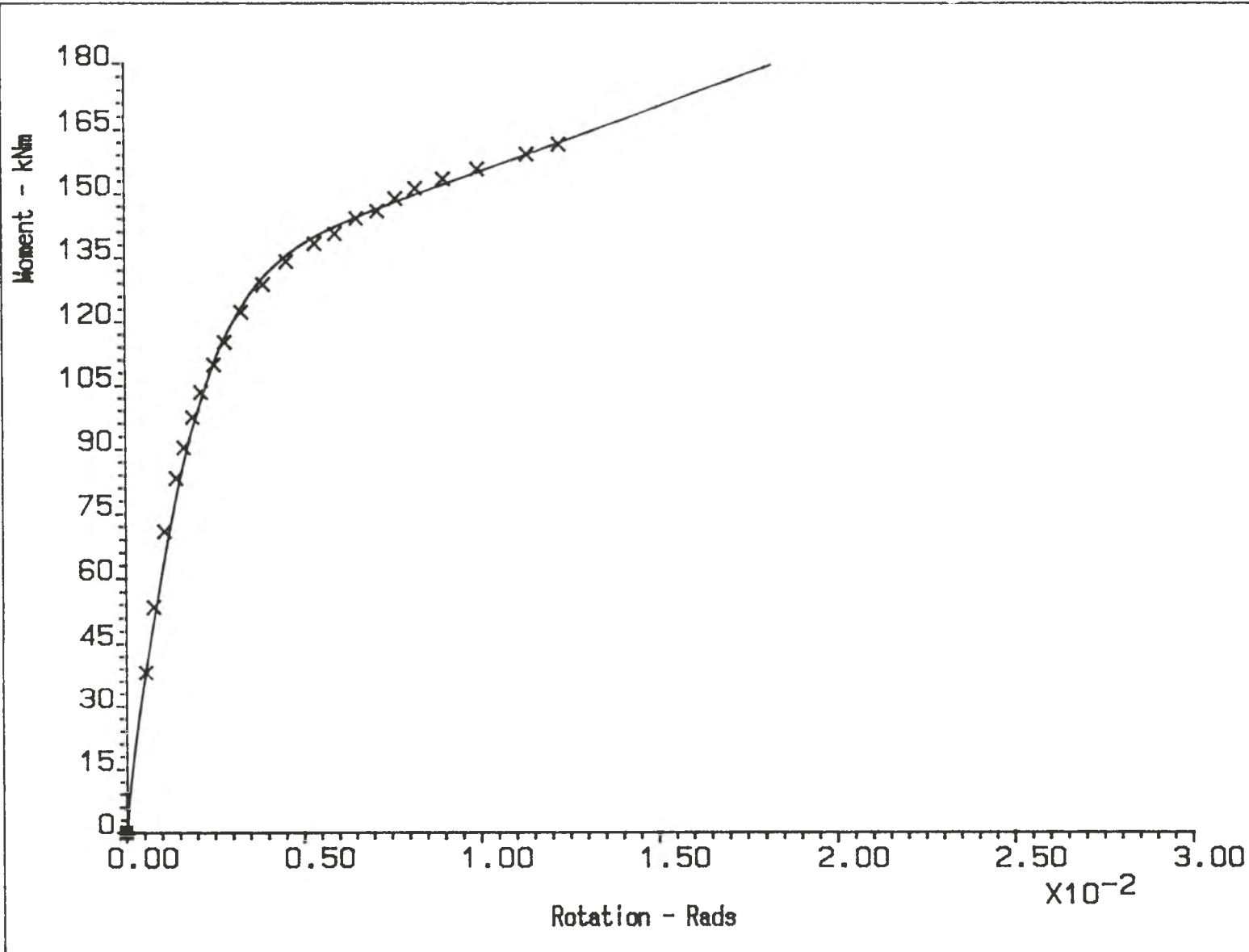
$M_p = 112. \text{ kNm}$
 $K_i = 50000. \text{ kNm/rad}$
 $K_p = 1500. \text{ kNm/rad}$

Decay factor = $2. \times 10^{-6}$

Figure 5.40

MODELLING OF CONNECTION
 DATA USING YEE MODEL.

Test A2



Connection Type :-
 Unstiffened
 Internal
 Beam Size -254x146 UB37
 Column Size -203x203 UC86
 4 M20 Tension Bolts
 Grade HSFG -Pretensioned
 Endplate Thickness = 20mm

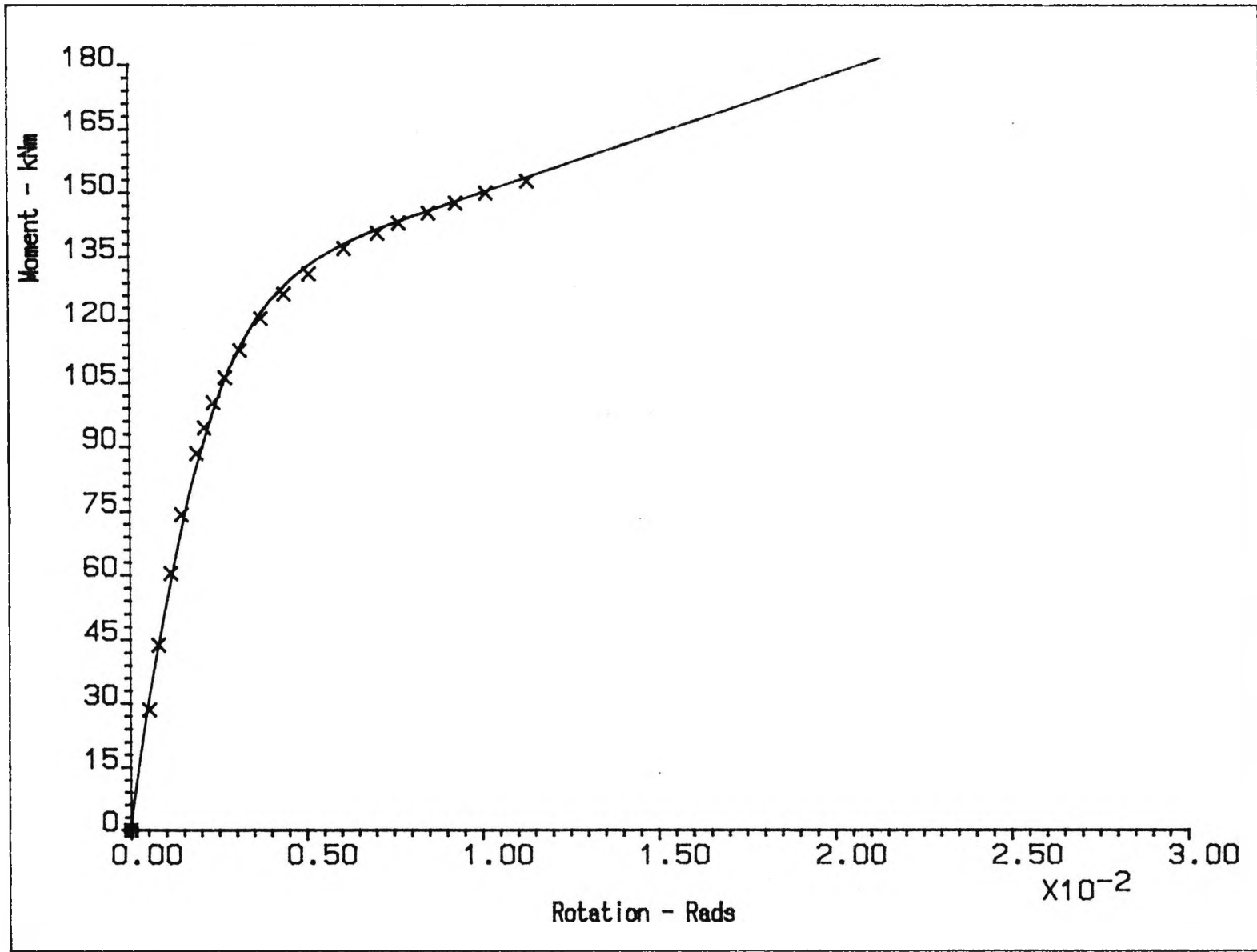
$M_p = 125. \text{ kNm}$
 $K_i = 70000. \text{ kNm/rad}$
 $K_p = 3000. \text{ kNm/rad}$

Decay factor = $7. \times 10^{-6}$

Figure 5.41

MODELLING OF CONNECTION
 DATA USING YEE MODEL.

Test A3



Connection Type :-
Unstiffened
Internal
Beam Size -254x146 UB37
Column Size -203x203 UC71
4 M20 Tension Bolts
Grade HSFG -Pretensioned
Endplate Thickness = 25mm

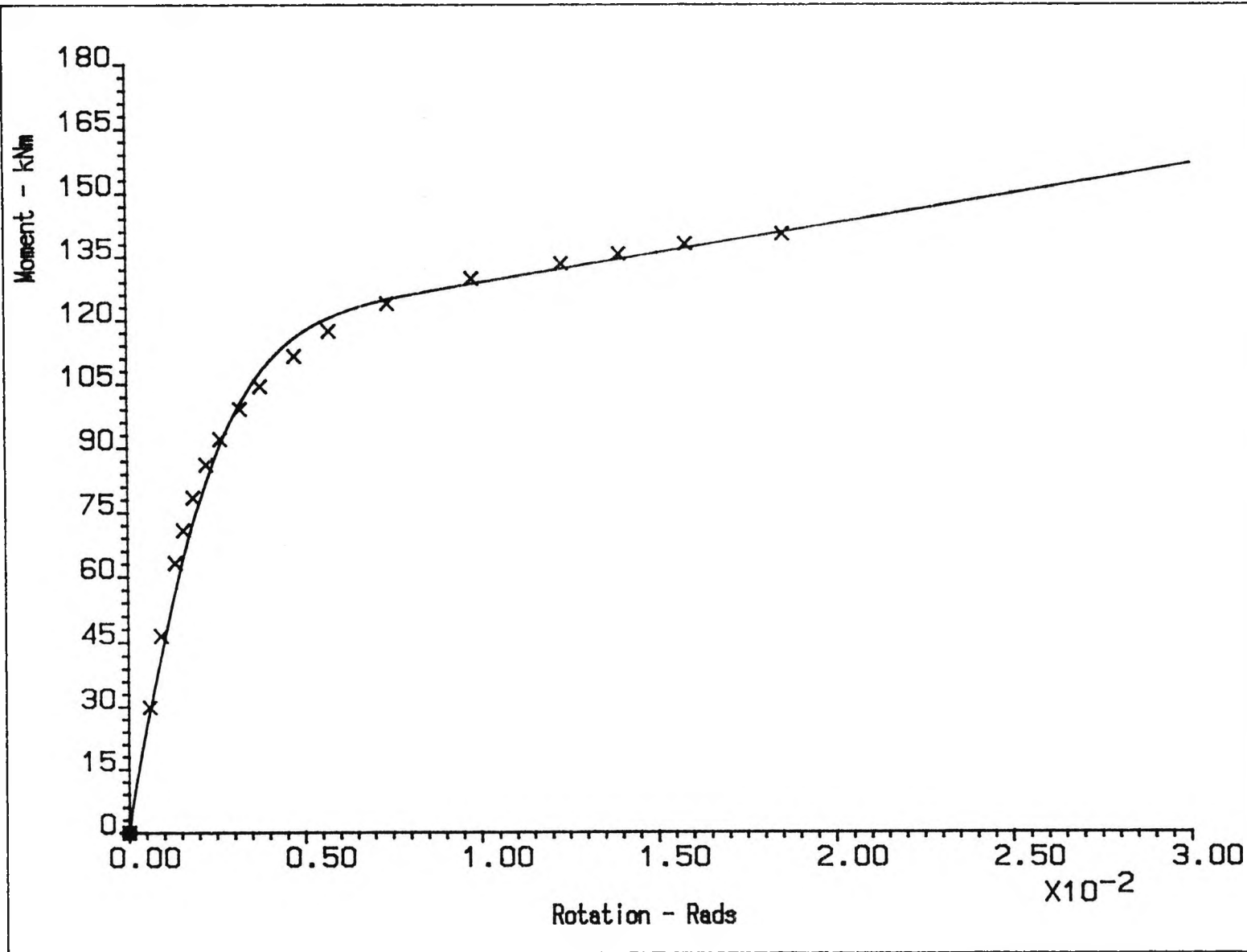
$M_p = 122. \text{ kNm}$
 $K_i = 60000. \text{ kNm/rad}$
 $K_p = 2800. \text{ kNm/rad}$

Decay factor = $6. \times 10^{-6}$

Figure 5.42

MODELLING OF CONNECTION
DATA USING YEE MODEL.

Test A4



Connection Type :-
 Unstiffened
 Internal
 Beam Size -254x146 UB37
 Column Size -203x203 UC71
 4 M20 Tension Bolts
 Grade HSFG -Pretensioned
 Endplate Thickness = 15mm

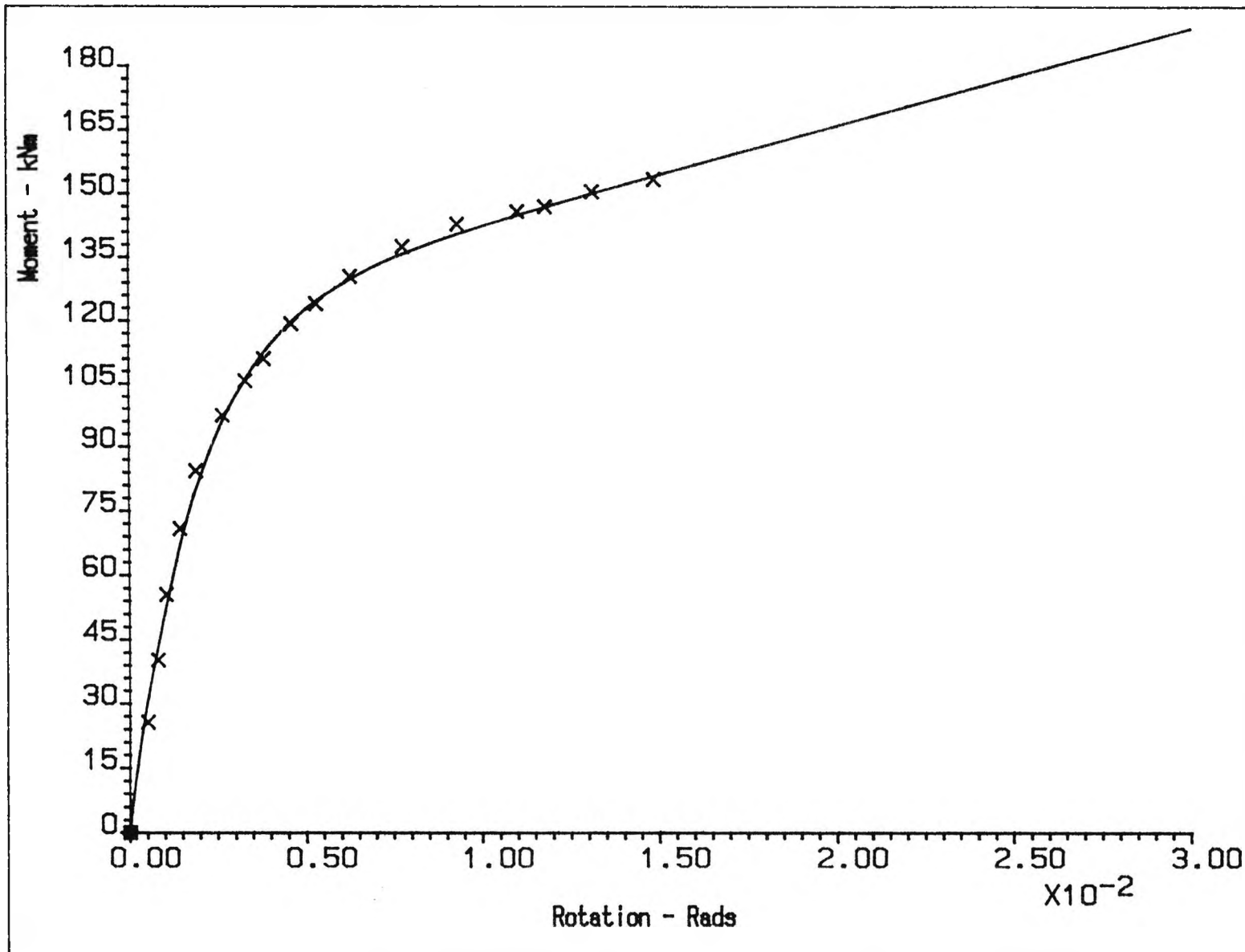
$M_p = 115. \text{ kNm}$
 $K_i = 50000. \text{ kNm/rad}$
 $K_p = 1400. \text{ kNm/rad}$

Decay factor = $5. \times 10^{-6}$

Figure 5.43

MODELLING OF CONNECTION
 DATA USING YEE MODEL.

Test A5



Connection Type :-
 Stiffened
 Internal
 Beam Size -254x146 UB37
 Column Size -203x203 UC60
 4 M20 Tension Bolts
 Grade HSFG -Pretensioned
 Endplate Thickness = 20mm

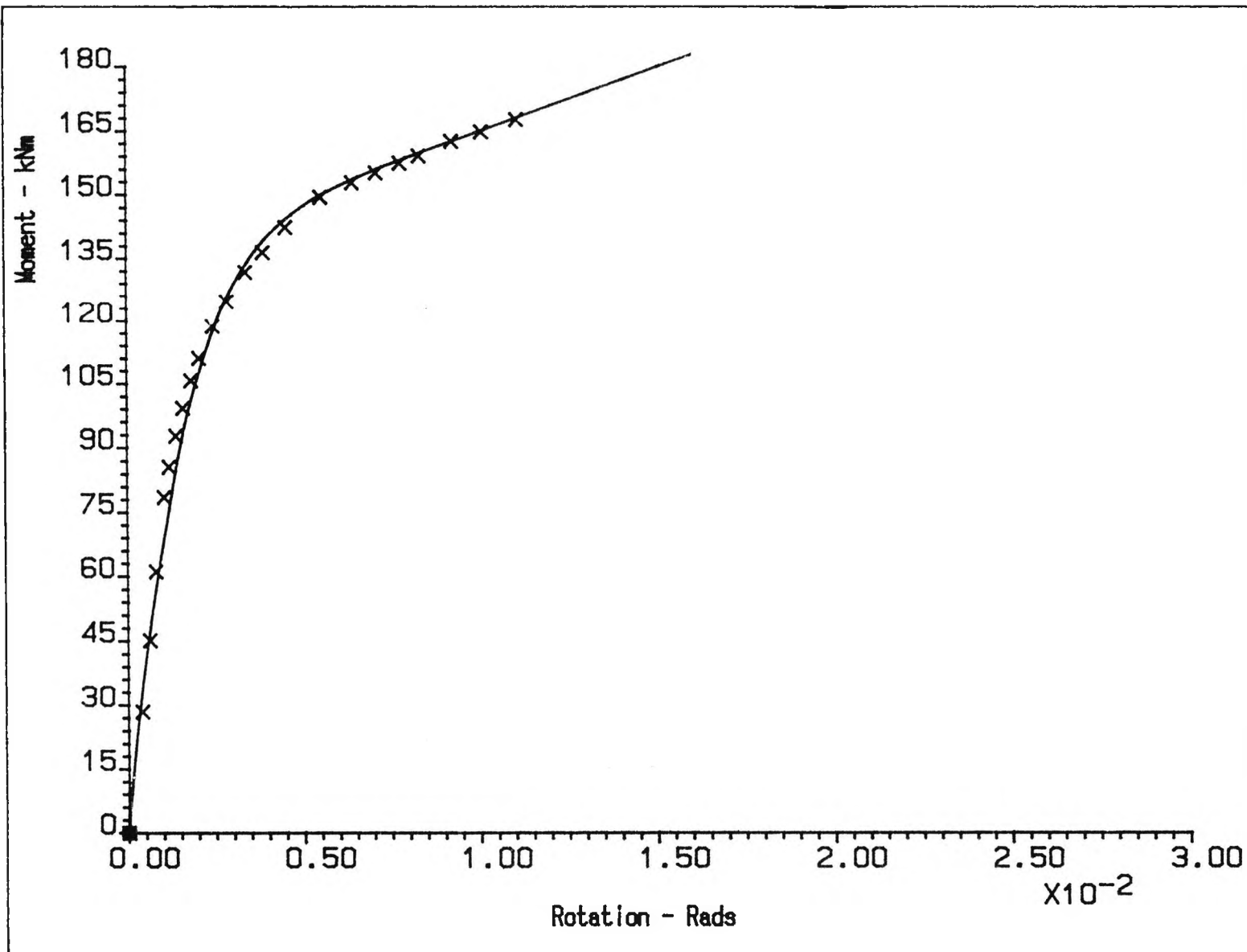
$M_p = 120. \text{ kNm}$
 $K_i = 65000. \text{ kNm/rad}$
 $K_p = 2300. \text{ kNm/rad}$

Decay factor = 0.0

Figure 5.44

MODELLING OF CONNECTION
 DATA USING YEE MODEL.

Test A6



Connection Type :-
 Stiffened
 Internal
 Beam Size -254x146 UB37
 Column Size -203x203 UC71
 4 M20 Tension Bolts
 Grade HSFG -Pretensioned
 Endplate Thickness = 20mm

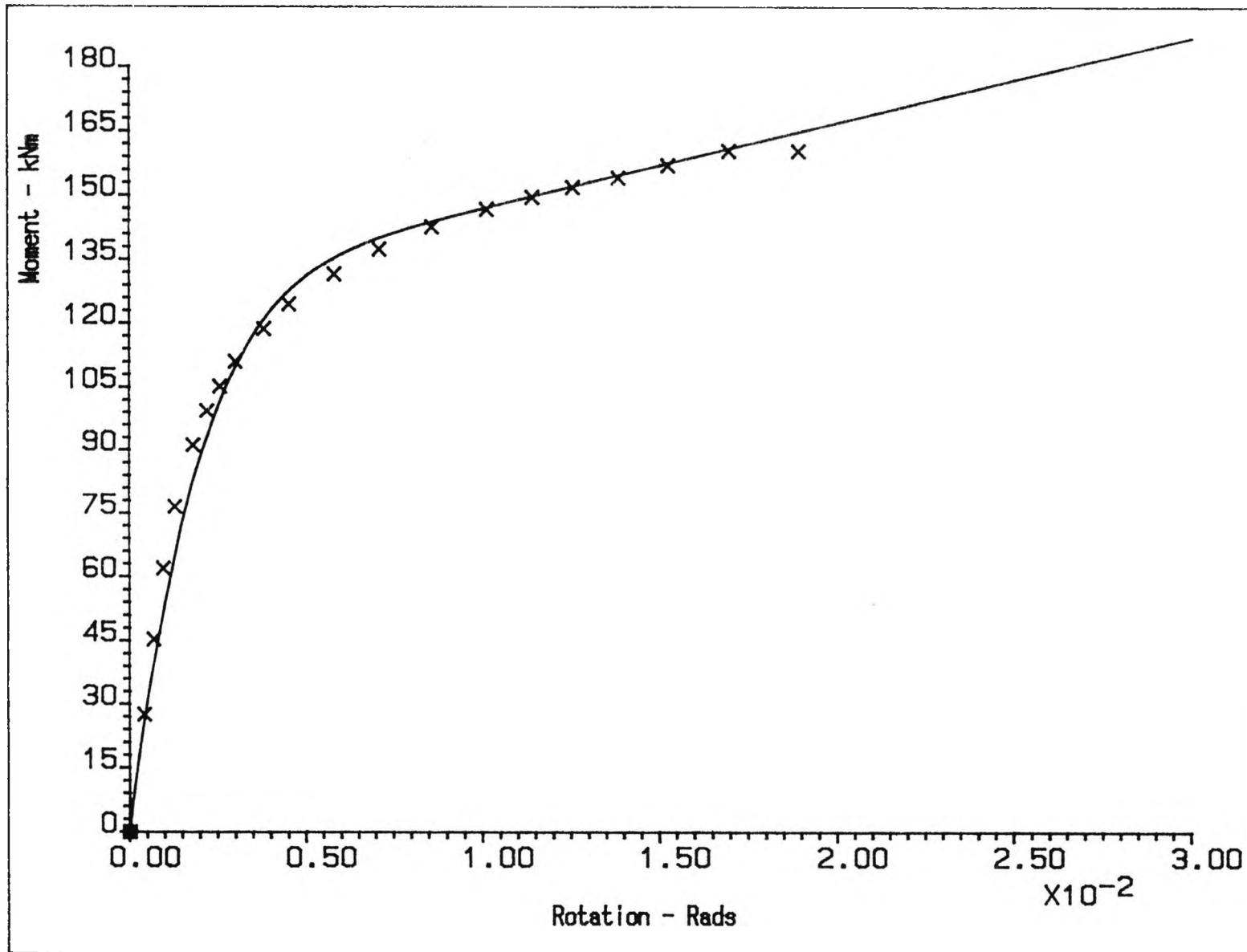
$M_p = 135. \text{ kNm}$
 $K_i = 85000. \text{ kNm/rad}$
 $K_p = 3000. \text{ kNm/rad}$

Decay factor = $5. \times 10^{-6}$

Figure 5.45

MODELLING OF CONNECTION
 DATA USING YEE MODEL.

Test A7



Connection Type :-
 Unstiffened
 Internal
 Beam Size -254x146 UB37
 Column Size -203x203 UC71
 4 M20 Tension Bolts
 Grade HSFG -Pretensioned
 Endplate Thickness = 20mm

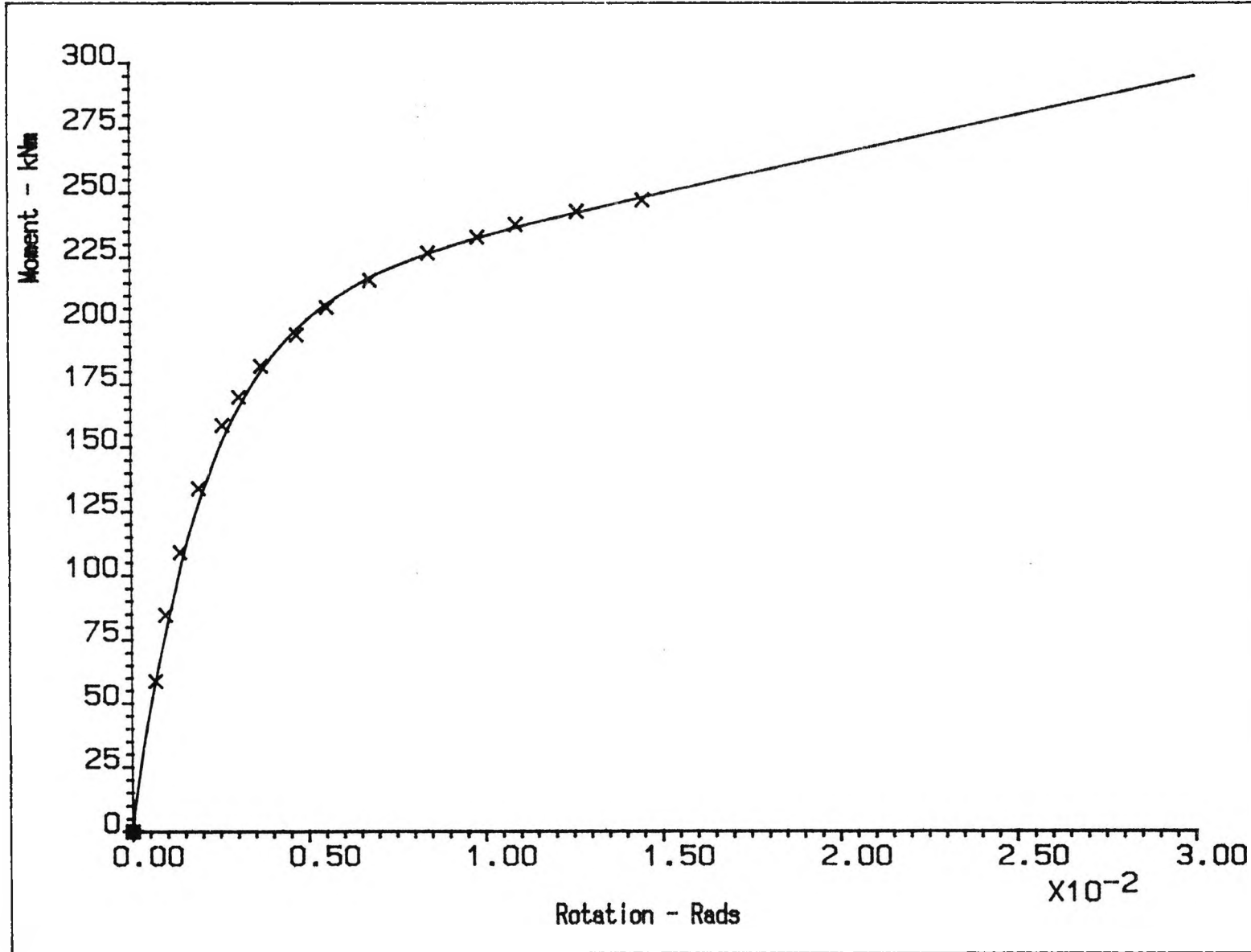
$M_p = 127. \text{ kNm}$
 $K_i = 65000. \text{ kNm/rad}$
 $K_p = 2000. \text{ kNm/rad}$

Decay factor= $3. \times 10^{-6}$

Figure 5.46

MODELLING OF CONNECTION
 DATA USING YEE MODEL.

Test A8



Connection Type :-
 Unstiffened
 Internal
 Beam Size -356x171 UB51
 Column Size -254x254 UC89
 4 M22 Tension Bolts
 Grade HSFG -Pretensioned
 Endplate Thickness = 25mm

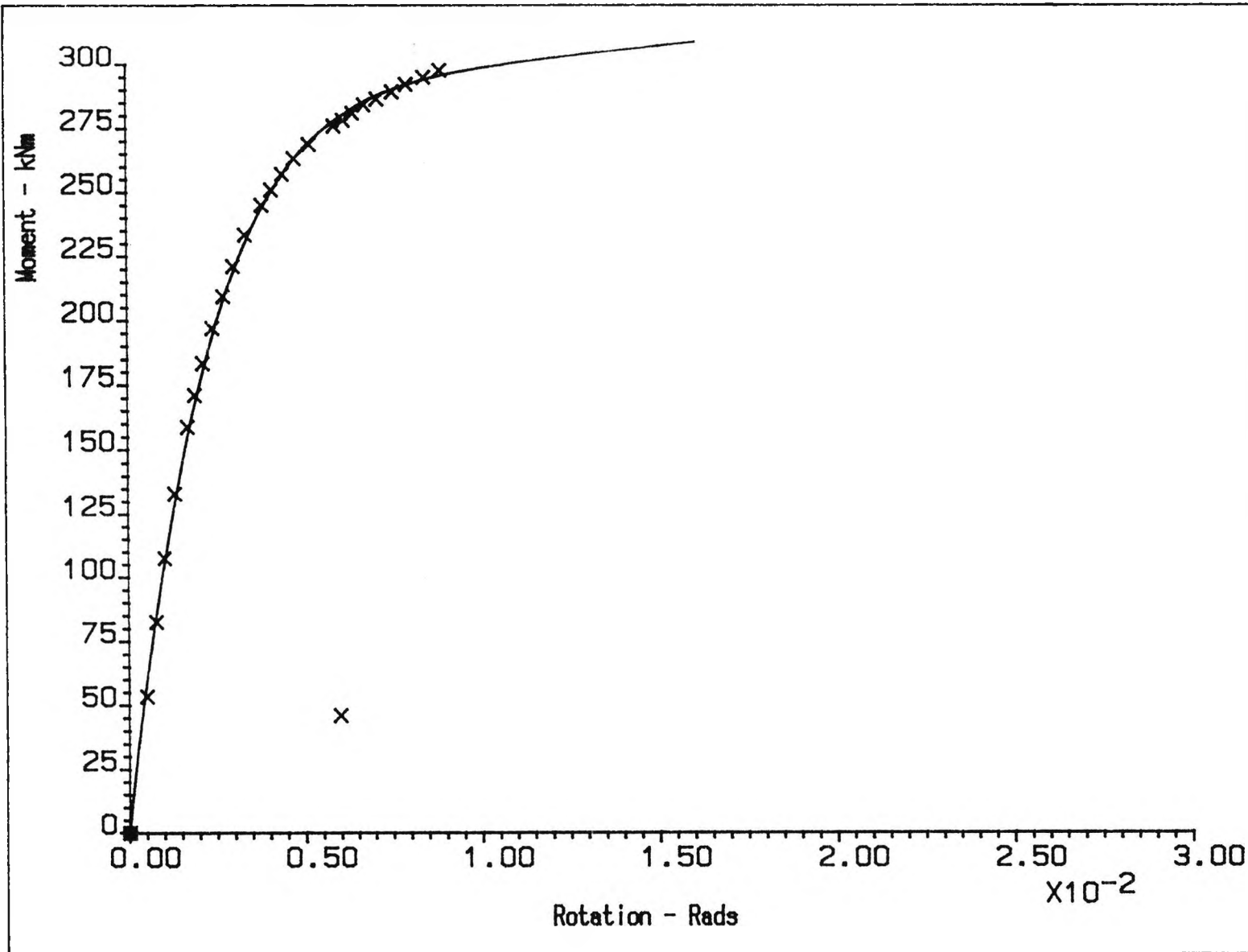
$M_p = 205. \text{ kNm}$
 $K_I = 100000. \text{ kNm/rad}$
 $K_p = 3000. \text{ kNm/rad}$

Decay factor=0.0

Figure 5.47

MODELLING OF CONNECTION
 DATA USING YEE MODEL.

Test B1



Connection Type :-
 Stiffened
 Internal
 Beam Size -356x171 UB51
 Column Size -254x254 UC89
 4 M22 Tension Bolts
 Grade HSFG -Pretensioned
 Endplate Thickness = 25mm

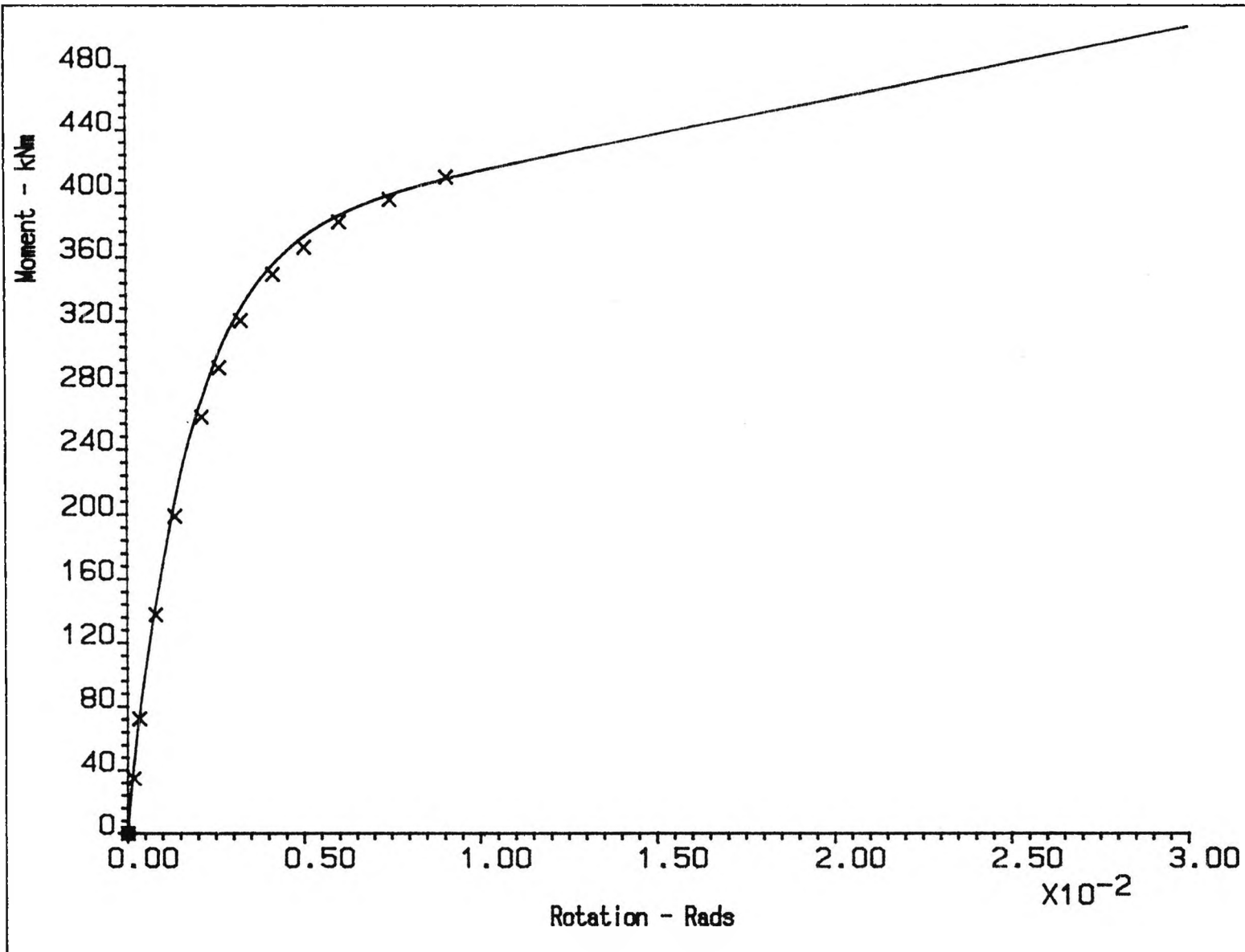
$M_p = 285. \text{ kNm}$
 $K_i = 125000. \text{ kNm/rad}$
 $K_p = 1500. \text{ kNm/rad}$

Decay factor = $3. \times 10^{-6}$

Figure 5.48

MODELLING OF CONNECTION
 DATA USING YEE MODEL.

Test B2



Connection Type :-
 Unstiffened
 Internal
 Beam Size -457x191UB74
 Column Size -305x305UC137
 6 M24 Tension Bolts
 Grade HSFG -Pretensioned
 Endplate Thickness = 25mm

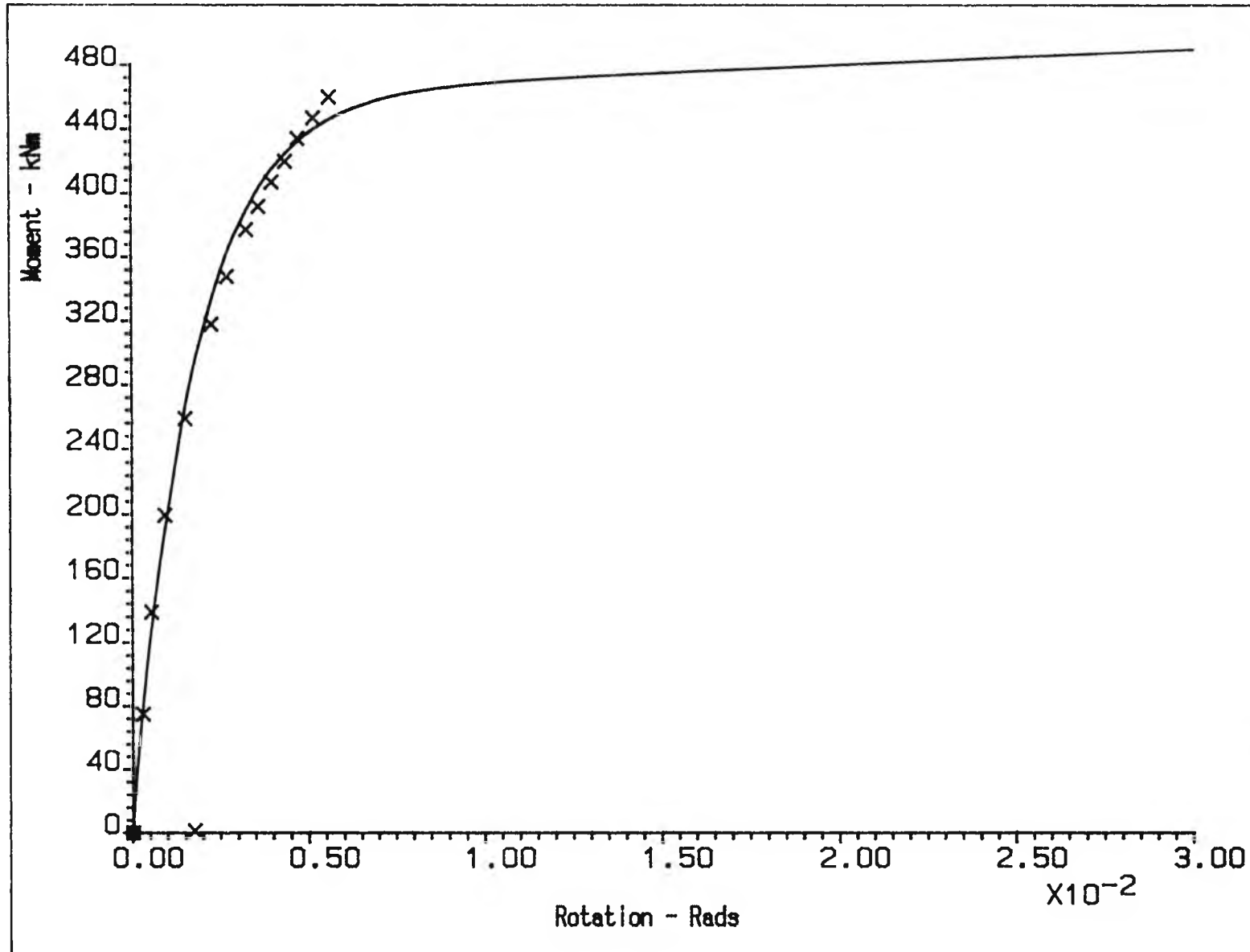
$M_p = 370. \text{ kNm}$
 $K_i = 220000. \text{ kNm/rad}$
 $K_p = 4500. \text{ kNm/rad}$

Decay factor=0.0

Figure 5.49

MODELLING OF CONNECTION
 DATA USING YEE MODEL.

Test C1



Connection Type :-
 Stiffened
 Internal
 Beam Size -457x191UB74
 Column Size -305x305UC137
 6 M24 Tension Bolts
 Grade HSFG -Pretensioned
 Endplate Thickness = 25mm

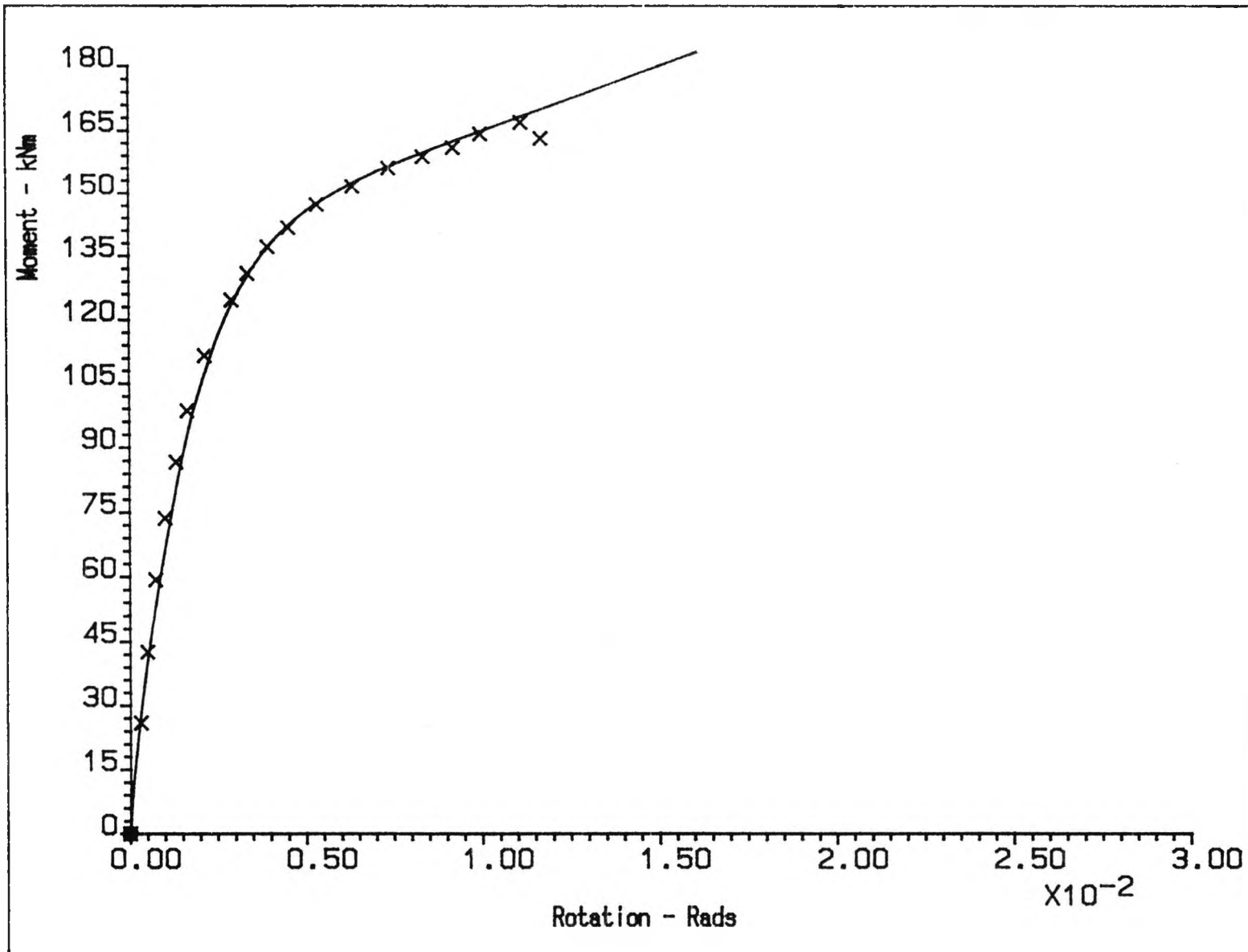
$M_p = 460. \text{ kNm}$
 $K_i = 260000. \text{ kNm/rad}$
 $K_p = 1000. \text{ kNm/rad}$

Decay factor=0.0

Figure 5.50

MODELLING OF CONNECTION
 DATA USING YEE MODEL.

Test C2



Connection Type :-
 Unstiffened
 Internal
 Beam Size -254x146UB37
 Column Size -305x305UC137
 4 M20 Tension Bolts
 Grade HSFG -Pretensioned
 Endplate Thickness = 20mm

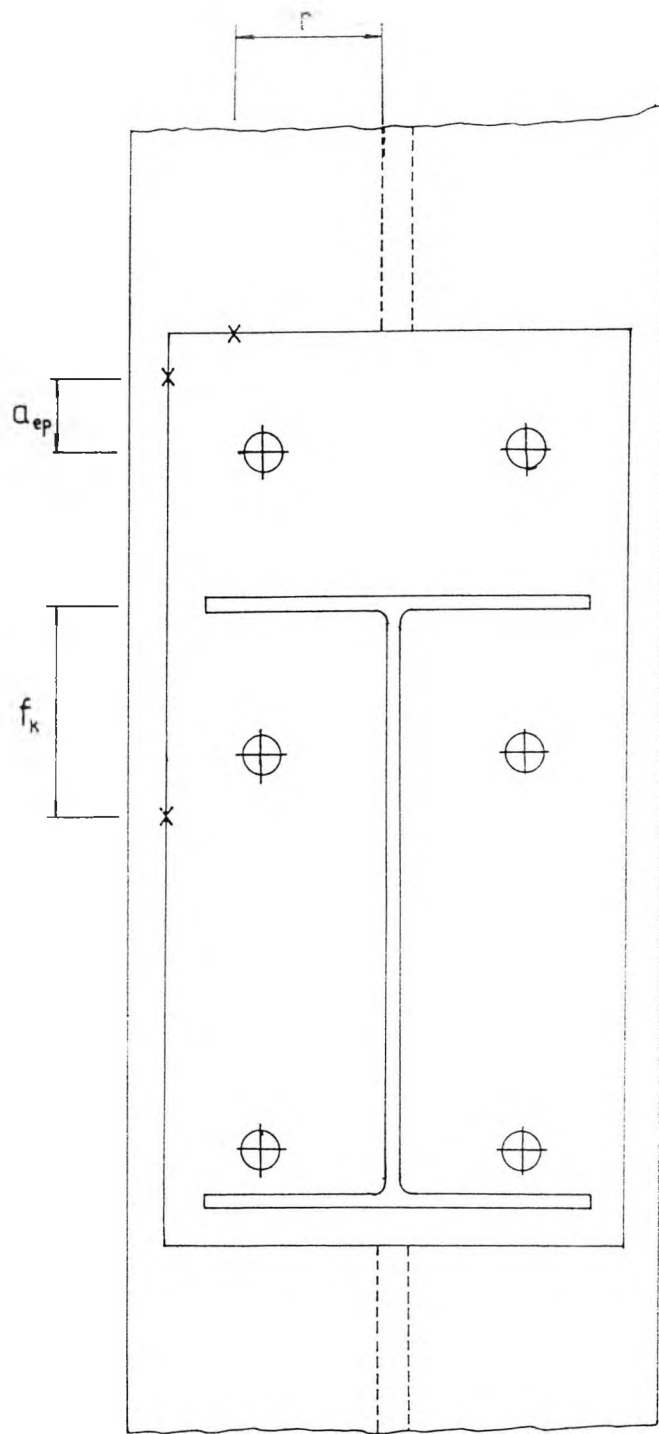
$M_p = 135. \text{ kNm}$
 $K_i = 85000. \text{ kNm/rad}$
 $K_p = 3000. \text{ kNm/rad}$

Decay factor = $2. \times 10^{-6}$

Figure 5.51

MODELLING OF CONNECTION
 DATA USING YEE MODEL.

Test D1

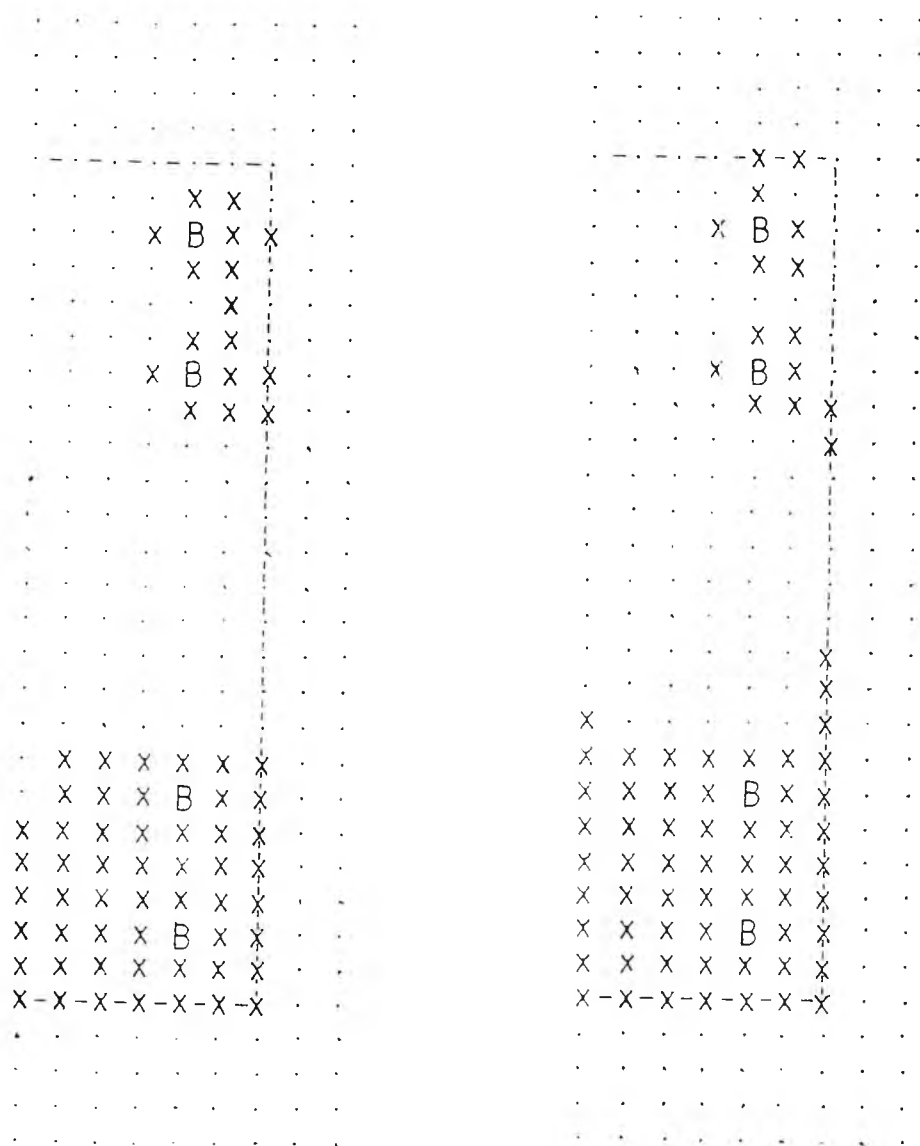


r = Relative rigidity factor

a_{ep} = Varying endplate 'a' dimension

f_k = Depth of contact point near compression region

Figure 5.52 Factors used to Define Contact Positions.



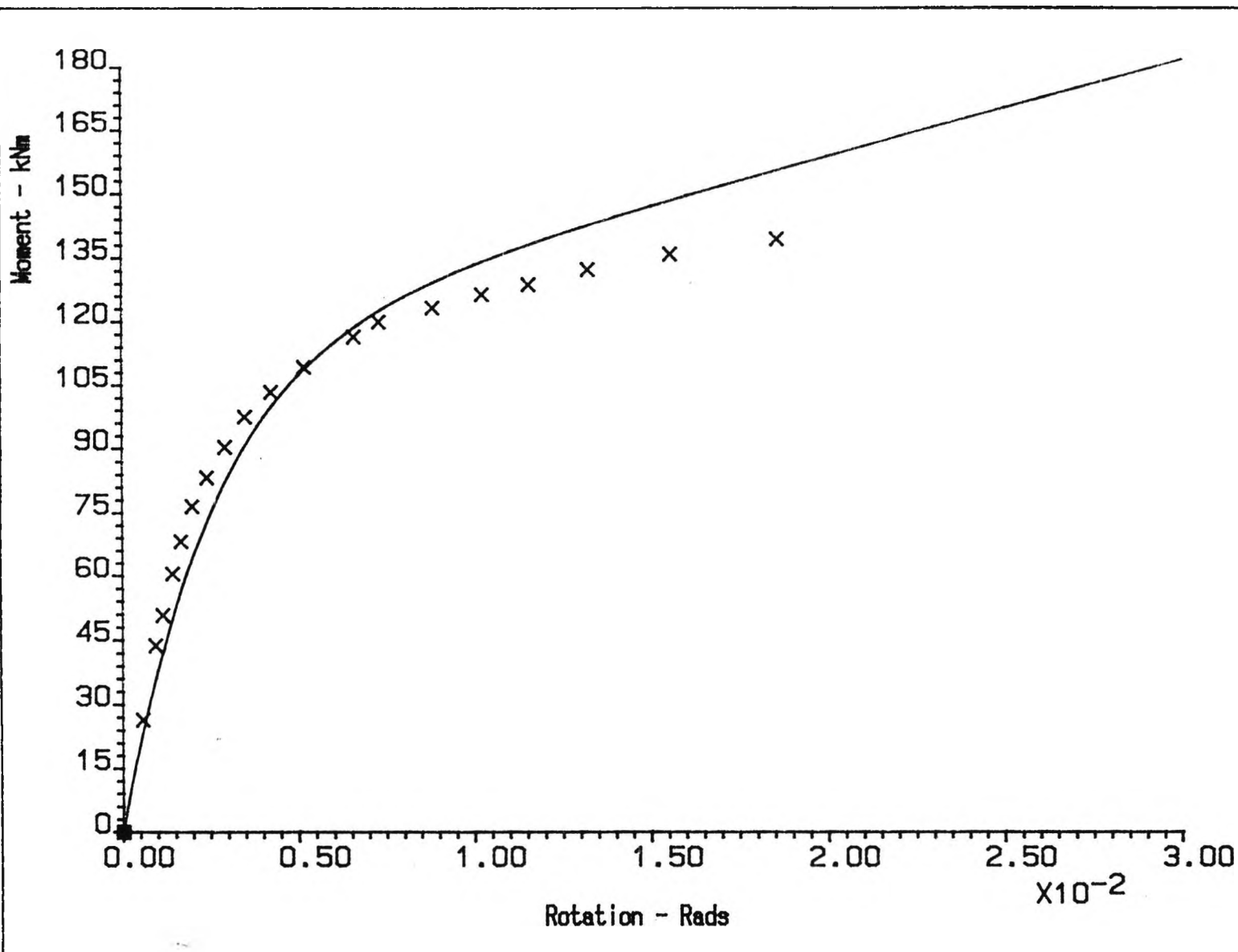
a) 2" Endplate

b) 3/4" Endplate

B = Bolt position

x = Contact node.

Figure 5.53 Contact Positions for Endplates and Column Flanges of Varying Thickness as Derived by Ioannides (Reference 10).



Connection Type :-
 Unstiffened
 Internal
 Beam Size -254x146 UB37
 Column Size -203x203 UC60
 4 M20 Tension Bolts
 Grade HSFG -Pretensioned
 Endplate Thickness = 20mm

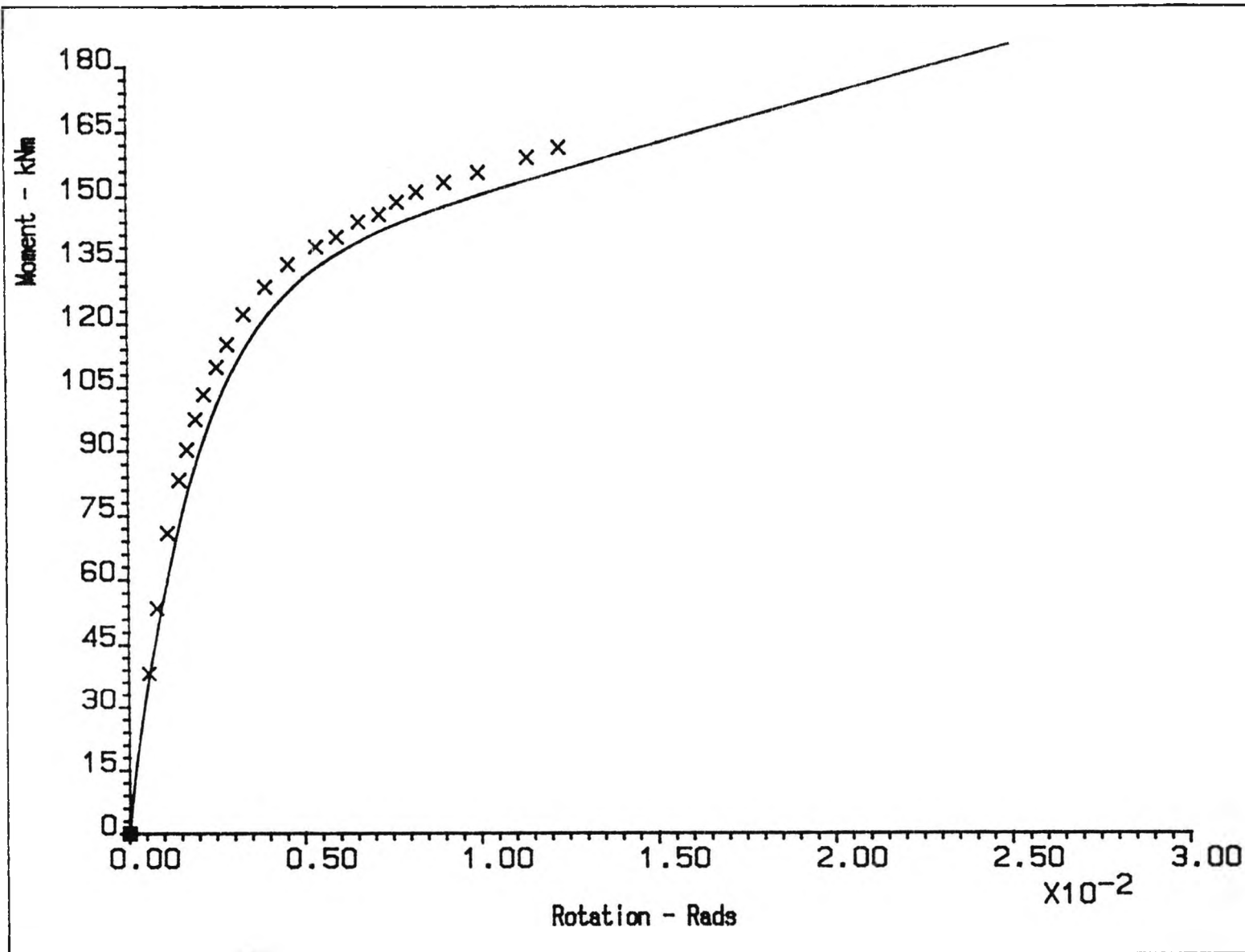
$M_p = 113. \text{ kNm}$
 $K_i = 45000. \text{ kNm/rad}$
 $K_p = 2300. \text{ kNm/rad}$

Decay factor=0.0

Figure 5.54

COMPARISON OF PREDICTION
 WITH CONNECTION DATA.

Test A2



Connection Type :-
 Unstiffened
 Internal
 Beam Size -254x146 UB37
 Column Size -203x203 UC86
 4 M20 Tension Bolts
 Grade HSFG -Pretensioned
 Endplate Thickness = 20mm

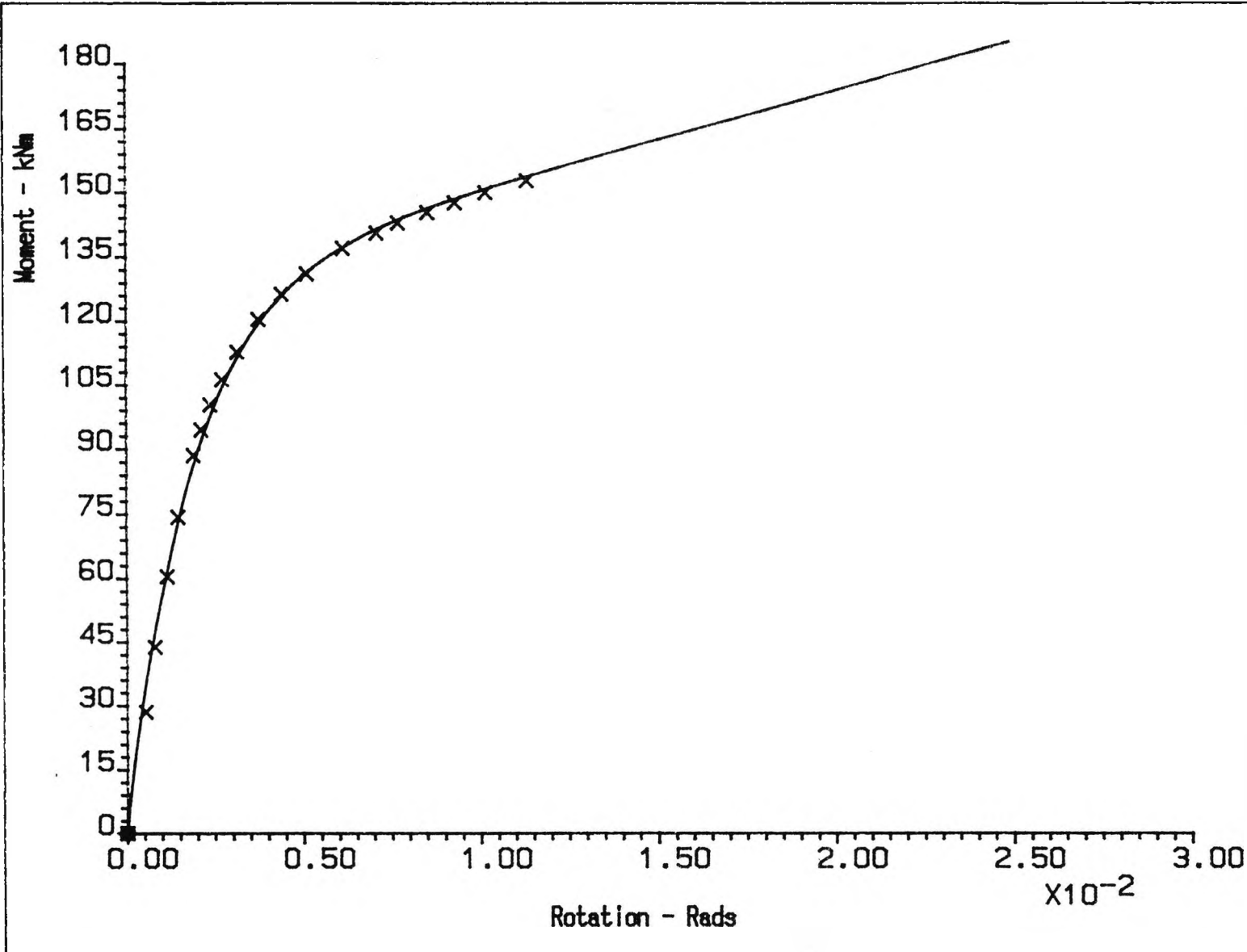
$M_p = 128. \text{ kNm}$
 $K_i = 71000. \text{ kNm/rad}$
 $K_p = 2300. \text{ kNm/rad}$

Decay factor=0.0

Figure 5.55

COMPARISON OF PREDICTION
 WITH CONNECTION DATA.

Test A3



Connection Type :-
 Unstiffened
 Internal
 Beam Size -254x146 UB37
 Column Size -203x203 UC71
 4 M20 Tension Bolts
 Grade HSFG -Pretensioned
 Endplate Thickness = 25mm

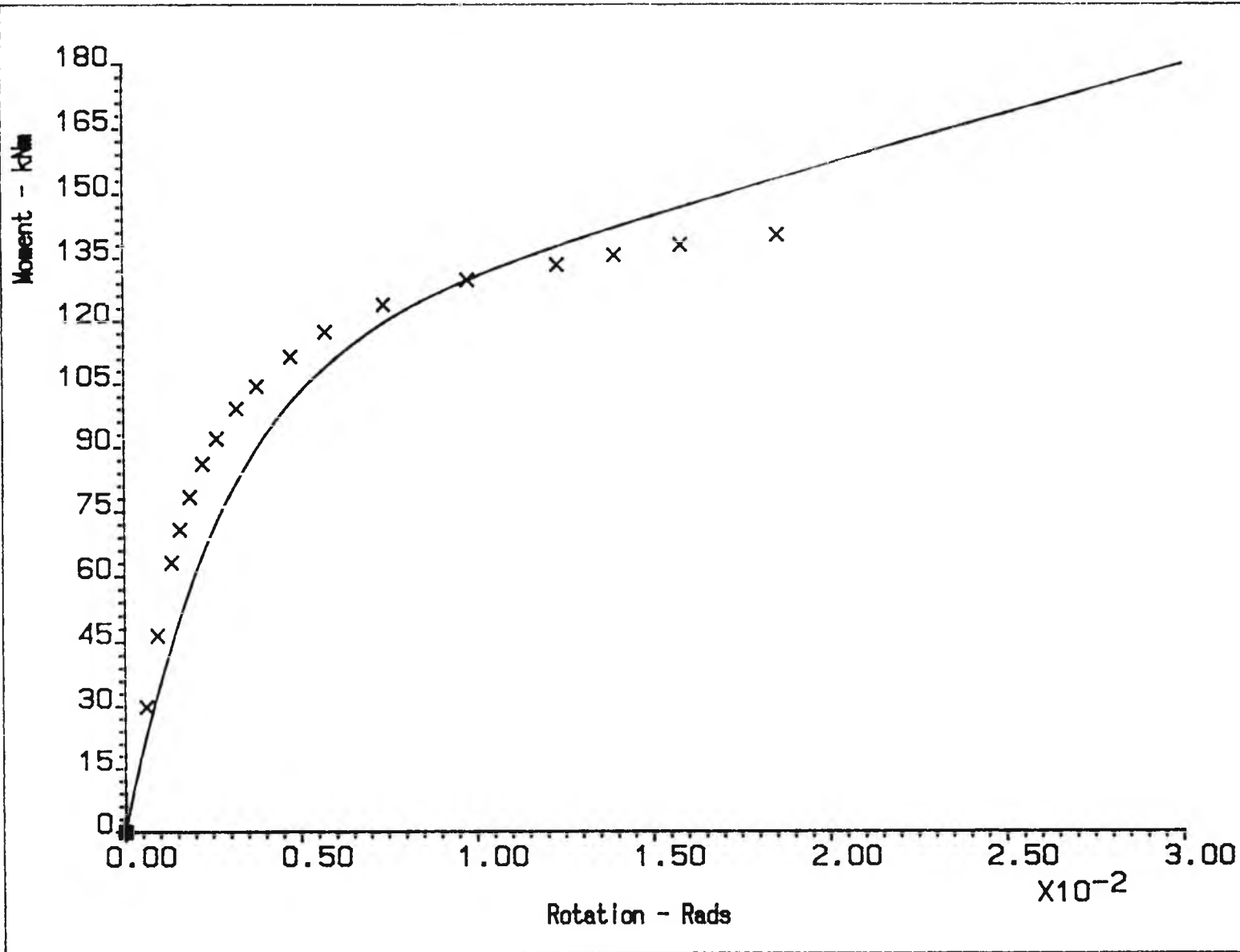
$M_p = 128. \text{ kNm}$
 $K_i = 66000. \text{ kNm/rad}$
 $K_p = 2300. \text{ kNm/rad}$

Decay factor=0.0

Figure 5.56

COMPARISON OF PREDICTION
 WITH CONNECTION DATA.

Test A4



Connection Type :-
 Unstiffened
 Internal
 Beam Size -254x146 UB37
 Column Size -203x203 UC71
 4 M20 Tension Bolts
 Grade HSFG -Pretensioned
 Endplate Thickness = 15mm

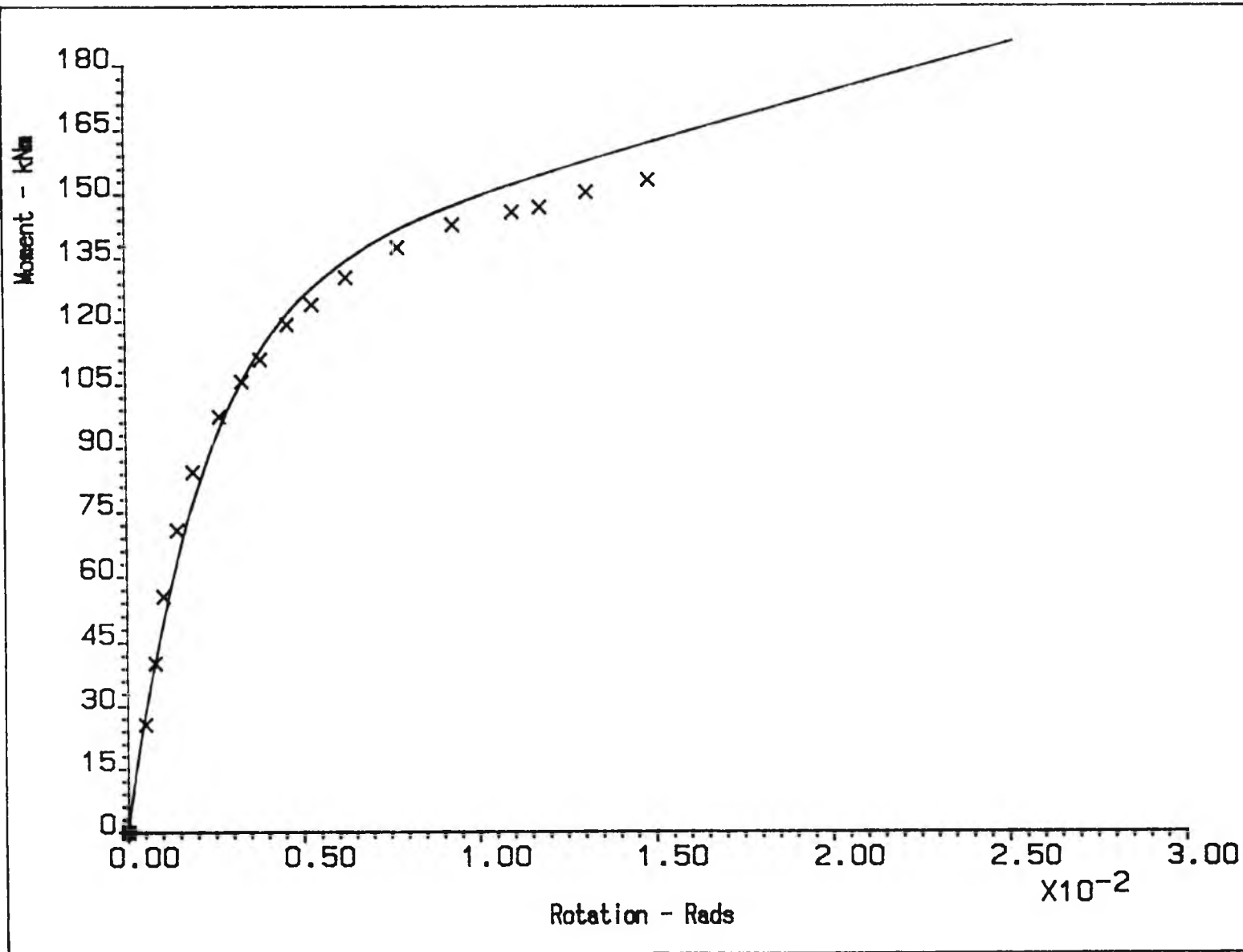
$M_p = 111. \text{ kNm}$
 $K_i = 41000. \text{ kNm/rad}$
 $K_p = 2300. \text{ kNm/rad}$

Decay factor=0.0

Figure 5.57

COMPARISON OF PREDICTION
 WITH CONNECTION DATA.

Test A5



Connection Type :-
 Stiffened
 Internal
 Beam Size -254x146 UB37
 Column Size -203x203 UC60
 4 M20 Tension Bolts
 Grade HSFG -Pretensioned
 Endplate Thickness = 20mm

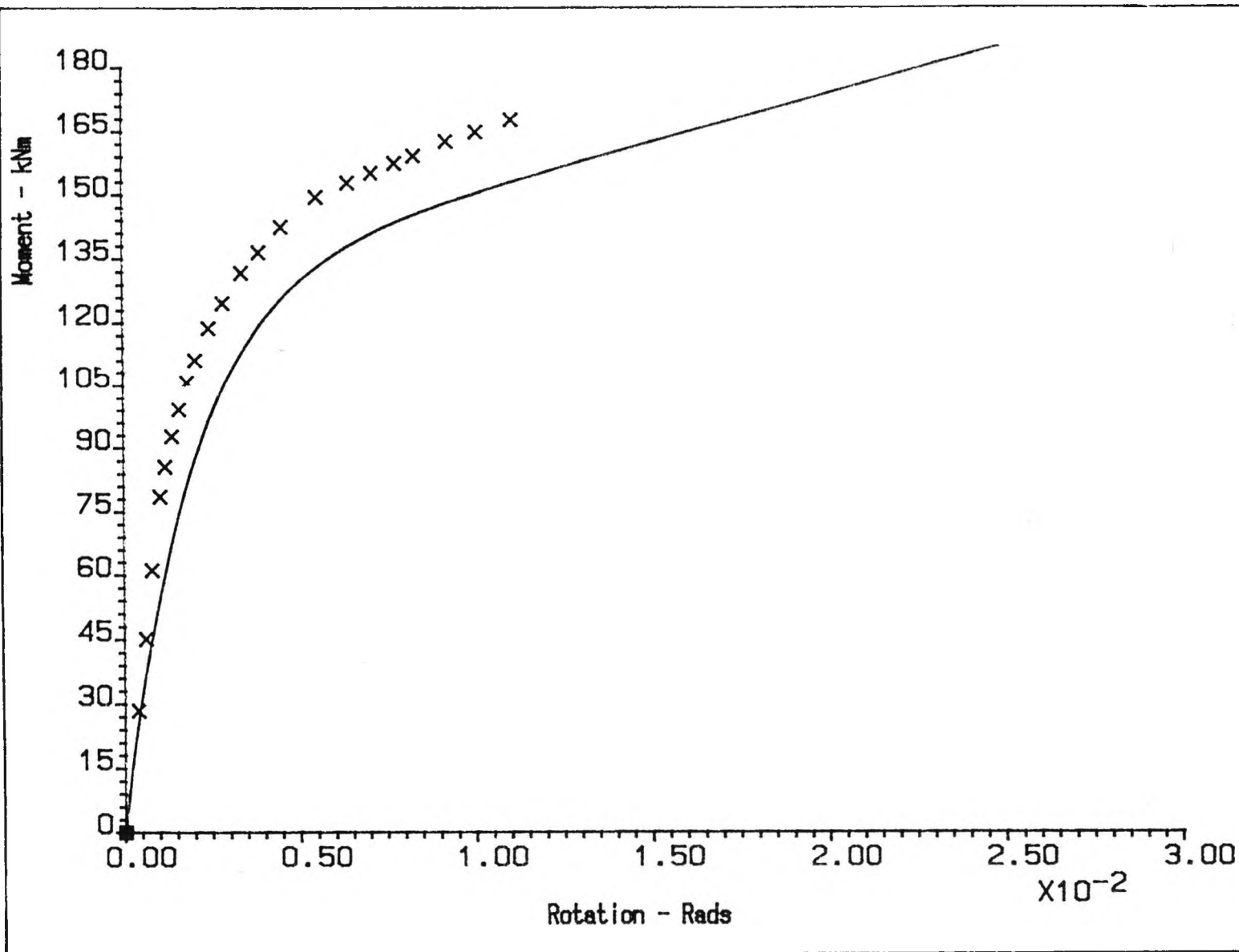
$M_p = 128. \text{ kNm}$
 $K_i = 59000. \text{ kNm/rad}$
 $K_p = 2300. \text{ kNm/rad}$

Decay factor=0.0

Figure 5.58

COMPARISON OF PREDICTION
 WITH CONNECTION DATA.

Test A6



Connection Type :-
 Stiffened
 Internal
 Beam Size -254x146 UB37
 Column Size -203x203 UC71
 4 M20 Tension Bolts
 Grade HSFG -Pretensioned
 Endplate Thickness = 20mm

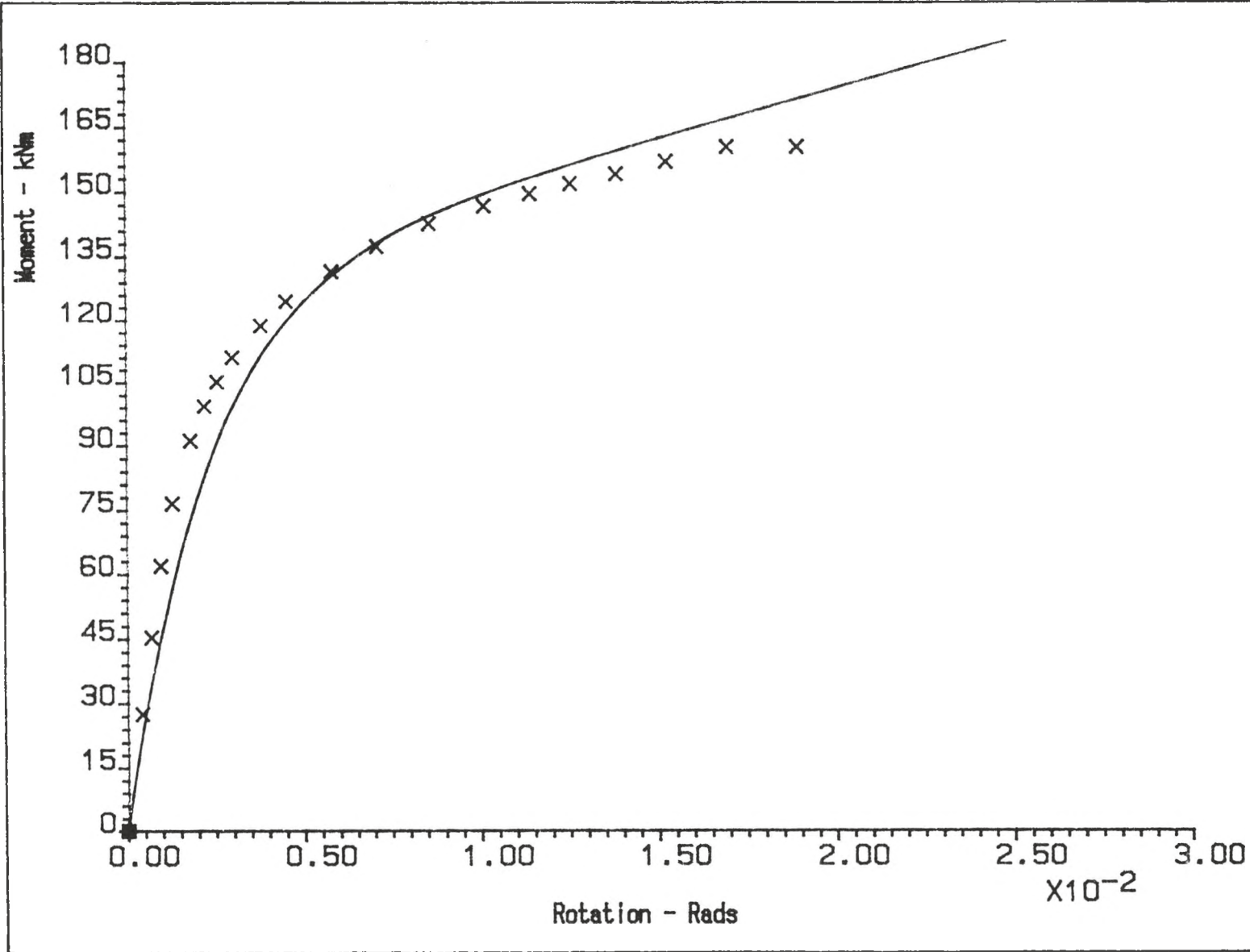
$M_p = 128. \text{ kNm}$
 $K_I = 68000. \text{ kNm/rad}$
 $K_p = 2300. \text{ kNm/rad}$

Decay factor=0.0

Figure 5.59

COMPARISON OF PREDICTION
 WITH CONNECTION DATA.

Test A7



Connection Type :-
 Unstiffened
 Internal
 Beam Size -254x146 UB37
 Column Size -203x203 UC71
 4 M20 Tension Bolts
 Grade HSFG -Pretensioned
 Endplate Thickness = 20mm

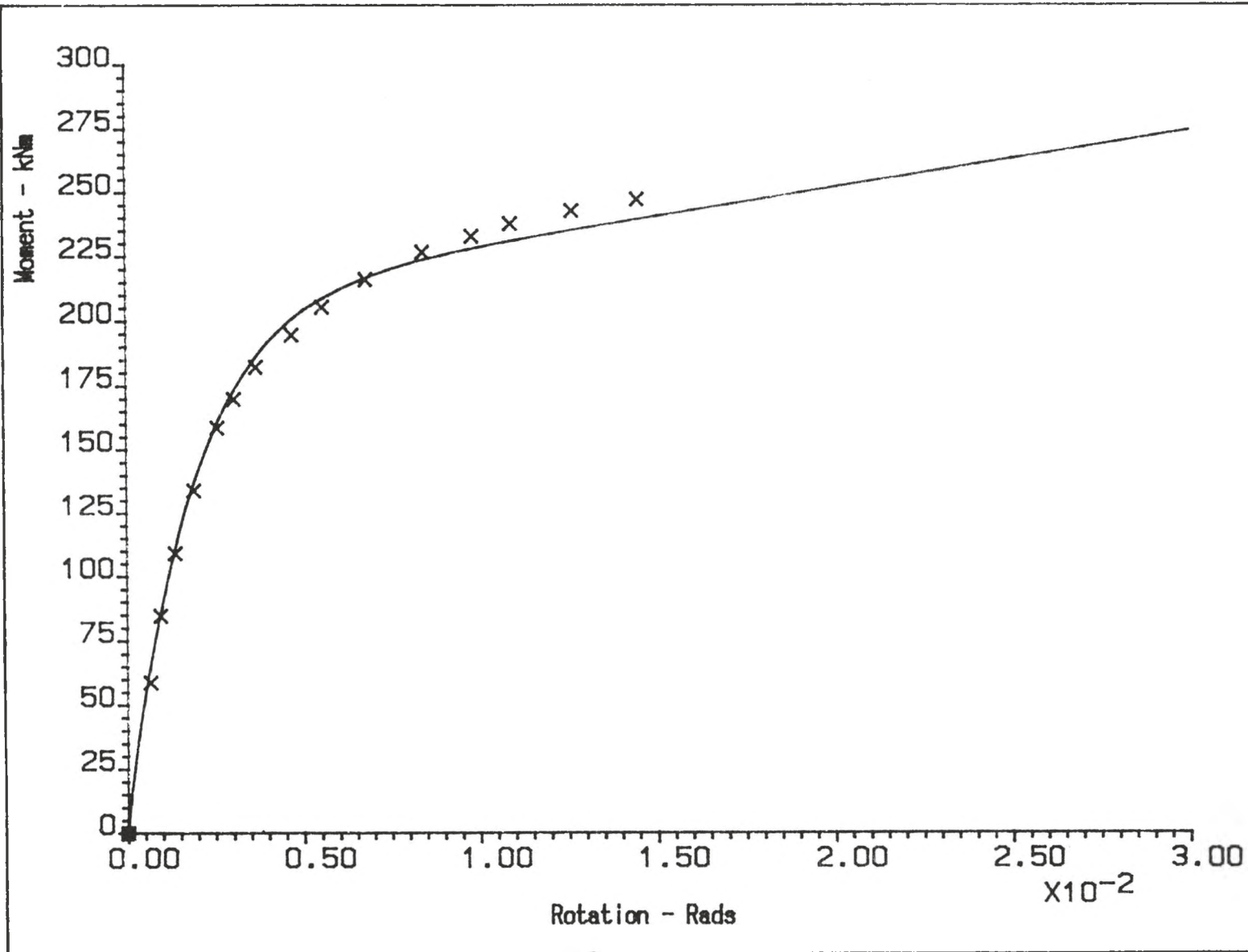
$M_p = 128. \text{ kNm}$
 $K_i = 57000. \text{ kNm/rad}$
 $K_p = 2300. \text{ kNm/rad}$

Decay factor=0.0

Figure 5.60

COMPARISON OF PREDICTION
 WITH CONNECTION DATA.

Test A8



Connection Type :-
 Unstiffened
 Internal
 Beam Size -356x171 UB51
 Column Size -254x254 UC89
 4 M22 Tension Bolts
 Grade HSFG -Pretensioned
 Endplate Thickness = 25mm

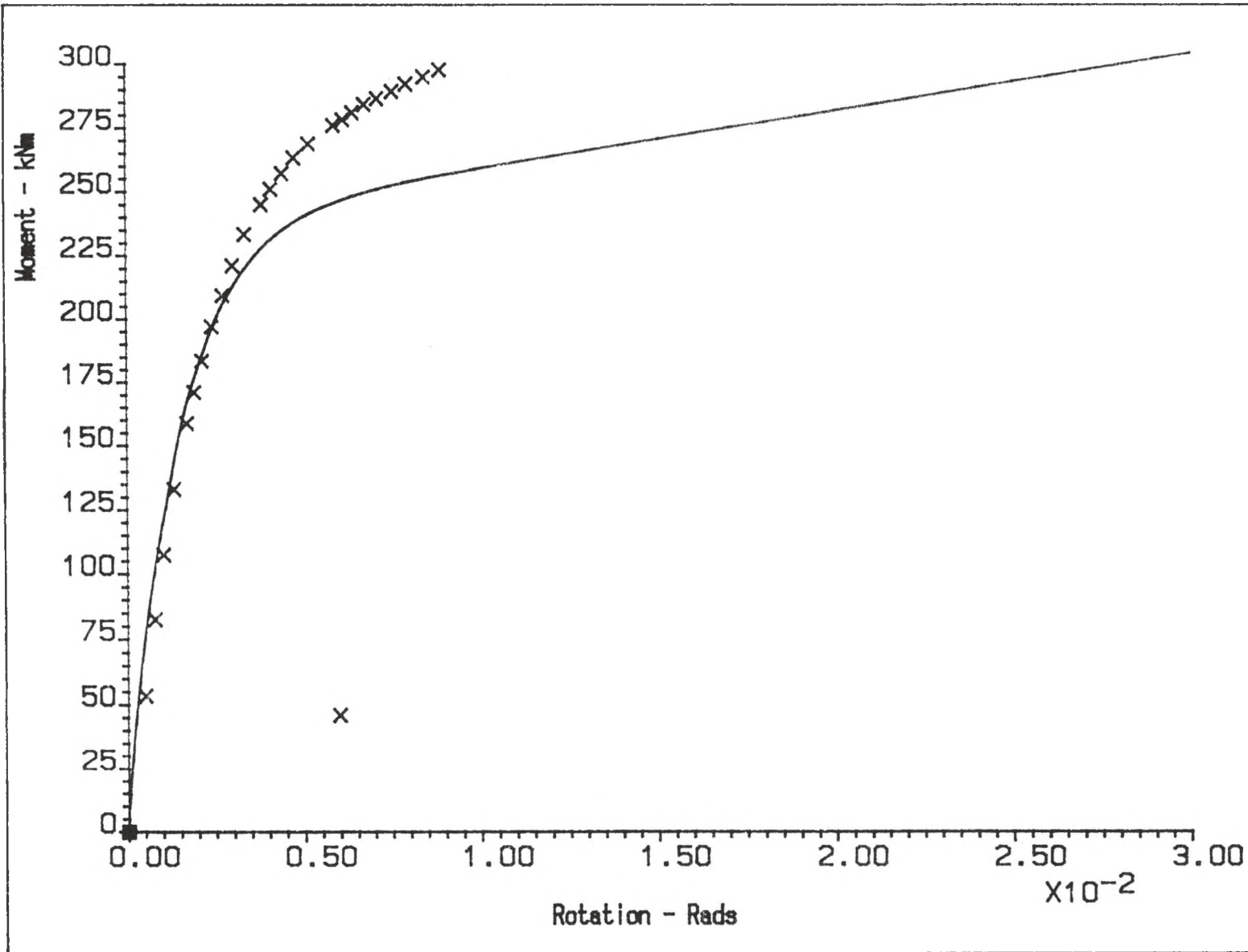
$M_p = 207. \text{ kNm}$
 $K_i = 113000. \text{ kNm/rad}$
 $K_p = 2250. \text{ kNm/rad}$

Decay factor=0.0

Figure 5.61

COMPARISON OF PREDICTION
WITH CONNECTION DATA.

Test B1



Connection Type :-
 Stiffened
 Internal
 Beam Size -356x171 UB51
 Column Size -254x254 UC89
 4 M22 Tension Bolts
 Grade HSFG -Pretensioned
 Endplate Thickness = 25mm

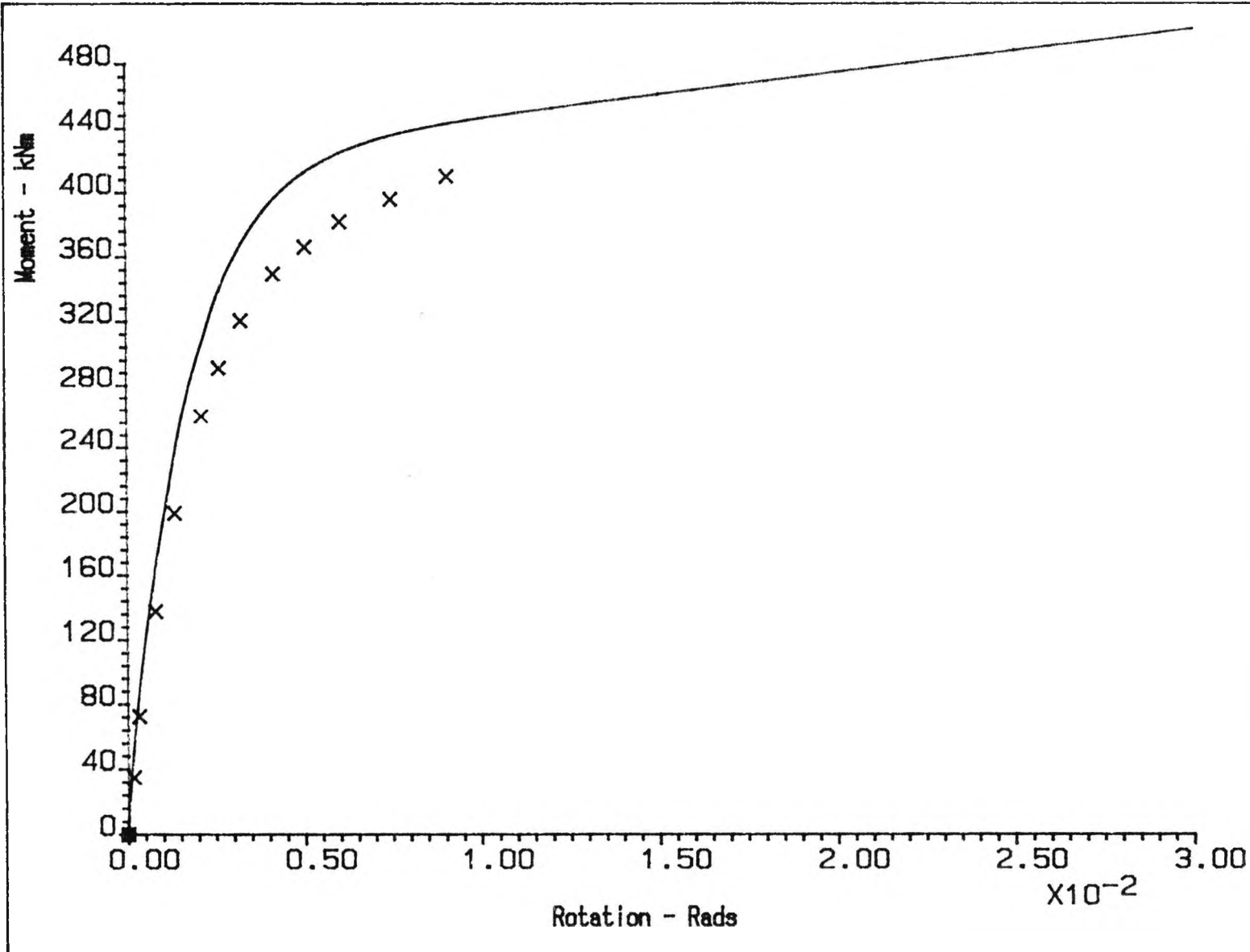
$M_p = 237. \text{ kNm}$
 $K_I = 164000. \text{ kNm/rad}$
 $K_p = 2250. \text{ kNm/rad}$

Decay factor=0.0

Figure 5.62

COMPARISON OF PREDICTION
WITH CONNECTION DATA.

Test B2



Connection Type :-
 Unstiffened
 Internal
 Beam Size -457x191UB74
 Column Size -305x305UC137
 6 M24 Tension Bolts
 Grade HSFG -Pretensioned
 Endplate Thickness = 25mm

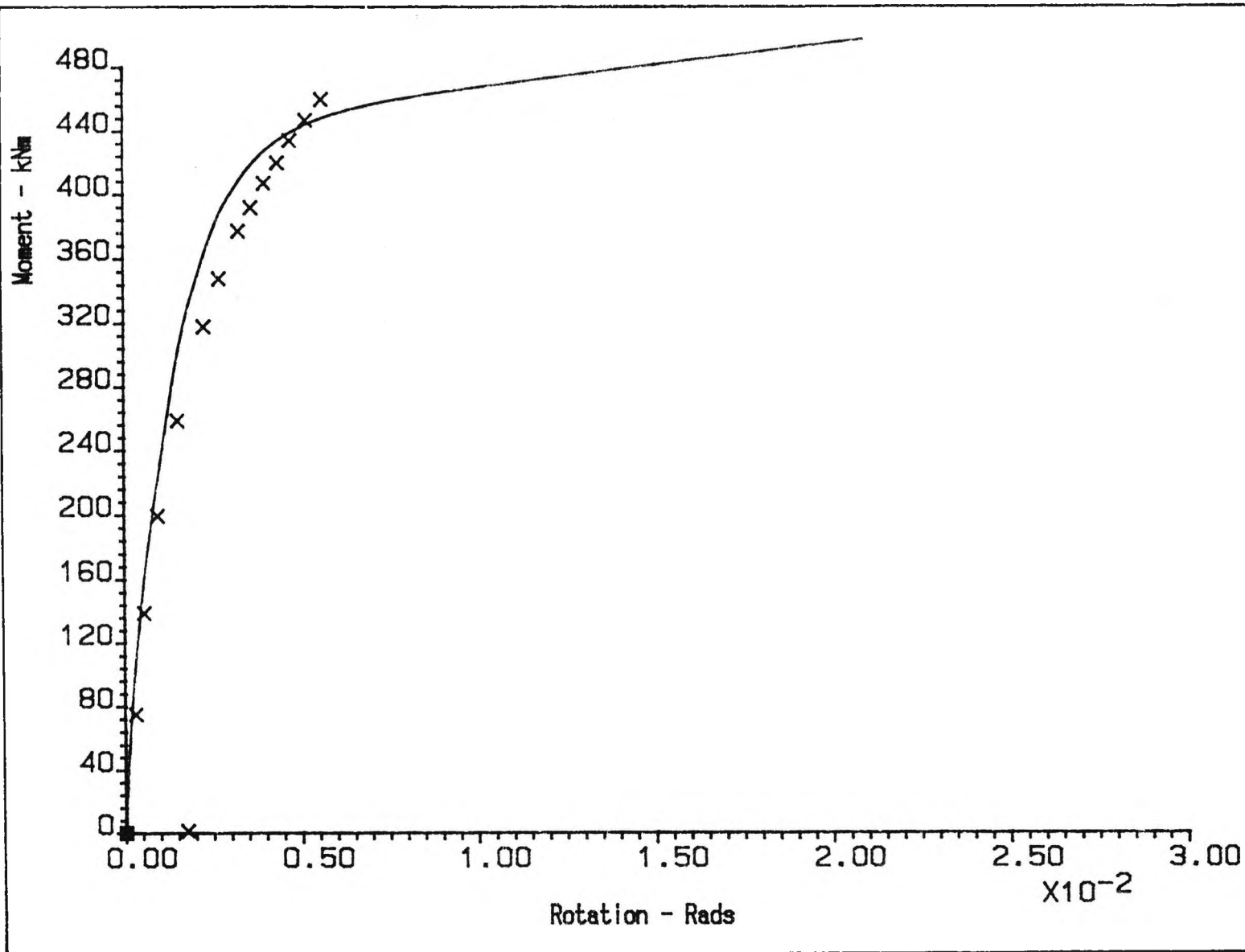
$M_p = 420. \text{ kNm}$
 $K_i = 253000. \text{ kNm/rad}$
 $K_p = 2750. \text{ kNm/rad}$

Decay factor=0.0

Figure 5.63

COMPARISON OF PREDICTION
 WITH CONNECTION DATA.

Test C1



Connection Type :-
 Stiffened
 Internal
 Beam Size -457x191UB74
 Column Size -305x305UC137
 6 M24 Tension Bolts
 Grade HSFG -Pretensioned
 Endplate Thickness = 25mm

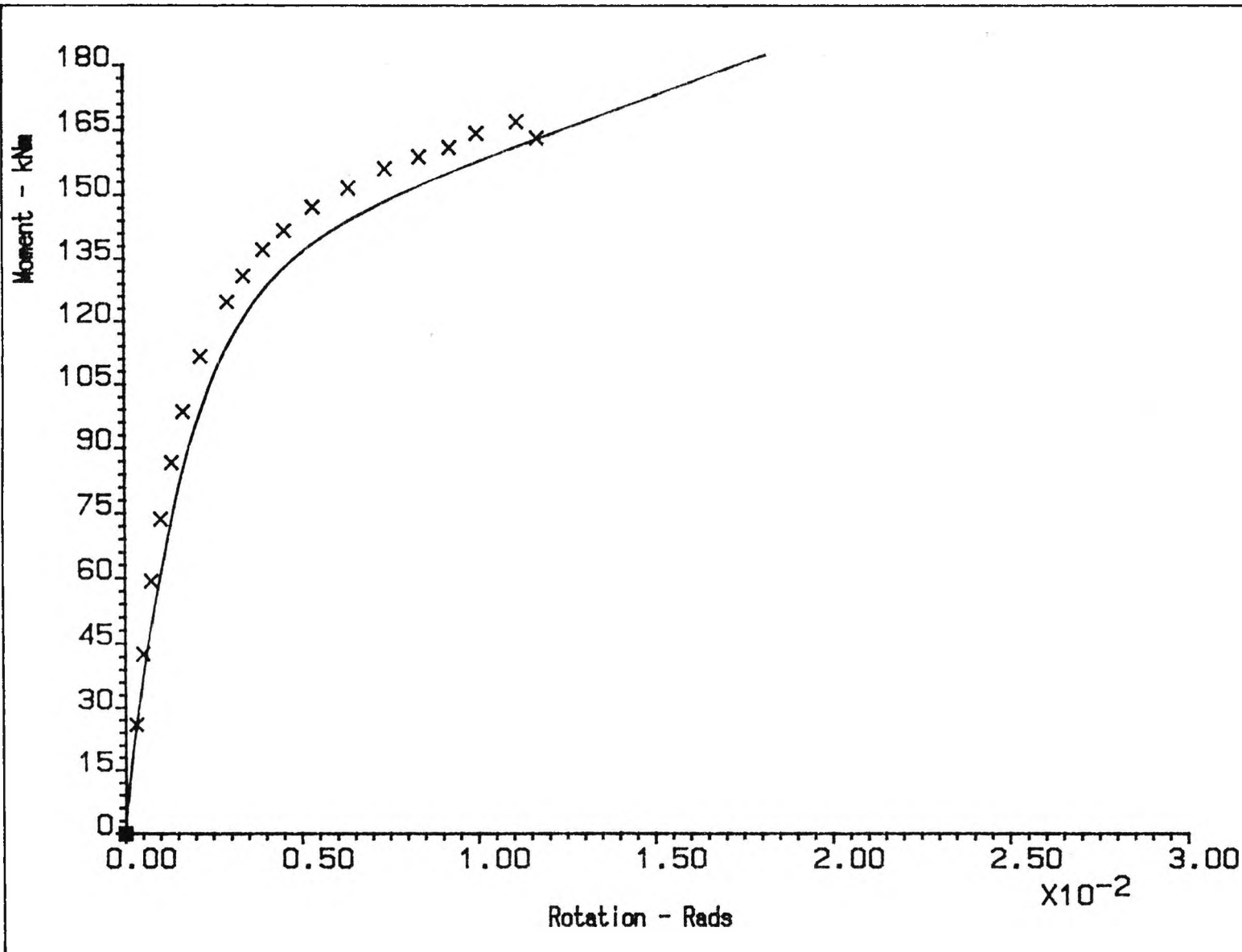
$M_p = 440. \text{ kNm}$
 $K_i = 325000. \text{ kNm/rad}$
 $K_p = 2750. \text{ kNm/rad}$

Decay factor=0.0

Figure 5.64

COMPARISON OF PREDICTION
 WITH CONNECTION DATA.

Test C2



Connection Type :-
 Unstiffened
 Internal
 Beam Size -254x146UB37
 Column Size -305x305UC137
 4 M20 Tension Bolts
 Grade HSFG -Pretensioned
 Endplate Thickness = 20mm

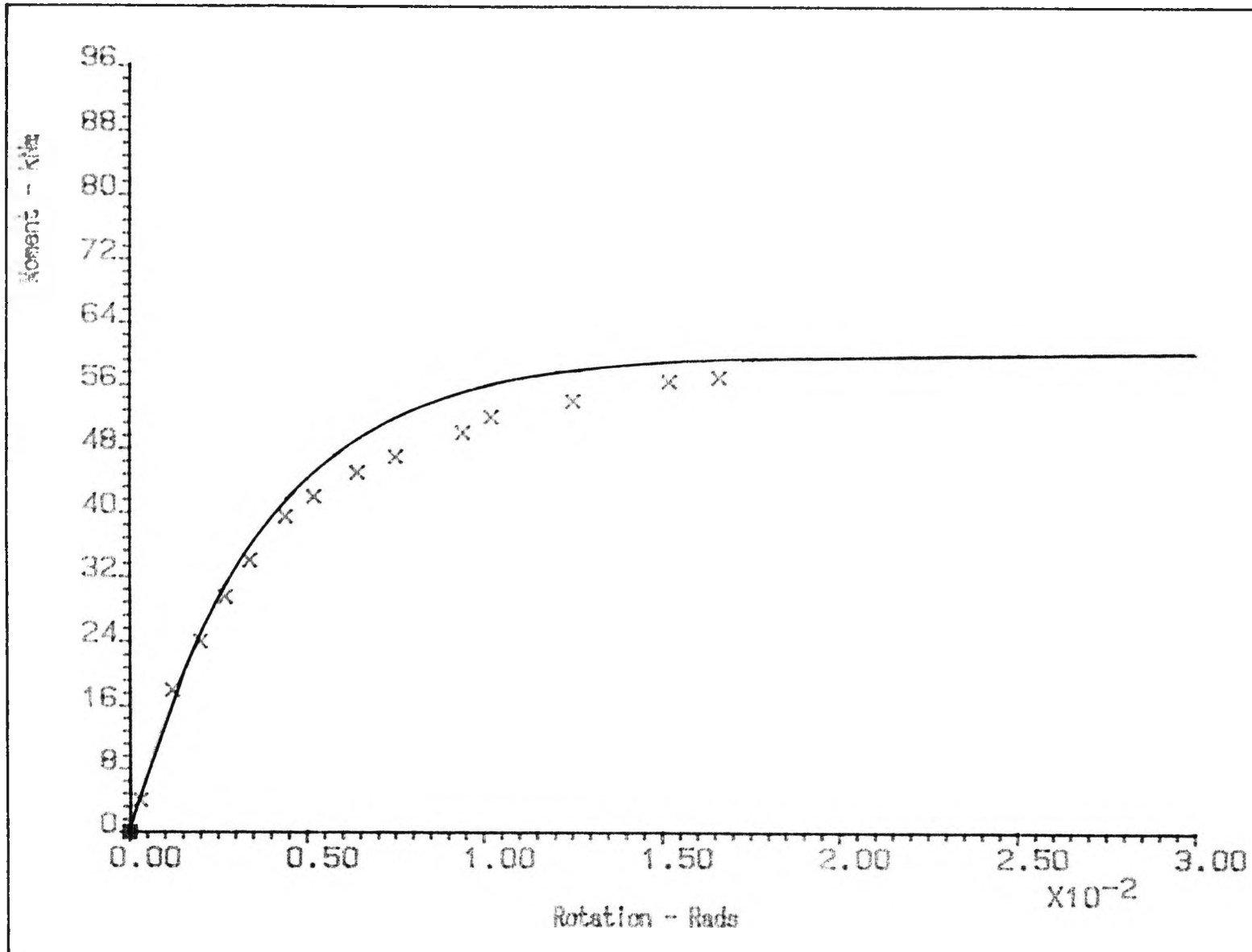
$M_p = 128. \text{ kNm}$
 $K_i = 79000. \text{ kNm/rad}$
 $K_p = 3000. \text{ kNm/rad}$

Decay factor=0.0

Figure 5.65

COMPARISON OF PREDICTION
WITH CONNECTION DATA.

Test D1



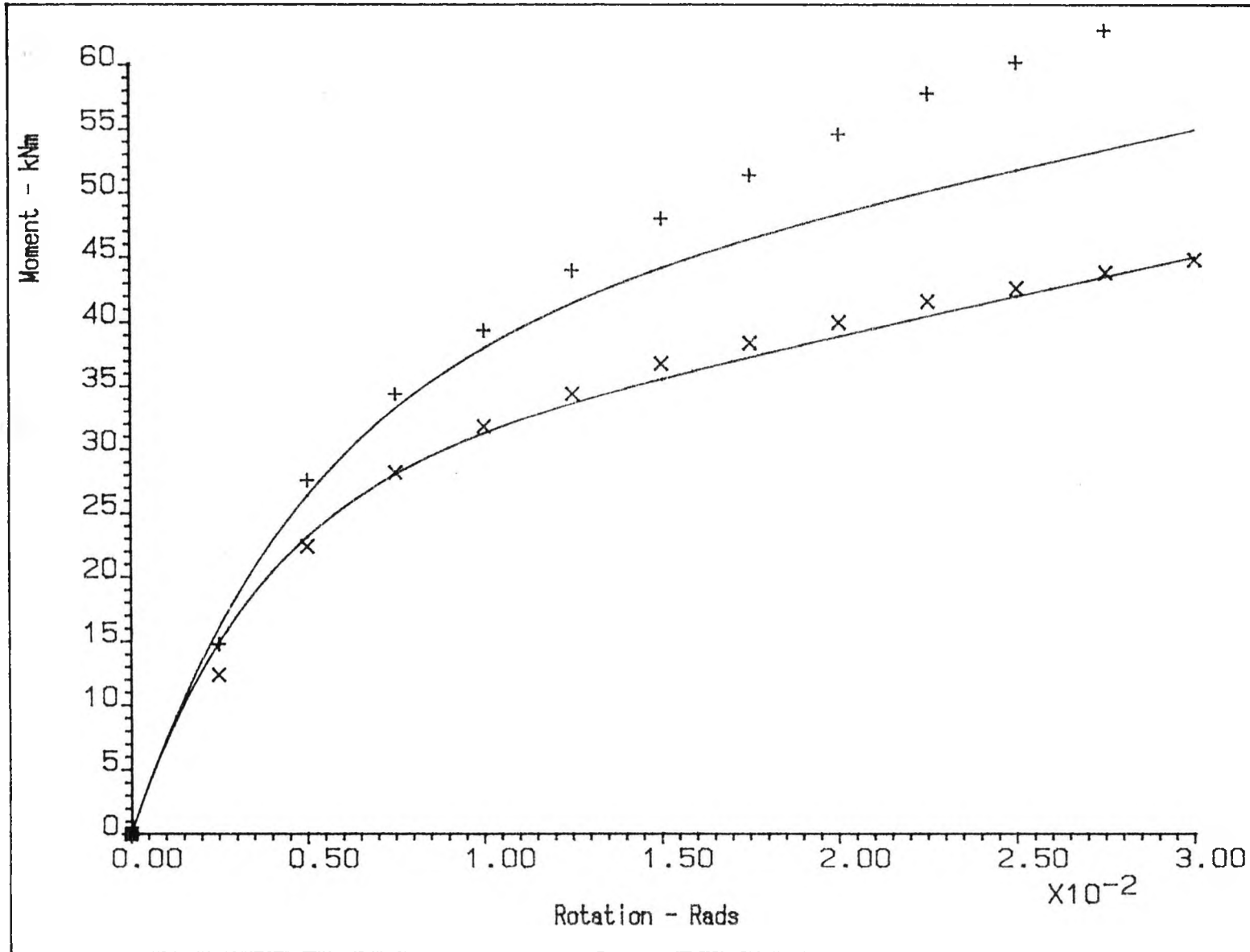
Connection Type :-
 Stiffened
 Internal
 Beam Size -254x102 UB22
 Column Size -152x152 UC23
 4 M16 Tension Bolts
 Grade 8.8-Pretensioned
 Endplate Thickness = 15mm

x = Test 13/B

Figure 5.66

COMPARISON OF PREDICTION
 AND OTHER TEST DATA.

Davison (14)



Connection Type :-
 Unstiffened
 Internal
 Beam Size -254x102 UB22
 Column Size -152x152 UC23
 4 M16 Tension Bolts
 Grade 8.8-Snugfit
 Endplate Thickness = 15mm

x = Test 3
 + = Test 4

Figure 5.67

COMPARISON OF PREDICTION
 AND OTHER TEST DATA.

Moore & Simms(18)

CHAPTER 6

ASSESSMENT OF THE APPLICABILITY OF MOMENT-ROTATION CURVES.

6.1 Introduction

In this chapter an assessment of the applicability of predicted moment-rotation curves to the analysis and design of steel frameworks is made.

The methods of including semi-rigid behaviour in more traditional forms of analysis including moment-distribution, slope-deflection etc. have been outlined elsewhere (2). Most of these methods are based upon the assumption of linear moment-rotation behaviour (see section 2.3.2). The effects of including moment-rotation relationships on the overall framework behaviour are examined in this chapter by the use of nonlinear semi-rigid plane framework analyses. These analyses are based upon a matrix method developed by Goto and Chen (44). A computer program written by the author based upon this method is outlined later.

The analysis program is used to assess the effect of the difference between the actual and predicted moment-rotation curves on framework behaviour. After examining the results of these analyses, it is hoped to be able to give guidance on the precision and accuracy required of any method of prediction on this connection type.

A plane framework employing extended and flush endplate connections was tested at the Building Research Establishment by Hatfield Polytechnic (7). An analysis of this framework is carried out using moment-rotation curves generated using the proposed method of prediction. The experimental and theoretical results of the framework analysis are compared.

6.2 A semi-rigid plane framework analysis program.

The method used to account for the semi-rigidity of connections in framework analysis is a matrix method. Its development is outlined elsewhere (44) and only a basic outline will be given here.

Semi-rigidity and other effects, such as the p-delta effect and the effect of bowing on axial force, are classed as second-order effects. They make the stiffness matrix of the frame dependent upon nodal displacements and axial force. This means that some form of nonlinear analysis is required to obtain a solution. The nonlinear method adopted in this analysis program is the secant stiffness method, chosen by its authors (44) for its stability and ease of application. The bowing effect on axial force has been found to be negligible for both rigid and flexible frames (44) and is, therefore, omitted here.

The general element stiffness equation for a beam-column element can be written as :-

$$\begin{Bmatrix} N_1 \\ S_1 \\ M_1 \\ N_2 \\ S_2 \\ M_2 \end{Bmatrix} = \frac{EI}{l^3} \begin{bmatrix} \frac{Al^2}{I} & 0 & 0 & -\frac{Al^2}{I} & 0 & 0 \\ 0 & 12\phi_1 & 6l\phi_2 & 0 & -12\phi_1 & 6l\phi_2 \\ 0 & 6l\phi_2 & 4l^2\phi_3 & 0 & -6l\phi_2 & 2l^2\phi_4 \\ -\frac{Al^2}{I} & 0 & 0 & \frac{Al^2}{I} & 0 & 0 \\ 0 & -12\phi_1 & -6l\phi_2 & 0 & 12\phi_1 & -6l\phi_2 \\ 0 & 6l\phi_2 & 2l^2\phi_4 & 0 & -6l\phi_2 & 4l^2\phi_3 \end{bmatrix} \begin{Bmatrix} u_1 \\ v_1 \\ \alpha_1 \\ u_2 \\ v_2 \\ \alpha_2 \end{Bmatrix} + \begin{Bmatrix} 0 \\ -\frac{p_y l}{2} \\ -\frac{p_y l^2}{12} \left[\frac{3}{2\phi_3 + \phi_4} \right] \\ 0 \\ -\frac{p_y l}{2} \\ \frac{p_y l^2}{12} \left[\frac{3}{2\phi_3 + \phi_4} \right] \end{Bmatrix}$$

(6.1)

where all the quantities are defined in Figure 6.1, except ϕ_i which are stability functions expanded as a power series to avoid numerical difficulty at low axial load.

This is simply expressed as

$$\{F_m\} = [K_{m1}] \{d_1\} + \{f_m\}$$

(6.2)

where

$\{F_m\}$	=	Element end force matrix
$[K_{ml}]$	=	Element stiffness matrix
$\{d_l\}$	=	Element end displacement matrix
$\{f_m\}$	=	Element end force matrix due to internal loading

The flexibility of the connection is taken into account by assuming a linear relationship between the beam end moment and connection rotation at any stage as

$$M = K_c(\theta, M) \theta$$

(6.3)

where $K_c(\theta, M)$ is the secant stiffness of the connection.

A modified member stiffness equation for the beam-column including connection flexibility can be obtained by eliminating the rotational degree of freedom at the end of the beam by static condensation. This leaves a modified stiffness equation with the same number of degrees of freedom as equation 6.1. This member stiffness equation for a beam column member with connection flexibility can be expressed as

$$\{F_m^c\} = [K_{ml}^c] \{d_l^c\} + \{f_m^c\}$$

(6.4)

where the superscript c denotes a modified matrix and the components of $[K_{ml}^c]$ and $\{f_m^c\}$ are given in reference 44.

To save unnecessary computer input, members of any frame are defined as beams or columns. Columns have member stiffness equations (6.2) and beams have member stiffness equations (6.4). Beams need the definition of connection parameters for both ends of the beam.

The flow chart for the computer program is shown in Appendix H. The initial connection stiffness is used for the first load increment. The member stiffness equations are then assembled in the global stiffness matrix. This stiffness matrix is solved in the normal manner and the element end forces calculated using the relevant member stiffness equations. These element end forces are compared with the element end forces used to calculate connection secant stiffness and the stability functions. If these forces do not come within the required tolerance then the new element end forces are used to recalculate connection stiffness and the stability functions. The procedure is repeated until the forces come within tolerance. This process is shown diagrammatically for one connection in Figure 6.2. Once the analysis has converged the internal displacements and forces can be calculated.

It should be noted that once nonlinearity is introduced to the analysis, the behaviour of any framework becomes load-history dependent. For this reason loads should be split into increments and great care taken in the order in which they are applied.

6.3 Selection of moment rotation curves for analysis.

Each end of the beam requires the selection of a set of connection parameters. These connection parameters are dependent on the connection geometry, the connection's position in the frame and on the load applied to the frame. Methods which could be used to incorporate the effect of these factors in the moment-rotation data are explained below.

One factor which affects the moment-rotation curve is axial load. The axial load carried by a column affects the value of allowable yield stress available for bending. Axial load can be accounted for by a simple reduction in the yield stress used to calculate the column failure modes. The effect on the moment-rotation curve is the same as reducing the plastic moment of the model as shown in Figure 5.39.1 if the overall failure mode is in the column. The effect of axial load on the buckling and crippling capacity of the column web has already been investigated (45). Further work needs to be done on the effect of the axial load on other column failure modes.

Another load factor which affects the moment-rotation behaviour of the connection is the out-of-balance moment across the connection. This results in a shear force across the connection and the derivation of its effect on the initial stiffness has already been outlined in section 3.23. The out-of-balance moment is directly related to the load applied to the connection and the spans of the beams framing into the column.

The above effects mean that the moment-rotation curves themselves are nonlinear in terms of axial load and moment across the connection. It would be too complex to include these nonlinear effects in the frame analysis. However, as extended endplates are nominally rigid connections, a rigid analysis of the frame under the same load conditions would give a good approximation of the force distribution at each connection. Appropriate connection parameters can then be chosen based on this information for the load level required.

The above demonstrates the ease in which relatively complex effects can be included in a simple model by the careful consideration of the structural action of the connection. It would be difficult to incorporate these effects into a curve-fitted or standardised model.

6.4 The effect of actual and predicted moment-rotation curves on frame behaviour.

As discussed in the previous section, the moment-rotation behaviour of any connection is dependent upon the load state at that connection. This load state is based upon the geometry of and the load applied to the frame. The moment-rotation curves from the experimental study were obtained from balanced internal/internal type tests. Therefore, any frame selected to examine the differing effects of these curves should reflect this behaviour. It was decided to examine a subassemblage of a framework to mirror the load conditions at the experimental

connection and minimize the effect of other connections in a total frame. This subassemblage is outlined in Figure 6.3. The behaviour of the middle beam in this subassemblage will be examined. Load will be applied in five vertical uniformly distributed increments up to the plastic moment of the beam. The values of interest are the central deflection and the end moment of the middle beam.

The correlation between the central deflection and the end moment of subassemblages using the actual and the predicted curves will be the criteria used to ascertain whether a predicted curve is accurate enough. It should be noted that actual curves here are the 'best' fit curves as outlined in section 5.5. When the deviation in actual and predicted curves is examined it will be seen that the difference in behaviour due to this approximation is negligible.

The graphs of central deflection and end moment for each test subassemblage (except test series C) are given in Figures 6.4 to 6.13. Test series C results are not presented as test C1 is not valid and test C2 did not reach failure, therefore, making it difficult to model connection behaviour accurately (see Figure 5.50).

Firstly, the effect of including the flexibility of extended endplate connections will be examined. The deflection and end moment of a rigid subassemblage is shown as a straight line in Figures 6.4 to 6.13. The inclusion of semi-rigid connections

makes a substantial difference to the behaviour of the framework. The difference in central deflection varies from test to test. For test series A, the deflection is 19% to 32% greater initially than the rigid case. In the later stages of loading this increases to 29% to 56%. For end moment, the decrease is 4.5% to 8% initially. Near the plastic moment of the beam there is a reduction in end moment of 7% to 14.5% of the rigid end moment. It would appear, therefore, that the greatest effect of including the flexibility of extended endplate connections is on the serviceability aspects of frame behaviour.

Test series B subassemblages show a more pronounced increase in deflection in comparison to rigid behaviour than test series A especially the unstiffened connection. This is despite initial stiffness being significantly larger.

The test D1 connection has less effect on the subassemblage deflections and moments than any series A test. For comparison purposes, a run of the predicted method of test C1 was carried out to obtain an estimate of the overall increase in deflection and decrease in end moment for this size of connection. This run showed a 36% to 69% increase in central deflection and a 9% to 18% decrease in end moment over the load range.

It is evident that the semi-rigidity of extended endplate connections has a significant effect on the behaviour of a framework even though it is classed as a rigid connection. In fact, this second order effect has far more significance than

other effects such as the p-delta or bowing effects, especially for low to medium rise steel frameworks.

The ability of the predicted curves to mirror the behaviour of the actual curves was examined next. If the predicted curves are examined (Figures 5.54 to 5.65), it can be seen that some deviations from actual behaviour appear to be quite significant. These deviations are more pronounced in the later stages of loading and it is this stage where the most substantial differences in frame behaviour occur.

The worst cases for the prediction of central deflection are tests A5 and A7 where there are increases in deflection of between 6% and 10% over actual connection behaviour. All other test connections have deviations below 5% for all the loading range. This is deemed accurate enough for engineering purposes. For tests A5 and A7 the predicted method underestimates initial stiffness by 9000 and 17000 kNm/rad respectively. The test A7 subassemblage deviations from actual behaviour are no worse than those of the test A5 subassemblage. It appears, therefore, that the stiffer a connection is the less accurate the initial stiffness needs to be for a corresponding deviation in frame behaviour. This is borne out by the test B2 connection where a overestimation in initial stiffness of 39000 kNm/rad results in only a 5% deviation in framework central deflection.

The variation in moment behaviour is less pronounced than deflection behaviour. All predicted connection subassemblages

deviate less than 5% over the loading range from actual connection subassemblages. Most connections, in fact have differences of less than 3% for the entire load range. This is less severe than the change in deflection. Therefore, there is a corresponding scaling down in deviation.

The above results are for a span of 6m which is considered to be a typical length beam. Increasing or decreasing the span would scale the corresponding deviations up or down respectively. Overall, it can be said that the prediction method performs satisfactorily for normal span beams. It can be seen that the accuracy required of the connection parameters varies with the stiffness of the connection considered. Typically a 7000kNm/rad or 13% deviation in initial stiffness for a 55000 kNm/rad initial stiffness connection will result in deviations in central deflection of less than 5% and deviations in end moment of less than 3% from experimentally obtained connection behaviour.

Also included in Figures 6.4 to 6.13 is the behaviour of the subassemblage taking the offset rotation as the connection curve. This leads to overestimation of deflection by 15% to 20% over actual connection subassemblage behaviour. This is accompanied by a 5% to 10% decrease in end moment. This demonstrates that offset stiffness can contribute a significant amount of rotation in connection tests and that great care must be exercised before using the results of these tests in framework analysis.

A common approximation is the representation of connection behaviour as a straight line model. It was decided to examine the difference in a straight line assumption and actual connection behaviour. This was done by comparing the deflection and moment at the elastic design moment of the beam. This value was chosen as it was the limit of the elastic range. The actual initial stiffness of the connection was used for the straight line model. The difference in central deflection and end moment is given on Table 6.1. From the table it can be seen that the error in end moment calculation is less than 5% (except for test B1). The deviation in central deflection is greater, being up to 27% less than the deflection due to actual connection. This indicates that a straight line approximation may be acceptable for the calculation of end moment in frames utilising extended endplate connections.

6.5 The Hatfield test frame.

6.5.1 Introduction

A three storey, two bay frame (see Figure 6.14) which included extended and flush endplate connections was tested at the Building Research Establishment by Hatfield Polytechnic (17). Two frames were tested under a variety of load conditions. The first frame was tested to examine the overall behaviour of the structure. The second frame was tested to confirm the results of the first test and to examine any irregularities. Measurements taken at various sections included deflection and

moment derived from strain gauge readings. Connection rotations were also monitored. Full details are given in reference 17. Some of the measurements will be compared with the results obtained from a semi-rigid analysis of the test frame using predicted moment-rotation curves.

6.5.2 Moment-rotation data generation.

If the test frame is examined it can be seen that all types of connection classified by their position in the frame are present i.e. external/eave, etc.. In addition each test was carried out with bolts pretensioned and snuggest. This means that connection parameters used are different for virtually every connection.

To accurately define internal/internal connection stiffness, the load distribution at the connection is needed as outlined in section 6.3. A difficulty arises in the selection of moment-rotation data in this case due to the mixture of endplate connections. Flush endplates are nominally pinned and extended endplates are nominally rigid. It was decided, however, that the initial stiffness of the connection would be chosen on the basis of a rigid analysis of the framework. The connection parameters for the flush endplate were estimated by the consideration of several research papers on connections of this type (14, 46).

The endplate dimensions are based upon the standardised endplates, dependent on beam size, as given in Jenkins, Tong and

Prescott's paper (16). The endplates varied in thickness only. All extended endplate connections were stiffened with compression and tension stiffeners. The parameters calculated for the hand tight and preloaded bolted connections are shown in Table 6.2. The only difference in the external and internal initial stiffness is in the amount of shear deflection assumed to be contributing to initial stiffness. In the external connection, shear accounts for approximately 50% of initial connection flexibility. The difference in handtight and preloaded initial stiffness is taken into account by the assumption of a different bolt stiffness in accordance with Agerskov's theory (40) (see Appendix B). Due to the lack of information relating to strain hardening stiffness, it is assumed to be negligible. The model in this case, is reduced to a two parameter model.

6.5.3 Comparison of analysis and experimental results.

The Hatfield test frames were tested in two different modes, sway and non-sway. In the non-sway case the frames were restrained laterally. The sway case only will be examined here.

Test frame 1 behaved peculiarly in that a noticeable lack of fit occurred at one of the extended endplate joints (17). This made this connection behave like a pinned joint for a substantial portion of the load range, and, therefore, only the results of test frame 2 will be considered. In each test loads were applied at the quarter points of the beams up to the equivalent of either dead load, dead and live load and factored design load. In the

analysis, rigid nodes were introduced at the quarter points of the beams and the loads were applied here so that the experimental behaviour was closely modelled. The rigid nodes had a very high initial stiffness and plastic moment equal to the plastic moment of the beam.

The results for two tests, test 11 (hand-tight bolts) and test 40 (preloaded bolts) are given in Table 6.3. The relevant node and element numbers are defined in Figure 6.15. It should be noted that these results are a 'snapshot' of how the frame behaved in a particular test. Over 40 tests were carried out on test frame 2 with the frame being constantly loaded and unloaded. The results at a particular load did vary from test to test but not significantly. These results are taken from Prescott's thesis (17) where the measurements from a limited number of tests were presented.

It can be seen from Table 6.3 that the majority of the predicted values are in good agreement with the experimental values. Agreement is good for both deflections and end moment. The former usually being predicted within 1mm and the latter to within 3kNm. It should be noted that central deflection was measured relative to the beam ends in the tests and, therefore, joint displacements were subtracted from the analysis results.

Values for dead load and dead plus live load only are presented as two connections theoretically failed in the analysis which was

terminated. This was due to assuming that strain hardening was negligible. It should be noted, however, that in the experimental test frame the same two connections were yielding significantly at the factored design load. The test frame experimental results were subject to local irregularities. This is borne out by the measured end moments being greater than the those of a nominally rigid connection in the same places.

The connection rotation results for some of the tests are also presented in Prescott's thesis (17). It is admitted by Prescott that these results are erratic. The explanation given is that this was due to variable instrumentation behaviour. It was noted, though, that the connection rotation curves that were obtained were more linear than those obtained in the laboratory specimen tests. The author feels that this could be due to the behaviour of connections under cyclic loads. Gertsle (47), amongst others, noted that when a connection unloads it invariably unloads along a line approximately equal to the initial stiffness of the connection. It follows the same load path on reloading before joining the original connection curve. This is shown diagrammatically in Figure 6.16. This behaviour could have taken place in the test frame as the frame was continuously loaded and unloaded. This process is the equivalent of work hardening or 'shakedown' in the connection.

Overall predicted results compare well with experimental results. This is despite the assumptions made at the beginning of the analysis. These assumptions include, that

i) the state of stress at internal connections can be assumed to be the same as a rigid connection for the selection of the initial connection parameters

ii) there is no lack of fit in any of the connections

and iii) connections are loaded from the 'virgin' state.

6.6 Applicability of moment-rotation curves.

It is well known that there is a need for methods of predicting moment-rotation behaviour and initial stiffness of connections (48). These methods should be applicable in both research and design. It is the lack of consistent data for use in research that is restricting the more widespread use of moment-rotation data in design. It has been demonstrated in this chapter that the proposed method of prediction gives moment-rotation curves that can predict overall frame behaviour within acceptable limits given that nominal properties were used in the analyses. An outline of the applicability of these predicted moment-rotation curves in research and design will be given in this section.

The principal aim of research into semi-rigid connections is to develop simplified design codes which accurately reflect the real behaviour of frameworks hence, leading to more economic and efficient design. This aim can be achieved in two ways.

Firstly, by expanding knowledge of how frameworks actually behave. This is directly related to connection behaviour as it is the present lack of knowledge of the actual method of load transfer from beams to columns that make present design codes so conservative. Once it is known how frameworks behave with different connection types and under different load conditions, the appropriate factors in the design codes can be reduced. For example, in the present limit state design code there are three statistical factors which cover variability of material strength, loading and structural performance. It is envisaged that the latter factor could be reduced depending upon which type of connections are used in the frame. This factor would still be conservative, but less so than before.

The second way of achieving economic design is to directly include connection behaviour in framework analysis. This is the most complex way and relies on sufficient data being available for all connection types and sizes. This solution would require a computer but would result in the most economic design in terms of least weight since the solution would be tailored to a specific frame. This method of incorporating semi-rigidity is not possible in the immediate future since connection behaviour in real frameworks has hardly been considered at present.

These realities include three-dimensional behaviour such as the effect of minor axis connections and torsion. In addition, the effects of cladding and the restraint offered by floors etc. also need to be considered. For the present, though, the problems offered by plane framework behaviour need to be examined and fully understood before these other effects are studied.

The applications of moment-rotation curves in the design office are limited at the present. One immediate use is the checking of connection behaviour in plastically designed frames. The connections need to be checked in plastically designed frames to ensure that the assumptions made in the design are feasible in reality. Witteveen et al. (49) outlined the criteria that need to be satisfied for extended endplate connections. These criteria are given in Figure 6.17. The ideal connection passes through the shaded areas fulfilling the requirements at the serviceability limit state of the frame and in the strain hardening phase of the loading.

A simplified way of incorporating the moment-rotation behaviour of a connection in beam behaviour is the beam-line method. This involves calculating the interception of a moment-rotation curve and the line representing beam end behaviour for all possible end fixity conditions for the load considered. This is demonstrated graphically in Figure 6.18. The moment and rotation at the interception represent the design conditions at the end of the beam with that particular connection. This obviously is a cumbersome process for very large frameworks and does not take

into account the effect of other beams on the individual behaviour of any other beam.

6.7 Summary

Summarizing, design applications are limited due to the lack of moment-rotation data on which to base research into frame behaviour. It is hoped that this research will help in establishing a method of predicting connection moment-rotation relationships. This research has demonstrated that by working within a limited model and using nominal section properties a satisfactory approximation of connection behaviour can be made. It is also hoped that this method of prediction will find wider application to other connection types as it is perfectly general. Although, it must be added that other connections may exhibit more variable behaviour than extended endplate connections.

Test	Deviation in Central Deflection %	Deviation in End Moment %
A2	21	5
A3	10	2
A4	10.5	2.5
A5	15	4
A6	16	4
A7	9	2
A8	12.5	3
B1	27	7
B2	21	3.5
D1	10	3

Table 6.1 Difference in Central Deflection and End Moment
for a Straight Line Model and Actual Connection
Curve at the Beam Elastic Design Moment.

Connection No.	Type	M_p kNm	K_i kNm/rad	K_p kNm/rad	c
1	External/Eave	130.	27800	0.0	0.0
2	External/Internal	140.	45822	0.0	0.0
3	External/Internal	140.	45822	0.0	0.0
4	Internal/Eave	130.	43844	0.0	0.0
5	Internal/Internal	140.	60193	0.0	0.0
6	Internal/Internal	140.	62811	0.0	0.0

a) Hand-Tight Bolts

Connection No.	Type	M_p kNm	K_i kNm/rad	K_p kNm/rad	c
1	External/Eave	130.	31747	0.0	0.0
2	External/Internal	140.	57023	0.0	0.0
3	External/Internal	140.	57023	0.0	0.0
4	Internal/Eave	130.	54588	0.0	0.0
5	Internal/Internal	140.	81101	0.0	0.0
6	Internal/Internal	140.	85927	0.0	0.0

b) Pretensioned Bolts

Table 6.2 Parameters used for Connections in the Hatfield Test Frame Analysis.

Element	Dead Load			Dead + Live Load		
	Predict.	Expt.	Rigid	Predict.	Expt.	Rigid
1	11.4	11.0	9.9	13.0	12.2	11.3
4	8.8	8.8	7.7	13.6	12.5	11.4
7	9.3	9.0	8.0	14.2	13.3	11.7

i) Test 40 - Preloaded Bolts - Sway Frame

Element	Dead Load			Dead + Live Load		
	Predict.	Expt.	Rigid	Predict.	Expt.	Rigid
1	11.8	14.7	9.9	13.4	16.0	11.3
4	9.2	9.8	7.7	14.4	14.0	11.4
7	9.8	10.0	8.0	14.9	15.0	11.7

ii) Test 11 - Hand-Tight Bolts - Sway Frame

a) Central Deflection (mm)

Node	Dead Load			Dead + Live Load		
	Predict.	Expt.	Rigid	Predict.	Expt.	Rigid
1	48.4	51.0	53.5	56.0	58.0	62.4
5	66.3	66.0	75.7	74.9	77.0	86.0
2	61.2	68.0	66.4	87.8	100.0	96.3
6	68.8	70.0	74.6	99.1	103.0	109.8
3	57.8	54.0	62.1	84.2	84.0	91.6
7	68.9	75.0	74.8	99.5	99.0	110.3

i) Test 40 - Preloaded Bolts - Sway Frame

Node	Dead Load			Dead + Live Load		
	Predict.	Expt.	Rigid	Predict.	Expt.	Rigid
1	47.7	50.0	53.5	55.2	57.0	62.4
5	64.8	37.0	75.7	73.2	47.0	86.0
2	60.1	60.5	66.4	86.0	89.0	96.3
6	67.2	66.0	74.6	96.5	96.0	109.8
3	56.8	49.0	62.1	82.6	74.0	91.6
7	67.3	65.0	74.8	96.8	95.0	110.3

ii) Test 11 - Hand-Tight Bolts - Sway Frame

b) End Moment (kNm)

Table 6.3 Comparison of Results of the Hatfield Frame Test and the Predicted Analysis.

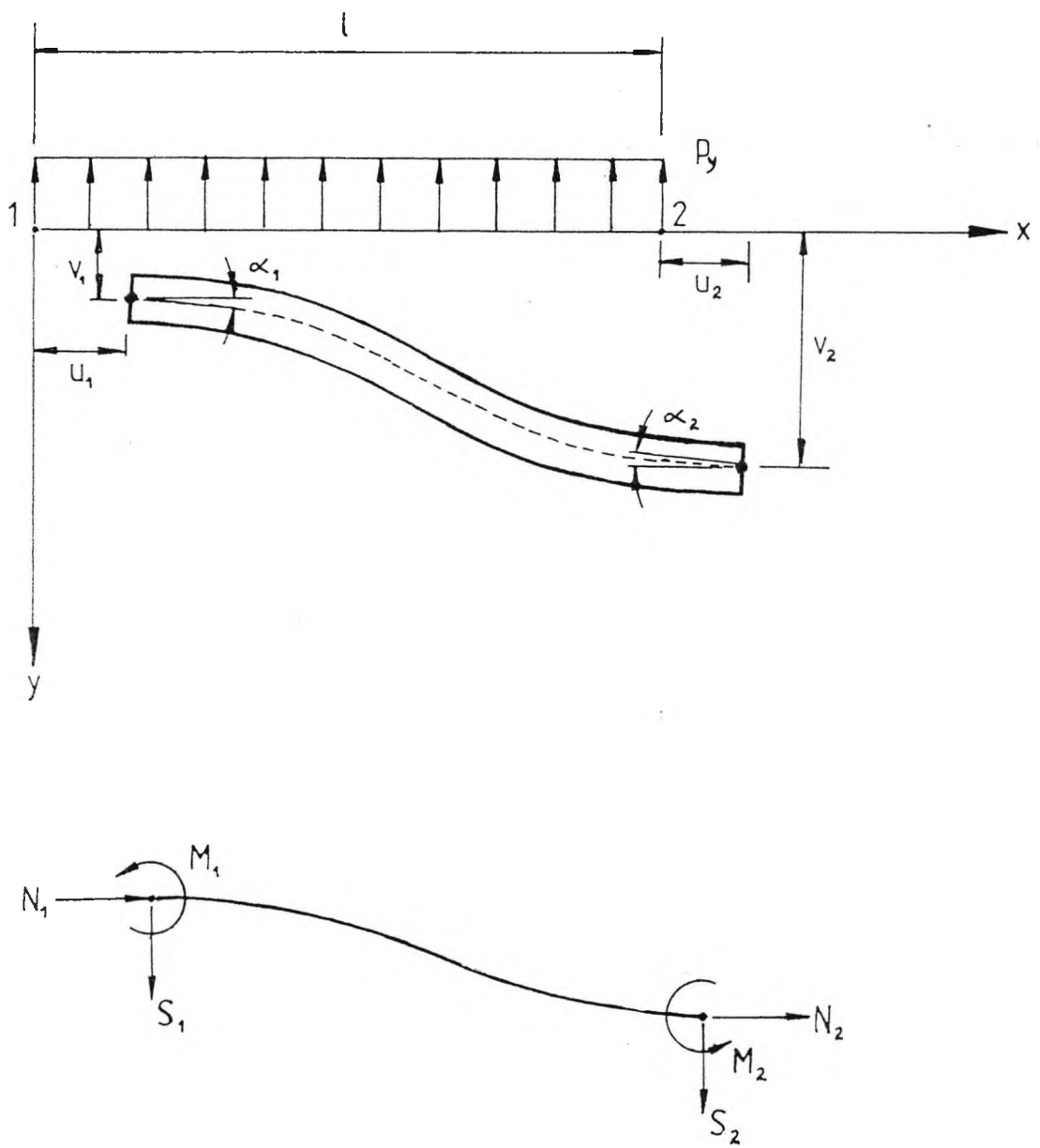
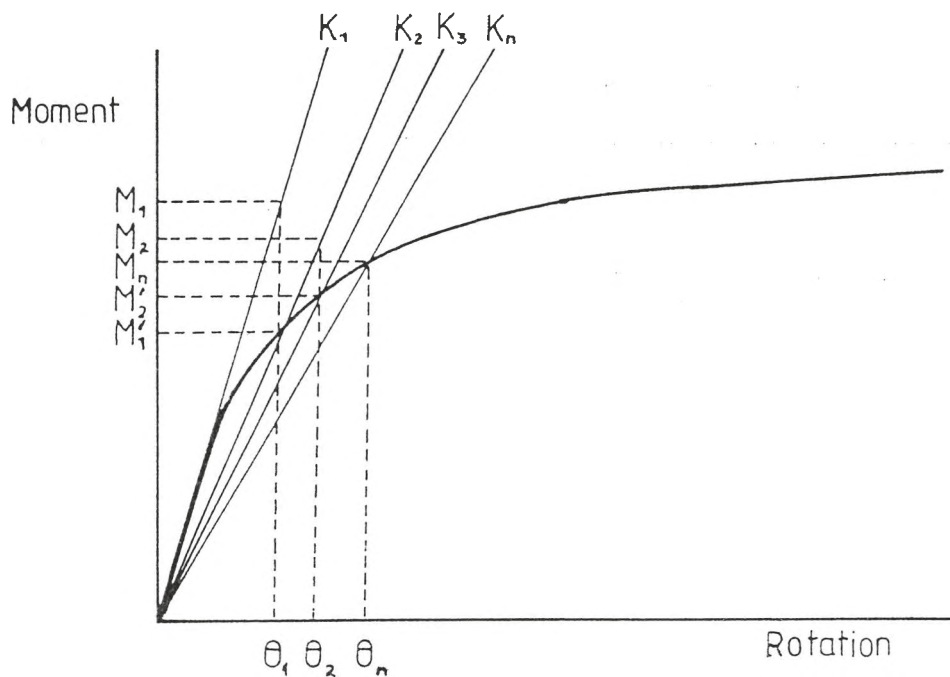


Figure 6.1 Definition of Beam Stiffness Equation Parameters.



- Steps
1. Assume K_1 , calculate M_1 .
 2. Calculate θ_1 from M_1/K_1 .
 3. Calculate M_1' from Yee's equation.
 4. Compare M_1 and M_1' .
 5. Calculate K_2 from M_1'/θ_1
 6. Repeat

Figure 6.2 Convergence of Solution at the End of the Beam.

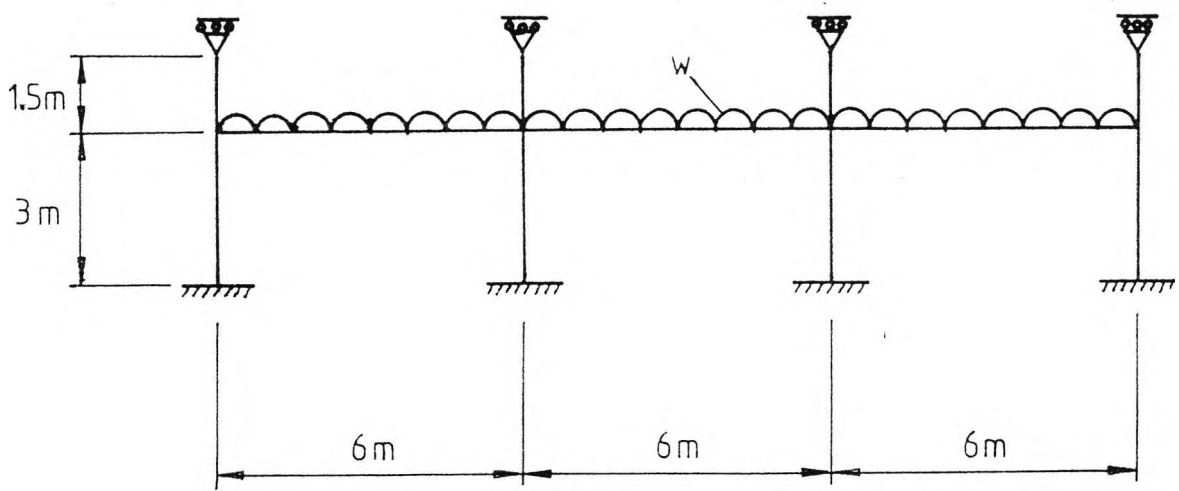


Figure 6.3 Subassemblage used to Examine the Effect of Semi-rigidity.

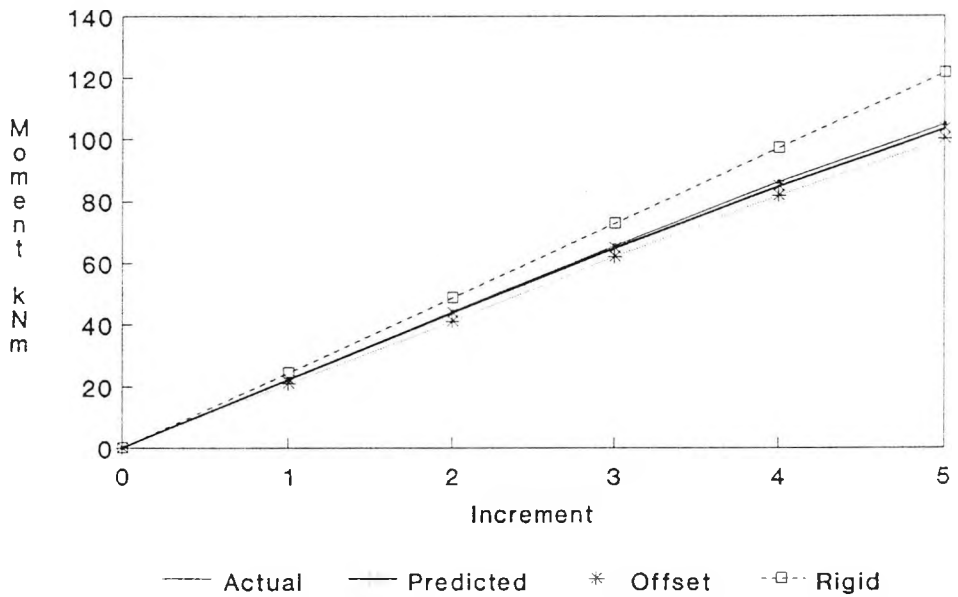
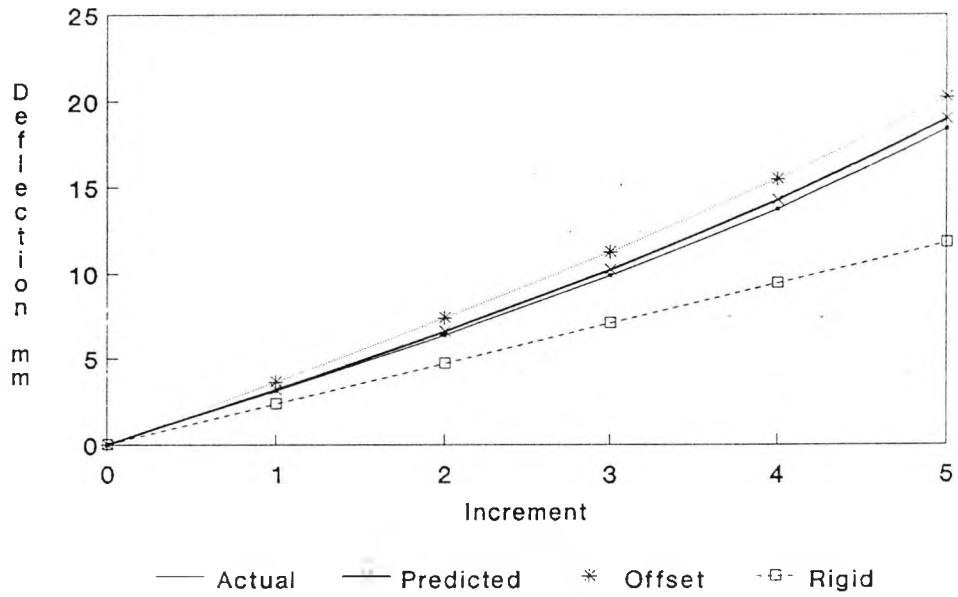


Figure 6.4 Comparison of the Effect of Actual, Predicted, Offset and Rigid Connections on Framework Behaviour - Test A2.

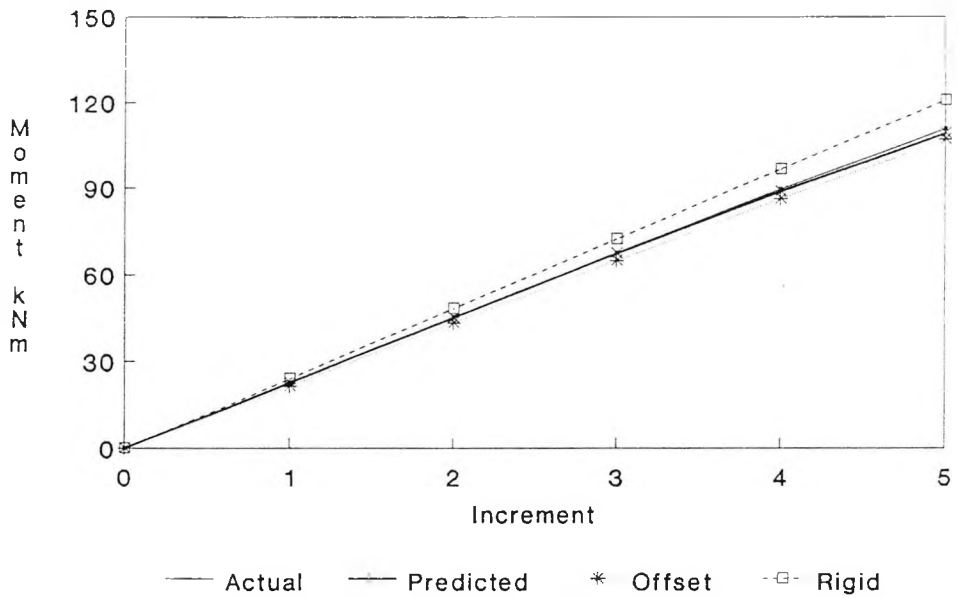
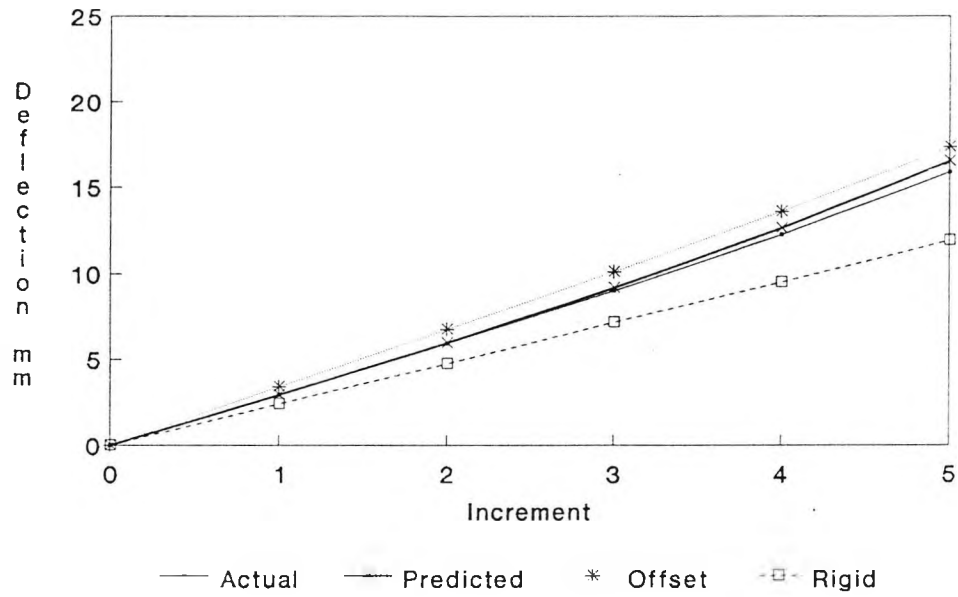


Figure 6.5 Comparison of the Effect of Actual, Predicted, Offset and Rigid Connections on Framework Behaviour - Test A3.

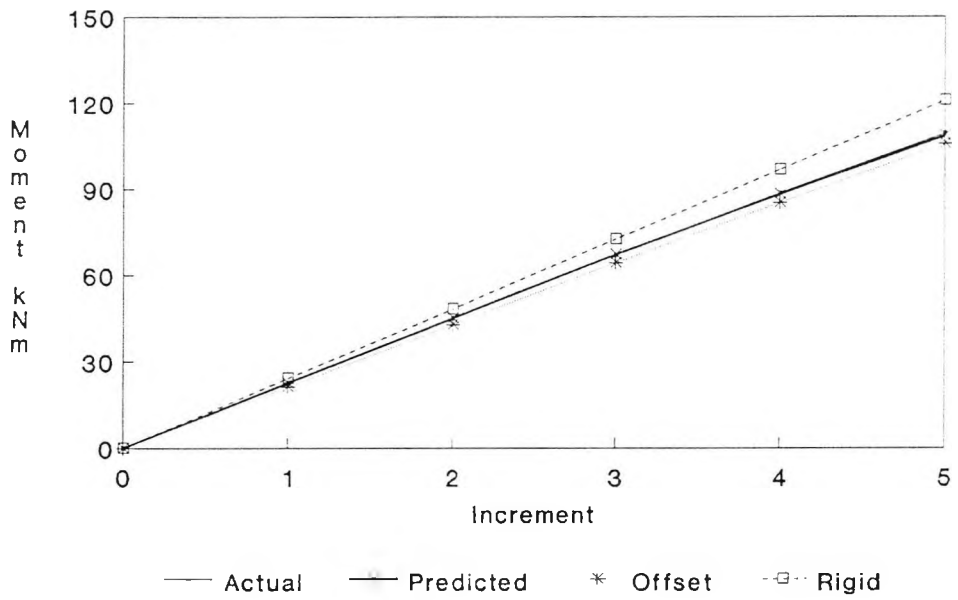
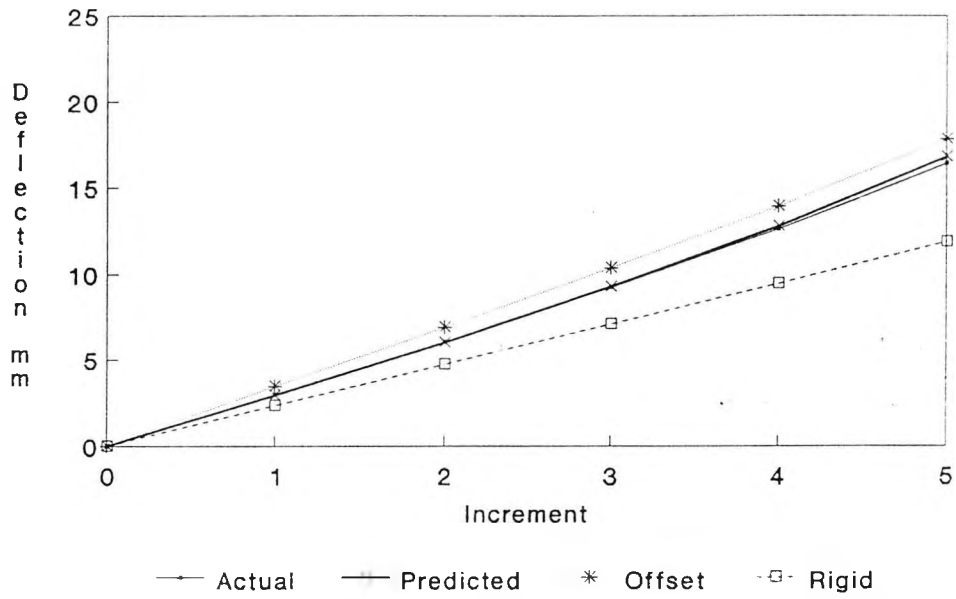


Figure 6.6 Comparison of the Effect of Actual, Predicted, Offset and Rigid Connections on Framework Behaviour - Test A4.

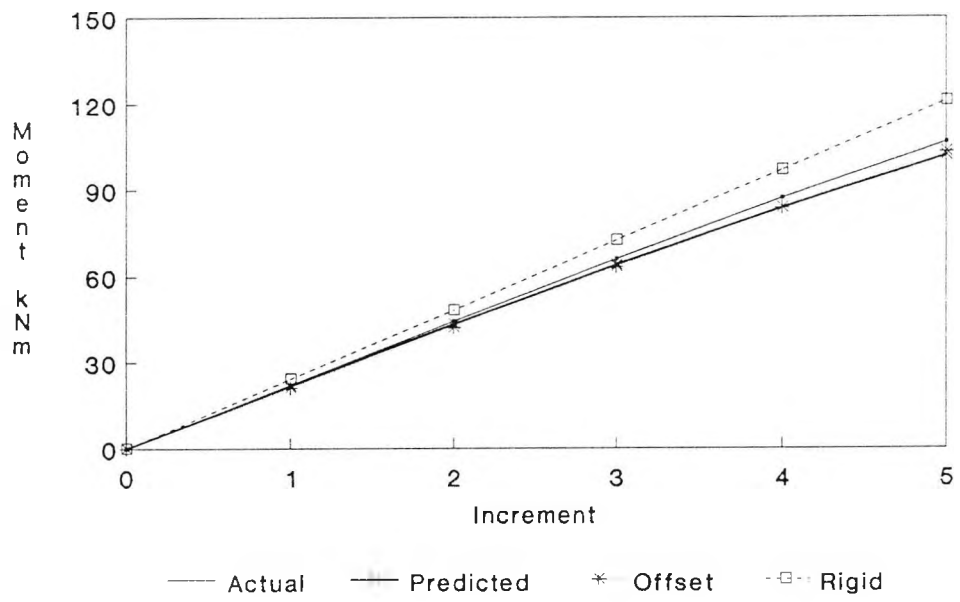
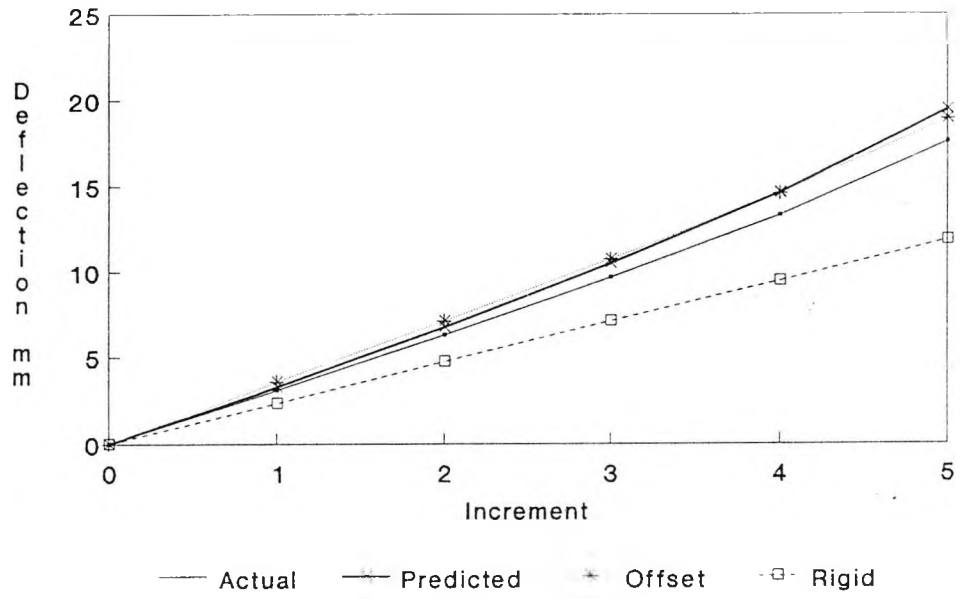


Figure 6.7 Comparison of the Effect of Actual, Predicted, Offset and Rigid Connections on Framework Behaviour - Test A5.

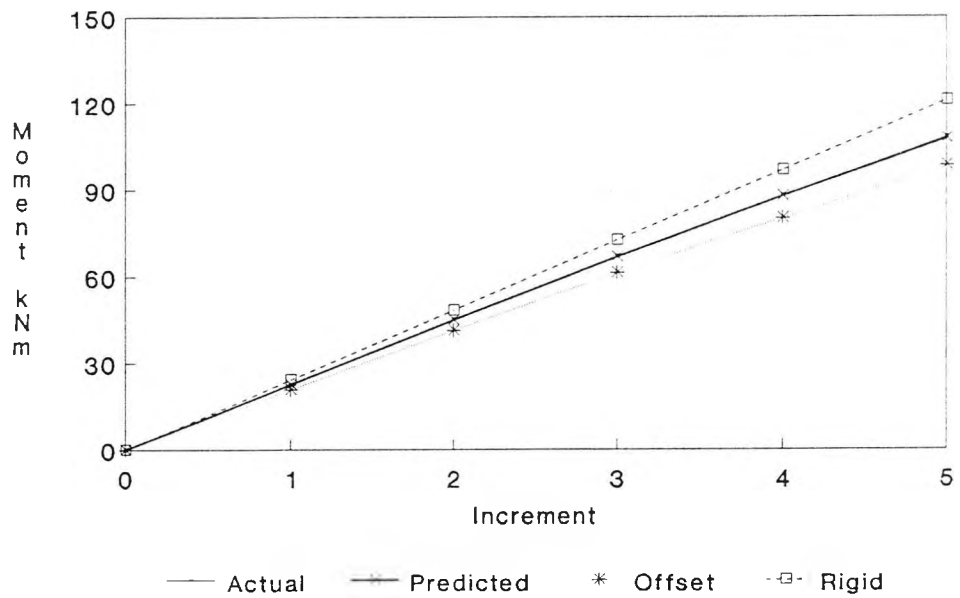
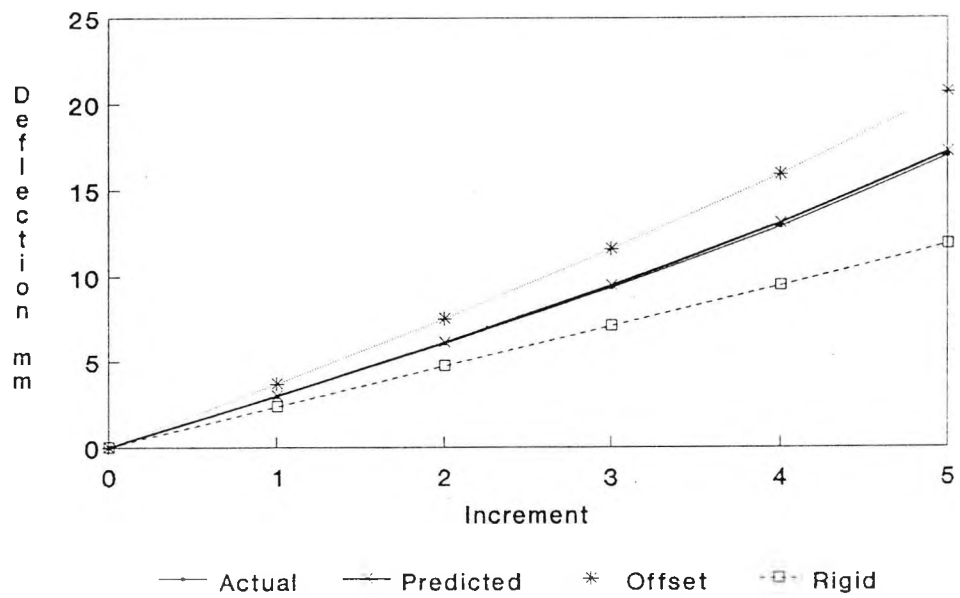


Figure 6.8 Comparison of the Effect of Actual, Predicted, Offset and Rigid Connections on Framework Behaviour - Test A6.

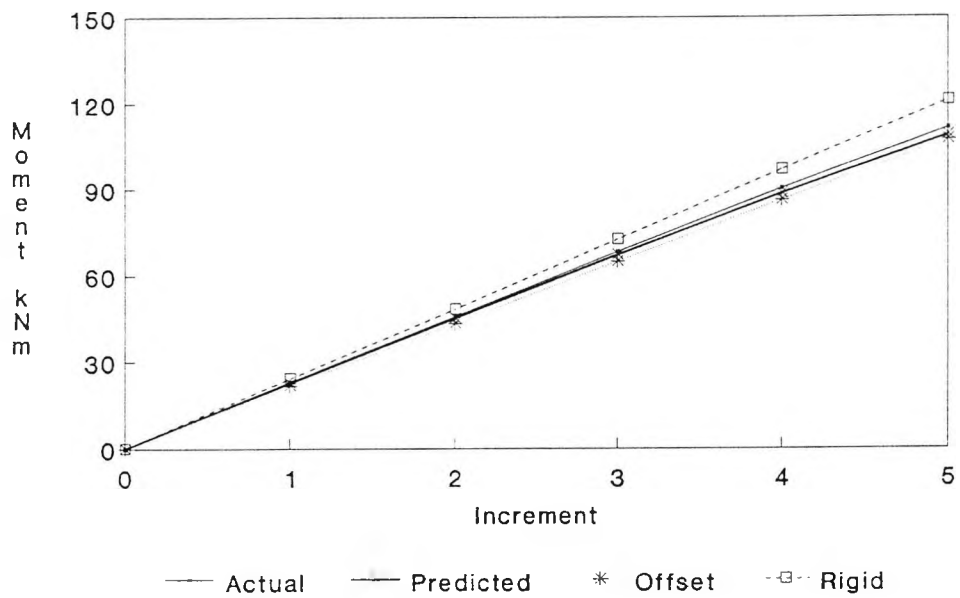
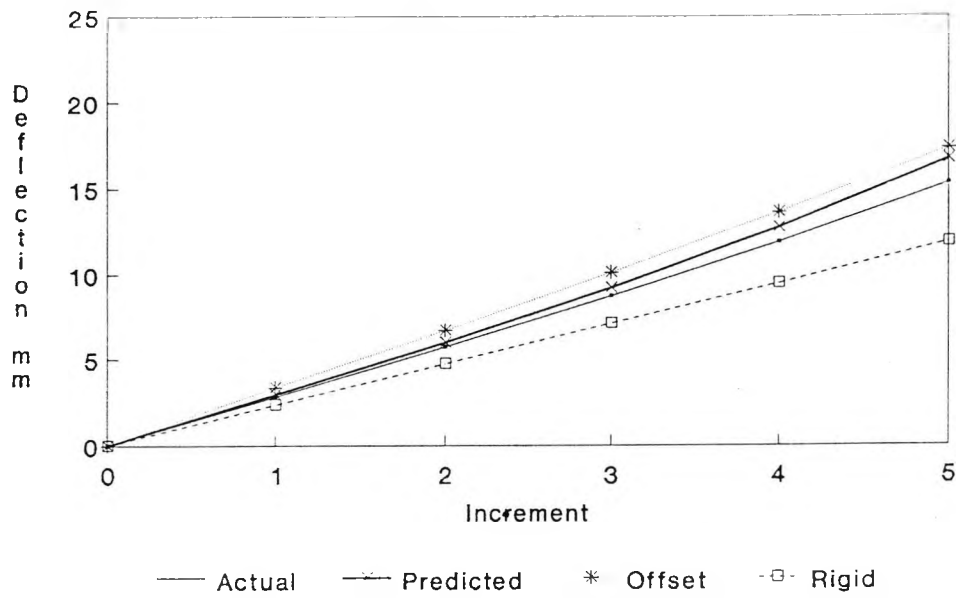


Figure 6.9 Comparison of the Effect of Actual, Predicted, Offset and Rigid Connections on Framework Behaviour - Test A7.

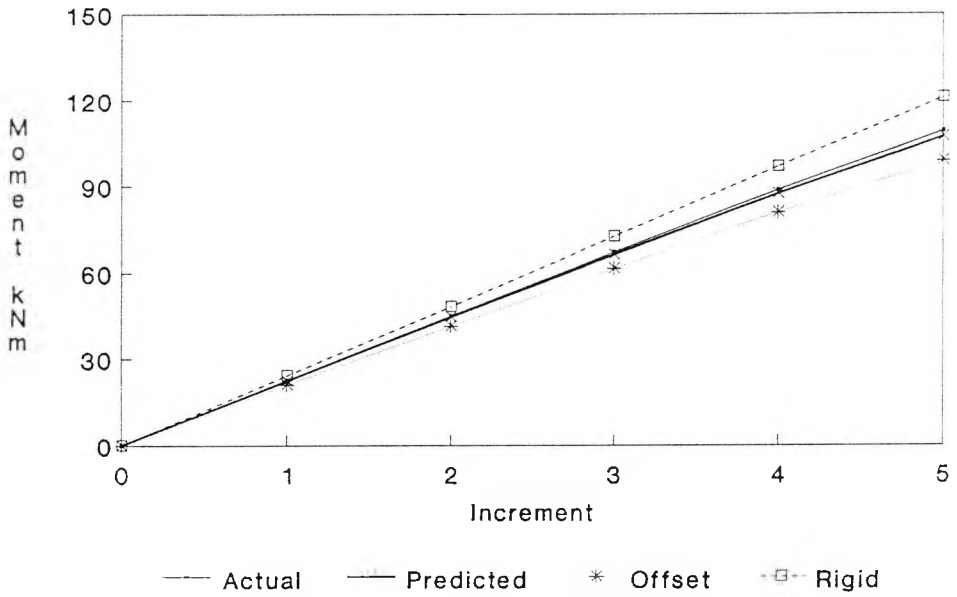
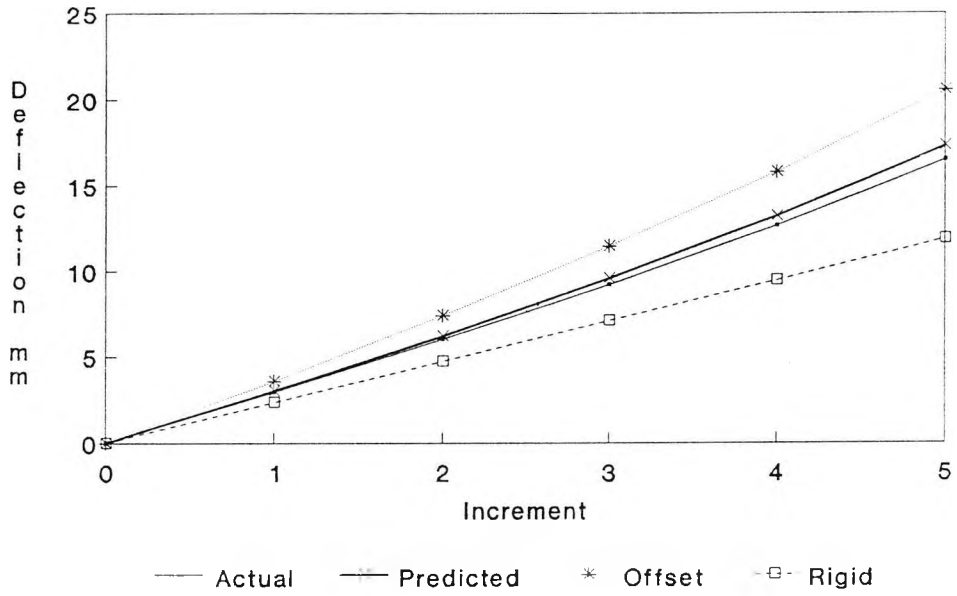


Figure 6.10 Comparison of the Effect of Actual, Predicted, Offset and Rigid Connections on Framework Behaviour - Test A8.

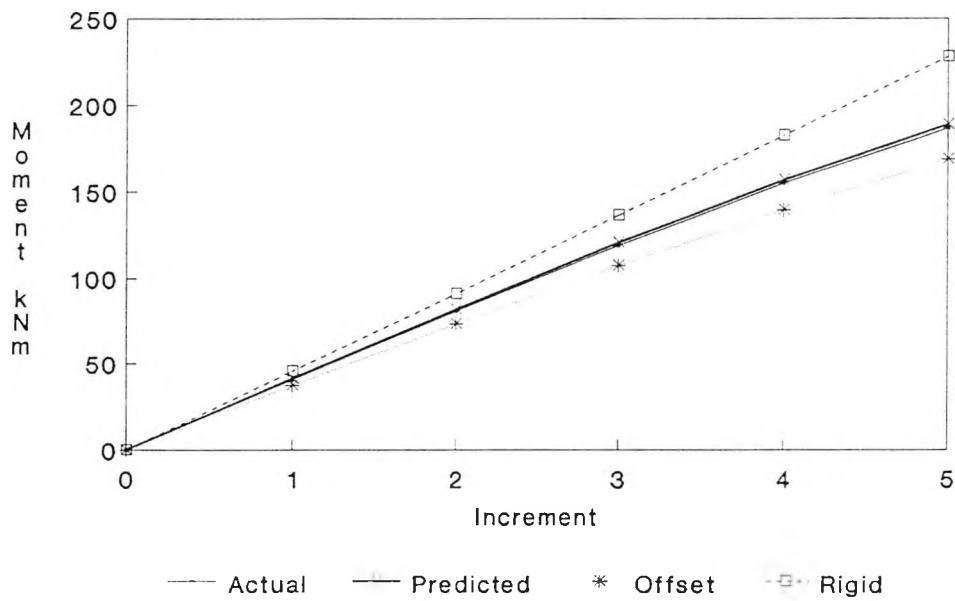
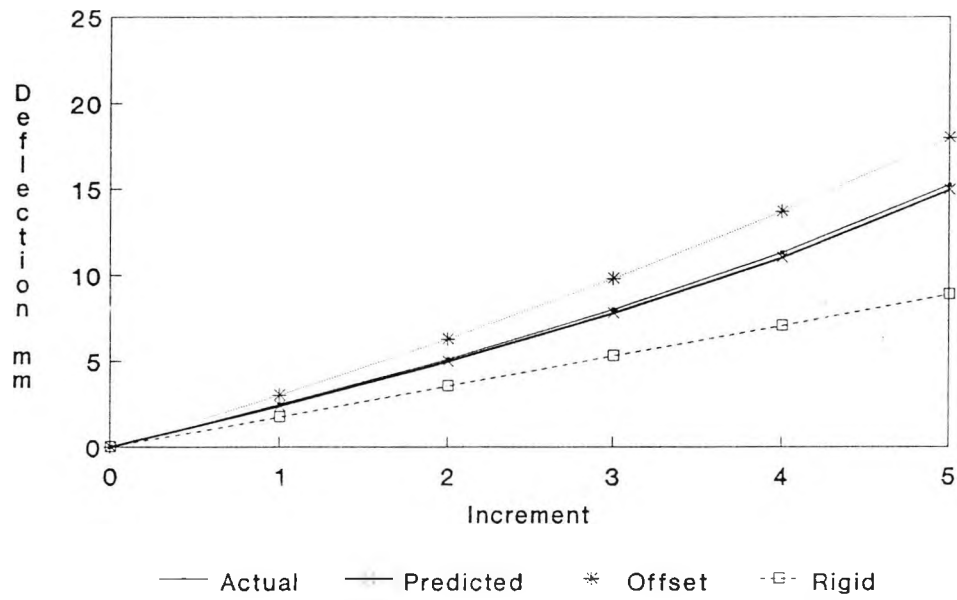


Figure 6.11 Comparison of the Effect of Actual, Predicted, Offset and Rigid Connections on Framework Behaviour - Test B1.

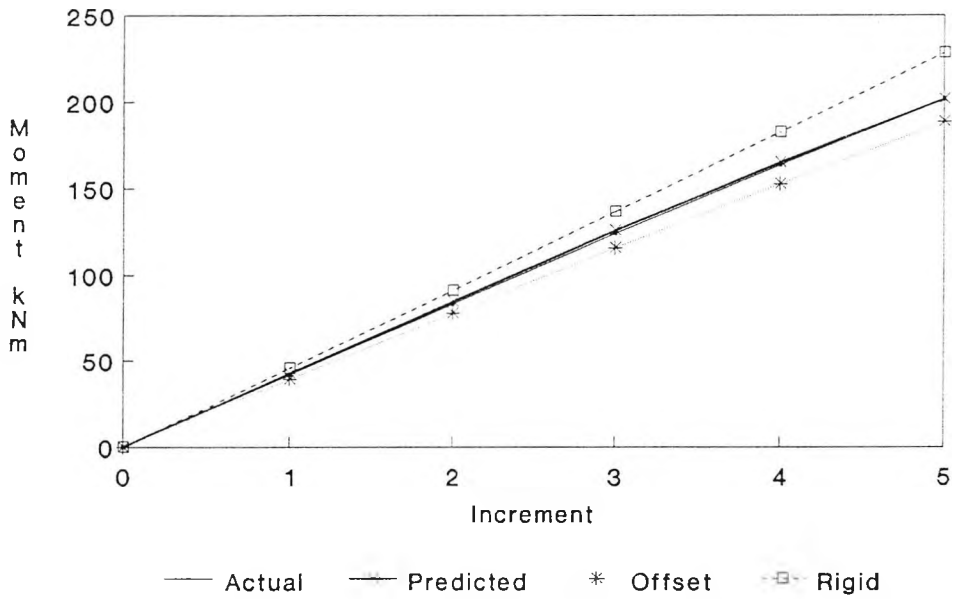
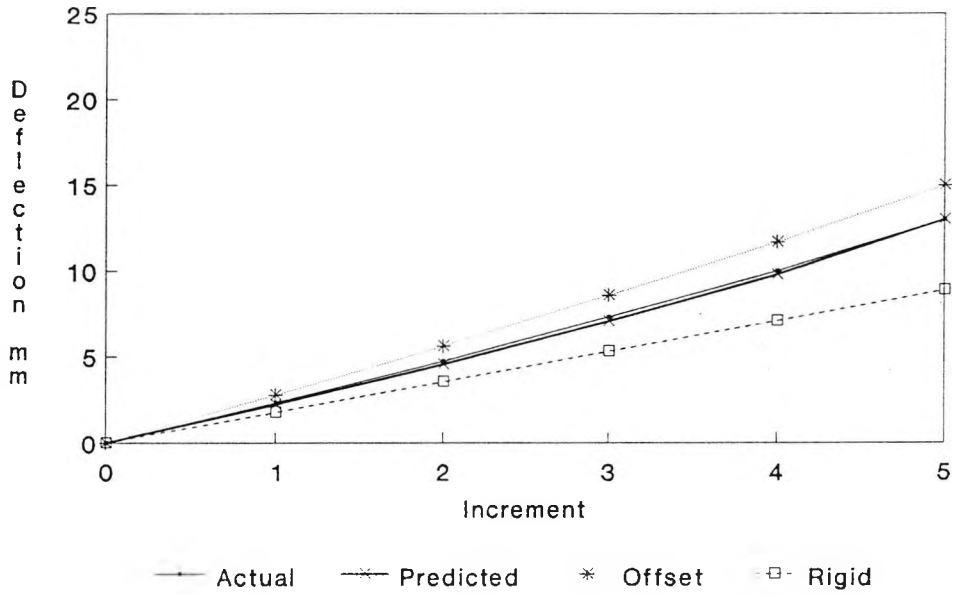


Figure 6.12 Comparison of the Effect of Actual, Predicted, Offset and Rigid Connections on Framework Behaviour - Test B2.

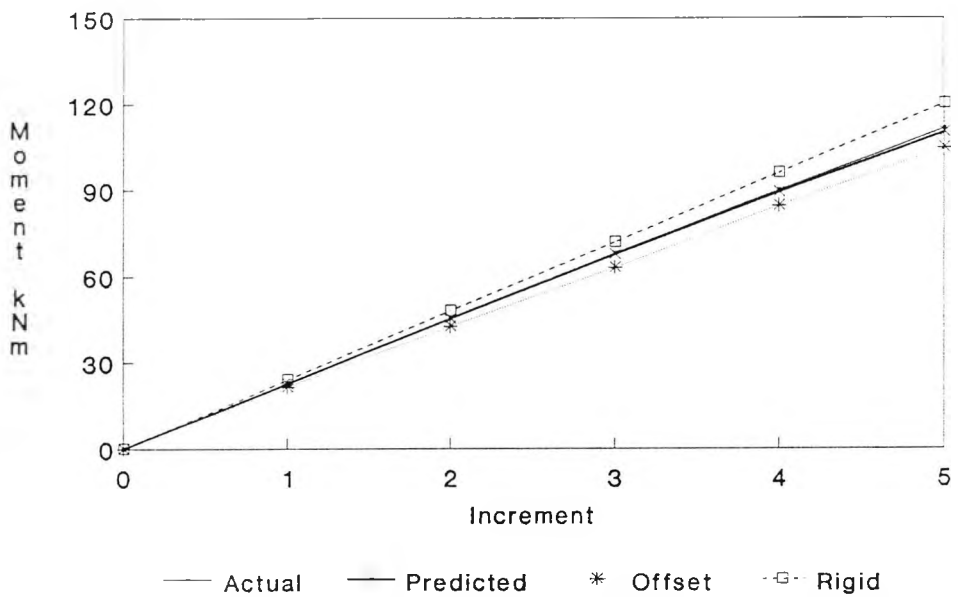
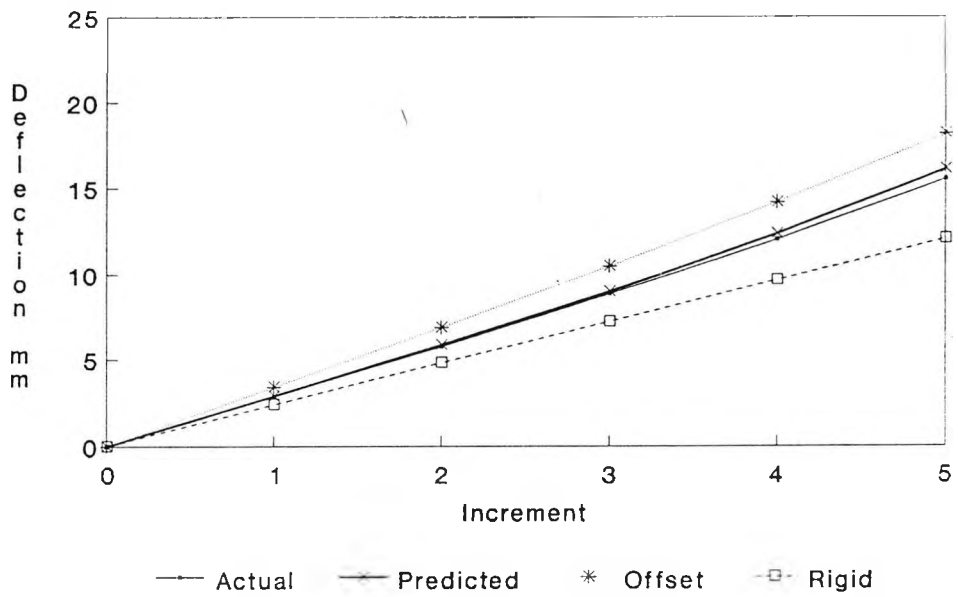
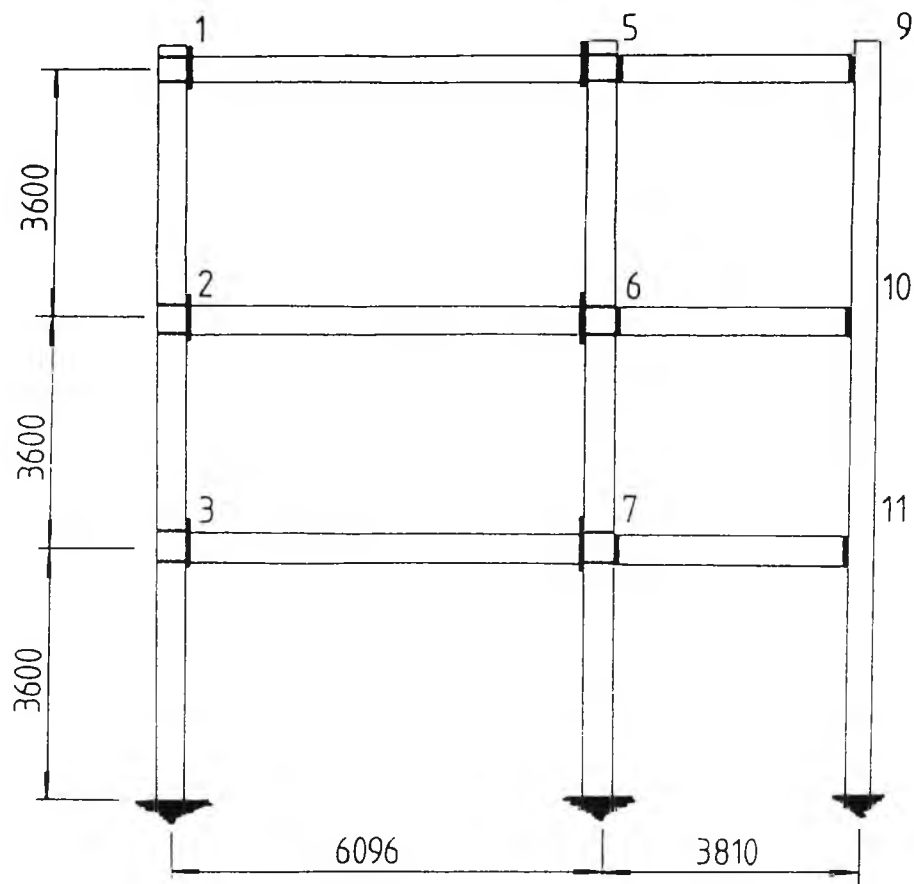


Figure 6.13 Comparison of the Effect of Actual, Predicted, Offset and Rigid Connections on Framework Behaviour - Test D1.



Columns 203 x 203 x 71 UC

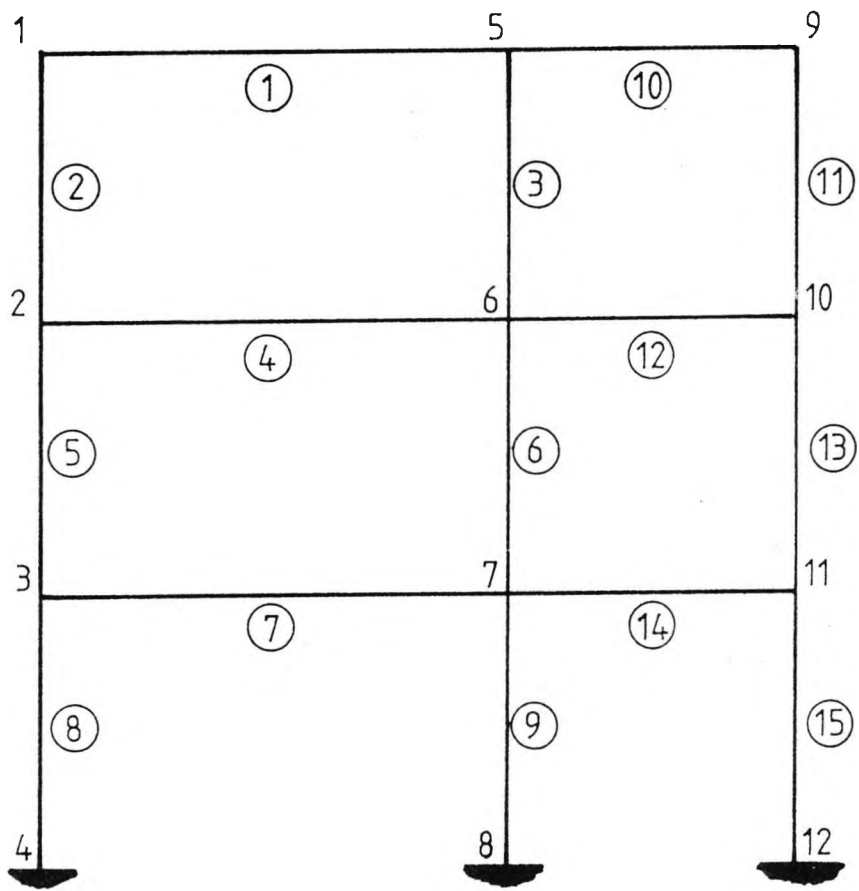
Beams 254 x 146 x 43 UB

Extended Endplate Connections :-

No's 1,5 - 20mm thick endplate

No's 2,3,6,7 - 25mm thick endplate

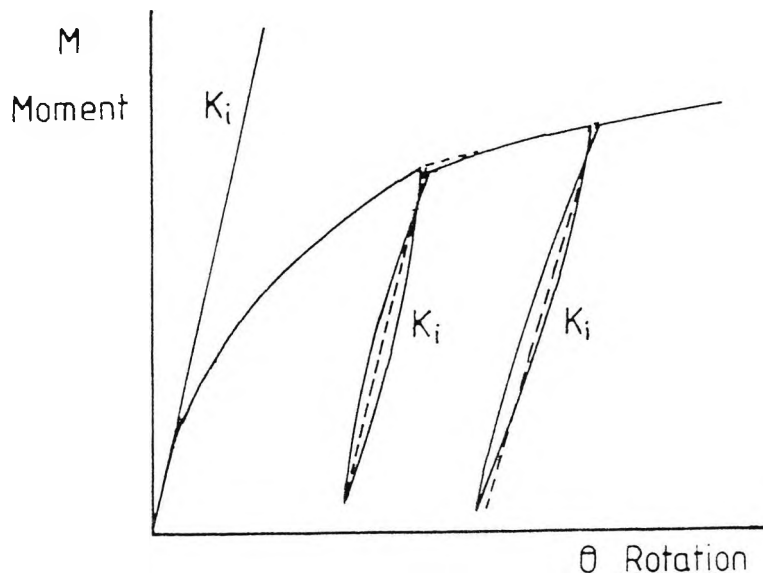
Figure 6.14 Hatfield Test Frame - Dimensions and Detailing.



1 = Node Number.

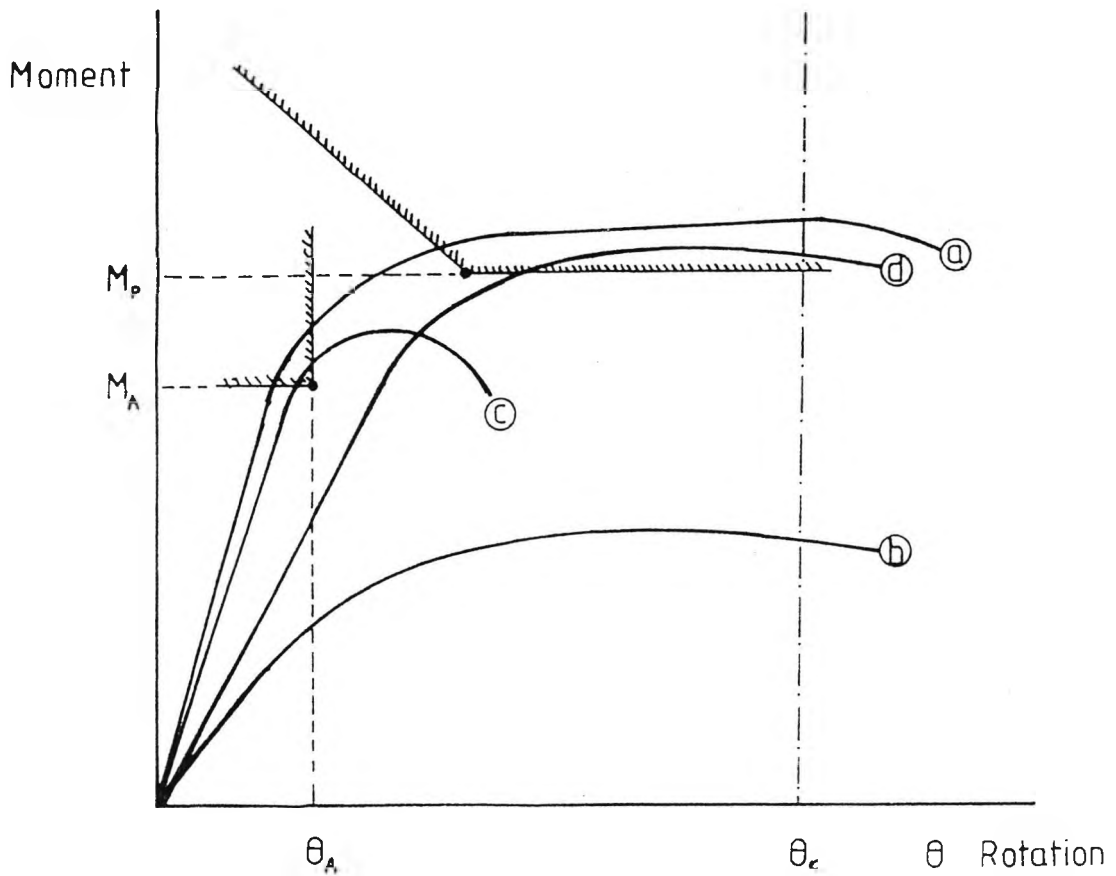
② = Element Number.

Figure 6.15 Hatfield Test Frame - Numbering System.



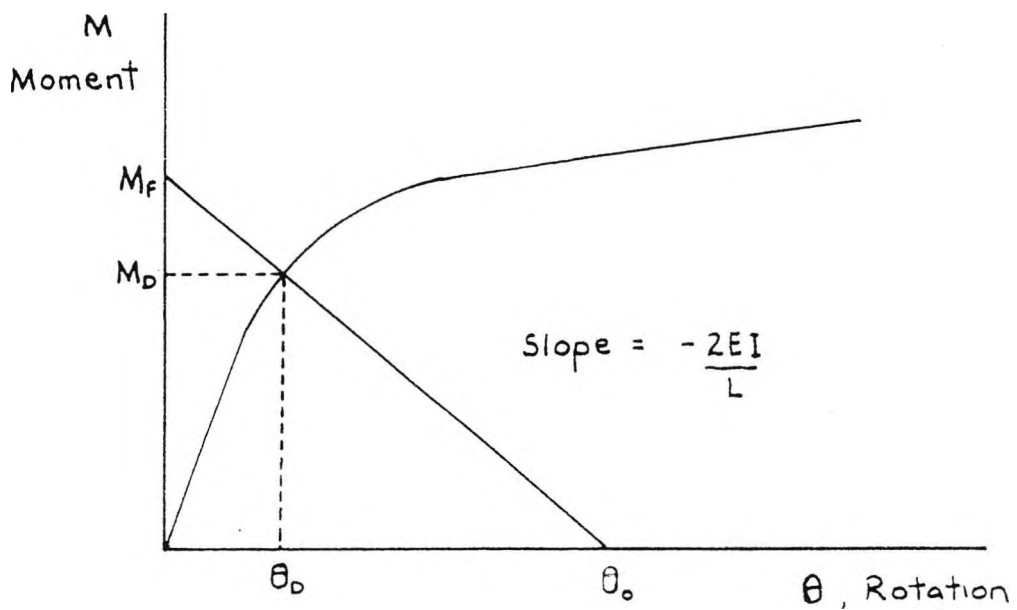
----- Assumed Behaviour
 ———— Actual Behaviour

Figure 6.16 Unloading and Reloading Behaviour of Connection.



- a = Acceptable connection
- b = Not strong enough
- c = Not flexible enough in the strain hardening range
- d = Too flexible at serviceability limit state
- θ_c = Desirable rotation for plastic hinge at beam centre

Figure 6.17 Criteria for Connections in Plastically Designed Frames (after Witteveen et al. (49)).



- M_F = Fixed end moment at beam end
- θ_0 = Pinned rotation at beam end
- M_D = Semi-rigid beam end design moment
- θ_D = Semi-rigid rotation at beam end design moment

Figure 6.18 Beam-Line Method (after Batho (19)).

CHAPTER 7

CONCLUSIONS AND RECOMMENDATIONS.

7.1 Conclusions.

The conclusions resulting from the author's research may be summarized as follows.

1. Moment-connection rotation behaviour is not always presented in previous connection tests. Great care must be taken when using the results from previous tests to ensure that the correct behaviour has been obtained.
2. Considering the possible combinations of beam and column sizes and the various types of extended endplate connection, it is highly unlikely that all structural effects will be able to be incorporated in a statistically fitted curve representation of moment-rotation behaviour. A physically based approach is, therefore, considered to be the best method of incorporating all the features required for one connection type in one model.
3. The model chosen to represent moment-rotation behaviour should be simple. It should represent the moment-rotation behaviour with as few parameters as possible. The Yee model chosen is a four parameter model and gives a good fit

to extended endplate connection data. It has been demonstrated in this thesis that this can be reduced to a three parameter model for internal extended endplate connections with little effect on overall frame behaviour.

4. A rigorous method of determining the tension component of extended endplate connections is presented. In most cases, this performs only a little better than the t-stub concept. However, the method is more rational in its treatment of unstiffened and stiffened connections and many useful results can be obtained from it. It may also be applied to many other types of connection as its derivation is perfectly general.
5. Overall, five methods of rotation measurement were used in this study. It was concluded that the best method of measurement was a transducer based method. This was because a direct measurement of connection rotation could be made and it enabled component deflections to be related to connection rotation.
6. The photogrammetry method was not precise enough to measure extended endplate connection rotation. However, it allowed an overall assessment of connection behaviour and helped in the placement of more precise measuring instruments. It would be useful for studies of more flexible connections where displacements are greater since a great deal of information can be deduced from the photographs obtained.

7. It is important to realise that connection specimen tests do not always behave in the manner they might in a framework. This was demonstrated by the initial settlement of each test due to the lack of total restraint in the direction longitudinal to the beam axis. This initial settlement has to be extracted from measurements to obtain the true moment-rotation behaviour in the initial stages of loading.
8. Connection rotation can be extracted from load-deflection relationships. However, the method is erratic and only strictly valid for the initial stages of loading, where elastic theory is applicable.
9. Deflection in the compression region is more complex than first thought due to the presence of column flange bending in addition to column web compression. For this reason an average value of deflection in the compression region is used in the deduction of connection rotation from test measurements.
10. An attempt was made to assess individual component contribution to connection rotation. This was not wholly successful, in that the expected trends did not appear. This was due to the precision of the measurements taken and the assumptions made in the analysis. These measurements were useful, though, in obtaining a qualitative guide to each component's contribution to connection rotation .

11. The parameter c , which is introduced to control the rate of decay of the curve, is needed to account for the varying rates of decay of the component contributions.
12. The Yee model can represent internal extended endplate connection behaviour very well.
13. The rigorous method of calculating initial endplate/column flange tension deflection can explain the variation in initial stiffness by changing the assumed contact positions of the endplate and column flange. The results obtained agree with the general trends observed by Zoetmeijer and Ioanniddes.
14. The four bolt tension region model performs just as well as the six bolt tension region model for the calculation of the initial stiffness of test series C. This is logical as the extra layer of bolts is introduced for extra strength at the plastic moment of the connection and, therefore, has little effect initially.
15. Considering individual components, compression web deflection is predicted very well. This indicates that the assumptions made in its derivation are closely fulfilled.
16. Tension region deflection tends to be overestimated. This is offset by neglecting column flange bending in the compression region in the prediction method.

17. Overall predicted initial stiffness is in good agreement with experimentally obtained values.
18. The rigorous method of calculating tension region deflection can be speeded up considerably by using a database of column flange factors and the assumption that stiffened flange factors can be calculated using simply supported edges at the stiffener positions.
19. Due to the many variables that can affect strain hardening stiffness, an average value for each connection size is adopted. It is recommended that a single strain hardening value based upon experimental results is adopted for other sizes of connection.
20. The plastic moment of the connections is accurately predicted using the strength criteria outlined and yield stress values from BS5950.
21. Agreement of the prediction method with existing experimental data is reasonable. This agreement is based upon limited data and estimates of connection parameters using methods presented in the appendices.

22. The criteria used to assess the accuracy of a method of prediction should be based on the difference in framework behaviour using both predicted and actual moment-rotation curves.
23. The moment-rotation behaviour of a connection is not only based on connection geometry, but also on the load state at a particular connection. The loads which could affect behaviour the most are the axial load and those causing the unbalanced moment across the connection. These effects can easily be incorporated into the physically based model.
24. The effect of including the semi-rigid behaviour of extended endplate connections on a 6m span beam is to increase deflection by up to 40% initially and 70% in the later stages of loading in comparison with a rigidly connected beam. This is accompanied by a decrease in end moment of up to 10% initially and 18% in the later stages of loading.
25. The effect of including semi-rigidity is far more significant than other second order effects such as the p-delta or bowing effects.
26. For a 6m span, the difference in frame behaviour is usually less than 5% for central deflection and 3% for end moment using predicted and actual moment-rotation curves.

27. The effect of using offset rotation curves instead of connection rotation curves is to increase the central deflection of a 6m span beam by up to 20% and decrease end moment up to 10% over actual connection rotation behaviour.
28. The difference in the assumption of a straight line model and actual connection behaviour at the elastic moment of a 6m span beam is to underestimate central deflection by up to 27% and to overestimate end moment by up to 5%.
29. A theoretical framework analysis of the Hatfield test frame using predicted moment-rotation curves shows good agreement with the experimentally obtained results. Central deflection is usually predicted within 1mm and end moments within 3kNm of experimentally obtained values.
30. Design applications of semi-rigid framework behaviour are hindered by the lack of moment-rotation data. Using a method of prediction such as the one used in this research does not give an 'exact' solution, but gives a better approximation to overall framework behaviour than the assumption of rigid connections.

7.2 Recommendations for future research.

1. For completeness sake, the derivation of connection parameters for all types of extended endplate in a plane framework have been presented. Some parts of this theory are experimentally unsubstantiated. Therefore further experimental work could be carried out on:-
 - a) Internal/eave type connections
 - b) External/internal type connections
 - c) Varying load conditions at the endplate connection i.e the effect of unbalanced moment and axial force.
 - d) Various stiffening arrangements, in particular the initial stiffness of column flanges with backing plates.
 - e) Deep beam connections.
- 2) The effect of cladding and the restraining effect of floors, etc. on the behaviour of extended endplate connections needs to be examined.
- 3) Three dimensional effects such as minor axis connections and torsion need to be assessed.
- 4) Ideally connection behaviour in real frameworks needs to be carefully examined.

5) Further work could be carried out on the extension of this method of prediction to other connection types. The procedure would be to :-

- a) Establish a valid load transfer mechanism through the connection.
- b) Relate the forces acting on the connection components to the moment at the end of the beam.
- c) Relate component deflection to connection rotation.
- d) Calculate component deflection by the use of suitable deflection theories and compatibility equations.
- e) Establish satisfactory strength criteria.
- f) Observe the value of strain hardening stiffness and adopt a suitable value.

REFERENCES

1. BS 5950 Structural Use of Steelwork in Building. Part 1- Code of Practice for Design in Simple and Continuous Construction: Hot Rolled Sections. British Standards Institute, London, 1985
2. Jones, S.W., Kirby, P.A. and Nethercot, D.A. "The Analysis of Frames with Semi-rigid Connections - A State of the Art Report." Journal of Constructional Steel Research, Volume 3, No.2, 1983, p.2
3. Lui, E.M. and Chen, W.F. "Steel Frame Analysis with Flexible Joints." Journal of Constructional Steel Research, Volume 8, 1987, p.161
4. Sherborne, A.N. "Bolted Beam-to-column Connections" The Structural Engineer, Volume 39, No.6, 1961, p.203
5. Bailey, J.R. "Strength and Rigidity of Bolted Beam-to-column Connections." Conference on Joints in Structures, Sheffield University, 1970, paper A4
6. Surtees, J.O. and Mann, A.P. "Endplate Connections in Plastically Designed Structures" Conference on Joints in Structures, Sheffield University, 1970, paper A5

7. Zoetmeijer, P. "A Design Method for the Tension Side of a Statically Loaded Bolted Beam-to-column Connection." Heron, Volume 20, No.1, 1974
8. Packer, J.A. and Morris, L.J. "A Limit State Design Method for the Tension Region of Bolted Beam-to-column Connections." The Structural Engineer, Volume 55, 1977, p.446
9. Dews, R.J. "Experimental Test Results on Exterior Endplate Moment Connections." Masters Thesis, Vanderbilt University, Nashville, Tennessee, 1978
10. Ioanniddes, S.A. "Column Flange behaviour in Bolted Endplate Moment Connections." Ph.D Thesis, Vanderbilt University, Nashville, Tennessee, 1978
11. Grundy, P., Thomas, I.R. and Bennetts, I.D. "Beam-to-column Moment Connections." Journal of Structures Division, ASCE, Volume 106, No. ST1, January 1980
12. Graham, J. "Beam-to-column Bolted Connections." Ph.D Thesis, Aston University, Birmingham, 1981
13. Yee, Y.L. "Prediction of Nonlinear Behaviour of Endplate Eave Connections." Ph.D Thesis, Monash University, Victoria, Australia, 1984

14. Davison, J.B. "Preliminary Report - Connection Performance." Sheffield University, 1985, Unpublished
15. Aggarwal, A.K. and Coates, R.C. "Moment-rotation Characteristics of Bolted Beam-to-column Connections." Journal of Constructional Steel Research, Volume 6, 1986, p.303
16. Jenkins, W.M., Tong, C.S. and Prescott, A.T. " Moment-transmitting Endplate Connections in Steel Construction and a Proposed Basis for Flush Endplate Design." The Structural Engineer, volume 64A, No.5, 1986, p.121
17. Prescott, A.T. " The Performance of Endplate Connections in Steel Structures and Their Influence on Overall Structural Behaviour" Ph.D Thesis, Hatfield Polytechnic, 1987
18. Moore, D.B. and Sims, P.A.C. "Preliminary Investigations into the Behaviour of Extended Endplate Steel Connections with Backing Plates." Journal of Constructional Steel Research, Volume 6, 1986, p.95
19. Steel Structures Research Committee, Final Report, Department of Scientific and Industrial Research, HMSO, London, 1936
20. Rathbun, J.C. "Elastic Properties of Riveted Connections" Transactions of ASCE, 1936, Volume 101, p.524

21. Johnston, B.G. and Mount, E.H. "Analysis of Building Frames with Semi-rigid Connections" Transactions of ASCE, 1942, Volume 107, p.993
22. Lionberger, S.R. and Weaver, W. "Dynamic Response of Frames with Non-rigid Connections" Journal of Engineering Mechanics Division, ASCE, February 1969, Volume 95, EM1, p.95
23. Romstad, K.M. and Subramian, C.V. "Analysis of Frames with Partial Connection Rigidity" Journal of Structural Division, ASCE, November 1970, Volume 96, ST 11, p.2283
24. Moncarz, P. and Gertsle, K.H., "Steel Frames with Nonlinear Connections" Journal of Structural Division, ASCE, 1981, Volume 107, p.1427
25. Melchers, R.E. and Kaur, D., "Behaviour of Frames with Flexible Joints" Proceedings of the Eighth Australian Conference on Mechanics of Structural Materials, Newcastle, Australia, p.27.1
26. Lothers, J.E. "Elastic Restraint Equations for Semi-rigid Connections" Transactions of ASCE, 1951, Volume 116, p.480

27. Huang, J.S., Chen, W.F., and Beedle, L.S. "Behaviour and Design of Steel Beam-to-Column Moment Connections" Welding Research Council Bulletin, No.188, October 1973, p.1
28. Sommer, W.H. "Behaviour of Welded Header Plate Connections" Masters Thesis, University of Toronto, Ontario, Canada, 1969
29. Frye, M.J., and Morris, G.A., "Analysis of Flexibly Connected Steel Frames" Canadian Journal of Civil Engineers, September 1975, Volume 2, No.3, p.280
30. Ang, K.M., and Morris, G.A., "Analysis of Three Dimensional Frames with Flexible Beam-Column Connections" Canadian Journal of Civil Engineers, 1984, Volume 11, p.245
31. Batho, C. and Lash, S.D. "Further Investigations on Beam and Stanchion Connections Encased in Concrete" Final Report, Steel Structures Research Committee, Department of Scientific and Industrial Research, HMSO, London, 1936, p.276
32. Krishnamurthy, N., Huang, H.T., Jeffrey, P.K. and Avery, L.K. "Analytical Moment-Rotation Curves for Endplate Connections" Journal of Structural Division, ASCE, Volume 105, 1979, p.133

33. Colson, A. and Louveau, J.M. "Connections Influence on the Inelastic Behaviour of Steel Structures" Euromech Colloquium 174, October 1983
35. Lipson, S.L. and Hague, M.I. "Elastic-Plastic Analysis of Single Angle Bolted-Welded Connections using the Finite Element Method" Computers and Structures, December 1978, Volume 9, No.6, p.533
36. Patel, K.V. and Chen, W.F. "Nonlinear Analysis of Steel Moment Connections" Journal of Structural Engineering, ASCE, Volume 110, No.8, August 1984, p.1861
37. Lowe, P.G. "Classical Theory of Structures" First Edition, Cambridge University Press, 1971
38. Jarimillo, T.J. "Deflection and Moments due to a Concentrated Load on a Cantilever Plate of Infinite Length" Journal of Applied Mechanics, ASME, Volume 17, 1950, p.67
39. Timoshenko, S.P. and Woinowsky-Krieger, S. "Theory of Plates and Shells" Second Edition, McGraw-Hill, 1959
40. Agerskov, H. "High Strength Bolted Connections subject to Prying" Journal of Structural Division, ASCE, January 1976, Volume 102, p.161

41. Roark, R.J. and Young, W.C. "Formulas for Stress and Strain" McGraw-Hill International Book Company, Fifth Edition, 1975
42. Chen, W.F. and Newlin, D.E. " Column Web Strength in Steel Beam-to-Column Connections" Journal of Structural Division, ASCE, Volume 99, September 1973, p.1978
43. Horne, M.R. and Morris, L.J. "Plastic Design of Low Rise Frames" Granada Publishing Ltd., 1981
44. Goto, Y. and Chen, W.F. "On Computer Based Design Analysis of Flexibly Jointed Frames" Journal of Constructional Steel Research, Volume 8, 1987, p.203
45. Bose, S.K., McNeice, G.M. and Sherborne, A.N. "Column Webs in Steel Beam-to-Column Connections - Part 2:Design Recommendations" Computers and Structures, Volume 2, 1972, p.281
46. Philips, J and Packer, J.A. "The effect of Plate Thickness on Flush Endplate Connections " Section 2.10A, Joints in Structural Steelwork, Proceedings of International Conference at Teeside Polytechnic, April 1981, Edited Howlett, J.H., Jenkins, W.M. and Stainsby, R., Pentech Press

47. Gertsle, K.H. "Flexibly Connected Steel Frames" Stability of Framed Structures, Edited R. Naranayan
48. Bjorhovde, R., Brozzetti, J. and Colson, A. "Announcement - Connections and Steel Structures" Journal of Constructional Steel Research, Volume 7, 1987, p.391
49. Witteveen, J., Stark, J.W.B., Bjilaard, F.S.K. and Zoetmeijer, P. "Welded and Bolted Beam-to-Column Connections" Journal of Structural Division, ASCE, Volume 108, February 1982, p.433
50. Cooper, M.A.R. "Fundamentals of Survey Measurement and Analysis" Granada Publishing , 1980

APPENDIX A

DEFLECTION OF AN INFINITELY LONG CANTILEVER PLATE UNDER CONCENTRATED LOAD. (AFTER JARAMILLO)

Figure A1 defines the problem to be solved and some of the terms used in its solution. The coordinate system is coincident with the middle plane of the plate and the point of application of the load. The plate is divided into two strip-shaped regions separated by the line $x = c$ to simplify the solution of the problem. Functions related to these regions will be denoted by the subscripts 1 for the region bounded by $x = 0$ to $x = c$ and subscript 2 for the region bounded by $x = c$ to $x = a$, where a is the width of the cantilever plate.

Neglecting the weight of the plate the transverse deflections, $w_j(x, y)$ ($j=1,2$), according to classical small deflection theory, are characterized by the homogeneous biharmonic equation.

$$\nabla^4 w_j(x, y) = 0 \quad (j=1,2)$$

(A1)

which is valid throughout the regions under consideration except for the singular load point, A.

The equations relating deflections to shearing forces, bending moments and twisting moments are

$$\begin{aligned}
 Q_{jx} &= -D(w_{j,xxx} + w_{j,xyy}) \\
 M_{jx} &= -D(w_{j,xx} + \nu w_{j,yy}) \\
 M_{jxy} &= -M_{jyx} = D(1 - \nu)w_{j,xy}
 \end{aligned}
 \tag{A2}$$

where ν = Poissons ratio and D = the flexural rigidity of the plate.

Subscripts x and y attached to functions indicate partial derivatives e.g. $w_{j,xyy} = \frac{\partial^3 w_j}{\partial x \partial y^2}$

Considering equations (A2), the boundary conditions written in terms of deflections, w are as follows :-

Along the fixed edge $x = 0$

$$w_1(0, y) = w_{1,x}(0, y) = 0
 \tag{A3}$$

and along the free edge $x = a$, $M_{2x} = Q_{2x} = M_{2y} = 0$, therefore

$$(w_{2,xx} - \nu w_{2,yy})_{(a,y)} = 0
 \tag{A4}$$

$$(w_{2,xxx} + (2 - \nu) w_{2,xyy})_{(a,y)} = 0 \quad (A5)$$

In addition to the above four boundary equations the solution must take into account the transition conditions at $x = c$. From continuity requirements for deflections, slopes and bending moments we have

$$w_1(c, y) = w_2(c, y) \quad (A6)$$

$$w_{1,x}(c, y) = w_{2,x}(c, y) \quad (A7)$$

$$(w_{1,xx} + \nu w_{1,yy})_{(c,y)} = (w_{2,xx} + \nu w_{2,yy})_{(c,y)} \quad (A8)$$

The shearing force, Q_x , however has a discontinuity at the point of application of the load, A. This is dealt with by replacing the load, P with a force function $F(y)$ which is equal to p for $|y| \leq \delta$ and zero elsewhere i.e. $P = 2p\delta$. As δ tends to zero the function $F(y)$ can be represented by a fourier integral.

Therefore the boundary condition becomes

$$-D(w_{1,xxx} + w_{1,yyx})_{(c,y)} + D(w_{2,xxx} + w_{2,yyx})_{(c,y)} = \int_0^\infty \frac{2p \sin \alpha \delta}{\pi \alpha} \cos \alpha y \, d\alpha \quad (A9)$$

An arbitrary function that will satisfy equation (A1) and the boundary and transition conditions (A2 - A9) is given by

$$w_j(x, y) = \int_0^{\infty} f_j(x, \alpha) \cos \alpha y \, d\alpha \quad (j=1, 2)$$

(A10)

where $f_j(x, \alpha) = (A_j + B_j \alpha x) \cosh \alpha x + (C_j + D_j \alpha x) \sinh \alpha x$ (A11)

and provided the improper integral (A10) and its required partial derivative exists.

Since equations (A2 - A9) are to be satisfied, we have from these and equations (A10) and (A11).

$$\begin{aligned} f_1(0, \alpha) &= f_{1,x}(0, \alpha) = 0 \\ f_{2,xx}(a, \alpha) - \alpha^2 \nu f_2(a, \alpha) &= 0 \\ f_{2,xxx}(a, \alpha) - \alpha^2 (2 - \nu) f_{2,x}(a, \alpha) &= 0 \\ f_1(c, \alpha) - f_2(c, \alpha) &= 0 \\ f_{1,x}(c, \alpha) - f_{2,x}(c, \alpha) &= 0 \\ f_{1,xx}(c, \alpha) - f_{2,xx}(c, \alpha) &= 0 \\ f_{2,xxx}(c, \alpha) - f_{1,xxx}(c, \alpha) &= \frac{P}{\pi D} \end{aligned}$$

(A12)

Substitution of equations (A10) and (A11) into equations (A12) leads to eight simultaneous equations in eight unknowns, A_j , B_j , C_j and D_j ($j = 1, 2$). Solving gives the complete integral representation of the deflections $w_j(x, y)$.

The solution in terms of dimensionless coordinates is given by

$$w_j(\xi, \eta, \zeta) = \frac{Pa^2}{8\pi D} \int_0^\infty \frac{\phi_j(\xi, \zeta, \mu)}{\mu^3 \Delta(\mu)} \cos \mu \eta \, d\mu \quad (\text{A13})$$

$$\text{where } \Delta(\mu) = \mu^2 + \gamma^2 + (2\gamma + 1) \cosh^2 \mu$$

$$\gamma = \frac{1 + \nu}{1 - \nu} \quad (\text{A14})$$

$$\text{and } \xi = \frac{x}{a}; \quad \eta = \frac{y}{a}; \quad \zeta = \frac{c}{a}; \quad \mu = \alpha a.$$

also for $j = 1$ ($0 \leq \xi \leq \zeta$)

$$\begin{aligned} \phi_1(\xi, \zeta, \mu) = & (1 + 2\gamma) [S_1 + \mu(\zeta - \xi)C_1 - (1 + 2\mu^2\xi\zeta)S_2 - \mu(\xi + \zeta)C_2] \\ & + [1 + 2\gamma + 2\gamma^2 + 2\mu^2(1 - \xi)(1 - \zeta)]S_4 + \mu(2 - \xi - \zeta)C_4 \\ & - [1 + 2\gamma + 2\gamma^2 + 2\mu^2(1 - \zeta + \xi)]S_5 \\ & - [2 - \zeta + (1 + 2\gamma)^2\xi + 4\mu^2\xi(1 - \zeta)]\mu C_5 \end{aligned} \quad (\text{A15})$$

where

$$\begin{aligned}
 S_1 &= \sinh(2 - \zeta + \xi) \mu; C_1 = \cosh(2 - \zeta + \xi) \mu \\
 S_2 &= \sinh(2 - \zeta - \xi) \mu; C_2 = \cosh(2 - \zeta - \xi) \mu \\
 S_3 &= \sinh(2 + \zeta - \xi) \mu; C_3 = \cosh(2 + \zeta - \xi) \mu \\
 S_4 &= \sinh(\zeta + \xi) \mu \quad ; C_4 = \cosh(\zeta + \xi) \mu \\
 S_5 &= \sinh(\zeta - \xi) \mu \quad ; C_5 = \cosh(\zeta + \xi) \mu
 \end{aligned}$$

(A16)

For $j = 2$ ($\zeta \leq \xi \leq 1$)

$$\phi_2(\xi, \zeta, \mu) \equiv \phi_1(\zeta, \xi, \mu)$$

(A17)

This follows from the Maxwell reciprocal theorem applied to the deflections $w_j(x, y)$.

The improper integral, equation (A13), now has to be solved to give the full solution for the deflections, w . As numerical integration is cumbersome, the integral is evaluated using contour integration. This leads to an expansion of the integral as a series in terms of the residues at the singularities. The singularities of the integral are simple poles and occur when equation (A14) is equal to zero. As $\gamma > 0$ (see equation (A14)), $\Delta(\mu)$ has no real roots therefore the roots of the equation must be complex.

The roots of equation (A14) can be given in the form

$$\begin{aligned}\mu_n &= \pm\alpha_n + i\beta_n \quad (n = 0, 1, 2, \dots, \infty) \\ \alpha_0 &= 0, \alpha_n > 0 \\ \beta_n &> 0\end{aligned}$$

Expanding equation (A14) in terms of the complex function, μ , gives two transcendental equations in α_n and β_n corresponding to the real and imaginary parts of the equation. Solving this by Newton's method gives monotonically increasing values for α_n and β_n for $n \geq 1$ which tend to infinity with n .

Therefore by the residue theorem

$$\int_0^\infty \frac{\phi_j(\xi, \zeta, \mu)}{\mu^3 \Delta(\mu)} \cos \mu \eta \, d\mu = \pi i \sum_{n=0}^{\infty} R_n$$

(A18)

where R_n is the residue at the simple pole μ_n of $\frac{\phi_j(\xi, \zeta, \mu)}{\mu^3 \Delta(\mu)} e^{i\eta\mu}$

By evaluating the residues the function for w is given by

$$w_j(\xi, \eta, \zeta) = -\frac{Pa^2}{\pi D} K_j(\xi, \eta, \zeta) \quad (j = 1, 2)$$

(A19)

where

$$K_1 = \frac{\pi}{8} \left(R_0 + 2 \sum_{n=1}^{\infty} [p_n(\xi, \zeta) \sin \alpha_n \eta + q_n(\xi, \zeta) \cos \alpha_n \eta] e^{-\beta_n} \right)$$

(A20)

where $R_0 = q_0(\xi, \zeta) e^{-\beta_0 \eta}$ as $\alpha_0 \rightarrow 0$

(A21)

and

$$p_n(\xi, \zeta) = f_n r_n(\xi, \zeta) + g_n t_n(\xi, \zeta)$$

$$q_n(\xi, \zeta) = f_n r_n(\xi, \zeta) - g_n t_n(\xi, \zeta)$$

(A22)

$$f_n = \frac{E_n}{E_n^2 + F_n^2} ; g_n = \frac{F_n}{E_n^2 + F_n^2}$$

$$E_n = 2\alpha_n + (2\gamma + 1) \sinh 2\alpha_n \cos 2\beta_n$$

$$F_n = 2\beta_n + (2\gamma + 1) \cosh 2\alpha_n \sin 2\beta_n$$

(A23)

The functions r_n and t_n in equations (A22) relate to the real and imaginary parts of the function $\frac{\phi_j(\xi, \zeta, \mu)}{\mu^3}$ and will be defined

with the aid of the auxiliary functions

$$\delta_n = \frac{\alpha_n}{\alpha_n^2 + \beta_n^2} ; \epsilon_n = \frac{\beta_n}{\alpha_n^2 + \beta_n^2}$$

$$\lambda_n = \frac{\alpha_n^2 - 3\beta_n^2}{(\alpha_n^2 + \beta_n^2)^2} ; \rho_n = \frac{3\alpha_n^2 - \beta_n^2}{(\alpha_n^2 + \beta_n^2)^2}$$

(A24)

and in terms of functions S_i, C_i, s_i, c_i ($i = 1, 2, 3, 4, 5$).

Here S_i, C_i are given by equations (A16) with μ replaced by α_n ; s_i, c_i are given by the corresponding trigonometric functions with μ replaced by β_n .

Therefore

$$\begin{aligned}
& (1 + 2\gamma) [\lambda_n \delta_n S_1 C_1 + e_n \rho_n C_1 S_1 \\
& + (\zeta - \xi) \frac{\lambda_n + \rho_n}{4} C_1 C_1 + 2(\zeta - \xi) \delta_n e_n S_1 S_1 \\
& - (\lambda_n \delta_n + 2\xi\zeta\delta_n) S_2 C_2 - (\rho_n e_n + 2\xi\zeta e_n) C_2 S_2 \\
& - (\xi + \zeta) \frac{\lambda_n + \rho_n}{4} C_2 C_2 - 2(\xi + \zeta) \delta_n e_n S_2 S_2] \\
& + [(1 + 2\gamma + 2\gamma^2) \lambda_n \delta_n + 2(1 - \xi)(1 - \zeta) \delta_n] S_4 C_4 \\
& + [(1 + 2\gamma + 2\gamma^2) \rho_n e_n + 2(1 - \xi)(1 - \zeta) e_n] C_4 S_4 \\
x_n(\xi, \zeta) = & + (2 - \xi - \zeta) \frac{\lambda_n + \rho_n}{4} C_4 C_4 + 2(2 - \xi - \zeta) \delta_n e_n S_4 S_4 \\
& - [(1 + 2\gamma + 2\gamma^2) \delta_n \lambda_n + 2(1 - \zeta + \xi) \delta_n] S_5 C_5 \\
& - [(1 + 2\gamma + 2\gamma^2) \rho_n e_n + 2(1 - \zeta + \xi) e_n] C_5 S_5 \\
& - [2 - \zeta + (1 + 2\gamma)^2 \xi + 4\xi(1 - \zeta)(\alpha_n^2 - \beta_n^2)] \frac{\lambda_n + \rho_n}{4} C_5 C_5 \\
& - [2 - \zeta + (1 + 2\gamma)^2 \xi + 4\xi(1 - \zeta)(\alpha_n^2 - \beta_n^2)] 2\delta_n e_n S_5 S_5 \\
& + 8\alpha_n \beta_n \xi (1 - \zeta) \left[\frac{\lambda_n + \rho_n}{4} S_5 S_5 - 2\delta_n e_n C_5 C_5 \right]
\end{aligned}$$

and

$$\begin{aligned}
& (1 + 2\gamma) [\lambda_n \delta_n C_1 S_1 - e_n \rho_n S_1 C_1 \\
& + (\zeta - \xi) \frac{\lambda_n + \rho_n}{4} S_1 S_1 - 2(\zeta - \xi) \delta_n e_n C_1 C_1 \\
& - (\lambda_n \delta_n + 2\xi\zeta\delta_n) C_2 S_2 + (\rho_n e_n + 2\xi\zeta e_n) S_2 C_2 \\
& - (\xi + \zeta) \frac{\lambda_n + \rho_n}{4} S_2 S_2 - 2(\xi + \zeta) \delta_n e_n C_2 C_2] \\
& + [(1 + 2\gamma + 2\gamma^2) \lambda_n \delta_n + 2(1 - \xi)(1 - \zeta) \delta_n] C_4 S_4 \\
& - [(1 + 2\gamma + 2\gamma^2) \rho_n e_n + 2(1 - \xi)(1 - \zeta) e_n] S_4 C_4 \\
t_n(\xi, \zeta) = & + (2 - \xi - \zeta) \frac{\lambda_n + \rho_n}{4} S_4 S_4 - 2(2 - \xi - \zeta) \delta_n e_n C_4 C_4 \\
& - [(1 + 2\gamma + 2\gamma^2) \delta_n \lambda_n + 2(1 - \zeta + \xi) \delta_n] C_5 S_5 \\
& + [(1 + 2\gamma + 2\gamma^2) \rho_n e_n + 2(1 - \zeta + \xi) e_n] S_5 C_5 \\
& + [2 - \zeta + (1 + 2\gamma)^2 \xi + 4\xi(1 - \zeta)(\alpha_n^2 - \beta_n^2)] \frac{\lambda_n + \rho_n}{4} S_5 S_5 \\
& + [2 - \zeta + (1 + 2\gamma)^2 \xi + 4\xi(1 - \zeta)(\alpha_n^2 - \beta_n^2)] 2\delta_n e_n C_5 C_5 \\
& - 8\alpha_n \beta_n \xi (1 - \zeta) \left[\frac{\lambda_n + \rho_n}{4} C_5 C_5 - 2\delta_n e_n S_5 S_5 \right]
\end{aligned}$$

(A25)

Equations (A19) to (A25) represent a complete solution for the deflections $w(\xi, \eta, \zeta)$. The series rapidly converges for deflections with only the first seven or eight roots needed for a solution everywhere. Convergence was slower around the point of loading but this was expected due to the discontinuity introduced by the concentrated load. This solution was chosen as the deflections could be determined under the point of loading. In other solutions, namely fourier series, the deflection under the point of load cannot be evaluated as the solution tends to infinity at this point (see reference 39-Timoshenko and Woinowsky-Krieger).

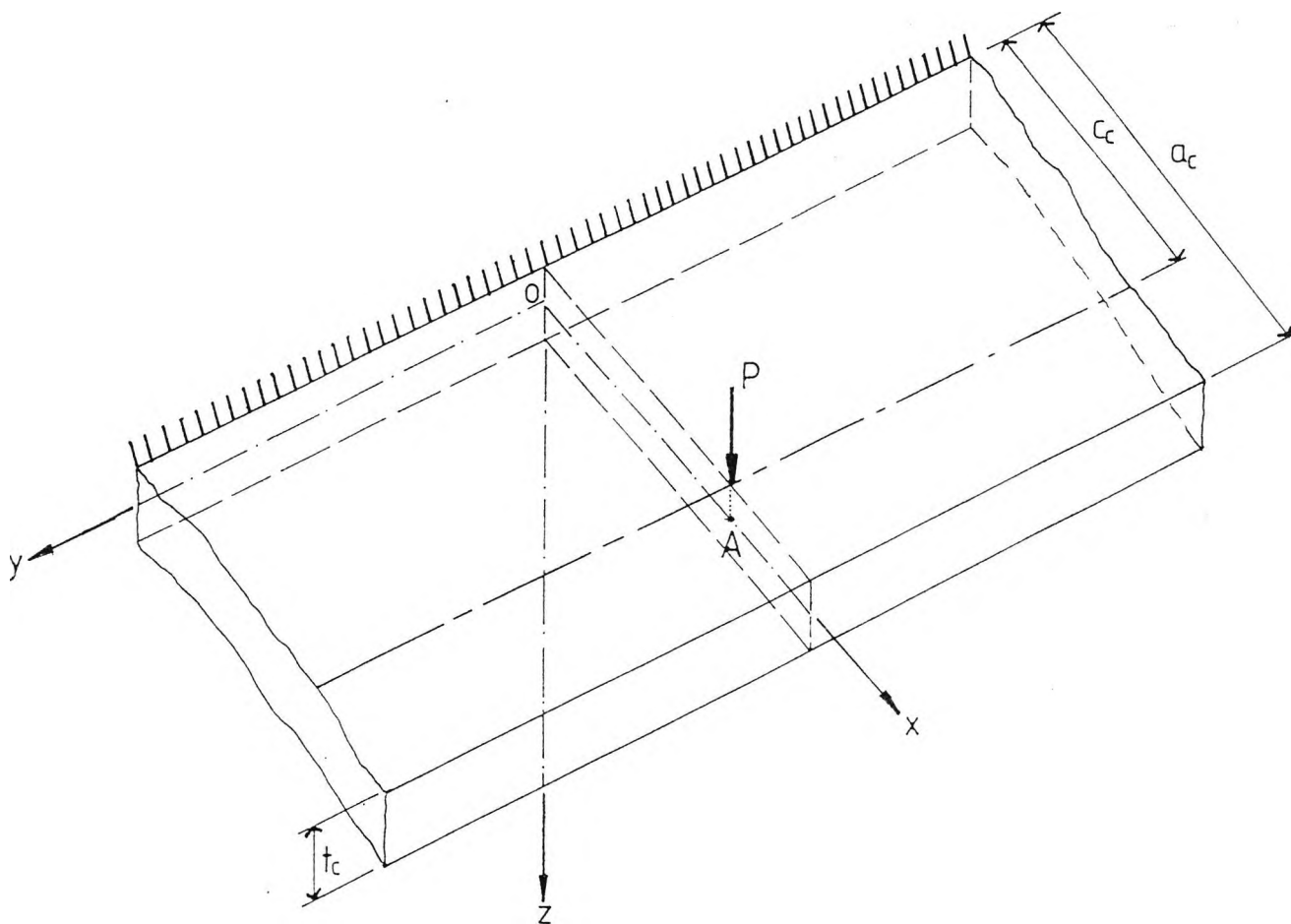


Figure A1 Cantilever Plate - Loading and coordinate system (after Jaramillo)

APPENDIX B

DERIVATION OF BOLT STIFFNESS (AFTER AGERSKOV(40))

The stiffness of any bolt is required in two cases. Firstly for bolts that are hand tight and secondly for bolts that are pretensioned. The stiffness of both these cases can be derived by considering bolt behaviour throughout the loading range of the connection.

If a bolt is pretensioned an equal and opposite force is set up in the endplate and column flange which is due to the compression of the endplate and column flange around the bolt head and nut respectively. When the endplate is loaded, this compression is gradually released until no compressive force is present. This point marks the separation of the endplate and column flange at the boltline. If it is assumed that the relationship between this compressive force, C , the actual bolt force, \bar{B} , and the applied force, F , is linear then the net bolt force, B , at any stage of loading is given by

$$B = \bar{B} - C$$

(B1)

The assumed relationships of all the forces with applied load are shown in Figure B1(a). The model of the bolt used to calculate bolt deformation is given in Figure B1(b).

From Agerskov's paper (40), bolt elongation, Δl_b is given by

$$\Delta l_b = \Delta \bar{B} \left(\frac{l_s}{EA_s} + \frac{l_t}{EA_t} + \frac{1}{2} \frac{l_n}{EA_t} \right)$$

(B2)

Deformation of the nut and washer respectively are given by

$$\Delta l_n = \frac{\Delta \bar{B} l_n}{2EA_n}$$

(B3)

and

$$\Delta l_w = \frac{\Delta \bar{B} l_w}{EA_w}$$

(B4)

The deformation of the plates due to the compressive force, C , is given by

$$\Delta l_p = \frac{\Delta C (t_{ep} + t_{cf})}{EA_p}$$

(B5)

At the instant of separation

$$\Delta l_b = \Delta l_p - \Delta l_n - \Delta l_w$$

(B6)

From experimental observation, the areas of each bolt part can be related to the bolt shank area by

$$A_p = 5.0A_s ; A_n = 2.5A_s ; A_w = 2.5A_s ; A_t = 0.7A_s$$

(B7)

Substituting equations (B7) into equations (B2), (B3), (B4) and (B5) and then substituting (B2), (B3), (B4) and (B5) into (B6) gives

$$\frac{\Delta \bar{B}}{EA_s} (l_s + 1.43l_t + 0.91l_n + 0.4l_w) = \frac{\Delta C}{5EA_s} (t_{ep} + t_{cf})$$

(B8)

Let L_{ebi} = effective bolt length
 $= l_s + 1.43l_t + 0.91l_n + 0.4l_w$

(B9)

From Figure B1(a), by similar triangles

$$C = \frac{\bar{B}_0 (\bar{B}'_0 - \bar{B})}{(\bar{B}'_0 - \bar{B}_0)}$$

(B10)

where \bar{B}_0 = initial pretension

and \bar{B}'_0 = bolt force at separation

At separation

$$\Delta \bar{B} = \bar{B}'_0 - \bar{B}_0 \text{ and } \Delta C = \bar{B}_0$$

(B11)

Substituting for $\Delta \bar{B}$ and ΔC in equation (B8) and rearranging gives the bolt force at separation as

$$\bar{B}'_0 = \bar{B}_0 \left(1 + \frac{(t_{ep} + t_{cf})}{5L_{ebl}} \right)$$

(B12)

or

$$\frac{\bar{B}'_0}{\bar{B}_0} = \left(1 + \frac{(t_{ep} + t_{cf})}{5L_{ebl}} \right)$$

(B13)

Now substituting for C (equation (B10)) in equation (B1) and rearranging gives

$$B = \bar{B}'_0 \frac{(\bar{B} - \bar{B}_0)}{(\bar{B}'_0 - \bar{B}_0)}$$

(B14)

ΔC in equation (B5) $\bar{B}_0 - C$ (as $\bar{B}_0 = C_0$ initially)

Substituting for C (equation (B10)) and rearranging gives

$$\bar{B}_0 - C = \bar{B}_0 \frac{(\bar{B} - \bar{B}_0)}{(\bar{B}'_0 - \bar{B}_0)} \quad (B15)$$

Therefore

$$\bar{B}_0 - C = \frac{\bar{B}_0}{\bar{B}'_0} B \quad (B16)$$

Substituting for $\frac{\bar{B}_0}{\bar{B}'_0}$ from equation (B13) gives

$$\bar{B}_0 - C = \left[\frac{5L_{ebl}}{5L_{ebl} + (t_{ep} + t_{cf})} \right] B \quad (B17)$$

Substituting for (B17) in (B5) and noting that the deflection of the bolt is the deflection of the middle surface of the plates, then

$$\delta_b = \left[\frac{5L_{ebl}}{5L_{ebl} + (t_{ep} + t_{cf})} \right] \frac{(t_{ep} + t_{cf})}{10EA_s} B \quad (B18)$$

This is in the form $\delta_b = K_b B$ and is for a pretensioned bolt

where $K_b =$ bolt stiffness

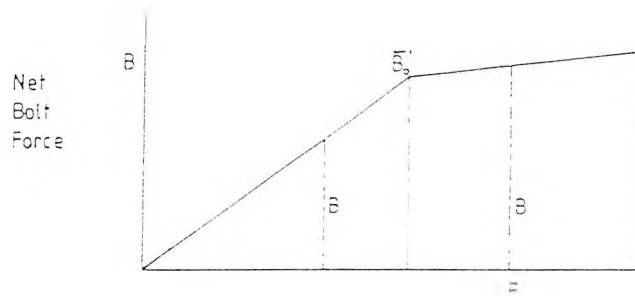
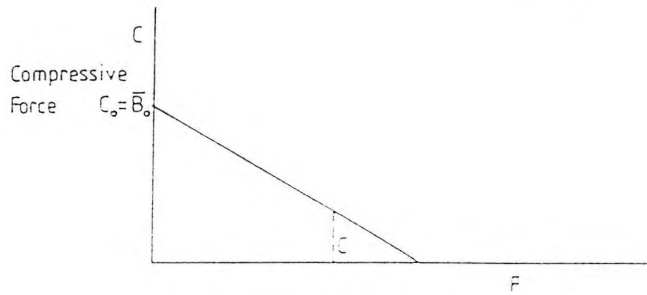
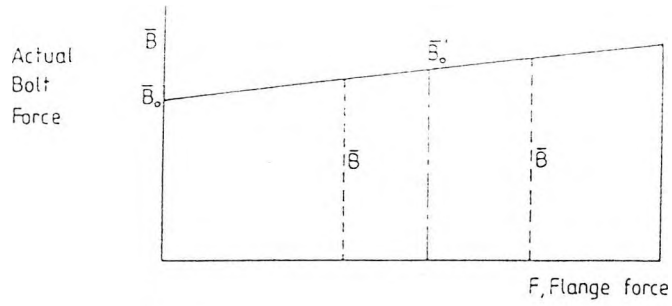
For a hand tight bolt, $\bar{B}_0 = 0$, therefore $B = \bar{B}$

and

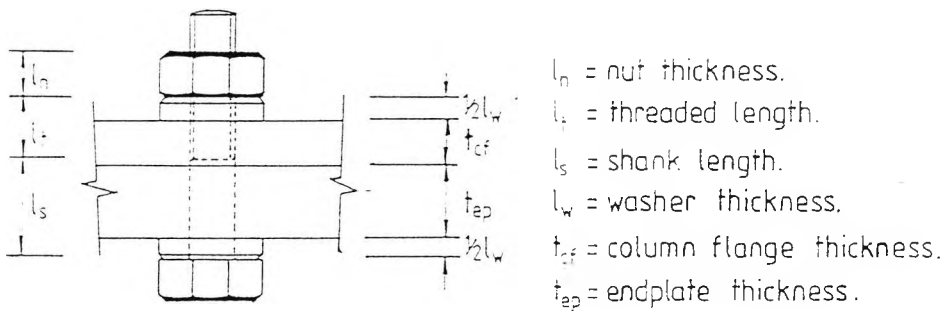
$$\begin{aligned}\delta_b &= \frac{1}{2} (\text{elongation of the bolt}) \\ &= \frac{L_{ebi}}{2EA_s} B\end{aligned}$$

(B19)

This expression is for a snug tight bolt.



a) Assumed variation of bolt force with flange force.



b) Model for calculation of bolt deformation.

Figure B1 Assumed Bolt Force Variation with Flange Force for Derivation of Bolt Stiffness

APPENDIX C

EXAMPLE OF CONNECTION DESIGN FOR PLASTIC MOMENT OF BEAM

Series A Connection

Section Details

Beam Section 254x146x37 kg/m; $Z_p = 485.3\text{cm}^3$

Column Section 203x203

Grade 43 Steel ; $\sigma_y = 265\text{ N/mm}^2$

1. Tension Force

Plastic Moment, $M_p = Z_p \sigma_y$.

$$M_p = 485.3 \times 265 \times 10^{-3} = 128.6\text{ kNm}$$

$$D_{bf} = D_b - t_{bf} = 256 - 10.9 = 245.1\text{ mm}$$

$$\text{Tension force, } F_t = \frac{128.6 \times 10^3}{245.1} = 524.7\text{ kN}$$

2. Bolt Diameter

$$\text{Proof load of bolt } \geq \frac{F_t}{4} = \frac{524.7}{4} = 131.2\text{ kN}$$

M20 HSFG Bolt Proof Load = 144 kN

Therefore use 4 M20 HSFG bolts in the tension region and 2 M20 HSFG bolts in the compression region.

3. Weld Sizes

$$\text{a.) Flange weld} = \frac{t_{bf}}{\sqrt{2}} = \frac{10.9}{\sqrt{2}} = 7.7\text{mm}$$

$$\text{b.) Web weld} = \frac{t_{bw}}{\sqrt{2}} = \frac{6.4}{\sqrt{2}} = 4.5\text{mm}$$

Therefore use an 8 mm fillet weld around the beam flange and a 5 mm fillet weld for the beam web. Carry the beam flange tension fillet weld 50 mm down the web.

4. Endplate Thickness

Adopt recommendations for endplate dimensions

$$W_{ep} = 9D; A_h = 5D; C_v = 6D; a_{ep} = 2.5D$$

Bolt diameter, $D = 20\text{mm}$

$$W_{ep} = 180\text{mm}; A_h = 100\text{mm}; C_v = 120\text{mm}; a_{ep} = 50\text{mm}$$

Rule of thumb endplate thickness

$$20\text{mm} < t_{ep} < 24\text{mm}$$

As t_{ep} is likely to be greater than t_{cf} use

$$t_{ep} = \sqrt{\frac{F_t m}{\sigma_{yep} W_{ep}}}$$

$$m = \frac{(C_v - t_{bf} - 2 \times \text{weld size})}{2} = \frac{(120.0 - 10.9 - 2 \times 8)}{2} = 46.5\text{mm}$$

Beam tension force = 524.7 kN

$$\text{Therefore } t_{ep} = \sqrt{\frac{524.7 \times 10^3 \times 46.5}{265 \times 180}} = 22.6 \text{ mm}$$

As a 25mm thick endplate would change the design - use a 20mm thick endplate.

5. Column Flange Thickness

$$1; F_{mb} = t_{cf}^2 \left[\frac{3.14(m + n') + 0.5C_v}{(m + n)} \right] \sigma_y + 4P_L \left[\frac{n}{(m + n)} \right]$$

$$2; F_{mc} = t_{cf}^2 \left[3.14 + \frac{(2n' + C_v - D')}{m} \right] \sigma_y$$

$$m = \frac{A_h - t_{cw} - 2 \times \text{root fillet}}{2} = \frac{100.0 - 10.3 - 2 \times 10.2}{2} = 34.7 \text{ mm}$$

$$n = \frac{W_{ep} - A_h}{2} = \frac{180.0 - 100.0}{2} = 40.0 \text{ mm}$$

$$n' = \frac{W_{cf} - A_h}{2} = \frac{206.2 - 100.0}{2} = 53.1 \text{ mm}$$

$$F_{mb} = t_{cf}^2 \left[\frac{3.14(34.7 + 53.1) + 0.5(120.0)}{(34.7 + 40.0)} \right] 265 \times 10^{-3} + 4 \times 144 \left[\frac{40.0}{74.7} \right]$$

$$= 1.187 t_{cf}^2 + 308.4$$

$$F_{mc} = t_{cf}^2 \left[3.14 + \frac{2 \times 53.1 + 120.0 - 22.0}{34.7} \right] 265 \times 10^{-3}$$

$$= 2.397 t_{cf}^2$$

For no stiffening $F_t < F_{mb}, F_{mc}$

$$\text{For } F_{mb}, t_{cf} = \sqrt{\frac{524.7 - 308.4}{1.187}} = 13.5\text{mm}$$

$$\text{For } F_{mc}, t_{cf} = \sqrt{\frac{524.7}{2.397}} = 14.8\text{mm}$$

Therefore UC 203x203x60 is adequate

UC 203x203x52 is inadequate

6. Column Web - Tension Zone

$$\text{Web tension zone capacity} = (C_v + 3.5m) t_{cw} \sigma_{yc}$$

Therefore for 203x203x60 UC

$$\text{Capacity} = (120.0 + 3.5(34.7)) 9.3 \times 265 \times 10^{-3} = 594 \text{ kN}$$

Therefore for 203x203x52 UC

$$\text{Capacity} = (120.0 + 3.5(35.2)) 8.0 \times 265 \times 10^{-3} = 515 \text{ kN}$$

Tension force = 524.7 kN

Therefore 203x203x60 UC adequate, 203x203x52 UC just inadequate

7. Column Web - Compression Zone

$$F_{wc} = (t_{bf} + t_{ep} + g_{ep} + 5k) t_{cw} \sigma_{yc}$$

$$\begin{aligned} F_{wc} &= (10.9 + 20 + 20 + 5 \times 24.4) 9.3 \times 265 \times 10^{-3} \\ &= 426 \text{ kN (UC 203x203x60)} \end{aligned}$$

$$F_{wc} = (10.9 + 20 + 20 + 5 \times 27.5) 10.3 \times 265 \times 10^{-3}$$
$$= 514 \text{ kN (UC 203x203x71)}$$

Therefore UC 203x203x71 just inadequate

Use an unstiffened 203x203x71 UC as the design connection to examine the design rules as only just inadequate.

8. Summary

Design Connection

Beam 254x146x37kg/m UB

Column 203x203x71kg/m UC

4 M20 HSFG bolts in tension region

Endplate 180mm wide x 20mm thick

No stiffening required

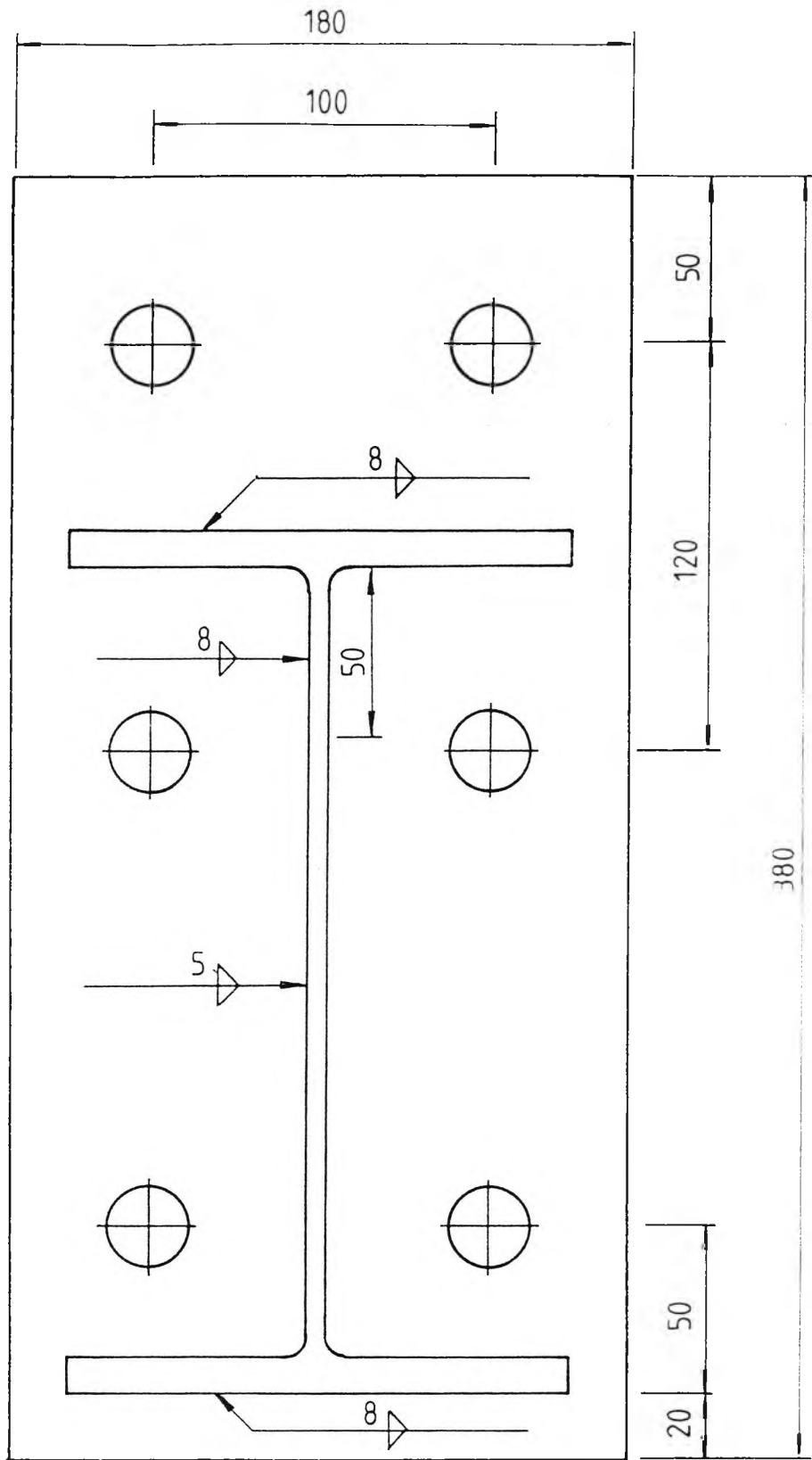


Figure C1 Endplate Detail - Series A

APPENDIX D

PHOTOGRAMMETRIC STUDY

1. Introduction.

Photogrammetry is the science of obtaining reliable data from the measurement of photographic images. It was used in this project as it afforded a means of recording the movement of several points relative to other moving points. The theory will be explained simplistically below.

The test arrangement is drawn schematically in Figure D1. The camera position (x_o, y_o) is found by resecting from the known target positions (T1, T2, T3). Once the position is known, the position of any point on the specimen can be found by knowing the vector of the point (v_1, v_2) and the height of the point above the fixed datum (h_1, h_2) . The resection and vector calculations are based on measurements taken from the photograph. These measurements are taken on a highly refined measuring device called a stereocomparator which measures the points to a high precision and then writes their coordinates to a data file. Existing computer software is then used to carry out the resection and the calculation of the coordinates of the required points.

As plane rotation only was required, one photograph was needed to measure the deflections in two dimensions. If deflections in

the third dimension were needed then a second photograph could be taken. This is known as stereophotogrammetry. In this case more control in the third dimension was given by the use of levelling to record the out-of-plane movement.

2. Feasibility of the photogrammetric study.

Before the study was embarked upon, the feasibility of measuring deflection to within ± 0.1 mm was investigated. The conditions needed to attain this specification are set out below.

2.1 Photographic measurement.

The camera used was a wide angled lens metric camera. The metric simply means that the internal geometry of the camera is known to a close tolerance. The focal length, f , of a wide angle lens camera is approximately 100mm. The scale of any photograph is defined as

$$\text{scale} = \frac{f}{H}$$

(D1)

where H = height of camera above the datum

The size of the photographic plate on which the image was to be developed was 150 x 100mm. Therefore the maximum scale possible was given by

$$\frac{150}{3000} = 0.05 \quad (\text{or } 1:20)$$

where 3000mm is the maximum distance required across the specimen.

Therefore, the height of the camera above the datum was given by,

$$H = \frac{100}{0.05} = 2000\text{mm}$$

This was easily attainable. From the scale, the smallest movement that could be measured could be found. Movement on the photograph can be measured to 5 microns, therefore movement on the specimen can be measured to 5 microns x 20 (scale) = 100 microns or 0.1mm.

2.2 Datum measurement.

If the movement to be measured was 0.1mm then the camera position needed to be calculated to at least 0.1mm. This meant that the fixed datum target coordinates had to be known to at least 0.1mm also. Therefore a scheme had to be devised of measuring the target positions within the required tolerance.

This was achieved by gluing six targets to the laboratory floor. The targets were white crosses on a black background with a hole, 0.5mm, drilled in the middle. Each target was measured from every other target several times using a calibrated, tensioned steel band. For each measurement, a different part of the band was used. The reduction of the measurements lead to the standard error of each distance being found. When these distances and standard errors were input into a computer program based on a least squares fit, the coordinates and standard errors of each target were found. If the coordinates were not found within the measured tolerance, then the least precise distances were remeasured until they were known to a higher precision. The target system was then reanalysed until the target coordinates were obtained within the required tolerance.

It was decided, therefore, that the photogrammetric study should proceed as deflections could be measured to 0.1mm.

3. Test Procedure.

3.1 Test set-up and specimen preparation.

Deflection needed to be measured to 0.1mm. Therefore, it was important that the points to be measured on the specimen were well defined. This was achieved by attaching small targets to the specimen. The targets were made of paper and fixed by, firstly sanding down the surface of the specimen and then gluing them in position. A special anti-glare spray was then applied to

minimize reflection from the paper surface. The positions of the targets for test A1 are shown in Figure D2.

The next step was to position the camera in the required position to take the photographs. The main requirement was that the camera had to be 2m above the specimen. This was achieved by erecting scaffolding and spanning the test rig with scaffolding beams. The camera was placed on the beams and directly over the area of interest on a sliding mounting. The camera was levelled before the test. The sliding mounting facilitated the change of photographic plates at each load increment. The camera position does not have to remain fixed as its position will be calculated relative to the fixed targets for each load increment.

Lastly, adequate lighting was provided to ensure the target area was clearly visible. The initial test set up is shown in Figure D3.

3.2 Test Procedure.

Before the test, preliminary photographs were taken to ensure that lighting conditions were correct and that all fixed targets and areas of interest were visible.

The test specimen was just loaded sufficiently to be held by the rollers and support points. An initial photograph was taken and the target positions were levelled. The photographic plate was changed and the next load increment applied. A photograph was

taken and the specimen again levelled to ensure that little out-of-plane movement was taking place. The photograph and load readings at the support points were taken simultaneously. A typical photograph obtained from this procedure is shown in Figure D4.

4. Analysis of results.

Each load increment photograph was analyzed on the stereocomparator. The results output were the coordinate positions of each target relative to the coordinate system defined by the fixed targets. These results needed to be reduced to obtain component deflection and connection rotation.

Component deflection relative to the column centreline is easily found from the coordinate data. Connection rotation, however, needs some definition before it can be calculated.

The main targets of interest for calculation of connection rotation are shown in Figure D5. The normal definition of connection rotation is the change of the angle between the beam and column centrelines. These lines are defined by 3-0-4 and 0-1-2 in Figure D5. To neglect beam flexure, it was attempted to measure the change in angle between lines 3-4 and lines 0-1. This change was found to be negligible up to the plastic moment of the beam in test A1. This was clearly not the case, if the deflections at the endplate tension and compression levels were considered. It was concluded that connection rotation along the

beam centreline in the column itself was negligible. That is, that connection rotation effectively started on the beam-column interface. The reason that target 1 did not deflect was that the beam web was distorted at the end of the beam due to being restrained by the bolted endplate. This means that pure connection rotation cannot be measured along the centreline of the beam but must be measured a distance away where beam flexure will also be included.

Therefore, connection rotation must be measured between points 0-2 and 3-4. There are two ways of defining this rotation. The change in angle between 0-4 and 0-2 (angle i - angle j), and the change in angle between 3-4 and 1-2 (angle i - angle k). Other methods of rotation measurement are the deflection at the beam flange levels divided by beam depth and the derivation of rotation from load-deflection readings. Connection rotation from all these methods of measurement are shown in Table D1. The connection rotation measured from beam flange level deflection readings is shown for measurements taken on the endplate and on the beam flanges.

It can be seen that there is reasonable agreement between the connection readings by the deflection method and those derived from the load deflection method. In the early stages of loading the rotation measurement between lines 3-4 and 1-2 slightly overestimates connection rotation by approximately the amount of the offset rotation as calculated in Appendix E. The connection rotation measured assuming a fixed centre point (column 1)

underestimates rotation, as expected. Therefore, it was concluded that it would be best to measure connection rotation from deflection readings at the beam flange levels. However a more precise method of measurement would be needed as initial deflections were of the same order as the precision of the photogrammetric deflection measurements.

Moment kNm	Connection rotation (10^{-3} rads)				
	$\angle i - \angle j$	$\angle i - \angle k$	$\frac{\Delta_u + \Delta_l}{D_{bf}}$	$\frac{\Delta_u + \Delta_l}{D_{bf}}$	Dial Gauge Reading
	$\theta_c + \theta_m$	$\theta_c + \theta_m$	Endplate θ_c	Beam Flange θ_c	θ_c
4.0*	0.0	0.0	0.0	0.0	0.0
37.8	0.6	1.5	0.8	0.9	0.6
73.3	1.8	3.3	2.1	0.3	1.7
107.1	2.7	4.2	4.7	4.7	4.3
123.1	4.7	8.3	7.8	7.2	7.9

* Initial reading

Table D1. Connection rotation values for test D1

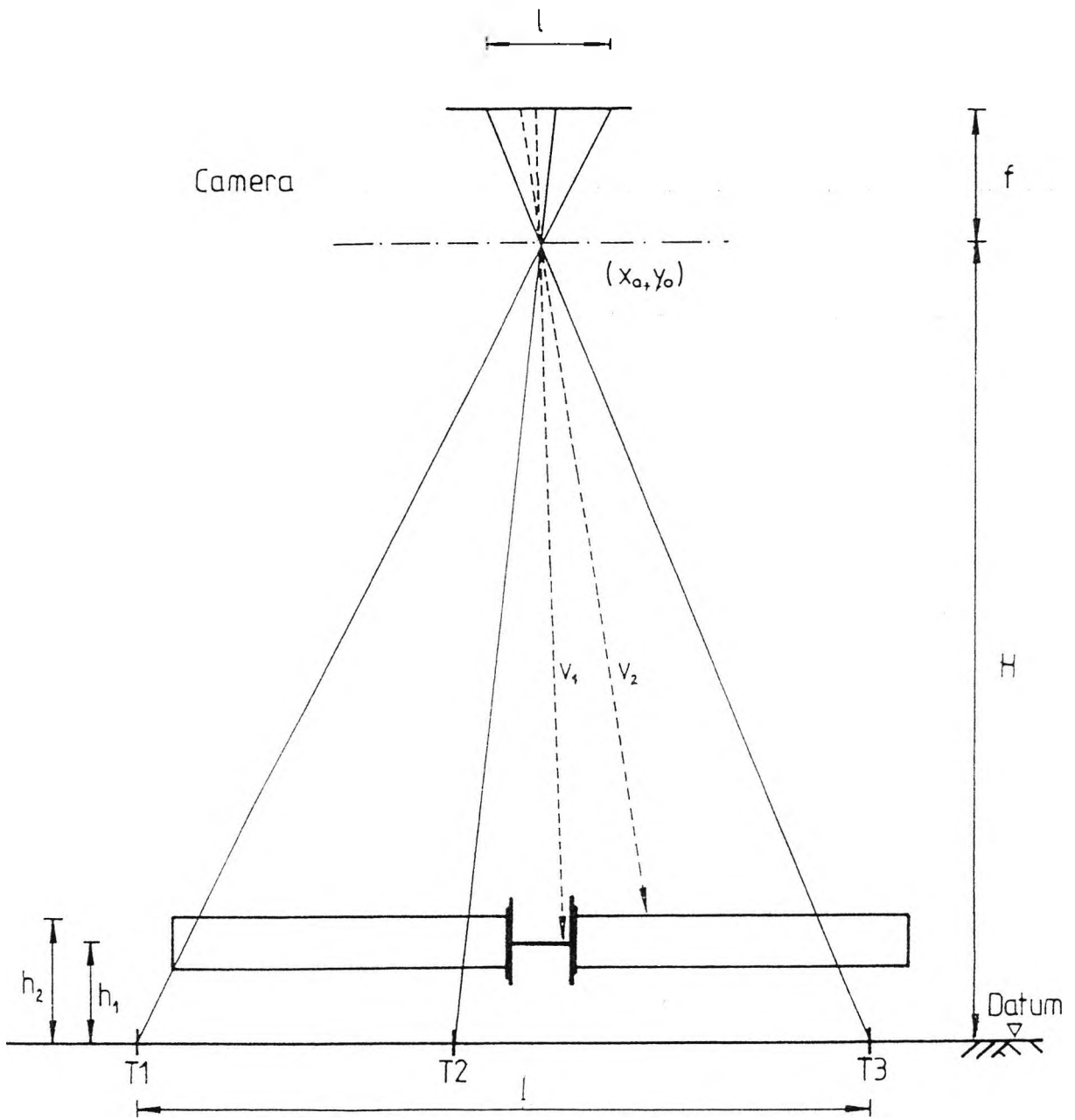
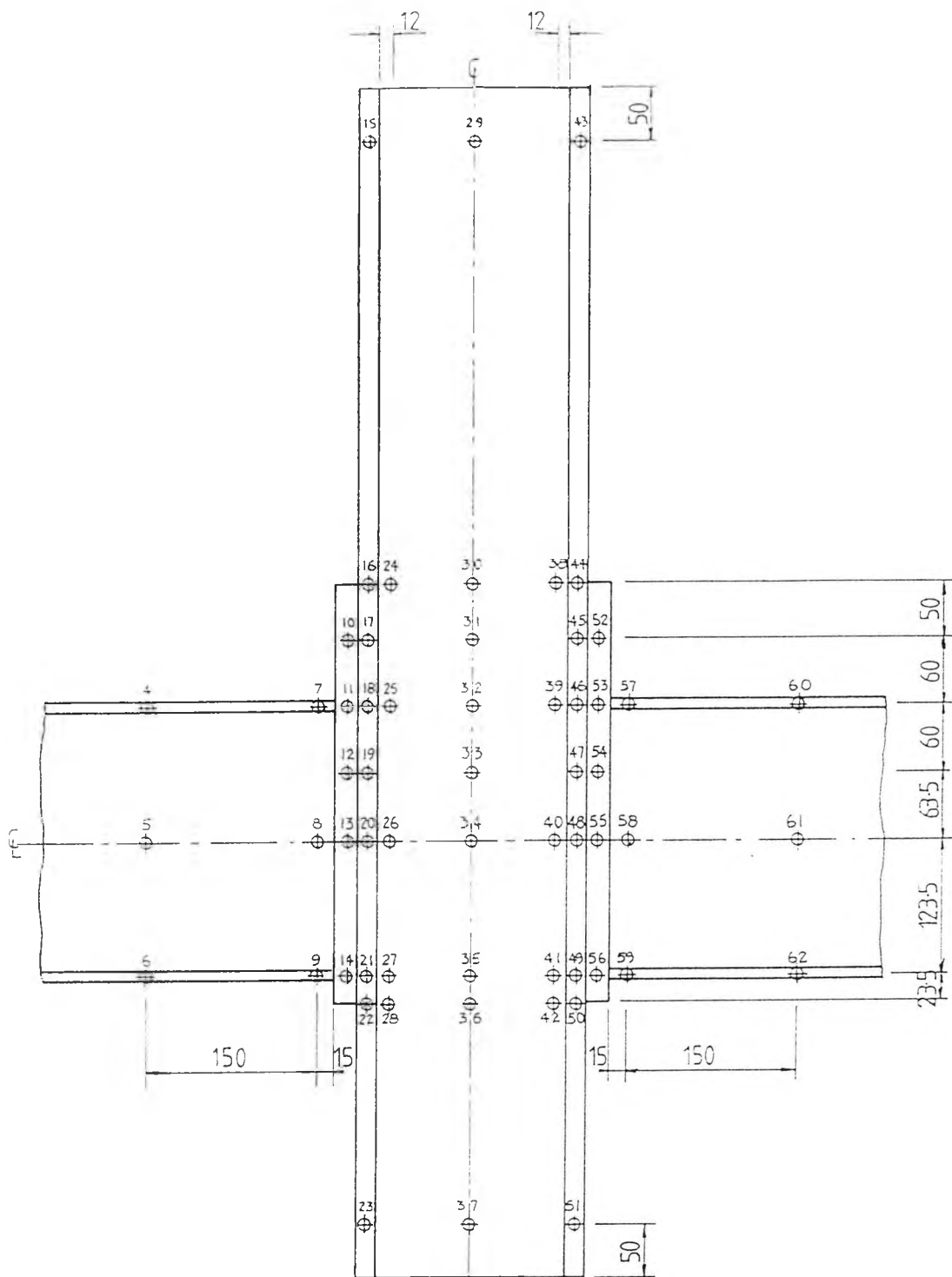


Figure D1. Photogrammetric Test Arrangement



Targets not dimensioned are positioned on centrelines of column flange and endplate.

Figure D2. Position and Numbering of Targets for Test A1



Figure D3 Test Set-up

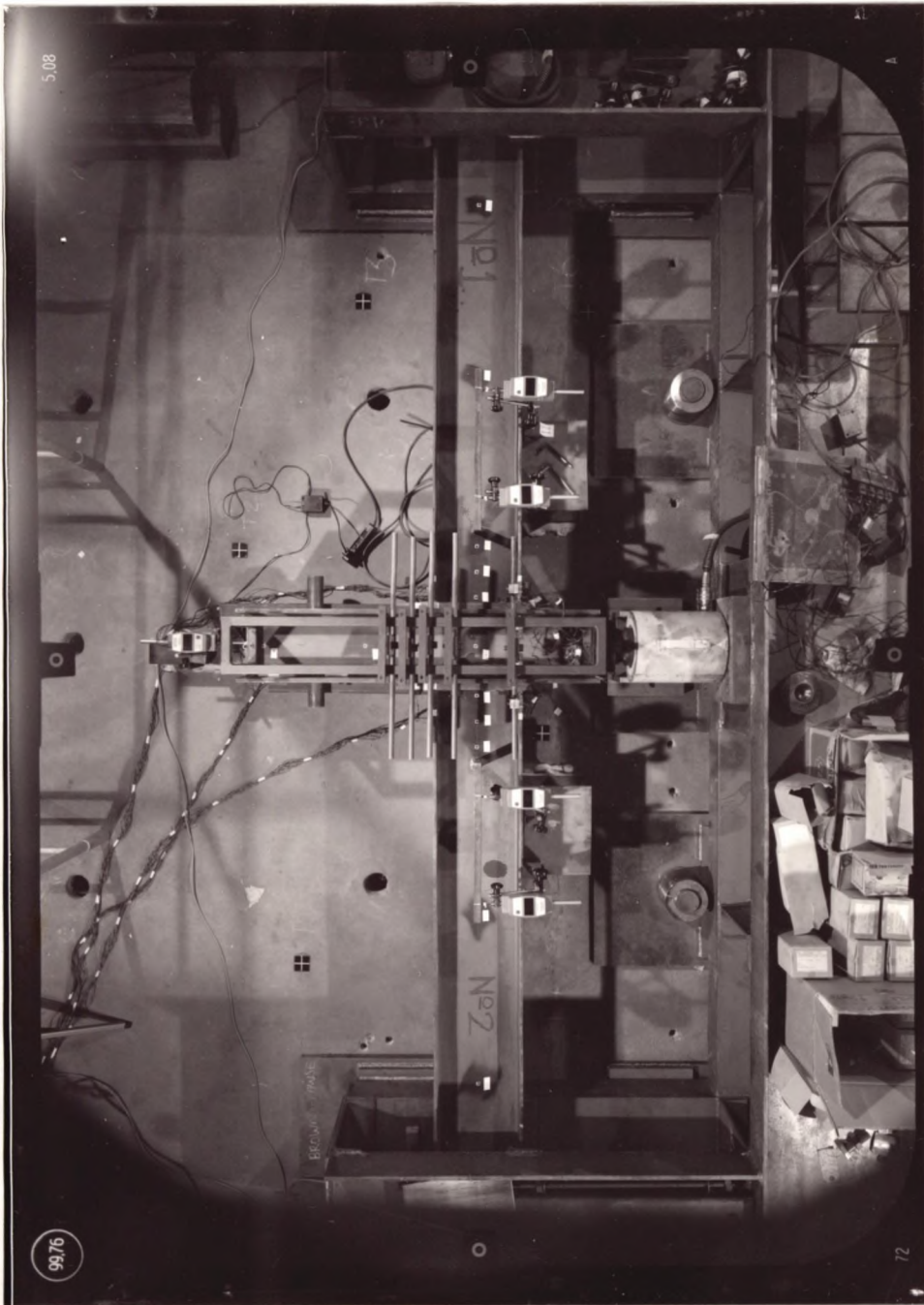
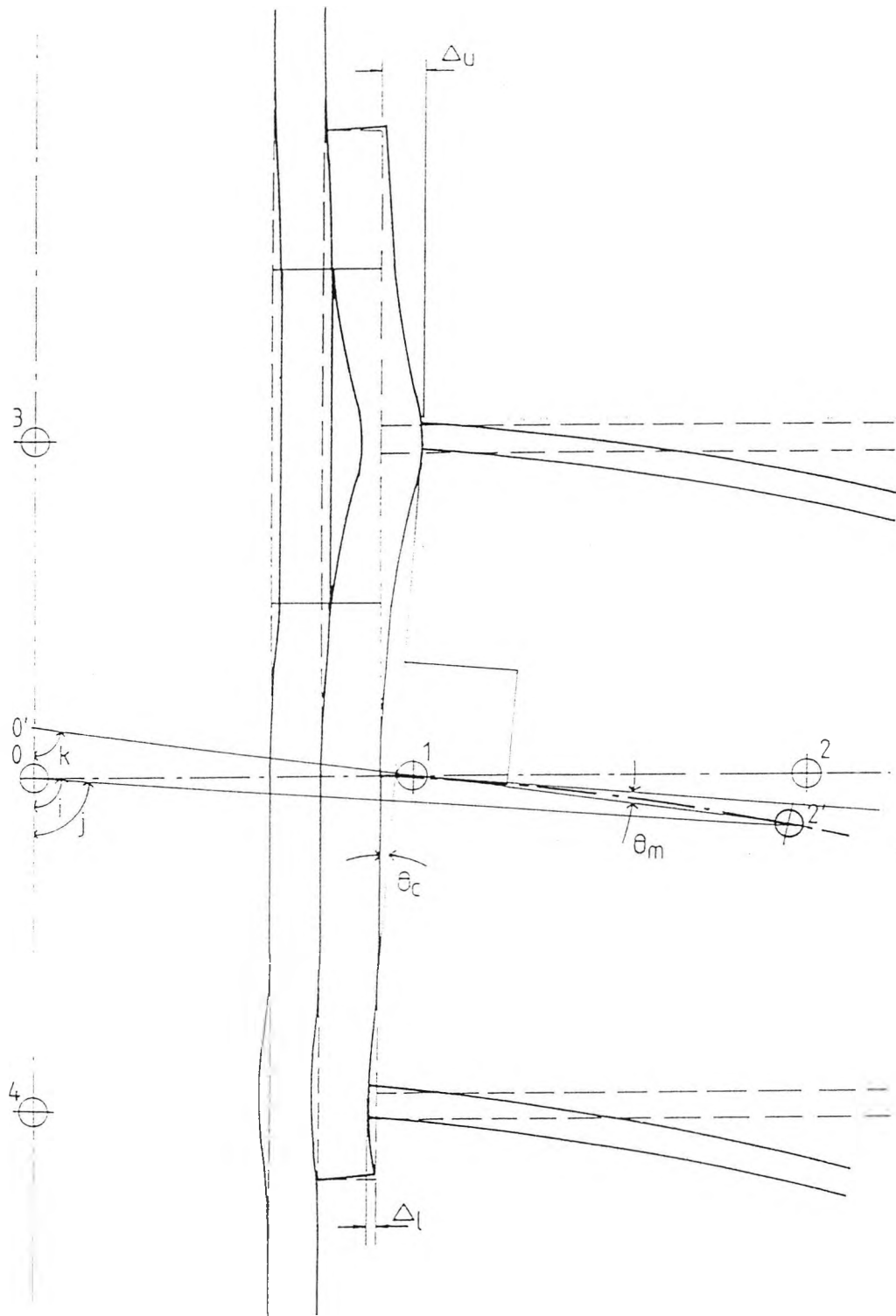


Figure D4. Typical Photogrammetric Plate



——— Deflected shape - - - - Deflected centreline
 - - - - Undeformed shape ——— Undeformed centreline

Figure D5. Definition of Connection Rotation

APPENDIX E

CALCULATION OF MOMENT-ROTATION DATA FROM LOAD-DEFLECTION DATA AND THE CALCULATION OF BEAM OFFSET FLEXURE.

1. Calculation of moment-rotation data

A typical internal/internal cruciform type specimen is shown in Figure E1(a). If the deflections in the y-direction due to the axial compression in the column section and bolt slip are neglected, this arrangement reduces to the simply supported beam representation shown in Figure E1(b). However there is a difference in that an ordinary simply supported beam would have a slope of zero at midpoint. If the connections at the beam/column interface were rigid then this would be the case. However as seen in the main body of the text each connection deforms to a certain extent under load. This deformation is represented by introducing a slope discontinuity at the central point of the beam as shown in Figure E1(b).

The deflection of the beam can be represented by the equation

$$w = Ax^3 + Bx^2 + Cx + D + \frac{Wz_1^3}{6EI} - \theta z_1 \quad (E1)$$

where $z_1 = (x - \frac{l}{2})$ and only exists if $z_1 > 0$

The four arbitrary constants can be found from the four boundary conditions at the end of the beams.

$$\begin{aligned} w = w'' = 0 & \quad \text{at } x = 0 \\ w = w'' = 0 & \quad \text{at } x = l \end{aligned}$$

(E2)

From the first two conditions $B = D = 0$

The third condition yields

$$Al^3 + Cl + \frac{Wl^3}{48EI} - \frac{\theta l}{2} = 0$$

(E3)

The fourth condition yields

$$6Al + \frac{Wl}{2EI} = 0$$

(E4)

Solving these boundary conditions gives

$$A = -\frac{W}{12EI} ; C = \frac{Wl^2}{16EI} + \frac{\theta}{2}$$

(E5)

Substituting into equation E1 gives

$$w = \left(\frac{Wl^2}{16EI} + \frac{\theta}{2} \right) x - \frac{W}{12EI} x^3 + \frac{Wz_1^3}{6EI} - \theta z_1$$

(E6)

The deflection at any point on the beam is now known in terms of the load acting on the beam, the beam geometric properties and

the slope discontinuity at the beam/column connections. If the position of a dial gauge reading on the beam specimen is known then the average rotation due to the connections can be deduced. The most common position for deflection readings is at the centre of the cruciform specimen. Therefore substituting $x = \frac{l}{2}$ into equation E6 gives

$$w_c = \frac{Wl^3}{48EI} + \frac{\theta l}{2} \quad (E7)$$

where w_c is the dial gauge reading at load W

Rearranging gives the average connection rotation

$$\frac{\theta}{2} = \frac{1}{l} \left(w_c - \frac{Wl^3}{48EI} \right) \quad (E8)$$

It will be noted that $\frac{Wl^3}{48EI}$ is the deflection of a simply supported beam of length twice the beam lever arm. Therefore the average connection rotation is simply the deflection reading less the deflection of a simply supported beam divided by the effective beam length of the cruciform specimen.

Moment at the connection is given by $M = \frac{Wl}{4}$ (E9)

2. Calculation of beam offset flexure.

If equation E6 is differentiated to give the slope of the beam at any value of x then

$$w' = \frac{Wl^2}{16EI} + \frac{\theta}{2} - \frac{W}{4EI}x^2 + \frac{Wz_1^2}{2EI} - \theta z_1$$

(E10)

If the offset flexure is defined as l_1 , as shown in Figure E1(b)

then at $x = \frac{l}{2} - l_1$

$$w' = \frac{\theta}{2} + \frac{W(ll_1 - l_1^2)}{4EI}$$

(E11)

Therefore the beam slope at the offset position can be split up into average connection rotation and the slope due to beam offset flexure. That is beam offset flexure is given by

$$\theta_m = \frac{W(ll_1 - l_1^2)}{4EI}$$

(E12)

This can be given in terms of connection moment as

$$\theta_m = \frac{M(ll_1 - l_1^2)}{EIl}$$

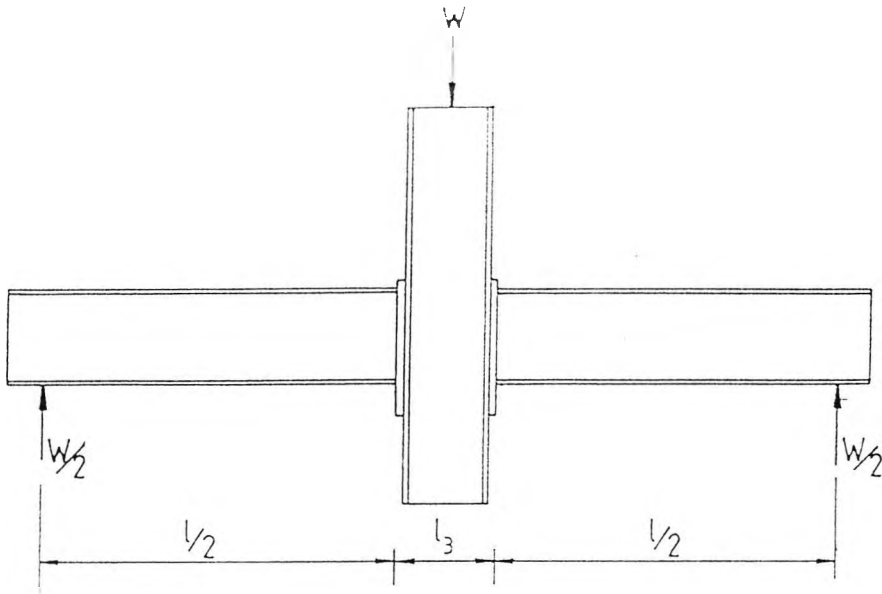
(E13)

If the offset flexure, l_1 , is small in comparison with the

effective beam length l then $l_1^2 \ll ll_1$, therefore the beam offset flexure can be estimated by the expression

$$\theta_m \approx \frac{Ml_1}{EI}$$

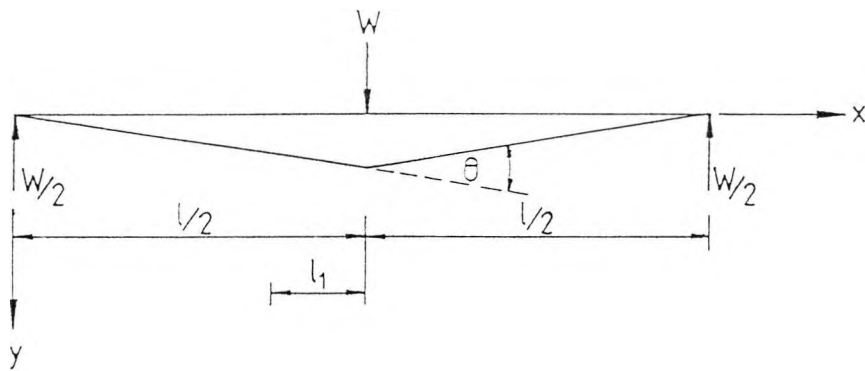
(E14)



$l/2$ = beam lever arm.

l_3 = column depth + 2 × endplate thickness

a) Connection specimen.



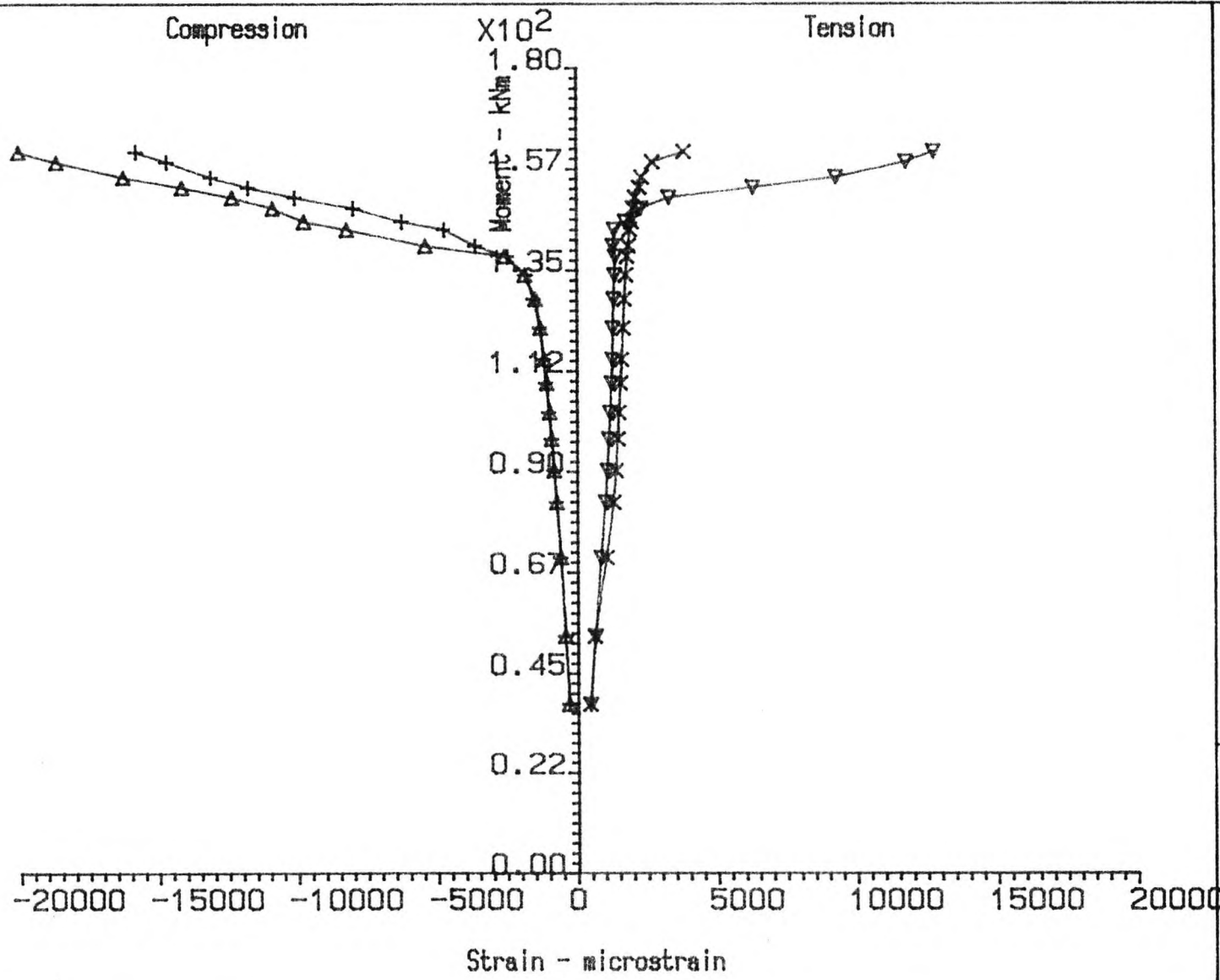
l_1 = offset length.

b) Representation of connection specimen

Figure E1 Definition of Cruciform Specimen Dimensions

APPENDIX F

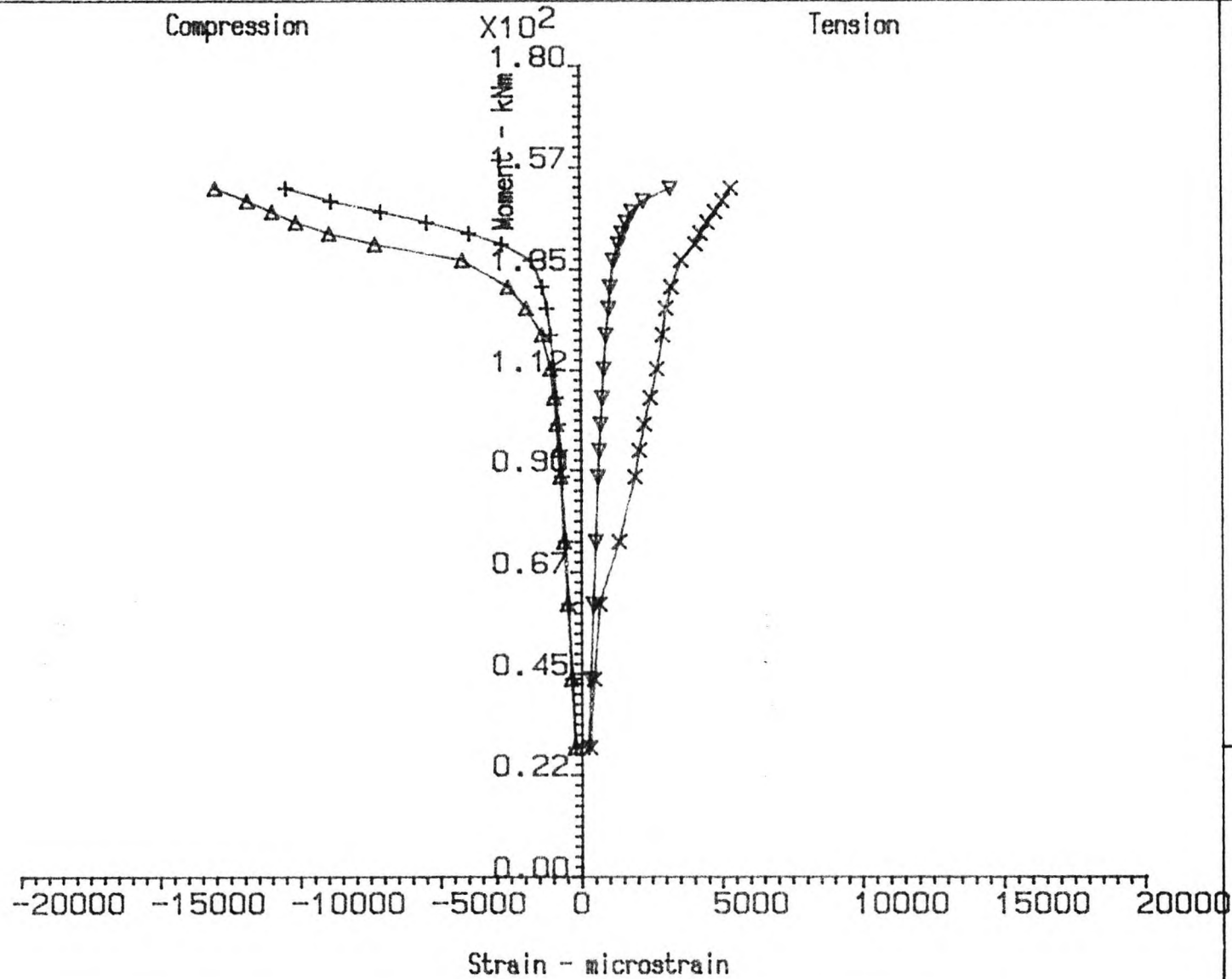
BEAM STRAIN GAUGE VERSUS LOAD READINGS



Connection Type :-
Unstiffened
Internal
Beam Size -254x146 UB37
Column Size -203x203 UC86
4 M20 Tension Bolts
Grade HSFG -Pretensioned
Endplate Thickness = 20 mm

∇, \triangle = Beam 1
 $\times, +$ = Beam 2

Figure F.1
STRAIN GAUGE READINGS
AGAINST BENDING MOMENT.
Test A3

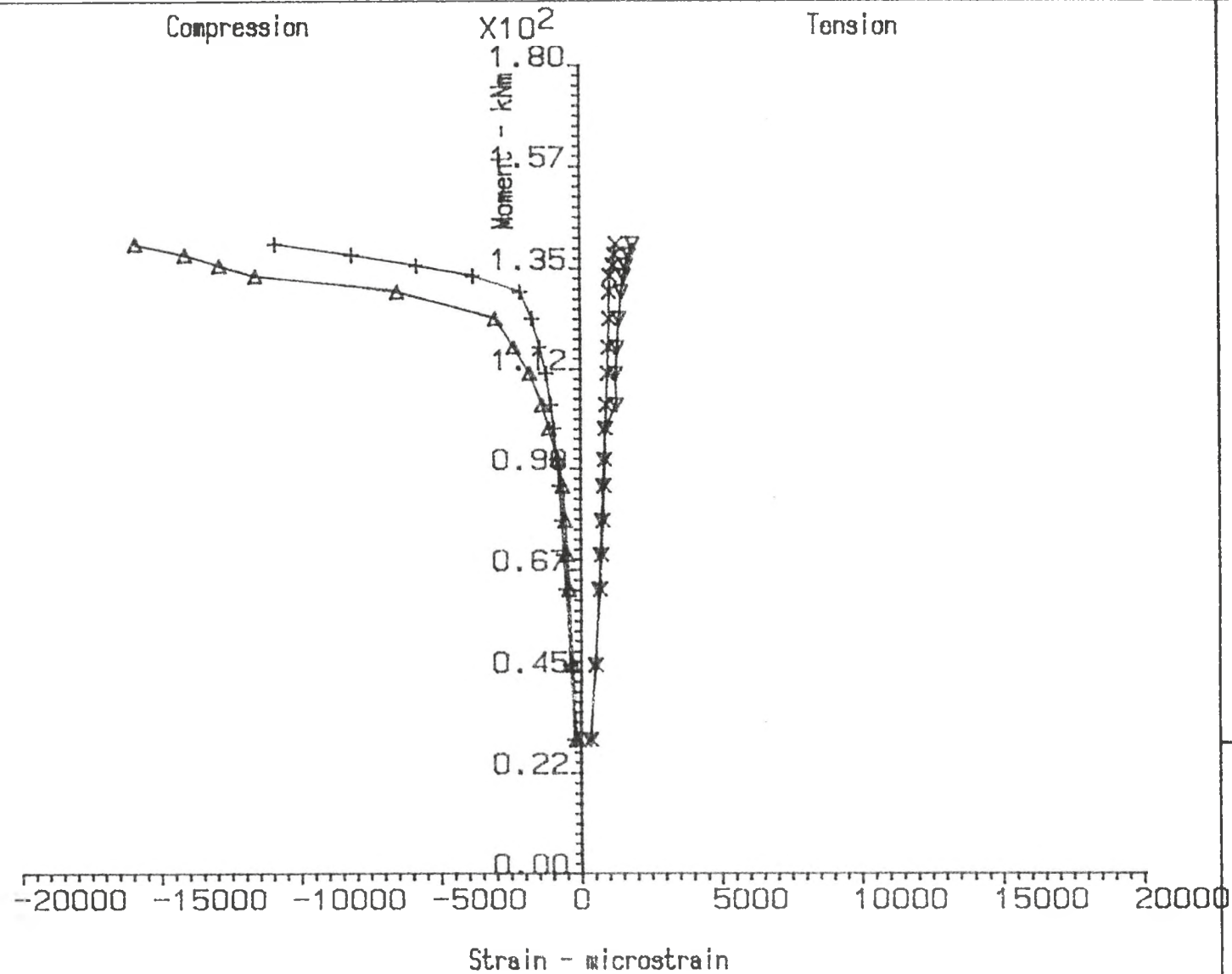


Connection Type :-
 Unstiffened
 Internal
 Beam Size -254x146 UB37
 Column Size -203x203 UC71
 4 M20 Tension Bolts
 Grade HSFG -Pretensioned
 Endplate Thickness = 25mm

∇, Δ = Beam 1
 $\times, +$ = Beam 2

Figure F.2.
 STRAIN GAUGE READINGS
 AGAINST BENDING MOMENT.

Test A4

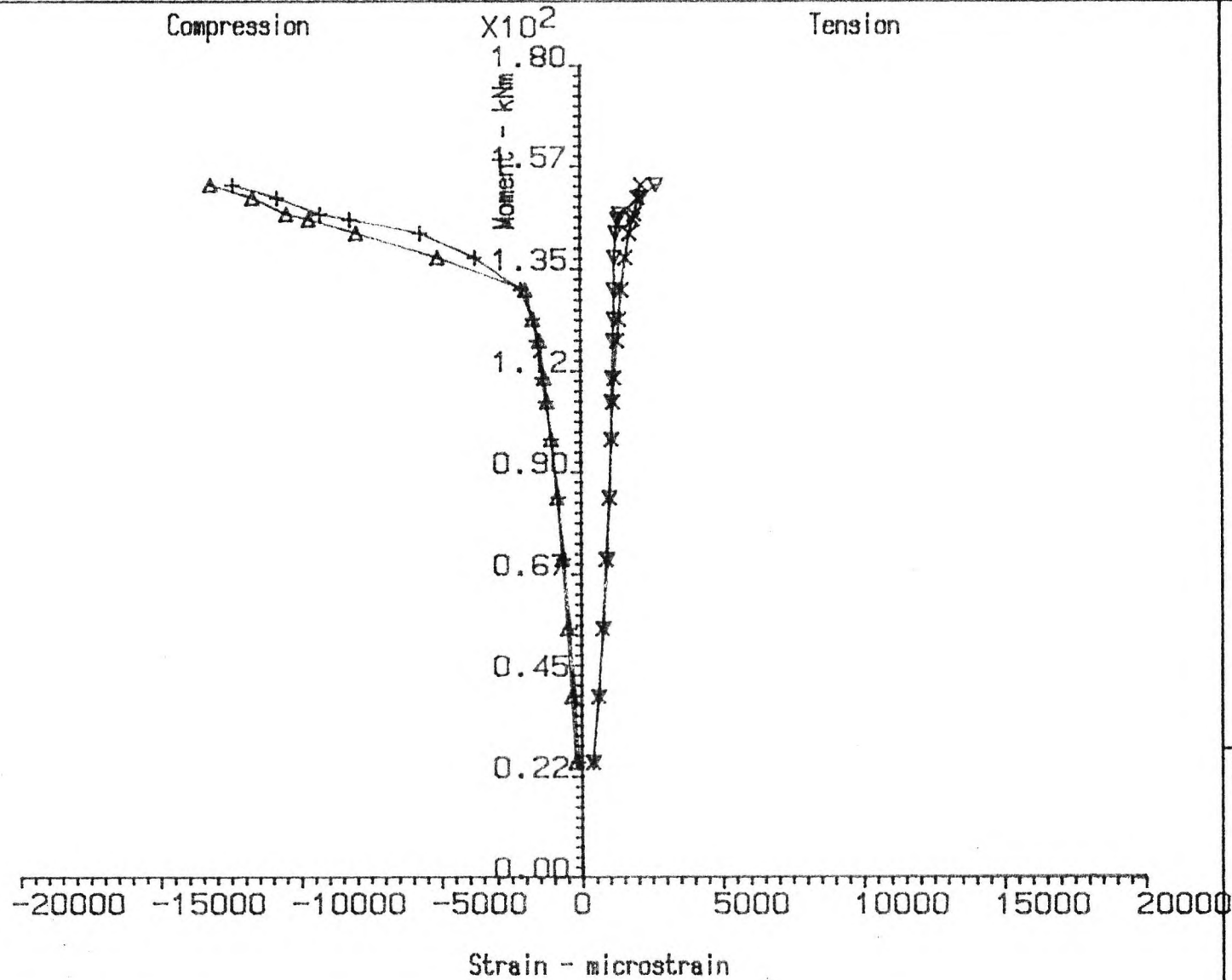


Connection Type :-
 Unstiffened
 Internal
 Beam Size -254x146 UB37
 Column Size -203x203 UC71
 4 M20 Tension Bolts
 Grade HSFG -Pretensioned
 Endplate Thickness = 15mm

∇, Δ = Beam 1
 $\times, +$ = Beam 2

Figure F.3.
 STRAIN GAUGE READINGS
 AGAINST BENDING MOMENT.

Test A5

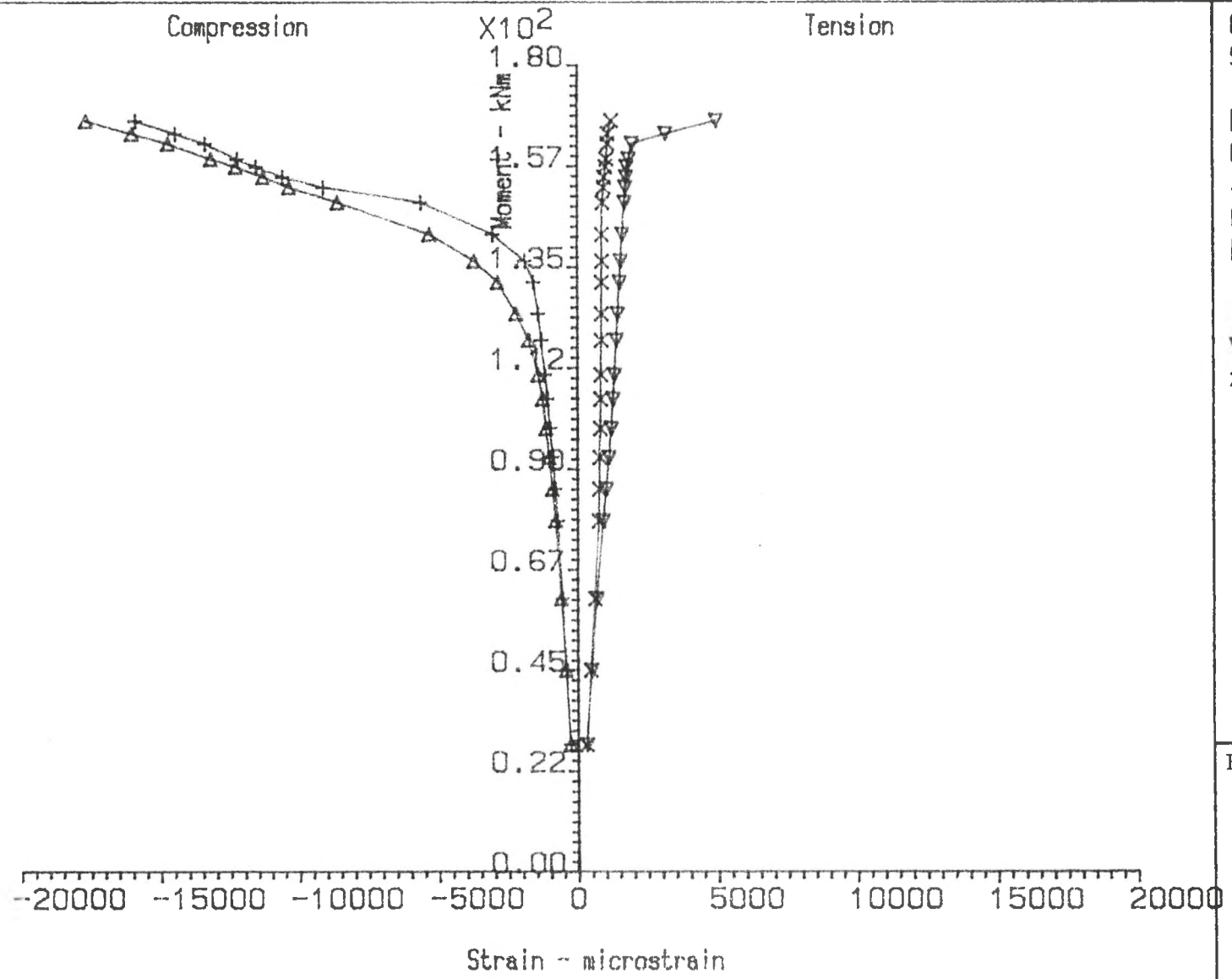


Connection Type :-
Stiffened
Internal
Beam Size -254x146 UB37
Column Size -203x203 UC
4 M20 Tension Bolts
Grade HSF8 -Pretensioned
Endplate Thickness = 20mm

∇, Δ = Beam 1
 $\times, +$ = Beam 2

Figure F.4.
STRAIN GAUGE READINGS
AGAINST BENDING MOMENT.

Test A6

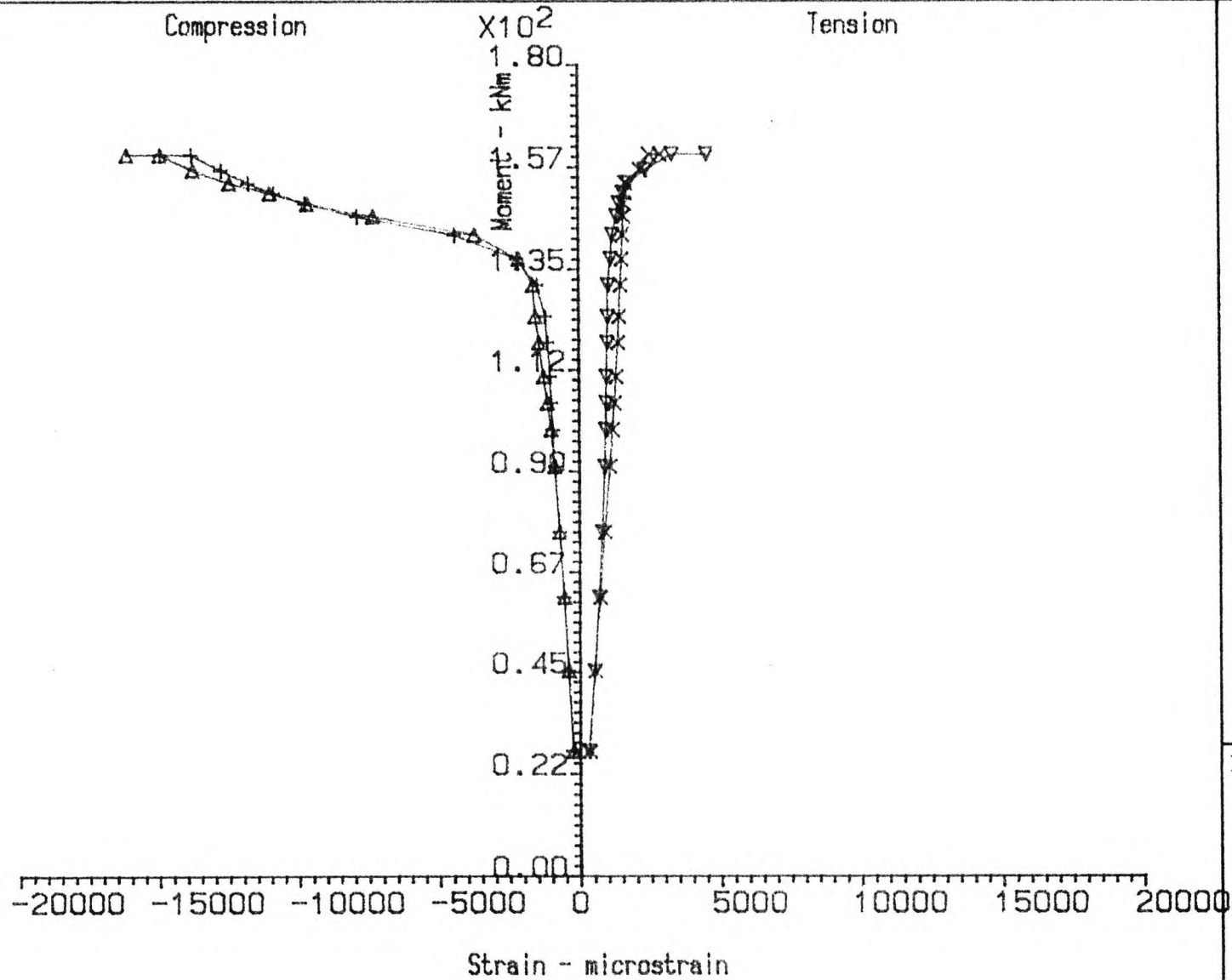


Connection Type :-
Stiffened
Internal
Beam Size -254x146 UB37
Column Size -203x203 UC71
4 M20 Tension Bolts
Grade HSFG -Pretensioned
Endplate Thickness = 20mm

∇, Δ = Beam 1
 $\times, +$ = Beam 2

Figure F.5.
STRAIN GAUGE READINGS
AGAINST BENDING MOMENT.

Test A7



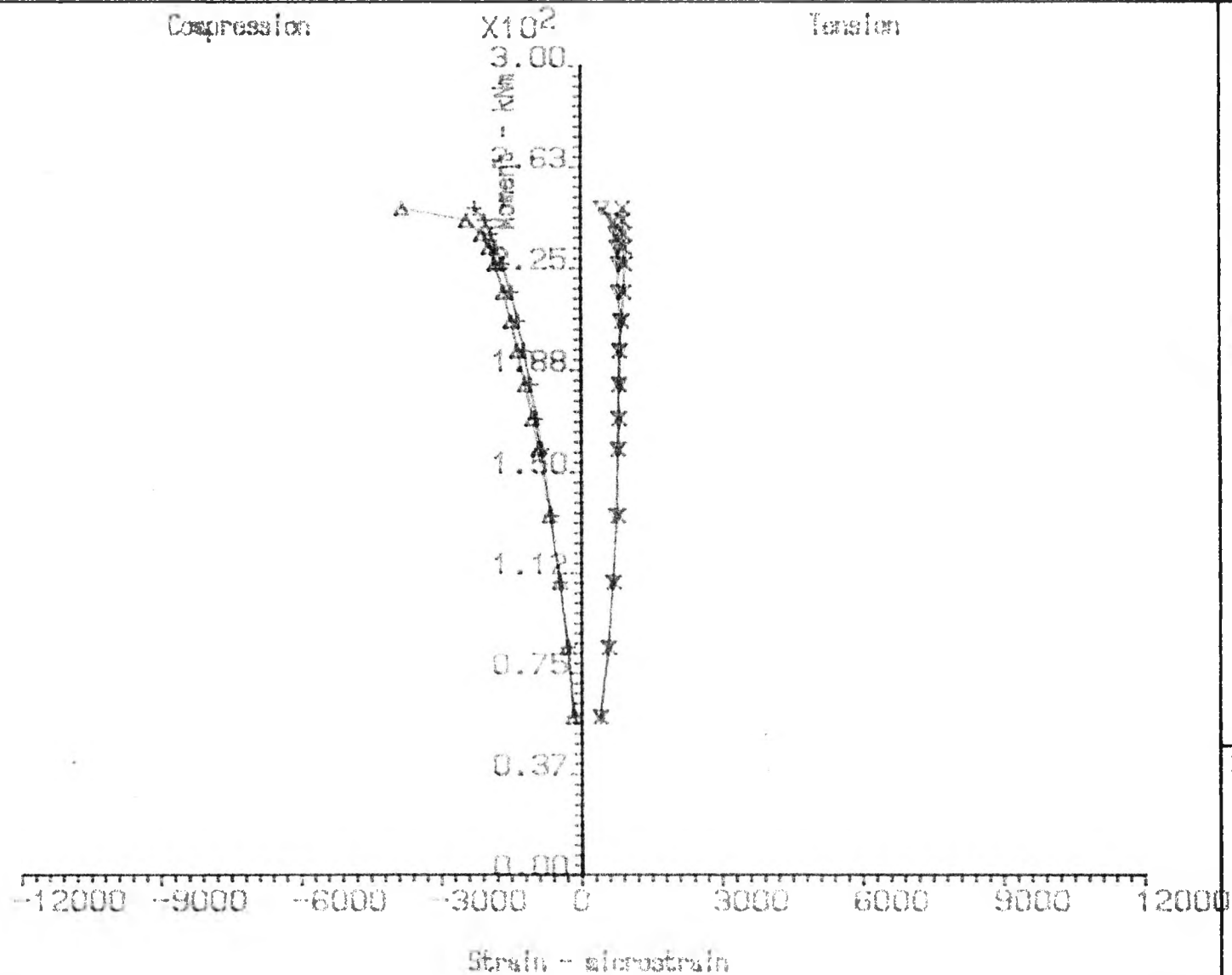
Connection Type :-
 Unstiffened
 Internal
 Beam Size -254x146 UB37
 Column Size -203x203 UC71
 4 M20 Tension Bolts
 Grade HSFG -Pretensioned
 Endplate Thickness = 20mm

∇, Δ = Beam 1
 $\times, +$ = Beam 2

Figure F.6.

STRAIN GAUGE READINGS
 AGAINST BENDING MOMENT.

Test A8

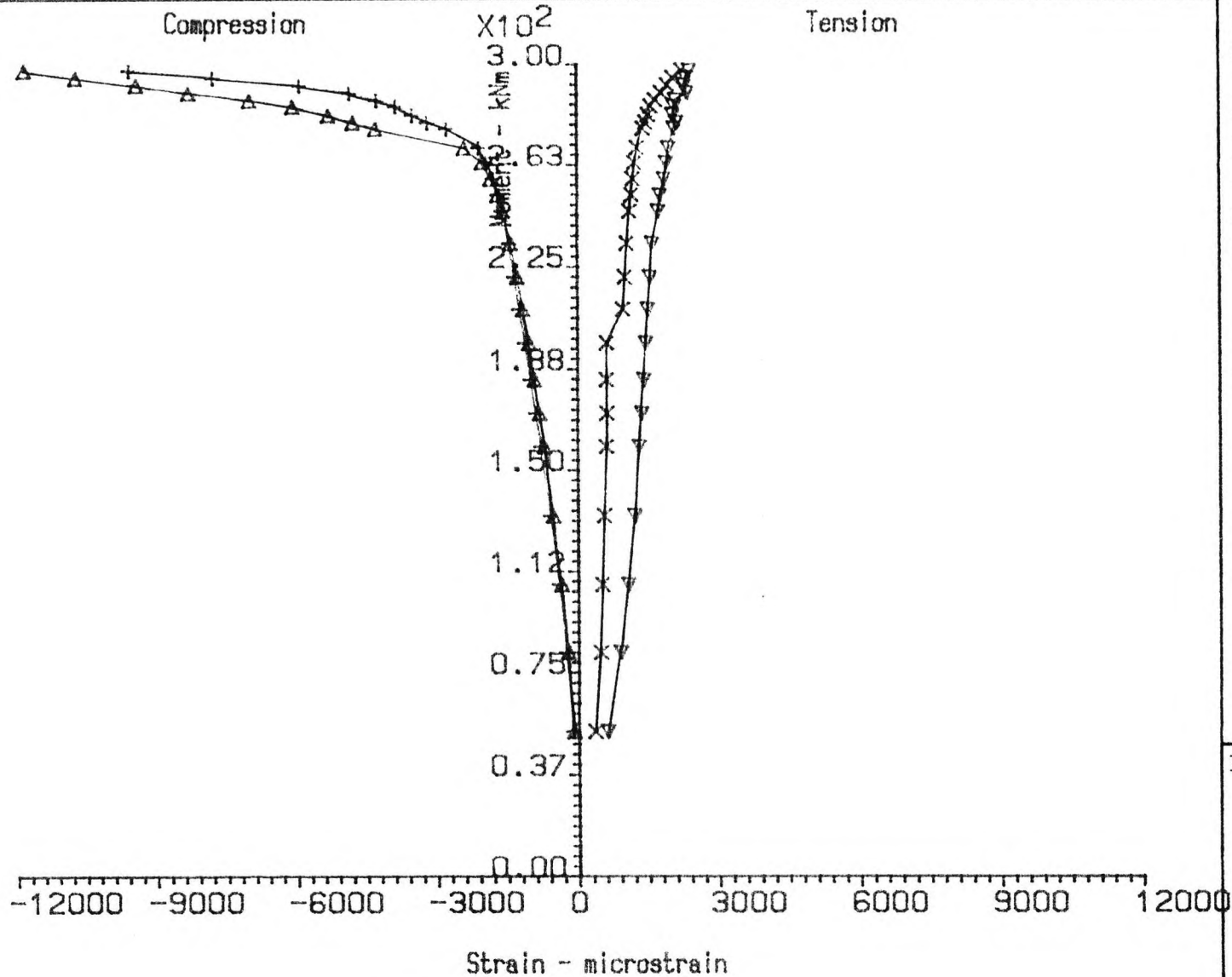


Connection Type :-
 Unstiffened
 Internal
 Beam Size -356x171 UB51
 Column Size -254x254 UC89
 4 M22 Tension Bolts
 Grade HSFG -Pretensioned
 Endplate Thickness = 25mm

▽,△ = Beam 1
 ×,+ = Beam 2

Figure F.7.
 STRAIN GAUGE READINGS
 AGAINST BENDING MOMENT.

Test B1

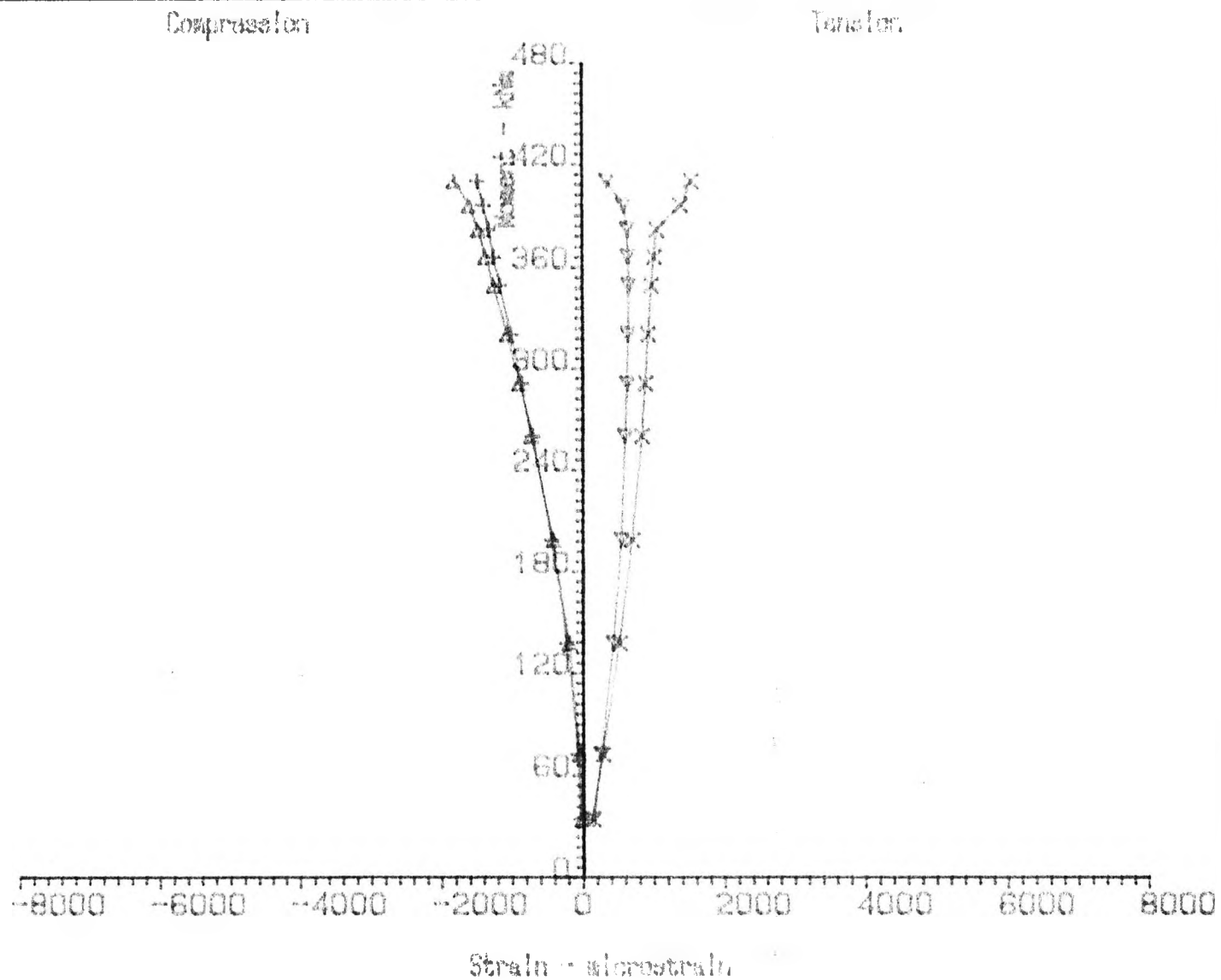


Connection Type :-
Stiffened
Internal
Beam Size -356x171 UB51
Column Size -254x254 UC89
4 M22 Tension Bolts
Grade HSFG -Pretensioned
Endplate Thickness = 25mm

▽,△ = Beam 1
x,+ = Beam 2

Figure F.8.
STRAIN GAUGE READINGS
AGAINST BENDING MOMENT.

Test B2



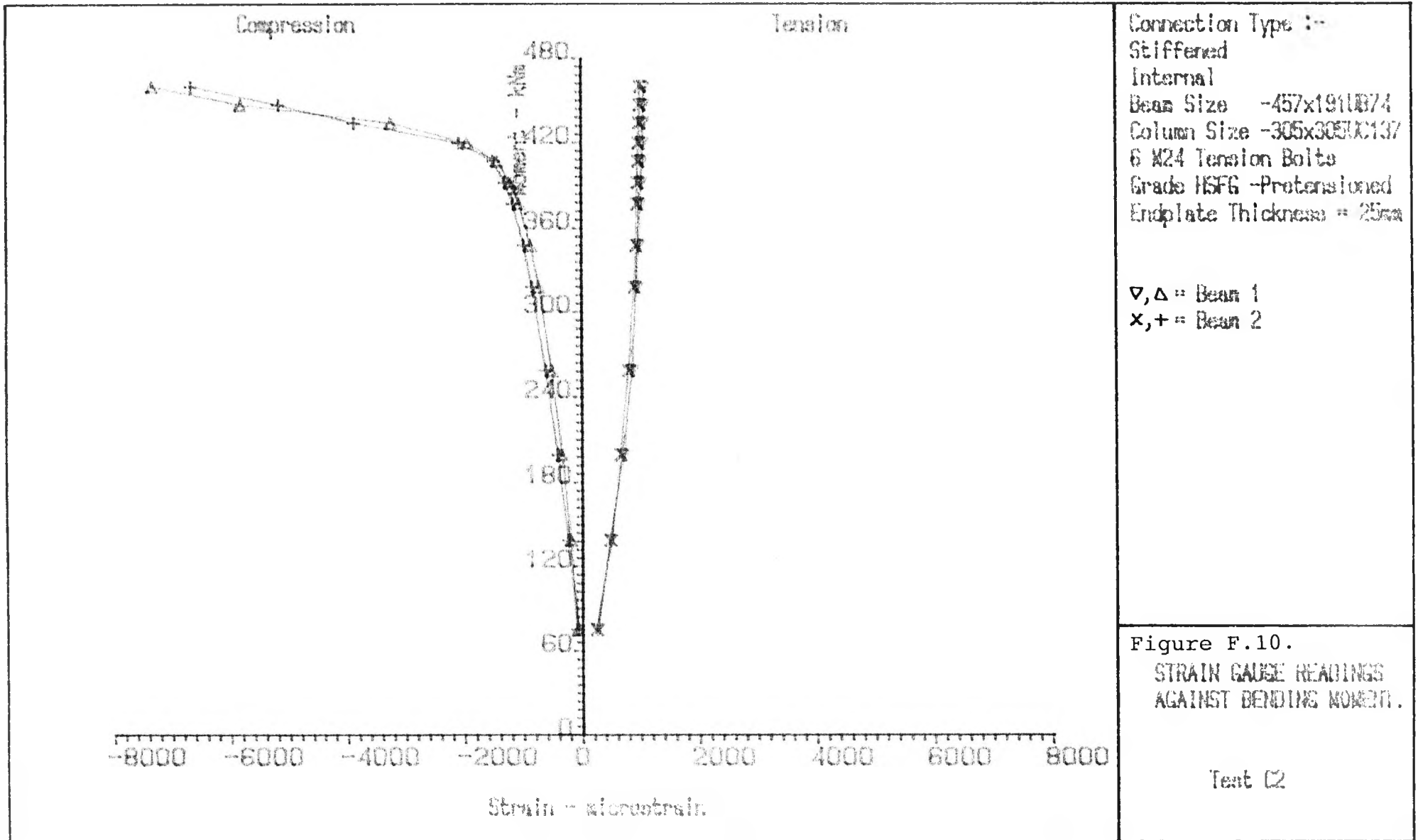
Connection Type :-
 Unstiffened
 Internal
 Beam Size --457x191UB74
 Column Size --305x305UC137
 6 M24 Tension Bolts
 Grade HSFG --Pre-tensioned
 Endplate Thickness = 25mm

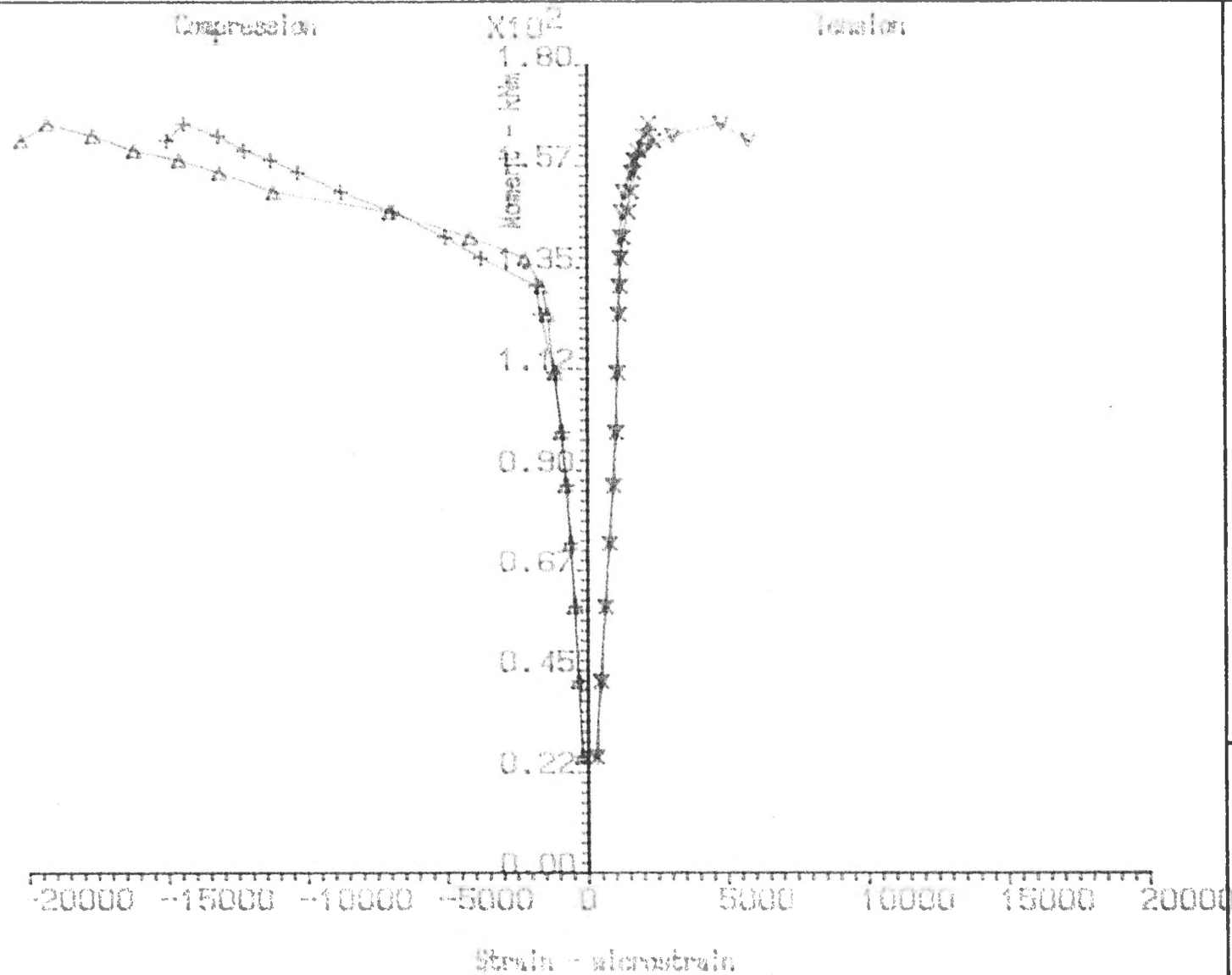
▽, Δ = Beam 1
 ×, + = Beam 2

Figure F.9.

STRAIN GAUGE READINGS
 AGAINST BENDING MOMENT.

Test C1





Connection Type :-
Unstiffened
Internal
Beam Size -254x146UC137
Column Size -305x305UC137
4 M20 Tension Bolts
Grade HSFG -Pretensioned
Endplate Thickness = 20mm

∇, Δ = Beam 1
 $\times, +$ = Beam 2

Figure F.11.
STRAIN GAUGE READINGS
AGAINST BENDING MOMENT.

Test D1

APPENDIX G

CALCULATION OF THE RELATIVE PRECISION OF DERIVED QUANTITIES BY THE PROPAGATION OF ERRORS.

From reference 50, it can be seen that the relative precision of a derived quantity can be determined by the relative precision of the measurements which make up that quantity by the propagation of errors.

Therefore for any quantity, Q , dependent upon x, y then the variance of that quantity is given by

$$\sigma_Q^2 = \left(\frac{\partial f}{\partial x}\right)^2 \sigma_x^2 + \left(\frac{\partial f}{\partial y}\right)^2 \sigma_y^2 + 2 \left(\frac{\partial f}{\partial x}\right)\left(\frac{\partial f}{\partial y}\right) \sigma_{xy}$$

(G1)

where $Q = f(x, y)$

The standard deviation of the quantity and a measurement of the relative precision of one reading is given by the square root of the variance. For uncoupled measurements the final term in the variance equation G1 is zero as σ_{xy} is zero.

Applying this theory to typical major quantities derived in this thesis gives the results outlined below

a) Rotation

$$\theta = \frac{\Delta_u + \Delta_l}{D_{bf}} \quad (\sigma_\Delta)^2 = (0.01\text{mm})^2$$
$$(\sigma_{D_{bf}})^2 = (0.5\text{mm})^2$$

Therefore typical $\sigma_\theta = \pm 1.1 \times 10^{-4}$ rads

b) Moment

$$M = Pl \quad (\sigma_P)^2 = (0.9\text{kN})^2$$
$$(\sigma_l)^2 = (0.5\text{mm})^2$$

Therefore typical $\sigma_M = \pm 1.3$ kNm

c) Initial Stiffness

$$K_i = \frac{Pl \cdot D_{bf}}{(\Delta_u + \Delta_l)} \quad (\sigma_\Delta)^2 = (0.01\text{mm})^2$$
$$(\sigma_{D_{bf,i}})^2 = (0.5\text{mm})^2$$
$$(\sigma_P)^2 = (0.9\text{kN})^2$$

Therefore typical $\sigma_{K_i} = \pm 1700$ kNm/rad

d) Flexibility

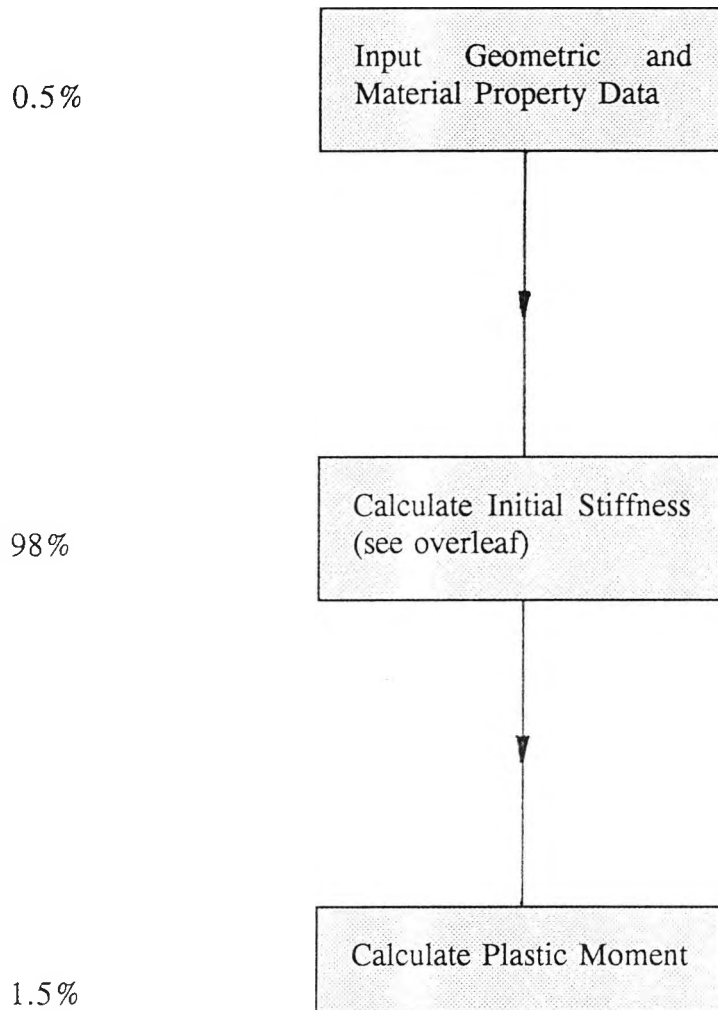
$$f_i = \frac{\Delta_c D_{bf}}{Pl} \quad (\sigma_\Delta)^2 = (0.01\text{mm})^2$$
$$(\sigma_{D_{bf,i}})^2 = (0.5\text{mm})^2$$
$$(\sigma_P)^2 = (0.9\text{kN})^2$$

Therefore typical $\sigma_{f_i} = \pm 0.06 \times 10^{-6}$ mm/kN

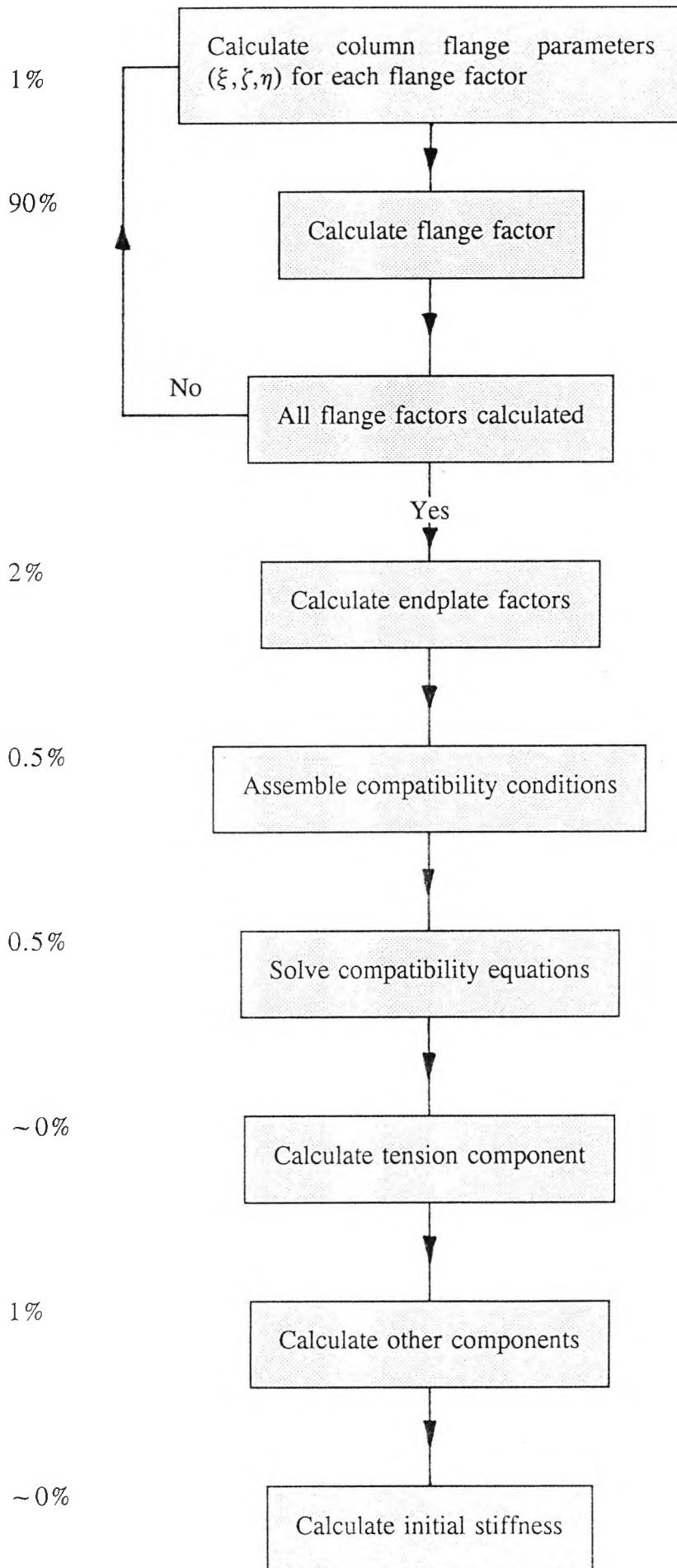
APPENDIX H

FLOW DIAGRAMS
FOR COMPUTER PROGRAMS

1. Calculation of Connection Parameters



Calculation of Initial Stiffness



2. Frame Program

